Application of Room Temperature Ionic Liquids as Electrochemical Solvents

Russell Griffith Evans

St. John's College

University of Oxford

Trinity Term 2005

A thesis submitted for the degree of

Doctor of Philosophy

RADCLIFFE SCIENCE LIBRARY OXFORD
DEPOSITED
- 7 FEB 2006
THESIS

APPLICATION OF ROOM TEMPERATURE IONIC LIQUIDS AS ELECTROCHEMICAL SOLVENTS

A thesis submitted for the degree of Doctor of Philosophy by Russell Griffith Evans, St. John's College, University of Oxford, Trinity Term 2005.

This thesis is concerned with investigating the suitability of room temperature ionic liquids as solvents in which to perform voltammetry, and in characterising electrochemical processes within these media. After providing a general introduction and a background to the ionic liquid field, the results of six original studies are presented, dealing in turn with the following subjects:

- The oxidation of N,N,N',N'-tetraalkyl-*para*-phenylenediamine (TAPD) in five ionic liquids each incorporating the bis(trifluoromethylsulfonyl)imide anion.

- The reduction of oxygen in four ionic liquids based on quaternary alkyl –onium cations and heavily fluorinated anions in which the central ion is either nitrogen or phosphorous.

- The simulation of double potential step chronoamperometry at a disk electrode for the case of unequal diffusion coefficients and its experimental validation using a variety of aqueous, traditional nonaqueous and ionic liquid solutions.

- The rate of diffusion of N,N,N',N'-tetramethyl-*para*-phenylenediamine (TMPD), its radical cation and dication as a function of temperature and ionic liquid viscosity and four such solvents.

- The temperature dependence of the viscosity of five ionic liquids along with the translational and rotational diffusion coefficients of dissolved 2,2,6,6-tetramethylpiperidine-N-oxyl (TEMPO).

- The kinetics of the reaction between N,N-dimethyl-*para*-toluidine (DMT) and its electrogenerated radical cation in an ionic liquid solvent.

The experimental strategy common to each report involves the application of cyclic voltammetry and chronoamperometry at disk electrodes immersed in μL-samples of ionic liquid solution. The data so measured is then analysed via the appropriate theoretical equations or, as is commonly necessary, by comparison with simulated voltammetry. Combined, these chosen redox systems provide access to information on various aspects of electrochemistry within ionic liquids, specifically (a) mass transport (b) the nature of the electron transfer process and (c) the rate of follow-up homogeneous reactions. It is the overall finding herein that while both diffusion and heterogeneous electron transfer are significantly slowed relative to the same processes in a conventional organic solvent, the rate of subsequent homogeneous chemistry remains largely unchanged.

Acknowledgements

First and foremost I wish to thank *Professor Richard Compton* for agreeing to let me work in his group for the last three years, for initiating my interest in room temperature ionic liquids and for his continuous guidance. I'm not sure either of us predicted such a long and (hopefully) productive association when I first arrived for interview at St. John's College almost nine years ago, and whatever caused me to pick that college in particular, I still consider it as a good move.

Modern scientific investigation is rarely a solitary pursuit, and I am indebted to several fellow researchers for their various contributions to the work reported herein. Thanks to *Professor Christopher Hardacre* and *Constanza Villagrán* in Belfast who crucially provided all the samples of ionic liquid, without which this project would not have gotten very far; *Professor David Walton* (Coventry) and *Paul Price* for synthesising the samples of TBPD and [TMPD][BF_4] respectively (the latter managed successfully only once, but once more than in my own attempts); *Professor Clive Hahn* for loan of a gas mixing pump; *Dr. Neil Rees* for assistance in fabricating microelectrodes and for many hours spent attempting fast-scan voltammetry in ionic liquids (virtually none of which made it into this thesis but was nonetheless appreciated); *Andrew Wain* for all the ESR spectroscopy; *Dr. Oleksiy Klymenko* for the large amount of programming he carried out allowing me to make sense of much of my data and finally *Marisa Buzzeo* for co-writing a review with me, for accompanying me to the First International Conference on Ionic Liquids in Austria, and generally for being my partner in ionic liquid electrochemistry for three years.

All RGC group members are acknowledged for offering help and advice when sought and for creating a fun environment to work in. Notable mentions go to *Dr. Peter Tomčík* for interesting conversations and the best reference I'll ever receive; *Dr. Debora Giovanelli* for contributing to some fun nights out and for having good taste in television; *Michael Hyde* for the T2 crossword, trips to the 'library' and being a dab hand with CorelDraw; CSI *Claire Forryan* for table tennis, shopping trips and cooking me several delicious meals; *Marisa Buzzeo and family* for copying all those CDs on my behalf and supplying the lab with copious quantities of confectionary; *Andrew Wain* for computer golf antics and renditions of 'Once More with Feeling'; *Nicole Fietkau* for sudoku, 24 and several handy lifts into London; *Antony Clegg* for being a gallant loser at Tardis Tennis and Slime Volleyball; and last, but not least, Greater Manchester's very own *Trevor Davies* for the Fantasy Compton League, spot the intro, megaquiz, acknowledging that pork pies are best served cold and that genuine Cornish pasties do not contain carrots, along with some memorable performances in the pub.

Finally, many thanks to my family, especially my parents, for all their support.

Contents

Abstract i
Acknowledgements ii
Contents iii
Glossary vii
1 Fundamentals of Electrochemistry 1
1.1 The Electrode | Solution Interface 1
1.1.1 Structure of the Interfacial Region 1
1.1.2 Faradaic and Nonfaradaic Processes 3
1.1.3 Stages of an Electrochemical Process 3
1.2 Mass Transport 4
1.2.1 Fick's Laws of Diffusion 5
1.2.2 The Diffusion Coefficient 8
1.3 Heterogeneous Electron Transfer 9
1.3.1 The Butler-Volmer Model 9
1.3.2 Electrochemical Reversibility 11
1.4 Practical Electrochemistry 12
1.4.1 The Electrochemical Cell 12
1.4.2 The Disk Electrode 14
1.5 Voltammetric Techniques 16
1.5.1 The Potential Step Method 16
1.5.2 The Potential Sweep Method 19
1.6 Matching Experiment with Theory 23
1.6.1 The Finite Difference Method 23
1.6.2 Data Fitting Methods 26
1.7 References 29
2 Room Temperature Ionic Liquids in Electrochemistry 31
2.1 Introduction 31
2.2 Properties of Ionic Liquid Solvents 35
2.2.1 Viscosity 37
2.2.2 Conductivity 39
2.2.3 Electrochemical Window 40

2.2.4 Double-Layer Capacitance....42
2.2.5 Solubility and Solvating Properties....43
2.2.6 Effect of Impurities....43
2.2.7 Voltammetry in Ionic Liquids....47
2.3 Electrochemical Applications of Ionic Liquids....49
2.3.1 Fundamental Voltammetric Studies....50
2.3.2 Electroanalysis....52
2.3.3 Electrodeposition....55
2.3.4 Electrosynthesis....57
2.3.5 Applications in Electrochemical Devices....59
2.4 Summary....60
2.5 The Aims of the Work Reported in this Thesis....63
2.6 References....64
3 General Experimental Methods....71
3.1 Chemical Reagents....71
3.2 Electrodes and Potentiostat....73
3.3 Additional Apparatus....74
3.4 References....76
4 Oxidation of N,N,N',N'-Tetraalkyl-*para*-phenylenediamines in a Series of Room Temperature Ionic Liquids Incorporating the Bis(trifluoromethyl-sulfonyl)imide Anion....78
4.1 Introduction....79
4.2 Experimental Section....82
4.3 Theory Section....83
4.3.1 Simulation of Cyclic Voltammetry....83
4.3.2 Determination of Diffusion Coefficients....85
4.4 Results and Discussion....86
4.4.1 Influence of Water Vapour on the RTIL Electrochemical Window....86
4.4.2 Potential Sweep Analysis of TAPD....88
4.4.3 Chronoamperometric Analysis of TAPD....90
4.4.4 Simulating the TAPD Voltammetry....91
4.4.5 Discussion....93
4.5 Conclusions....96
4.6 References....96

5 Electroreduction of Oxygen in a Series of Room Temperature Ionic Liquids Composed of Group 15-Centred Ions 99

5.1 Introduction 100

5.2 Experimental Section 103

5.3 Theory Section 103

5.3.1 Analysis of Chronoamperometric Transients 103

5.3.2 Simulation of Cyclic Voltammetry 104

5.4 Results and Discussion 105

5.4.1 Reduction of Oxygen in the Quaternary Ammonium RTILs 105

5.4.2 Reduction of Oxygen in the Quaternary Phosphonium RTILs 112

5.5 Conclusions 117

5.6 Appendix: Simulating the $\vec{E}C\vec{E}$ Mechanism 118

5.7 References 122

6 Double Potential Step Chronoamperometry at Disk Electrodes: Simulating the Case of Unequal Diffusion Coefficients 124

6.1 Introduction 124

6.2 Theory Section 126

6.2.1 The Mathematical Model 126

6.2.2 The Expanding Time Grid 130

6.2.3 Fitting and Computation 131

6.3 Experimental Section 132

6.4 Results and Discussion 133

6.4.1 Theoretical Results 133

6.4.2 Chemically Reversible, One-Electron Couples 138

6.4.3 Anodic Dimerisation of *p*-Chloroaniline 140

6.5 Conclusions 143

6.6 References 144

7 A Comparative Electrochemical Study of Diffusion in Room Temperature Ionic Liquid Solvents *versus* Acetonitrile 146

7.1 Introduction 146

7.2 Experimental Section 150

7.3 Results and Discussion 151

7.3.1 Analysis of Chronoamperometric Data 151

7.3.2 Results in Acetonitrile 153
7.3.3 Results in Room Temperature Ionic Liquids 155
7.3.4 Discussion 161
7.4 Conclusions 164
7.5 References 165
8 An Electrochemical and ESR Study on the Molecular Dynamics of TEMPO in Room Temperature Ionic Liquid Solvents 167
8.1 Introduction 167
8.2 Experimental Section 170
8.3 Results and Discussion 171
8.3.1 Viscosity 171
8.3.2 Translational Diffusion 171
8.3.3 Rotational Diffusion 173
8.4 Conclusions 178
8.5 References 179
9 A Kinetic Study of the Reaction between N,N-Dimethyl-*para*-toluidine and its Electrogenerated Radical Cation in a Room Temperature Ionic Liquid 181
9.1 Introduction 182
9.2 Experimental Section 185
9.3 Results and Discussion 185
9.3.1 Voltammetry of DMT in $[Py_{14}][NTf_2]$ 185
9.3.2 Diffusion 189
9.3.3 Heterogeneous Kinetics 191
9.3.4 Homogeneous Kinetics 194
9.4 Conclusions 200
9.5 Overall Conclusions of the Work Reported in this Thesis 201
9.6 References 202

Glossary

The following is a list of symbols and abbreviations commonly used throughout this thesis. In cases where a symbol has more than one meaning, the appropriate context is made clear in the text.

α	charge transfer coefficient
γ	activity coefficient
δ	diffusion layer thickness
η	dynamic viscosity
κ	specific conductivity
τ	dimensionless time parameter
τ_R	rotational correlation coefficient
ϕ	electrostatic potential
Λ_m	molar conductivity
a	hydrodynamic radius
A	area
C	homogeneous chemical reaction step
C_d	double-layer capacitance
D	diffusion coefficient
e^-	electron
E	heterogeneous electron transfer step
E	potential difference
E^0	standard electrode potential
E_f^0	formal electrode potential
E_a	activation energy
F	Faraday constant (96485 C mol^{-1})
H	ESR line width parameter
I	ESR line intensity
I	current
J	flux of material
k	(a) Boltzmann constant (1.380622 x 10^{-23} J K^{-1})
	(b) homogeneous rate constant

k_0	standard heterogeneous rate constant
M	molar mass
n	(a) number of electrons
	(b) a real integer > 0
O	general solution species prone to undergoing a one-electron reduction
r	cylindrical polar spatial coordinate
r_d	disk radius
R	general solution species prone to undergoing a one-electron oxidation
R	universal gas constant (8.3145 J K^{-1} mol^{-1})
R^2	least squares correlation coefficient
R_u	uncompensated resistance
t	time, temporal coordinate
T	absolute temperature
u	concentration
v	scan rate
V	volume
x	(a) Cartesian spatial coordinate
	(b) solvent association parameter
y	Cartesian spatial coordinate
z	cylindrical polar spatial coordinate

ADI	alternating direction implicit method
CE	counter electrode
CV	cyclic voltammetry/voltammogram
DMT	N,N-dimethyl-*para*-toluidine
ESR	electron spin resonance spectroscopy
EV^{2+}	ethylviologen
FIFD	fast implicit finite difference method
GC	glassy carbon
LSV	linear sweep voltammetry/voltammogram
PCA	*para*-chloroaniline
RE	reference electrode
RTIL	room temperature ionic liquid
TAPD	N,N,N',N'-tetraalkyl-*para*-phenylenediamine
TEMPO	2,2,6,6-tetramethylpiperidine-N-oxyl
UME	ultramicroelectrode
WE	working electrode

1 Fundamentals of Electrochemistry

As far as it applies in this thesis, the term *electrochemistry* may be defined as the study of chemical changes in solution brought about through the passage of an electrical current. Under appropriate conditions, measurement of this current along with other pertinent system variables, a process known as *voltammetry*, can provide both kinetic and thermodynamic data concerning the species undergoing the chemical change. It is the aim in this chapter to review some of these appropriate conditions along with their accompanying theory as far as they relate to the techniques employed in the collection and analysis of the experimental data that is subsequently reported. A much more comprehensive account can be found in standard electrochemistry textbooks.[1-6]

1.1 The Electrode | Solution Interface

Electrochemistry is a heterogeneous phenomenon, herein involving charge transfer between a solid metal electrode and a solution of ions. In designing and successfully interpreting the observations made during electrochemical experiments, it is therefore important to consider the local structure at this boundary and the types of current that may be induced to flow across it.

1.1.1 Structure of the Interfacial Region

In a typical voltammetric experiment, an electrode immersed in an ionic solution becomes charged relative that solution via the imposition of a potential difference across the interface from an external source. This causes the ions in the immediate vicinity of the electrode to redistribute themselves in an effort to maintain overall electroneutrality; ions of opposite charge are attracted towards its surface, those of

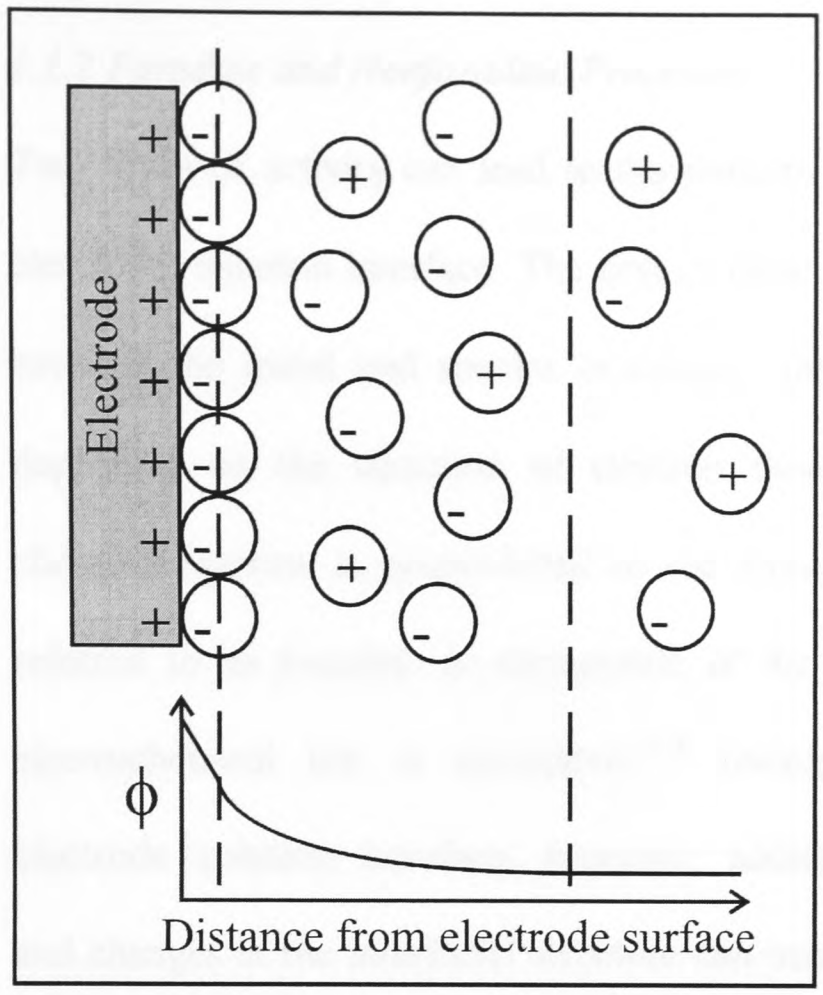


Figure 1.1
A schematic representation of the Stern model for the electrode | solution interface and the variation in electrostatic potential across it.

like charge repelled and an electric field gradient thus established extending out towards the bulk solution. There have been several attempts to model this assembly of ions and while further refinements have been made in subsequent years, Stern's approach,[7] proposed in 1924, is sufficient to broadly characterise the interfacial features in many traditional electrolyte solutions. This model of the electrode | solution interface is shown schematically in Figure 1.1. It is essentially a combination of two earlier theories, encompassing a Helmholz monolayer of specifically adsorbed ions at the electrode surface in series with a Gouy-Chapman diffuse layer in which electrostatic forces and thermal agitation are both significant in influencing the solution composition.[8-10] In terms of the potential, this corresponds to a linear drop followed by an approximately exponential fall off, tending to the bulk solution value. The existence of these two adjacent charge densities of equal but opposite sign creates in effect a capacitative arrangement, characterised for historical reasons by what is termed the double-layer capacitance, C_d.

1.1.2 Faradaic and Nonfaradaic Processes

Two types of activity can lead to the passage of external currents deriving from the electrode | solution interface. The first of these is associated with transfer of electrons between the metal and species in solution that either become oxidised or reduced depending on the direction of electron flow. In such processes, the amount of chemical reaction is proportional to the amount of charge passed and so they are referred to as *faradaic* in recognition of Sir Michael Faraday to whom this basic electrochemical law is accredited.[11] Owing to the capacitative nature of the electrode | solution interface, however, additional adsorption/desorption processes and changes in the interfacial structure can occur as the potential is varied, causing it to charge and discharge. Although there is no electron transfer, transient external currents are generated, resulting from these *nonfaradaic* processes. This charging current, I_c, is proportional to the double-layer capacitance, the electrode area, A, and the rate of change of the potential, known as the scan rate, v.

$$I_c = AC_d \frac{dE}{dt} = AC_d v \qquad (1.01)$$

In practical voltammetry, both types of current contribute to the overall measured response. The faradaic process is usually of sole interest, however, and appreciable levels of nonfaradaic current only serve to complicate data analysis, as decoupling the two it is generally not straightforward. Experimental conditions are therefore usually directed to probe regimes where the effects of the latter are sufficiently minimised.

1.1.3 Stages of an Electrochemical Process

A general electrode reaction consists of multiple steps, any of which, depending on the experimental conditions, may influence the overall rate. These steps may be classified as follows:

- Mass transport of material to and from the interfacial region
- Heterogeneous electron transfer
- Homogeneous chemical reactions that precede or follow the electron transfer

Such reactions are conveniently described using a form of mechanistic nomenclature introduced by Testa and Reinmuth,[12] whereby a heterogeneous electron transfer step is denoted 'E' and a homogeneous chemical reaction as 'C'. A stepwise two-electron reduction would then be represented as EE, while oxidation following a deprotonation step to give a radical which then dimerises is termed CEC. Further embellishments such as the inclusion of subscripts, C_n, to indicate the order of a homogeneous chemical step, or the addition of arrows denoting the relative direction of two or more heterogeneous electron transfers have also proved useful. This notation has been adopted to symbolize some of the chemical systems reported herein.

1.2 Mass Transport

In order to sustain any electrode process, fresh electroactive material must be transported from the bulk solution to the electrode surface. Mass transport is generally sub-divided into three categories, depending on the nature of the solution gradient along which a flow of material occurs. Movement of charged species in response to the potential difference between electrode and solution is known as *migration*. Motion along thermal or density gradients that arise as a consequence of reaction or deliberate mechanical pumping or stirring of the solution is termed *convection*. Finally, *diffusion* is the movement of species in solution due to the presence of a concentration gradient.

Any quantitative analysis of empirical data will have to account for mass transport

and so for each type of motion, electrochemists must tailor the experimental design such that it either occurs in a predictable manner, or is minimised to the extent that can be reliably ignored. In the case of migration, the latter option is almost always chosen. This is achieved by addition of a chemically and electrochemically inert salt, a *supporting electrolyte*, of concentration at least thirty times greater than the species under study. These ions then take on the bulk of the charge transport in solution. There are other advantages of increasing the ionic strength: the solution conductivity is increased and virtually the entire potential drop between metal and solution is contained within a small region of about 10-20 Å adjacent to the electrode surface. This distance is compatible with quantum mechanical tunnelling of electrons between the electrode and solution species. Turning next to convection, that which occurs naturally is chaotic and ill-defined, but usually safely ignored as long as the experimental timescale does not exceed 10-20 s. On the other hand, many electrochemical experiments do employ convection as the dominant form of mass transport, by applying an external force to stir or otherwise agitate the solution in a well-defined manner relative to a so-called *hydrodynamic* electrode.[13] The experiments described in this thesis, however, were conducted under diffusion-only conditions.

1.2.1 Fick's Laws of Diffusion

Adolf Fick, by deducing two laws that govern its behaviour, supplied a mathematical description of diffusion in 1855.[14,15] These laws take the form of differential equations relating the concentration of a species as a function of space and time and its *flux*, or number of moles passing through a plane of unit cross-sectional area per unit time. The laws in one spatial dimension may be derived by considering a

cylindrical solution volume with cross-section area A, in which there is a linear concentration gradient in the x-direction. During the time interval δt, a particle moves a distance of δx in either direction by random-walk. Taking a small section of length $2\delta x$ and further dividing it in half, as in Figure 1.2, the average number of particles per unit volume is defined as N_1 for the left-hand volume and N_2 on the right-hand side. The number of particles in each half is then obtained by multiplying by the volume, $A\delta x$, to give $N_1 A\delta x$ and $N_2 A\delta x$ respectively. Over the time interval δt, half the particles will move to the left and half to the right, thus the net number moving across the barrier from left to right will be $\frac{1}{2}(N_1 - N_2)A\delta x$. The net rate of transfer is then:

$$Rate = \frac{(N_1 - N_2)A\delta x}{2\delta t} \tag{1.02}$$

The difference between the average number of particles in each volume may also be related to the linear concentration gradient:

$$N_1 - N_2 = -\frac{\partial N}{\partial x}\delta x \tag{1.03}$$

Substituting into equation (1.02) gives:

$$Rate = \frac{A(\delta x)^2}{2\delta t}\frac{\partial N}{\partial x} \tag{1.04}$$

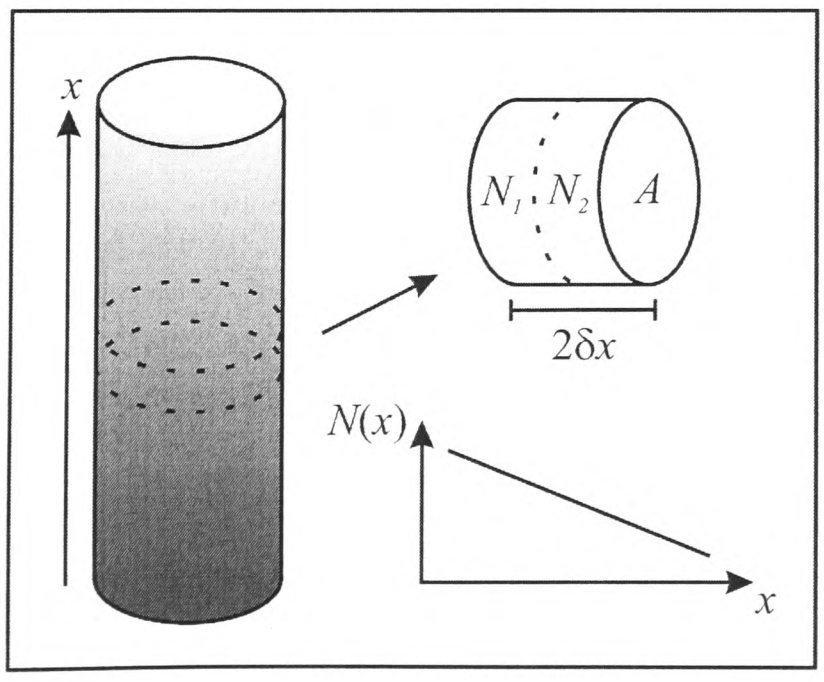


Figure 1.2
Model of diffusion in one dimension down a linear concentration gradient through a section of length $2\delta x$.

Finally, dividing by A and Avogadro's number gives the flux, J, in the standard units:

$$J = -D\frac{\partial C}{\partial x} \tag{1.05}$$

where D is the *diffusion coefficient*, given by:

$$D = \frac{(\delta x)^2}{2\delta t} \tag{1.06}$$

Equation (1.05) is Fick's first law of diffusion. The second law may be obtained by considering a volume element of unit cross-sectional area and thickness dx. The change in concentration over time within the element is given by the difference between the flux in, $J(x)$, and flux out, $J(x + dx)$, divided by the element volume, dx:

$$\frac{\partial C}{\partial t} = \frac{J(x) - J(x+dx)}{dx} = \frac{J(x) - [J(x) + (\partial J/\partial x)dx)]}{dx} = -\frac{\partial J}{\partial x} \tag{1.07}$$

Differentiating the first law (1.05) gives:

$$\frac{\partial J}{\partial x} = -D\frac{\partial^2 C}{\partial x^2} \tag{1.08}$$

and so by substitution, Fick's second law (1.09) is obtained:

$$\frac{\partial C}{\partial t} = D\frac{\partial^2 C}{\partial x^2} \tag{1.09}$$

These laws were obtained empirically by Fick based on the results of experiments involving diffusion along conically shaped vessels. For simplicity, they have been derived here for the one-dimensional case, however, the general formulation of Fick's second law is:

$$\frac{\partial C}{\partial t} = D\nabla^2 C \tag{1.10}$$

where ∇^2 is the Laplacian operator, whose form is specific to the geometry over which the equation is to be solved.

1.2.2 The Diffusion Coefficient

The last section introduced the concept of a diffusion coefficient as a measure of the rate at which material moves down a concentration gradient. Equation (1.06), however, does not provide the most useful definition of this quantity. An alternative formulation is obtained by applying hydrodynamic theory to give:

$$D = \frac{kT}{6\pi\eta a} \qquad (1.11)$$

which relates the diffusion coefficient to the viscosity of the solvent medium, η, and is known as the Stokes-Einstein equation.[16] Here a represents the radius of the diffusing species including its associated solvation shell. For a given molecule, equation (1.11) predicts an inverse linear relationship between diffusion coefficient and solvent viscosity. In the case of charged species, this correlation is more familiar as Walden's rule, which observes that the product of molar conductivity, Λ_m, and viscosity is roughly constant for the same ion in different solvents.[17] Since $\Lambda_m \propto D$, substituting for the diffusion coefficient in equation (1.11) does then imply that $\Lambda_m \propto 1 / \eta$, as required. In reality, varying degrees of solvation mean that not only the viscosity, but also the hydrodynamic radius changes with solvent and so over-reliance on the rule is inadvisable.

Wilke and Chang proposed another means by which to estimate diffusion coefficients from conveniently determined solution parameters by introducing the following semi-empirical correlation:[18]

$$D = 7.4 \text{ x } 10^{-8} \frac{T\sqrt{xM}}{\eta V^{0.6}} \qquad (1.12)$$

where D has the units $cm^2\ s^{-1}$ and the viscosity is in mPa s. Here, T is the absolute temperature, M is the molar mass of the solvent in g mol^{-1}, x is a solvent association parameter and V is the volume of the solute at its normal boiling point in $cm^3\ mol^{-1}$. For complex organic molecules, V is generally determined by summing individual atomic contributions, as tabulated by the authors. Equation (1.12) was based on data gathered across a variety of dilute aqueous and organic solutions and found to predict the diffusion coefficient to within an average of 10%.

Finally, diffusion is a thermally activated process and generally follows an Arrhenius relationship:

$$D = D_0 e^{-\frac{E_a}{RT}} \qquad (1.13)$$

where R is the universal gas constant, E_a is the diffusional activation energy and the coefficient of proportionality, D_0, is notionally the diffusion coefficient as $1/T \rightarrow 0$.

1.3 Heterogeneous Electron Transfer

Having reviewed the processes by which electroactive material is transported to an electrode surface, this section quantifies the rate of any ensuing electron transfer.

1.3.1 The Butler-Volmer Model

There have been several attempts to rationalise the rate of heterogeneous electron transfer, but the treatment by Butler and Volmer has found the most application and is assumed for all the work that follows in this thesis.[19-21] It is outlined here for the case of a general one-electron transfer involving two species, O and R:

$$O + e^- \underset{k_b}{\overset{k_f}{\rightleftharpoons}} R \qquad (1.14)$$

Here, k_f and k_b are heterogeneous rate constants for the forward and backward

electron transfer reactions respectively. Any current flow is proportional to the rate constant and the concentration of the corresponding species at the electrode surface, $[O]_0$ or $[R]_0$. The net current for the above reaction is then a sum of both the reductive and oxidative components:

$$I = I_b + I_f = FAk_b[R]_0 - FAk_f[O]_0 \tag{1.15}$$

Butler and Volmer's contribution was then to derive equations relating the forward and backward rate constants to the potential applied at the electrode:

$$\begin{aligned} k_f &= k_0 e^{-\alpha\theta} \\ k_b &= k_0 e^{(1-\alpha)\theta} \end{aligned} \tag{1.16}$$

where

$$\theta = \frac{F}{RT}\left(E - E_f^0\right) \tag{1.17}$$

This formulation contains three important parameters. The *formal electrode potential*, E_f^0, is the potential at which the forward and backward rate constants are equal. It may be related to the standard electrode potential, E^0, as:

$$E_f^0 = E^0 + \frac{RT}{F}\ln\left(\frac{\gamma_O}{\gamma_R}\right) \tag{1.18}$$

where γ_O and γ_R the activity coefficients of the redox species. The *standard heterogeneous rate constant*, k_0, is then the value of k_f and k_b at E_f^0. Finally, the *charge transfer coefficient*, α, may take a value between 0 and 1 and provides a measure of the symmetry of the energy barrier to reaction; for systems with $\alpha = 0.5$, the structure of the transition state equally reflects that of species O and R. Inserting the expressions for k_f and k_b into (1.15) gives the Butler-Volmer equation:

$$I = FAk_0\left([R]_0 e^{(1-\alpha)\theta} - [O]_0 e^{-\alpha\theta}\right) \tag{1.19}$$

A combination of this equation with Fick's second law is sufficient to model a simple electron transfer under diffusion only conditions.

1.3.2 Electrochemical Reversibility

This term provides a gauge of the rate of the electron transfer kinetics of a redox couple. If electron transfer is sufficiently facile that equilibrium is achieved on a short time scale and maintained as the potential is varied, the system is described as being *electrochemically reversible*. Under such conditions, equation (1.19) simplifies to the Nernst equation:[22]

$$E = E_f^0 + \frac{RT}{F} \ln \frac{[\mathrm{R}]_0}{[\mathrm{O}]_0} \qquad (1.20)$$

which provides the ratio of the concentrations of species O and R adjacent to the electrode surface at each potential. In the other extreme, for systems with very sluggish electron transfer kinetics, equilibrium is not attained at potentials close to E_f^0 on the same time scale and a significant overpotential must be applied to drive the reaction. Such redox couples are characterised as being *electrochemically irreversible*. Intermediate cases are said to display *quasireversibility*.

The time scale referred to in the above discussion, however, is entirely dependent on the experimental conditions and the degree of electrochemical reversibility is coupled to the prevailing rate of mass transport. In a potential sweep experiment, an electron transfer that initially appears reversible will eventually be rendered quasireversible as the scan rate is increased. Under a given set of experimental conditions, the reversibility can be assessed from the magnitude of the standard heterogeneous rate constant for the couple. Larger k_0 values indicate more rapid electrode kinetics.

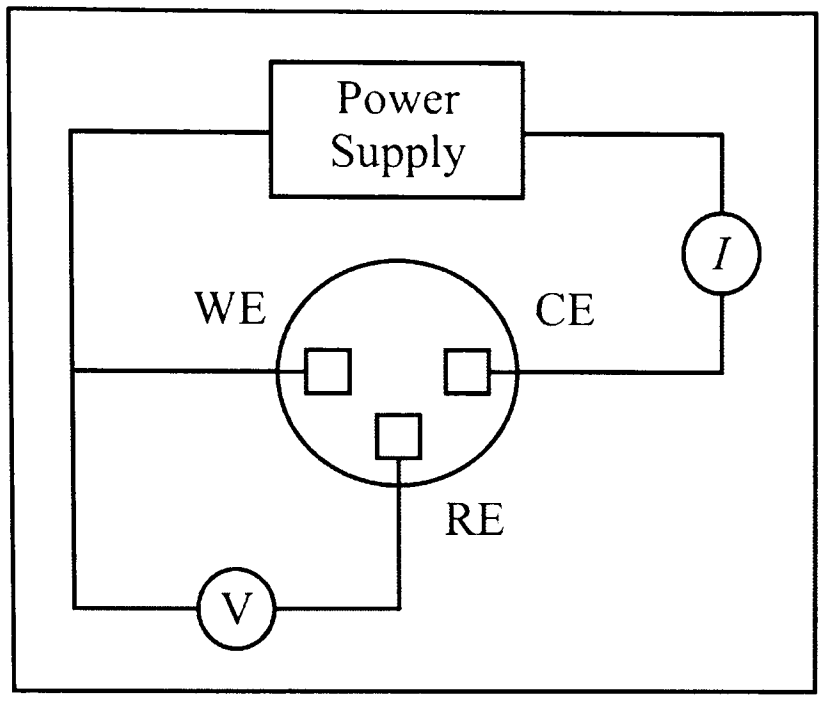


Figure 1.3
The standard configuration of a three-electrode electrochemical cell

1.4 Practical Electrochemistry

Having placed the various stages of the electrochemical process on a sound theoretical footing, this section moves on to consider some of the more empirical aspects involved in designing and conducting electrochemical experiments to measure the various parameters that have been introduced.

1.4.1 The Electrochemical Cell

In all the above, reaction has only been considered at a single electrode surface, henceforth termed the *working electrode*, WE. Basic electronics, however, decrees that at least one additional electrode be in contact with the solution to form a closed path. In fact, it is often preferable to employ a total of three electrodes in any electrochemical experiment in which it is intended to sustain a current. The essentials of the resulting electronic circuit are shown in Figure 1.3. In this arrangement, the current passes exclusively between the WE and a *counter electrode*, CE. Processes occurring at the CE have no bearing on the reaction of interest and its properties need only be such that it is able to pass sufficient current so as not to impede electron transfer at the WE. Practically this translates as a good electronic conductor with a

large surface area. The potential of the WE is then monitored relative to a third, *reference electrode*, RE. By ensuring that negligible current flows between them, the potential of the RE remains fixed throughout the experiment and thus changes in the externally applied potential, measured as (E_{WE} - E_{RE}), are directly related to those at the WE. The potentials of some reference electrodes are well characterised and thus measurements made against them in different systems may be directly related. In non-aqueous solvents, however, it is more common just to employ a gold or platinum wire as the RE, the rationale being that its potential, although unknown, is unlikely to change during a series of measurements. Such electrodes are known as *quasireferences* to distinguish that they must be calibrated against a true reference system to allow meaningful data comparison.

In reality, there is a third contribution to the measured potential, E_{app}, due to electrical resistance of the intervening solution to the passage of current:

$$E_{app} = E_{WE} - E_{RE} - IR_u \qquad (1.21)$$

where R_u represents uncompensated solution resistance. This phenomenon, known as ohmic drop, can be minimised by employing short WE – RE separations and reducing the amount of current passed through the use of small working electrodes. As such, this term can generally be ignored, but on occasion corrective measures are necessary before any meaningful interpretation of voltammetric data can occur. Another consequence of using a small WE is that the functions of the reference and counter can be combined, since the overall current passed is insufficient to cause any significant drift in its potential in this now two-electrode set up.

1.4.2 The Disk Electrode

A variety of working electrode geometries find routine use in electrochemistry, but the most prolific is the disk, which is used exclusively in the work reported herein. This abundance is no doubt due to practical considerations; a disk electrode is straightforward to fabricate by sealing a wire conductor into an insulating material (e.g. glass, PTFE) and then exposing a cross-section of the wire. Indeed, from a theoretical viewpoint it is one of the more complex arrangements, as diffusion to a disk surface is inherently a two-dimensional problem. The corresponding form of Fick's second law, cast in terms of cylindrical coordinates r, z for species R is:

$$\frac{\partial[\mathrm{R}]}{\partial t} = D_{\mathrm{R}}\left[\frac{\partial^2[\mathrm{R}]}{\partial r^2} + \frac{1}{r}\frac{\partial[\mathrm{R}]}{\partial r} + \frac{\partial^2[\mathrm{R}]}{\partial z^2}\right] \qquad (1.22)$$

where the coordinates r and z are as defined in Figure 1.4. Two components to the diffusion of species R can then be identified. So-called *planar diffusion* occurs to all points on the electrode along lines normal to the disk surface. At the disk edge, however, an additional *convergent diffusion* process may take place, radially with respect to the z-axis. These are illustrated on the right hand side of Figure 1.4. As a

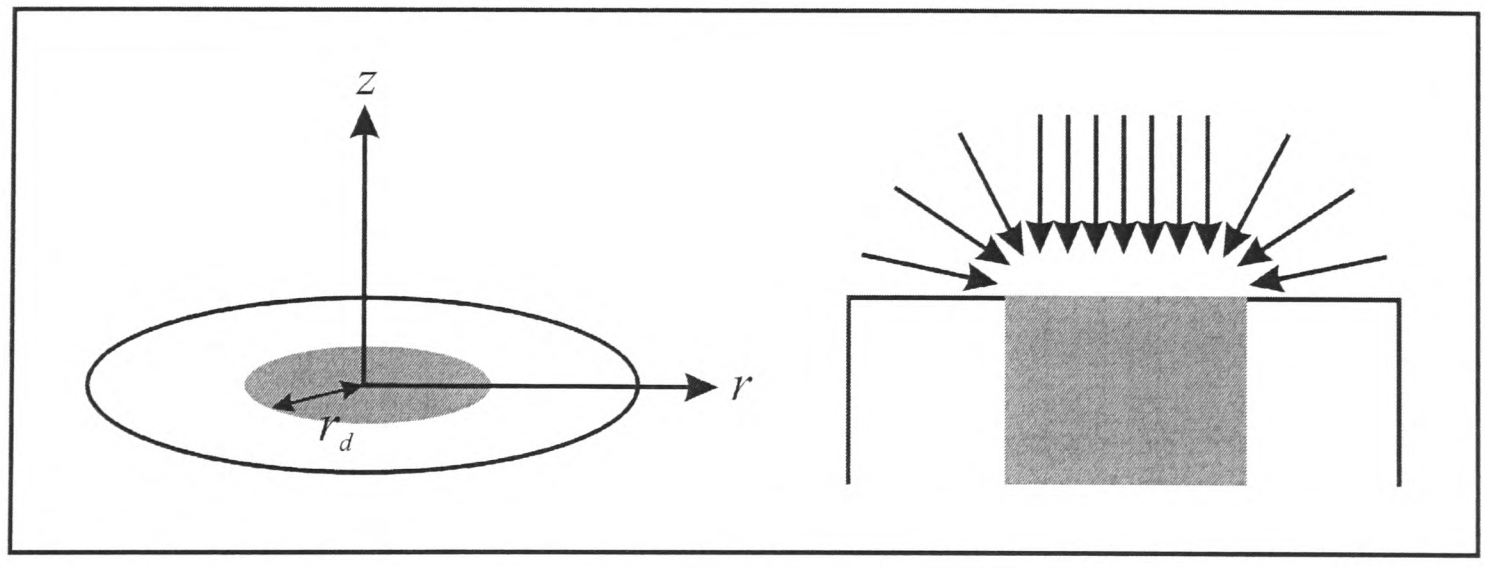


Figure 1.4
The disk geometry expressed in terms of cylindrical coordinates r, z and the pattern of diffusion to a disk surface.

consequence, the rate of mass transport varies locally over the electrode surface, with greatly increased current density at the disk edge.

In practice, either type of diffusion may dominate the electrode process or else they may both be significant, depending entirely on the experimental conditions. At each limit the transport problem may be adequately handled in one dimension (diffusion to a plane or a spherical surface, respectively), thus reducing the level of mathematical complexity required for its solution. For intermediate cases, however, it is inadvisable to attempt such a simplification.[23] An important criterion in determining the relative importance of planar and convergent diffusion is the length of an electrode's critical dimension relative to the size of the diffusion layer established in the adjacent solution. For a disk, this critical dimension is the radius, r_d and while there is no universally applicable definition of a diffusion layer thickness, from equation (1.06) it can be written as $\delta = \sqrt{2Dt}$. Disk electrodes with radii much larger than δ will display voltammetry consistent with an entirely planar diffusion profile. When the length of the diffusion layer exceeds the disk radius, however, the effects of convergent diffusion are primarily felt.

For a diffusion coefficient of 1 x 10^{-9} m^2 s^{-1}, typical for a conventional non-aqueous solvent, the diffusion layer thickness developed over 1 second is given from the above expression as ~ 50 μm. Consequently, the voltammetry from disk electrodes of radius r_d < 50 μm is commonly associated with the properties of convergent diffusion. Such electrodes are often termed *ultramicroelectrodes* or, more briefly, *microelectrodes* due to their small size. It is important to remember, however, that merely size alone does not determine the diffusional regime prevailing at their surface. Other advantages of miniaturisation are a reduction in the nonfaradaic

charging currents due to the appearance of the electrode area in equation (1.01) and, due to the smaller currents passed, a similar reduction in the amount of ohmic drop. The smaller current also make this one of the circumstances in which a two-electrode set up may be reliably employed.

1.5 Voltammetric Techniques

Having described the design and function of the various electrodes necessary to both accurately control the applied potential difference and measure the current response from an electrochemical system, it remains to consider the ways in which this potential difference may be most usefully perturbed in order to elicit electrochemical data from the system. Two general approaches are reviewed below, both in the context of the disk geometry under diffusion-only conditions.

1.5.1 The Potential Step Method

Known as *chronoamperometry*, this process involves monitoring with time the induced current resulting from an instantaneous change in the applied potential, usually from a region in which no faradaic process occurs to one in which oxidation or reduction proceeds at a diffusion-controlled rate (see Figure 1.5). For the oxidation of species R at a disk electrode, the current-time relationship following such a step is obtained by solving equation (1.22) with the following boundary conditions:

$$\begin{aligned} &t = 0; && [\mathrm{R}] = [\mathrm{R}]_{bulk} \\ &r \to \infty,\ z \to \infty; && [\mathrm{R}] \to [\mathrm{R}]_{bulk} \\ &r > r_d,\ z = 0; && \frac{\partial [\mathrm{R}]}{\partial z} = 0 \\ &r \le r_d,\ z = 0; && [\mathrm{R}] = 0 \end{aligned} \qquad (1.23)$$

Of these, the first four are general to an electrochemical process at a disk. The first specifies that the solution initially containing only species R and the second and third

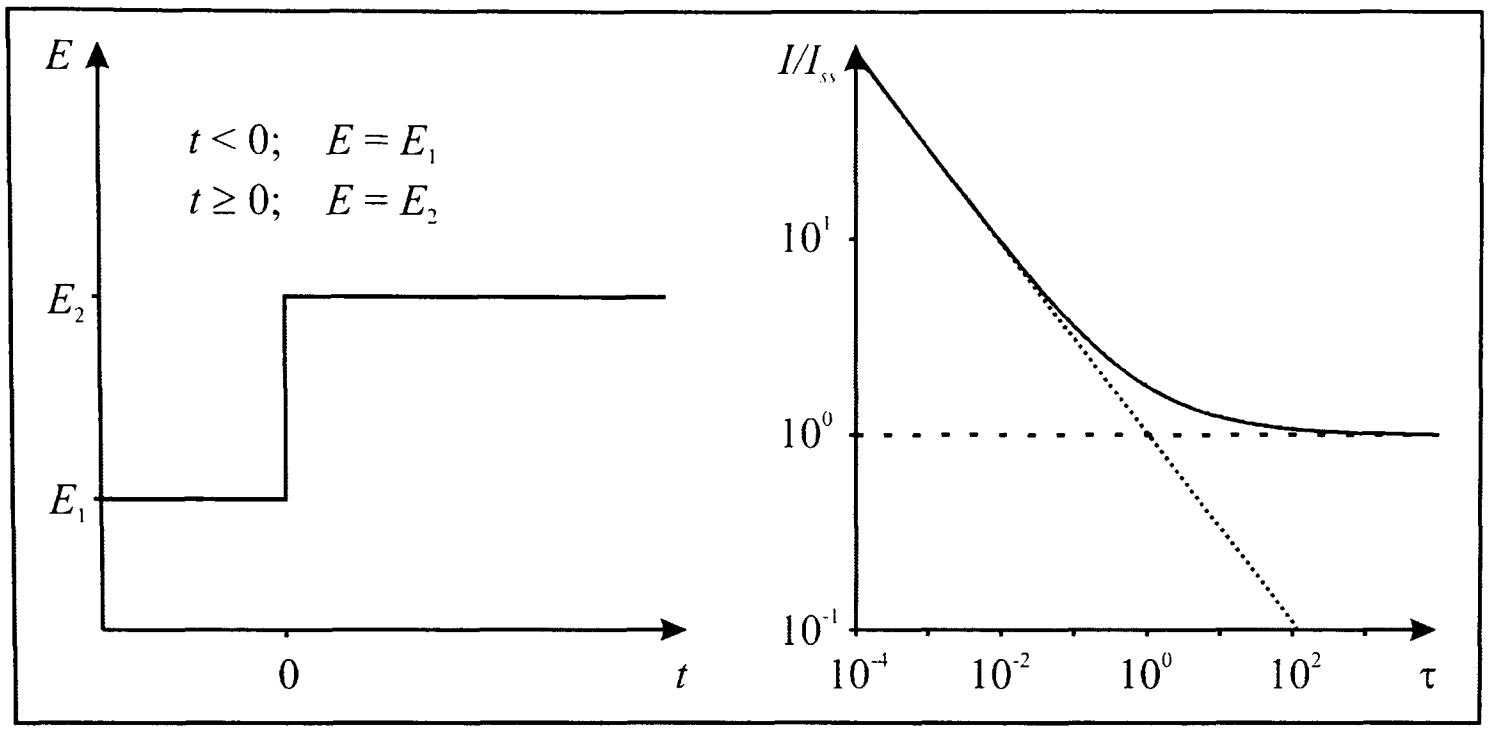


Figure 1.5
The potential waveform applied during a chronoamperometric experiment and the resulting time dependence of the current at a disk electrode as determined by Shoup and Szabo (——) and Cottrell (· · · ·) relative to the steady-state limiting value (- - -).

assume that the solution is sufficiently large that far from the electrode the concentration of R approaches the initial (bulk) value. The fourth defines the insulator boundary by specifying that no material may flow in or out of the plane containing the disk surface at $r > r_d$. Finally, the fifth condition establishes the potential step, which drives the surface concentration of R to zero at all times following its application. No exact solution to this problem exists and so to progress, numerical methods must be employed. Aoki and Osteryoung recast the equations in terms of a dimensionless parameter, τ:[24,25]

$$\tau = \frac{4Dt}{r_d^2} \tag{1.24}$$

and obtained the following solution:

$$I = \frac{4nFAD[\mathrm{R}]}{\pi r_d} f(\tau) \tag{1.25}$$

where n is the number of electrons transferred. The function $f(\tau)$ has two forms, appropriate to different time regimes. At short times when $\tau < 1.44$:

$$f(\tau) = \sqrt{\frac{\pi}{4\tau}} + \frac{\pi}{4} + 0.094\sqrt{\tau} \qquad (1.26)$$

whereas at longer times when $\tau > 0.82$:

$$f(\tau) = 1 + 0.71835\tau^{-1/2} + 0.05626\tau^{-3/2} - 0.00646\tau^{-5/2} \qquad (1.27)$$

The two curves overlap in the intermediate region $0.82 < \tau < 1.44$. Contemporary work by Shoup and Szabo via an alternative treatment yielded a single equation covering the entire range of τ.[26]

$$f(\tau) = 0.7854 + 0.8862\tau^{-1/2} + 0.2146e^{-0.7823\tau^{-1/2}} \qquad (1.28)$$

This relationship deviates from the true current by less than 0.6% at all times. Using either approach, the shape of the current decay can thus be analysed to determine the diffusion coefficient of species R. Of course, since the position of the potential step was designed to be sufficiently positive of the formal potential for the oxidation such that mass transport was rate limiting, heterogeneous kinetic terms to not appear in the equations and no assessment of the electrode kinetics can be made.

The above equations have been derived using the full, two-dimensional description of diffusion and are thus entirely general to the disk geometry. By re-examining equation (1.24), however, the parameter τ can be recognised as the squared ratio of the diffusion layer thickness to the disk radius. Following on from the discussion in the previous section therefore, in potential step experiments the magnitude of τ relates the importance of planar versus convergent diffusion and it is once more informative to examine the limiting cases. At very short times ($\tau < 10^{-2}$), the effects of convergent diffusion do not manifest appreciably and the corresponding current-time curve simplifies to the classical equation derived by Cottrell under the conditions of linear diffusion in one-dimension:[27]

$$I = \frac{nFAD^{1/2}[\mathrm{R}]}{\pi^{1/2}t^{1/2}} \tag{1.29}$$

The same result can be obtained from (1.25) and (1.26) in the limit of $\tau \to 0$. The overlap between this equation and the full treatment (plotted as the Shoup and Szabo form) can be seen in Figure 1.5 at low τ. At longer times, the effects of convergent diffusion begin to take effect and the current is seen to rise away from the ever-decreasing Cottrellian prediction. As τ becomes very large ($< 10^2$), the current approaches a *steady-state*, in the sense that it no longer varies with time. The magnitude of this steady-state current is found by extrapolating equations (1.25) and (1.27) to the limit of infinite τ:

$$I_{ss} = \frac{4nFAD[\mathrm{R}]}{\pi r_d} = 4nFr_dD[\mathrm{R}] \tag{1.30}$$

Graphical conformation is again provided in Figure 1.5.

The chronoamperometric technique can be extended by applying additional potential steps, with the resulting currents then dependent on the diffusion of multiple reaction species and/or homogeneous kinetic terms. This is considered further in a subsequent chapter.

1.5.2 The Potential Sweep Method

This complementary technique involves monitoring the current response as the potential is continually changed (usually linearly) with time. The resulting data, generally plotted as I versus E and termed a *voltammogram*, may be readily interpreted to provide much qualitative information regarding an electrochemical process. Quantitative analysis is also possible, but unlike the potential step method, there are no convenient equations of universal applicability and, short of simulating

the entire voltammetric wave, it is necessary to work in the limit of either planar of convergent diffusion. In potential sweep experiments, this is a property of the scan rate, such that the inequality:[2]

$$v \ll \frac{RTD}{nFr_d^2} \tag{1.31}$$

must be satisfied for convergent diffusion to dominate. Conversely, when the scan rate greatly exceeds this ratio, the electrode can be considered as planar. Under each of these conditions, some useful analytical equations can be derived.

At disk electrodes for which the only significant contribution to mass transport is convergent diffusion, the potential is generally ramped in a single direction in a process known as *linear sweep voltammetry* (LSV). For the oxidation of species O, the scan would most usefully be initiated within a region of zero faradaic activity and the potential then increased incrementally according to the scan rate until it reached and then exceeded the formal potential of the redox couple. This type of potential waveform and the corresponding *I-E* curve are illustrated in Figure 1.6. The

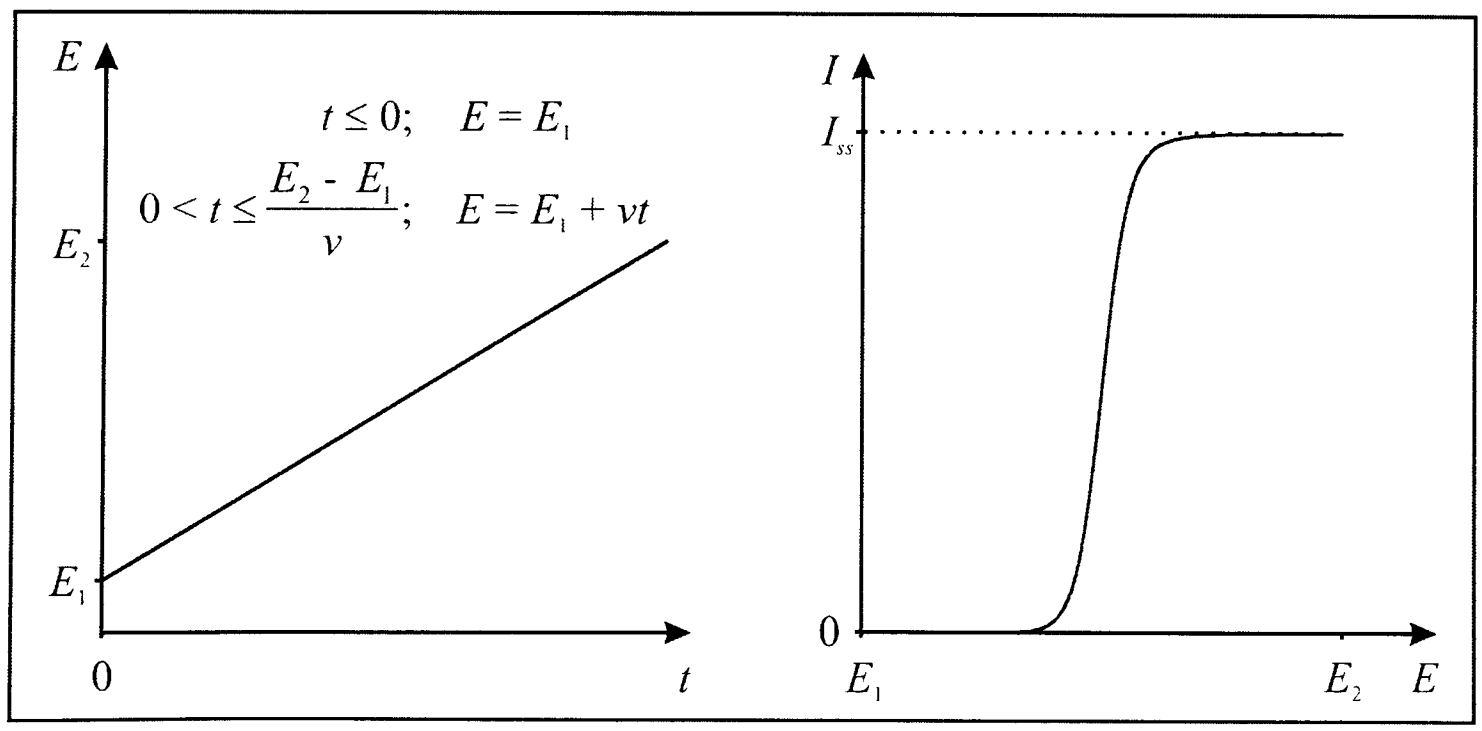


Figure 1.6
The potential waveform applied during a linear sweep voltammetric experiment and the resulting current generated at a disk electrode under a convergent diffusional regime.

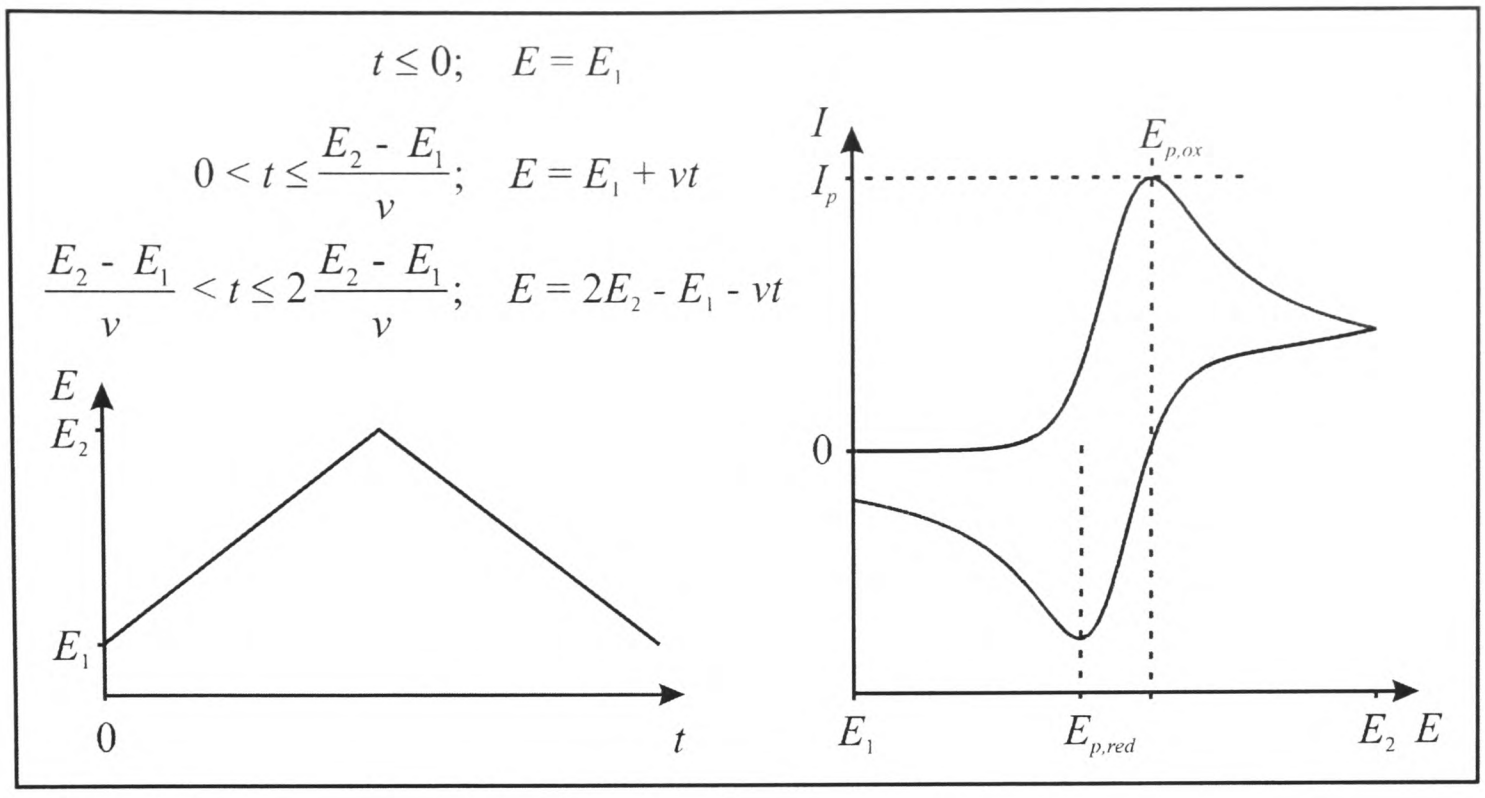


Figure 1.7
The potential waveform applied during a cyclic voltammetric experiment and the resulting current generated at a disk electrode under a planar diffusional regime.

voltammogram has a characteristic sigmoidal appearance and reaches a limiting, steady-state value that may be analysed according to equation (1.30) to provide the diffusion coefficient. Alternatively, such a procedure is commonly applied to electrochemically calibrate the radius of a small disk electrode in a solution where the diffusion coefficient of the electroactive species has been characterised independently. Depending on the reversibility, it is also possible to extract heterogeneous kinetic information contained within the curvature of the wave.[28-31]

In situations where diffusion to the disk is instead essentially planar, the potential sweep method is usually extended by reversing the sweep direction at the upper limit and continuing scan in the opposite direction. The particulars of this technique of *cyclic voltammetry* (CV) are summarised for a straightforward oxidative process in Figure 1.7, which demonstrates the transient, peak-shaped nature of the resulting *I-E* curves. In more complex systems, the location and relative size of the various voltammetric features as a function of scan rate can provide rapid insight into the

mechanism of an electrochemical process. For a reversible electron transfer, the separation of the peak potentials $\Delta E_p = E_{p,ox} - E_{p,red}$ is approximately equal to $59/n$ mV at 298 K. In this case, the peak current, I_p, is given by:

$$I_p = (2.69 \times 10^5) n^{3/2} A D^{1/2} [\mathrm{R}] v^{1/2} \qquad (1.32)$$

an equation usually credited to Randles and Sevcik.[32,33] If the electron transfer is instead sufficiently irreversible such that $\Delta E_p > 120/n$ the expression for the peak current becomes modified to:

$$I_p = (2.99 \times 10^5) \alpha^{1/2} A D^{1/2} [\mathrm{R}] v^{1/2} \qquad (1.33)$$

for the one-electron case. For intermediate electrochemical reversibility, the peak current is a complex function of numerous system parameters. The dependence of I_p on $v^{1/2}$ in the above expressions rationalises the choice of upper limit on the scan rate in practical voltammetry. As previously stated, the measured current results from a combination of faradaic and nonfaradaic processes. Given that the capacitative charging current scales directly with scan rate (equation 1.01), it will always eventually overwhelm the faradaic contribution as v is increased. The practical lower limit is also apparent from earlier discussion; the scan rate must not be so slow that the effects of natural convection begin to influence the mass transport on the experimental timescale.

While the peak current may not be an important diagnostic criterion in quasireversible systems, they do provide optimum conditions for probing the heterogeneous kinetics, for example, through the variation of ΔE_p with scan rate.[34] Precise methods of such analysis are more conveniently introduced in later chapters.

1.6 Matching Experiment with Theory

This chapter has served to introduce the various parameters that govern an electrochemical process and review the experimental methods employed to determine them in the work reported in this thesis. In this final section it remains to consider the process of relating theory and experiment by either (and more conveniently) fitting empirical data to appropriate analytical equations or, where necessary, simulating voltammetry. In the latter case, where equations cannot be solved exactly, numerical methods must be employed. There are various strategies with which to go about this, but all the simulations described within utilise the method of *finite differences.*

1.6.1 The Finite Difference Method

This approach involves discretising the interfacial region into a grid in both space and time and assuming that the concentrations of solution species vary linearly between these points. The partial differential equations that fully describe these concentrations can then be approximated as simple arithmetic operations on the absolute value of the concentrations at various combinations of grid points. Solving these now linear equations in concert generates a concentration profile and by considering the portion immediately adjacent to the electrode surface, a time-dependant current may be calculated. Since the closeness of the approximation increases with the number of grid points employed, the whole procedure is generally implemented using a computer in order to achieve accurate results on a reasonable timescale.

As an example, Figure 1.8 depicts the relationship between the different concentration values, $u^{t}_{x,y}$, for a given species at various grid points in one temporal and two spatial dimensions (t,x,y). With respect to the central point, the first time

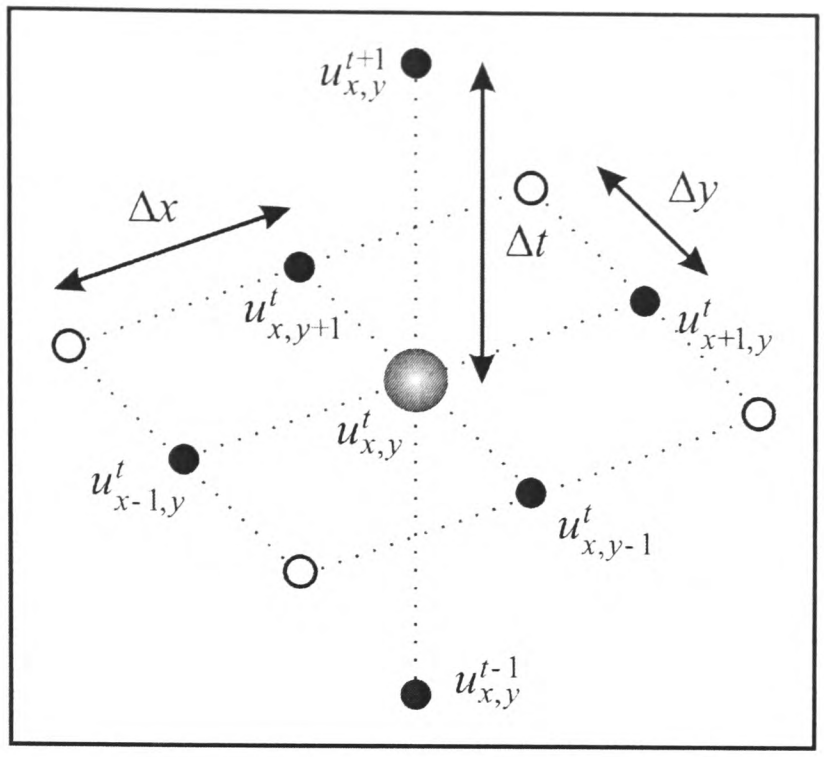


Figure 1.8
A grid illustrating the nomenclature used to describe the relationship between the value of the concentration, u, at discrete points in space (index x, y) and time (index t) with respect to the central point.

derivative may be expressed as the difference:

$$\frac{\partial u}{\partial t} \approx \frac{u^{t+1}_{x,y} - u^{t}_{x,y}}{\Delta t} \tag{1.34}$$

where Δt represents the spacing between to adjacent nodes along the t-axis. Similarly the second derivative with respect to time would be discretised as:

$$\frac{\partial^2 u}{\partial t^2} \approx \frac{u^{t+1}_{x,y} - 2u^{t}_{x,y} + u^{t-1}_{x,y}}{(\Delta t)^2} \tag{1.35}$$

Using this principle, an equation of more practical use, namely Fick's second law in one spatial dimension (1.09), may be converted into discrete form. With a function of two variables, however, there is a choice of expression, known respectively as *implicit* and *explicit* representations. In explicit form, the law is written as:

$$\frac{u^{t+1}_{x,y} - u^{t}_{x,y}}{\Delta t} = \frac{D}{(\Delta x)^2}\left(u^{t}_{x+1,y} - 2u^{t}_{x,y} + u^{t}_{x-1,y}\right) \tag{1.36}$$

and can be solved directly for $u^{t+1}_{x,y}$, the only unknown. The implicit equivalent is:

$$\frac{u^{t+1}_{x,y} - u^{t}_{x,y}}{\Delta t} = \frac{D}{(\Delta x)^2}\left(u^{t+1}_{x+1,y} - 2u^{t+1}_{x,y} + u^{t+1}_{x-1,y}\right) \tag{1.37}$$

In this case, there are three unknowns and clearly the equation cannot be solved in isolation. On the basis on this brief discussion it would therefore seem that the explicit method is wholly superior. In practice, however, it is given to computational instability and an implicit technique is often the best choice. The commercially available software DIGISIM® employs a *fast implicit finite difference* (FIFD) approach, adapted by Rudolph to simulate electrochemical problems in one spatial dimensional.[35,36]

In the case of the disk, where diffusion must be considered in two dimensions, a discretisation technique that has proved effective is the *alternating direction implicit* (ADI) method.[37,38] This treatment involves giving each grid point a mixture of implicit and explicit calculation. Fick's second law in two dimensions for the grid in Figure 1.8 is written as:

$$\frac{\partial u}{\partial t} = D\left(\frac{\partial^2 u}{\partial x^2} + \frac{\partial^2 u}{\partial y^2}\right) \tag{1.38}$$

To implement the ADI method, the time step is divided in half. At time t+½ the x-coordinate is treated implicitly, the y-coordinate explicitly and the equations solved:

$$\frac{1}{2}\frac{u_{x,y}^{t+1/2} - u_{x,y}^{t}}{\Delta t} = D\left(\frac{u_{x+1,y}^{t+1/2} - 2u_{x,y}^{t+1/2} + u_{x-1,y}^{t+1/2}}{\Delta x^2} + \frac{u_{x,y+1}^{t} - 2u_{x,y}^{t} + u_{x,y-1}^{t}}{\Delta y^2}\right) \tag{1.39}$$

Then, at the t+1 time step the y-coordinate is treated implicitly, with the previously calculated concentrations used for the explicit treatment of the x-coordinate:

$$\frac{1}{2}\frac{u_{x,y}^{t+1} - u_{x,y}^{t+1/2}}{\Delta t} = D\left(\frac{u_{x+1,y}^{t+1/2} - 2u_{x,y}^{t+1/2} + u_{x-1,y}^{t+1/2}}{\Delta x^2} + \frac{u_{x,y+1}^{t+1} - 2u_{x,y}^{t+1} + u_{x,y-1}^{t+1}}{\Delta y^2}\right) \tag{1.40}$$

Thus over the full time step both coordinates have been treated implicitly, while the number of unknowns at any given time step remains at three. This algebra has been

developed for a uniform rectangular spatial grid, however, it will be recalled from earlier discussions that the rate of diffusion varies locally across a disk surface and it is therefore preferable to include more grid points close to the disk edge. This can be achieved by an algebraic transformation of the coordinate system, a process known as *conformal mapping*.

In the above, the variation in concentration has only been considered in terms of diffusion. For the modelling of more complex electrochemical systems, it becomes necessary to incorporate homogeneous kinetic terms into the equations and this is relatively straightforward. For example, in the case of the following reaction scheme:

$$\mathrm{A} - e^{-} \rightleftharpoons \mathrm{B} \xrightarrow{k} \mathrm{C} \tag{1.41}$$

the transport equation for species B (in one-dimension) is modified as:

$$\frac{u_{x,y}^{t+1} - u_{x,y}^{t}}{\Delta t} = \frac{D_{\mathrm{B}}}{(\Delta x)^2}\left(u_{x+1,y}^{t} - 2u_{x,y}^{t} + u_{x-1,y}^{t}\right) - ku_{x,y}^{t} \tag{1.42}$$

where k is the homogeneous rate constant for the conversion of B to C. The effects of heterogeneous kinetics enter the simulation as boundary conditions, which provide external values of the concentration at various grid points independently from the differential equations thus facilitating the solution of the latter. These solution methods generally involve matrix formulation and iterative procedures and it is not proposed to detail them here.

1.6.2 Data Fitting Methods

When the necessary analytical equations are available such that the functional relationship between the controlled and measured variables is known to within the value of one or more system constants, the usual strategy for ascertaining these values is to determine the function's line of best-fit through the experimental points. This is

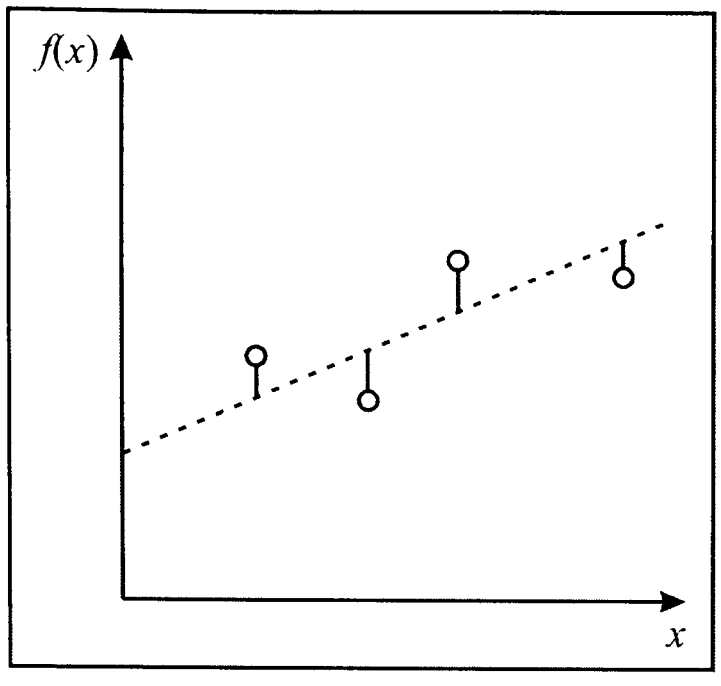


Figure 1.9
A plot indicating the vertical offsets of the points x_i,y_i from the line of best fit.

most simply achieved when the best fitting line is straight, and so wherever possible it is common practice to initially transform the data to conform to a linear relationship. The mathematical procedure for finding a line of best fit is known as *least squares linear regression* and was derived independently by Gauss and Legendre. It involves minimising the sum of the squares of the offsets of the points from the best-fit line (see Figure 1.9). The squares of the offsets are used to determine the absolute deviation, as the points may fall either above or below the line. If the line of best fit is defined as:

$$f(x) = mx + c \tag{1.43}$$

then the quantity to be minimised is given by the following sum:

$$\varepsilon = \sum_i \left[y_i - f(mx_i + c) \right]^2 \tag{1.44}$$

The minimum value of ε is found by setting to zero its derivatives with respect to m and c:

$$\begin{aligned} \frac{\partial \varepsilon}{\partial m} &= 2m\sum_i x_i^2 + 2c\sum_i x_i - 2\sum_i x_i y_i = 0 \\ \frac{\partial \varepsilon}{\partial c} &= 2Nc + 2m\sum_i x_i - 2\sum_i y_i = 0 \end{aligned} \tag{1.45}$$

where N represents the total number of data points. Solving these equations simultaneously then give the values of m and c:

$$m = \frac{ss_{xy}}{ss_{xx}} \qquad c = \bar{y} - m\bar{x} \tag{1.46}$$

where a bar above a quantity indicates its mean value and the ss_{jk} notation is defined below:

$$ss_{jk} = \sum_i (j_i - \bar{j})(k_i - \bar{k}) \tag{1.47}$$

The overall quality of the fit can be gauged in terms of the *correlation coefficient*, R^2:

$$R^2 = \frac{ss_{xy}^2}{ss_{xx} ss_{yy}} \tag{1.48}$$

The higher the value of R^2, the lower the amount of scatter in the data and the better the fit, up to a limit of $R^2 = 1$ for a perfect match.

When the function of interest cannot be expressed in a linearised form, fitting to a curve is possible, but more mathematically complex. Iterative numerical methods are required and best implemented with the assistance of a computer. Generic curve-fitting tools are provided within several commercially available analytical software packages. For this purpose, they generally employ the Levenberg-Marquardt algorithm, which provides an effective means of minimizing a sum of squares of several nonlinear functions that depend on a common set of parameters.[39,40]

This concludes a survey of the various principles that underpin the subject and methods described in this thesis, considered thus far from a general electrochemical viewpoint. The next chapter proceeds to focus the discussion on the field of room temperature ionic liquid electrochemistry.

1.7 References

[1] J. Albery, *Electrode Kinetics*, Clarendon Press, Oxford, **1975**.

[2] A.J. Bard, L.R. Faulkner, *Electrochemical Methods: Fundamentals and Applications: 2nd Edition*, John Wiley & Sons, New York, **2001**.

[3] C.M.A. Brett, A.M. Oliveira Brett, *Electrochemistry: Principles, Methods and Applications*, Oxford University Press, New York, **1993**.

[4] J.C. Eklund, A.M. Bond, J.A. Alden, R.G. Compton, *Advances in Physical Organic Chemistry* **1999**, *32*, 1.

[5] A.C. Fisher, *Electrode Dynamics*, Oxford University Press, New York, **1996**.

[6] P.H. Rieger, *Electrochemistry: 2nd Edition*, Chapman & Hall, New York, **1994**.

[7] O. Stern, *Z. Elektrochem.* **1924**, *30*, 508.

[8] H.L.F. von Helmholtz, *Ann. Physik.* **1853**, *89*, 211.

[9] G. Gouy, *Compt. Rend.* **1910**, *149*, 654.

[10] D.L. Chapman, *Phil. Mag.* **1913**, *25*, 475.

[11] M. Faraday, *Experimental Researches in Electricity*, Bernard Quaritch, London, **1839**.

[12] A.C. Testa, W.H. Reinmuth, *Anal. Chem.* **1961**, *33*, 1320.

[13] C.M.A. Brett, A.M.C.F. Oliveira Brett, *Compr. Chem. Kinet.* **1986**, *26*, 355.

[14] A. Fick, *Poggendorff's Annel. Physik* **1855**, *94*, 59.

[15] A. Fick, *Phil. Mag.* **1855**, *10*, 30.

[16] H.J.V. Tyrrell, K.R. Harris, *Diffusion in Liquids: A Theoretical and Experimental Study*, Butterworths & Co. Ltd., **1984**.

[17] P. Walden, *Z. Phys. Chem.* **1906**, *55*, 207.

[18] C.R. Wilke, P. Chang, *Am. Inst. Chem. Eng. J.* **1955**, *1*, 264.

[19] J.A.V. Butler, *Trans. Faraday Soc.* **1924**, *19*, 729.

[20] J.A.V. Butler, *Trans. Faraday Soc.* **1924**, *19*, 734.

[21] T. Erdey-Gruz, M. Volmer, *Z. Phys. Chem.* **1930**, *150A*, 203.

[22] W. Nernst, *Z. Phys. Chem.* **1888**, *2*, 613.

[23] J.A. Alden, F. Hutchinson, R.G. Compton, *J. Phys. Chem. B* **1997**, *101*, 949.

[24] K. Aoki, J. Osteryoung, *J. Electroanal. Chem.* **1981**, *122*, 19.

[25] K. Aoki, J. Osteryoung, *J. Electroanal. Chem.* **1984**, *160*, 335.

[26] D. Shoup, A. Szabo, *J. Electroanal. Chem.* **1982**, *140*, 237.

[27] F.G. Cottrell, *Z. Physik. Chem.* **1902**, *42*, 385.

[28] J. Tomes, *Collect. Czech. Chem. Commun.* **1937**, *9*, 12.

[29] J. Tomes, *Collect. Czech. Chem. Commun.* **1937**, *9*, 150.

[30] J. Tomes, *Collect. Czech. Chem. Commun.* **1937**, *9*, 81.

[31] M.V. Mirkin, A.J. Bard, *Anal. Chem.* **1992**, *64*, 2293.

[32] A. Sevcik, *Collect. Czech. Chem. Commun.* **1948**, *13*, 349.

[33] J.E.B. Randles, *Transactions of the Faraday Society* **1948**, *44*, 327.

[34] R.S. Nicholson, *Anal. Chem.* **1965**, *37*, 1351.

[35] M. Rudolph, *J. Electroanal. Chem.* **1992**, *338*, 85.

[36] M. Rudolph, D.P. Reddy, S.W. Feldberg, *Anal. Chem.* **1994**, *66*, 589A.

[37] J. Douglas, *J. Soc. Indust. Appl. Math.* **1955**, *3*, 42.

[38] D.W. Peaceman, H.H. Rachford, *J. Soc. Indust. Appl. Math.* **1955**, *3*, 28.

[39] K. Levenberg, *Quart. Appl. Math.* **1944**, *2*, 164.

[40] D.W. Marquardt, *J. Soc. Indust. Appl. Math.* **1963**, *11*, 431.

2 Room Temperature Ionic Liquids in Electrochemistry

Some twenty-five years after they first came to prominence as alternative electrochemical solvents, room temperature ionic liquids are currently being employed across an increasingly wide range of areas within chemistry. After providing a general introduction, this chapter reviews the current state of ionic liquid-based electrochemistry, with particular focus on the work of the last decade. Being composed entirely of ions and possessing wide electrochemical windows (frequently in excess of 5 Volts), it is not difficult to understand why these compounds are seen by electrochemists as attractive potential solvents. Accordingly, an examination of the pertinent properties of ionic liquids is presented, followed by an assessment of their application across the various electrochemical disciplines and some concluding remarks reflecting upon current problems and future directions. Sections of this chapter were published as part of a review article in *ChemPhysChem*,[1] but the text has been updated where appropriate to include any significant new developments.

2.1 Introduction

While there is no universally agreed upon definition, to the uninitiated, a room temperature ionic liquid (RTIL) may be conveniently described as a compound composed entirely of ions that exists in its liquid state at temperatures around 298 K and below. Although some compounds that would now be recognised as RTILs were known of much earlier (such as simple alkylammonium nitrates, for example, that were characterised early last century[2]), the field of modern ionic liquid chemistry really took off in the late nineteen seventies, when they were envisaged as lower-temperature alternatives for the molten alkali halide salts used as electrolytes in

thermal batteries.[3,4] Throughout the 1980's, ionic liquid-based research was primarily of an electrochemical nature as these materials were employed as alternative solvents in which to explore the redox properties of a whole host of different inorganic, organometallic and organic compounds.[5-7] With the advent of more air and moisture stable RTILs, however, the use of ionic liquids has expanded into many other fields including organic and inorganic synthesis, catalysis, polymerisation and industrial applications, to the extent that in the present day they are regarded by some as one of the most promising greener alternatives to the volatile organic solvents currently in widespread use. There is a healthy chemical literature on the application of RTILs across these various disciplines already in existence,[8-14] including the recent publication of two books devoted to the subject.[15,16] This account focuses on recent developments in the use of ionic liquids for the purpose for which they were originally conceived – as electrochemical solvents.

The first generation of room temperature ionic liquids was created by mixing aluminium halides (most usually the chloride) with the corresponding halide salt of an organic cation, commonly of the alkylpyridinium or 1,3-dialkylimidazolium types. These compounds have the advantage that they preclude the solvation, solvolysis and dissociative side reactions that often corrupt metal halide complexes and related compounds in simple molecular solvents. Accordingly, they have been utilized as solvents in many studies of solution electrochemistry, electrodeposition, electropolymerisation, and as electrolytes in electrochemical devices such as semiconductors and batteries. A novel aspect of these solvents is their tuneable Lewis acidity, which can be affected simply by varying the molar ratio of the two components. This class of RTIL have already been extensively reviewed and so will

not be dealt with in any further detail here. The interested reader is directed to the following publications.[5-7,17,18]

The principal drawback of haloaluminate RTILs is their sensitivity to atmospheric moisture, which reacts with the aluminium halide species to produce aluminium oxide halide complexes and protonic impurities. This inevitably increases the amount of effort and expense required to produce and maintain high quality melts, which must be handled under essentially anhydrous conditions. This situation was clearly not ideal, and in the early 1990's, the search began for alternative, water-stable anions to replace the haloaluminate. The most significant compounds to result from this investigation incorporated the tetrafluororoborate and hexafluorophosphate anions.[19,20] Unlike their haloaluminate analogues, this new breed of RTIL could be both prepared and safely stored outside of an inert atmosphere, the presence of water being much less detrimental (a single report concerning the decomposition of hexafluorophosphate to phosphate in a biphasic 1-butyl-3-methylimidazolium hexafluorophosphate | acidic aqueous system not withstanding[21]). While these compounds were generally unreactive with water, however, they were still prone to absorb considerable amounts of moisture resulting in significant changes to their physical and chemical properties; many of the beneficial traits possessed by ionic liquids over more conventional solvents were severely curtailed under these conditions. Thus, while exposure to water causes no permanent damage, venting within an inert atmosphere is still generally required prior to the commencement of any experiment. To combat this, ionic liquids based on more hydrophobic anions have been developed within the last few years, notably those containing bis(trifluoromethylsulfonyl)imide,[22,23] the 1,3-dialkylimidazolium salts of which

have a saturated water content of less than 2%. In addition, new, more electrochemically robust ionic liquids based on different cations have been synthesised such as those based on quaternary –onium cations in which the central atom is nitrogen, phosphorus or sulfur.[24-26] These advances have inevitably led to a broader spectrum of applications involving these liquids. Figure 2.1 shows the trend in electrochemical research papers involving the use of ionic liquids compiled using SciFinder® Scholar.

In the next section, the properties of non-haloaluminate ionic liquids are assessed with particular emphasis on those most relevant to electrochemical studies, ending with a brief consideration of the practicalities of applying standard electrochemical methodologies within these solvents. Following this, some recently reported voltammetric investigations are highlighted, covering solution electrochemistry, electrodeposition, electrosynthesis and the application of non-haloaluminate RTILs in electrochemical devices.

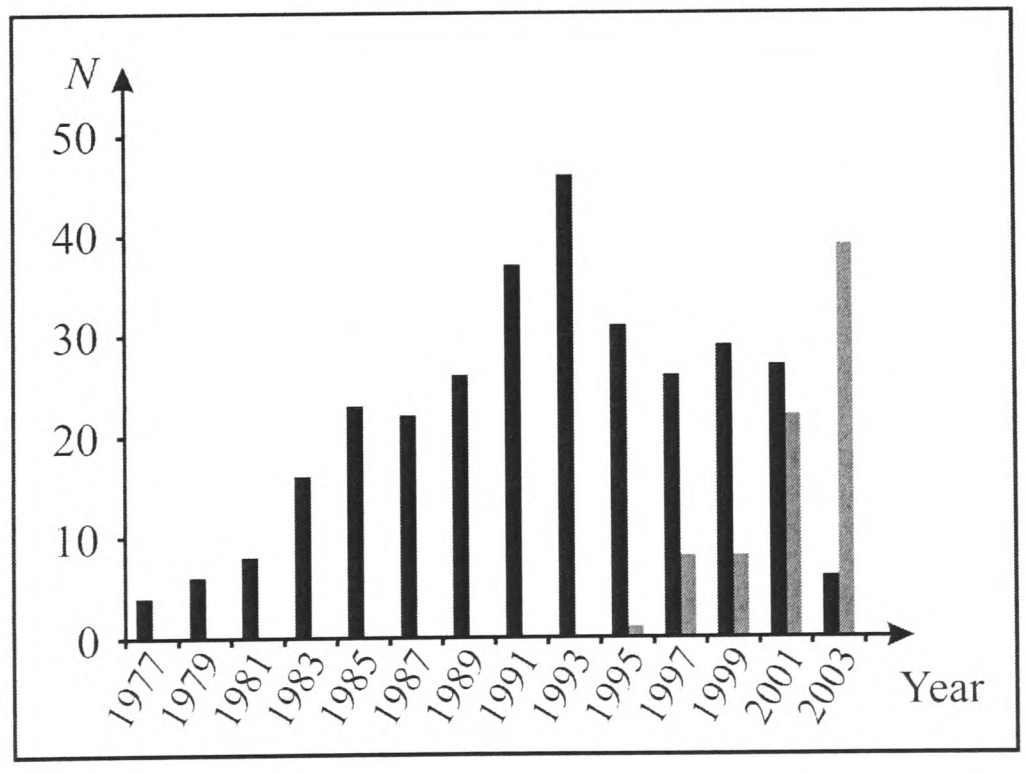


Figure 2.1
A bar chart showing the frequency in publication of electrochemical research papers involving haloaluminate (■) and non-haloaluminate (■) room temperature ionic liquids, compiled using SciFinder® Scholar 2002.

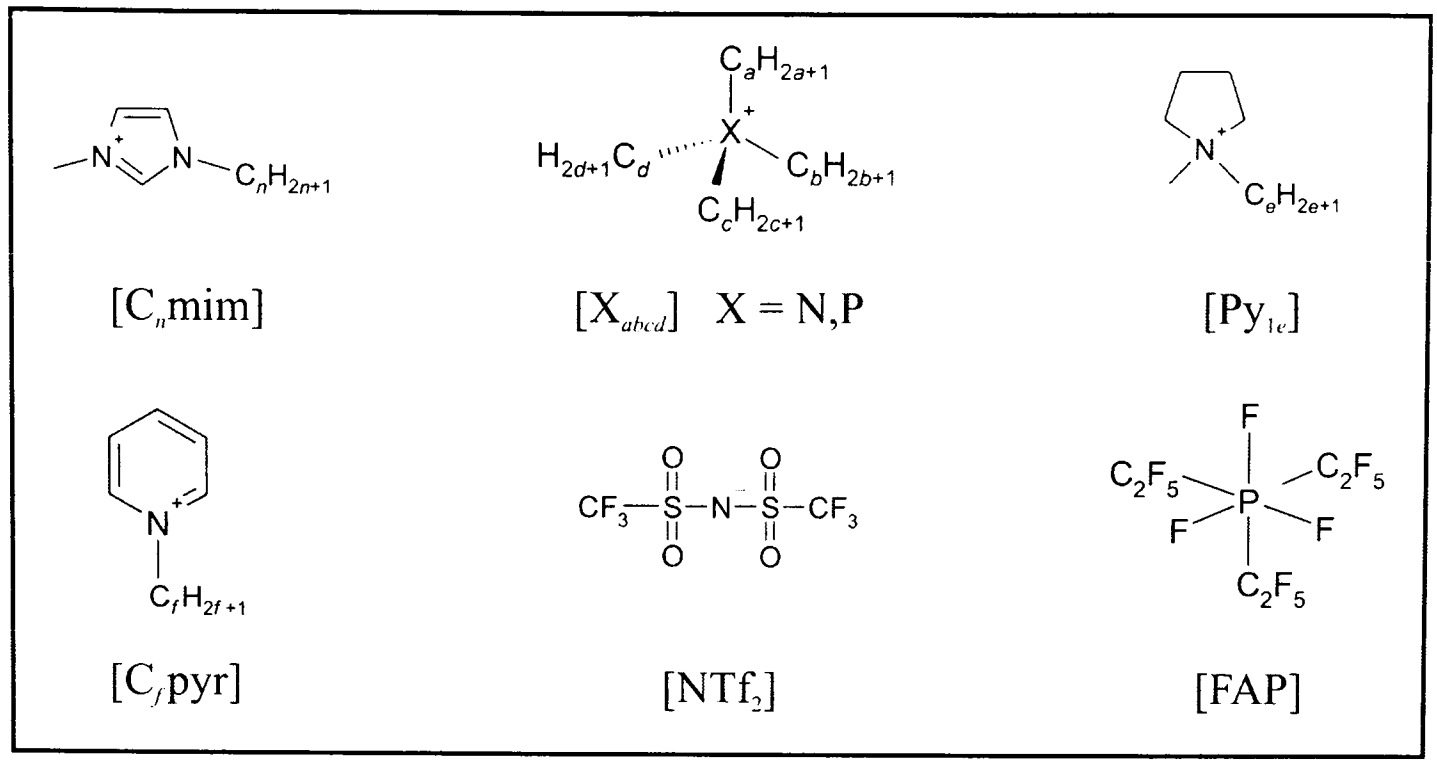


Figure 2.2
Molecular structures of several cations and anions commonly employed in the synthesis of room temperature ionic liquids and a guide to the nomenclature adopted to describe them.

2.2 Properties of Ionic Liquid Solvents

All non-haloaluminate ionic liquids share the general structural motif of a large, poorly coordinating inorganic anions combined with an unsymmetrical organic cation. So far, some of the most popular types of these compounds employed in electrochemical studies have incorporated the 1-alkyl-3-methylimidazolium, N-alkylpyridinium, N-methyl-N-alkylpyrrolidinium and tetraalkyl -onium cations. On the anionic side, the tetrafluoroborate, hexafluorophosphate, bis(trifluoromethyl-sulfonyl)imide (bistriflimide) and trifluorotris(pentafluoroethyl)phosphate have been most prevalent. Structures of the more complex ions and an explanation of the notation adopted to describe them are provided in Figure 2.2. However, this is by no means an exhaustive list of ionic liquids investigated for possible electrochemical applications, indeed numerous other compounds have been and continue to be studied in this regard (an assortment of additional cations and anions are catalogued in

Table 2.1). All these compounds possess the archetypal RTIL properties such as high thermal stability, non-volatility, high polarity, large viscosity, high intrinsic conductivity and wide electrochemical windows. Yet, altering the combination of cation and anion used, or even modifying the nature of one or more alkyl chains on a single class of cation allows for considerable variation within this general framework, providing the possibility for 'fine-tuning' the solvent properties to the particular task at hand. Although there is a tendency to regard any compound labelled as an ionic liquid to be inherently 'green' it should be recognised that, as with any other property, the relative toxicity of RTILs depends on their exact ionic composition. Full toxicological investigations have yet to be carried out, even for ionic liquids that are currently commercially available,[27] however, under certain circumstances, the generation of potential hazardous decomposition products (such as HF) has been reported.[21]

Table 2.1
A list of cations and anions that have been employed as components in non-haloaluminate room temperature ionic liquids and selected references exemplifying their study.

Cations	Reference	Anions	Reference
imidazolium	[28,29]	BF_4^-	[30-32]
1,3-dialkylimidazolium	[23,30]	PF_6^-	[30,33,34]
1,2,3-trialkylimidazolium	[22,23,33]	AsF_6^-	[30,33]
1,3,4-trialkylimidazolium	[23]	$N(SO_2CF_3)_2^-$	[23,33]
1-alkyl-3-methoxyalkylimidazolium	[23,35]	CTf_3^-	[22,33,36]
1-(2,2,2-trifluoroethyl)-3-methylimidazolium	[23]	$CH_3CO_2^-$	[23]
1-(ω-phenylalkyl)-3-methylimidazolium	[37]	$CF_3CO_2^-$	[23,38]
1-methyl-3-[2,6-(S)-dimethylocten-2-yl]imidazolium	[39,40]	$CH_3SO_3^-$	[41]
N-alkylpyridinium	[42,43]	$CF_3SO_3^-$	[23,36]
tetraalkylammonium	[24,44]	$CF_3CF_2CF_2CO_2^-$	[23]
methoxyalkyltrialkylammonium	[44,45]	$CF_3CF_2CF_2CF_2SO_3^-$	[23]
1,3-dialkylpyrrolidinium	[25,46]	SCN^-	[47]
tetraalkylphosphonium	[48]	$CH_3C_6H_4SO_3^-$	[41]
trialkylsulfonium	[26]	$N(CN)_2^-$	[49,50]
$Co(4,4'\text{-}(CH_3(OCH_2CH_2)_7OCO)_2\text{-}2,2'\text{-bipyridine})^{2+}$	[45]	$N(SO_2C_2F_5)_2^-$	[30]
$Fe(4,4'\text{-}(CH_3(OCH_2CH_2)_7OCO)_2\text{-}2,2'\text{-bipyridine})^{2+}$	[45]	$H(HF)_n^-$	[51,52]
$(N,N'\text{-}(CH_3(OCH_2CH_2)_3)_2\text{-}4,4'\text{-bipyridine})^{2+}$	[53]	DNA^-	[45]
$HOC_2H_4N(CH_3)_3^+$	[54]	$Co(CO)_4^-$	[55]

Later in this section, the effect of impurities on the behaviour of ionic liquids is noted and some subtleties of employing traditional electrochemical techniques remarked upon. First, however, the trends in the most electrochemically relevant properties of pure RTILs are summarised and contrasted with equivalent properties of more conventional solvent-electrolyte systems. For a more comprehensive discussion of the electrochemical properties of all types of room temperature ionic liquids, including extensive tables of physical data drawn from the literature, reference [15] should be consulted.

2.2.1 Viscosity

The viscosity of an ionic liquid is an important consideration in electrochemical studies due to its strong effect on the rate of mass transport within solution. In Table 2.2, the viscosities of several ionic liquids are listed alongside those of some more traditional molecular solvents. It is obvious that the former are between one and two orders of magnitude larger and as a direct consequence, diffusion of electroactive species in RTIL solvents is slowed by a similar factor. Identity of the anion has a large effect on the viscosity of an ionic liquid, in particular through their relative basicity and ability to participate in hydrogen bonding. For example, the perfluorinated BF_4^- and PF_6^- anions form much more viscous ionic liquids (containing strong H···F interactions)[34] than those formed by the weakly basic NTf_2^- anion, in which the negative charge is extensively delocalised over the two sulfoxide groups.[23] Altering the organic cation causes a more subtle change in viscosity, and this is attributed to the influence of van der Waals interactions; viscosity generally increases with increasing cationic size (for example, by increasing alkyl chain length).[23] The viscosities of non-haloaluminate ionic liquids are extremely

Table 2.2
A comparison of dynamic viscosity (η / mPa s) and specific conductivity (κ / mS cm^{-1}) for a representative selection of molecular solvents and non-haloaluminate room temperature ionic liquids. Unless otherwise stated, T = 298 K.

Solvent	Viscosity / mPa s	Conductivity / mS cm^{-1}	Reference
N,N-dimethylformamide	0.794	4.0[a]	[56,57]
Acetonitrile	0.345	7.6[a]	[56,57]
Ethanol	1.074	0.6[a]	[56,57]
Dimethylsulfoxide	1.987	2.7[a]	[56,57]
[C_2mim][NTf_2]	28	8.4	[30]
[C_4mim][NTf_2]	44[b]	3.9[c]	[23,37]
[C_6mim][NTf_2]	59[b]		[37]
[C_8mim][NTf_2]	74[b]		[37]
[C_2mim][BF_4]	43	13.0	[30]
[C_2mim][PF_6]		5.2	[30]
[C_4mim][PF_6]	275[b]	1.5	[34,37]
[N_{6222}][NTf_2]	167	0.67	[24]
[N_{6444}][NTf_2]	595	0.16	[24]
[Py_{13}][NTf_2]	63	1.4	[25]
[Py_{14}][NTf_2]	85	2.2	[25]

[a] Conductivity for organic solvent containing 0.1 M tetrabutylammonium perchlorate at 295 K
[b] Viscosity estimated from graphical data provided in the reference
[c] 293 K

temperature dependent, and a 20% change over 5 K is not uncommon around room temperature.[30] An Arrhenius-type relationship is approximately followed ($\eta = \eta_0 e^{Ea/RT}$ where E_a is the activation energy for viscous flow), although slight deviations from this behaviour at temperatures close to the freezing point have been reported, attributed to the onset of ion association and aggregation.[23,30]

Abbott has attempted to rationalise the high viscosity of RTILs by adapting a hole theory model used to account for the motion of ions in high temperature molten salts.[58] This theory assumes that ionic materials contain voids arising from thermally generated local density fluctuations: an ion may only move if there is an adjacent cavity of sufficient volume to accommodate it. Then, as the viscosity of molten salts is similar to that for simple molecular liquids, the decrease in average hole size with temperature combined with the larger size of the ions in RTILs results in considerably

more restricted ion mobility in the latter. Some empirical correlation was achieved with a relatively simple quantitative model based on this principle.

2.2.2 Conductivity

As with any solvent employed in an electrochemical process, the conductivity of an ionic liquid is of vital importance. Being composed entirely of ions, RTILs possess an abundance of charge carriers and so, based on this consideration alone, a large conductivity might initially be predicted. Overall, however, the conductivity of any solution depends on both the number of charge carriers and their mobility, and what ionic liquids make up for in the former category is counteracted by the extremely slow rate of mass transfer of their large constituent ions. Consequently, as Table 2.2 illustrates, RTILs have conductivities on a par with those of organic solvents with added inorganic electrolytes, but not significantly larger. While contributing little improvement over conventional nonaqueous solvents in terms of their absolute conductivity, however, ionic liquids do offer the advantage that this property is intrinsic to the pure liquid and does not require the addition of a separate salt. For example, this could be beneficial in the study of reactions in which a supporting electrolyte may interfere, or may simplify the extraction and purification of the product from an electrosynthetic process.

Among the various RTIL structures, conductivity seems to be most strongly linked to viscosity, likely due to the correlation between viscosity and ion mobility as noted in the previous section. For a given anion with a range of cations, conductivity generally decreases in the order 1-alkyl-3-methyimidazolium > N,N-dialkylpyrrolidinium > tetraalkylammonium and this has been identified with an decrease in planarity of the cationic core; the flatness of the imidazolium ring seems to confer a higher

conductivity than the tetrahedral arrangement of alkyl groups displayed by the ammonium salts, with the pyrrolidinium-based RTILs adopting an intermediate geometry and conductivity.[25] The variation of ionic liquid conductivity with temperature typically gives a distinctly curved Arrhenius plot at low temperatures, and the data may be fitted much more closely using the Vogel-Tammann-Fulcher (VTF) relationship,[30,46] an empirical equation developed for liquids that form glass phases: $\kappa = AT^{-½}\exp[-B(T-T_0)]$. Here, κ is conductivity, A and B are empirically determined constants, as is T_0, the ideal glass temperature (at which the conductivity drops to zero). At temperatures above $2T_0$, the more simple Arrhenius equation is sufficient to characterise the observed temperature dependence.

Finally, it should be noted that Hagiwara et al. have reported the synthesis of an ionic liquid significantly more conductive than all those considered above.[51] This salt, generated by reaction of 1-ethyl-3-methylimidazolium chloride with anhydrous hydrogen fluoride, is best described by the formula [C_2mimF·2.3HF] and is believed to be composed of oligomeric [$(HF)_nF$] anions. A conductivity of 100 mS cm^{-1} at 298 K was reported, along with a very low viscosity (4.85 mPa s) and modest electrochemical window (-0.6 V – +2.6 V vs Al wire in C_2mimCl·2$AlCl_3$ at a vitreous carbon electrode).

2.2.3 Electrochemical Window

Any solvent is only suitable for conducting a range of electrochemical experiments on species dissolved within it if these species are more easily oxidised or reduced than the solvent itself. In RTILs, it is generally found in practice that the constituent anions are oxidised at sufficiently large potentials, and at sufficiently low ones, the organic cations undergo reduction. The potentials at which these bulk processes are

initiated determine the accessible electrochemical window for each liquid. A detailed comparison of the various potential windows reported in the literature is not straightforward for a number of reasons. First, where the purity of a RTIL is uncertain, the presence of electroactive impurities can cause an apparent narrowing of the true potential window (see section 2.2.6); secondly, the potential of solvent breakdown may vary slightly on different electrode surfaces; finally, the data is reported against several different reference and quasireference systems, which are not easily interconverted. Most voltammetric investigations carried out in ionic liquid solvents have employed quasireference electrodes, often silver or platinum wires,[59-64] the data from which cannot be compared to a high degree of accuracy, let alone directly related to potentials determined in molecular solvents. Bond et al. have advocated the use of the metallocene derivatives as voltammetric reference standards for ionic liquids.[59] When tested in $[C_4mim][PF_6]$, a reversible, one-electron reduction process was observed for cobaltocene with a potential independent of electrode composition, concentration and scan rate. Ferrocene was found to be poorly soluble in this medium, but may function as a less expensive alternative for other ionic liquids.

Despite these difficulties in comparing the literature data, several general trends are apparent. There is little variation in the anodic potential limit for most of the currently popular RTILs since at most commonly used electrode materials, the oxidation potentials of ions such as BF_4^-, PF_6^- and NTf_2^- all lie in the same 0.5 V range. At the other extreme, however, the cathodic limit is more variable depending on the identity of the cation; 1-alkyl-3-methylimidazolium ions are around a Volt less stable to reduction than tetraalkylammonium or N,N-dialkylpyrrolidinium ions. The increased

vulnerability to reduction of these imidazolium cations has been attributed to initial attack on the acidic proton attached to the ring carbon between the two hetero-atoms, indeed additional alkylation of the ring at this site produces a RTIL with an enlarged cathodic window.[23] Overall then (and regardless of reference electrode), an electrochemical window of 4.5 – 6.0 V is typical for a pure non-haloaluminate RTIL[24,25,42,44,65] and this equals if not supersedes the corresponding windows observed for the commonly employed organic solvent/electrolyte combinations (acetonitrile/0.1 M tetrabutylammonium tetrafluoroborate, for example, has one of the largest electrochemical windows at 5.0 V[66]). This additional potential range may be exploited to study the direct oxidation or reduction of compounds whose solution phase electrochemistry has so far been inaccessible.

2.2.4 Double-Layer Capacitance

In addition to its inherent importance in the consideration of RTILs for electrochemical capacitor applications, measurement of the double-layer capacitance, C_d, and its variation with potential can be used to probe the structure of the interfacial region between an electrode and the RTIL solvent to which it is adjacent. Thus far however, there are only a handful of reports in existence that deal with such studies.[36,52,67] The data that is available suggests that ionic liquids possess double-layer capacitances comparable to those of nonaqueous solvent/electrolyte systems. For example, Nanjundiah et al. report C_d values of 10-15 μF cm^{-2} at potentials close to the potential of zero charge (PZC) for [C_2mim] salts of the anions $(CF_3SO_2)_3C^-$ CTf_3^-, NTf_2^-, $CF_3SO_3^-$ and BF_4^- at a dropping mercury electrode.[36] In the same experiments, the variation of C_d with potential was approximately parabolic and centred around the PZC, although at potentials far from the PZC the capacitance rose

much more rapidly. Despite the similarities in the C_d –E curve at potentials close to the PZC, the Stern diffuse double-layer model[68] usually applied in aqueous electrolyte systems is almost certainly inappropriate to describe ionic liquids. Instead, a multilayer model has been proposed in which the cations and anions adjacent to the electrode align to produce several layers of alternating positive and negative charge, with the excess charge on the RTIL being located several layers deep.[36,69] This model was able to account for the gross features of the C_d–E data described above.[36]

2.2.5 Solubility and Solvating Properties

Although not an electrochemical property per se, it remains of interest to consider the relative solvating ability of RTILs given that one may only interrogate the electrochemistry of any compound if it can be dissolved in sufficient quantity. A full, systematic study of the solvent properties of non-haloaluminate RTILs has yet to be reported. From the limited data available however, RTILs seem to behave most like dipolar, aprotic organic solvents and short chain alcohols in their interaction with organic solutes.[70-72] Clearly, solvating properties will vary depending on the exact nature of the RTIL constituent ions; anions possessed of high charge density and organic cations with short alkyl chains stabilise more polar molecules, while a more lipophilic RTIL may be generated by employing charge-diffuse anions and/or increasing alkyl substitution in the cation.

The haloaluminate predecessors of modern ionic liquids are particularly noted for their flexible solvating ability. In these binary mixtures, adding an excess of the organic salt would render the mixture Lewis basic owing to the presence of free halide ions, whereas addition of extra aluminium halide would create an overall Lewis acidic melt due to the presence of coordinately unsaturated aluminium cluster

species. The solvating properties at each extreme are considerably different, thus by tailoring the proportions accordingly, these ionic liquids are able to solubilize a wide range of inorganic and organometallic compounds. Non-haloaluminate ionic liquids on the other hand have a fixed acidity/basicity and are mostly virtually Lewis neutral due to the very weak acidic and basic donor properties of the ions that comprise them. Identifying this problem, Chen et al. explored the possibility of adding $[C_2mim][Cl]$ to the ionic liquid $[C_2mim][BF_4]$ to give a Lewis basic melt, which facilitated the dissolution and stabilisation of Cu(I) in this media.[73] Similarly, MacFarlane and coworkers have successfully synthesised RTILs containing the dicyanamide anion, $N(CN)_2^-$ in the hopes of creating improved solvent donor characteristics through the greater Lewis basicity of this anion.[49,50] In both these cases, the anodic potential windows of the resulting ionic liquids were considerably narrowed, an inevitable consequence of the fact that an anion with greater electron-donating abilities will naturally be more prone to oxidation. As regards Brønsted acidity/basicity, ionic liquid solvents are almost always aprotic. Watanabe et al. however, have described the synthesis of Brønsted acid-base ionic liquids derived from the combination of organic amines with bis(trifluoromethylsulfonyl)amine, $HNTf_2$, some of which were liquid at room temperature.[28] These materials were reported to conduct protons via a combination of Grotthuss and 'vehicle' type mechanisms, as evidenced by ^1H NMR chemical shift and self diffusion coefficient measurements, and have been envisaged for use as a new type of anhydrous proton conductor.[29]

2.2.6 Effect of Impurities

In the above sections it has been indicated that the properties of an ionic liquid can vary in no small measure according to its purity, indeed in the last section, the

deliberate addition of chloride was found to have a dramatic effect. Whether present intentionally or unintentionally, additives such as halide ions or molecular solvents can greatly influence the results of an electrochemical investigation. Thus, where their presence is undesirable, it is important to identify and eliminate these impurities as much as possible. Halide impurities are generally introduced during the two-step synthesis used to manufacture many RTILs. In this process, the cation is initially formed by alkylation of an imidazole or amine using an alkyl halide. A metathesis reaction with an alkali metal or silver salt of the desired anion then forms the ionic liquid together with the alkali metal or silver halide as a by-product. If this second reaction does not go to completion, unreacted halide ions from the first step remain and must be removed in additional synthetic steps. From an electrochemical point of view, halide impurities are likely to manifest themselves predominantly through their effect on the viscosity and electrochemical window. In the former case, a report by Seddon and coworkers observed that even relatively low concentrations of chloride caused a substantial increase in the viscosity of several imidazolium tetrafluoroborate and hexafluorophosphate RTILs.[74] As chloride and bromide ions are electroactive at potentials below those required to oxidise the heavily fluorinated constituent anions of RTILs, the effect of their presence on the solvent window is to narrow it at the anodic extreme or at the very least generate additional background signals which may interfere with the electrochemical process under investigation.

The most prevalent impurity affecting RTILs is undoubtedly water. Irrespective of their miscibility with H_2O, all ionic liquids are hygroscopic and if exposed to air will absorb atmospheric moisture to some extent. Furthermore, previous studies have demonstrated that even the presence of relatively low amounts of water can effect a

large change in the ionic liquid's properties.[39] As with halide impurities, a narrowing of the accessible potential window was observed, in this case at both the cathodic and anodic limit, likely due to the electrolysis of water. Whereas halide addition led to an increase in viscosity however, the presence of water was found to have the opposite effect, as evidenced by an increase in the rate of diffusion for the neutral molecule N,N,N',N'-tetramethyl-*para*-phenylenediamine.[39] While the diffusion coefficient for this molecule was found to double upon water saturation of a formally anhydrous ionic liquid solution, the effect on charged solutes was much more pronounced with the diffusion coefficients increasing by an order of magnitude. These findings led to speculation on the presence of an inhomogeneous 'nanostructure' in the wet ionic liquid whereby ionic species were able to undergo faster diffusion in more water concentrated regions while neutral species remained in relatively water-free, 'dry' locations. Seddon et al. studied the effect on viscosity of the addition of a range of molecular cosolvents, including water, and discovered that the reduction in viscosity followed essentially the same exponential relationship with mole fraction of added solvent, irrespective of which particular solvent was added.[74] For all the cosolvents under study, the data could be fitted to the single equation, $\eta = \eta_s \exp(-x_{cs}/a)$ where η_s is the viscosity of the pure ionic liquid at 293 K, x_{cs} is the mole fraction of the cosolvent and a is an empirical constant determined for each RTIL.

When undertaking any experiment involving ionic liquids, initial steps to purge the solvent of any water that may be present are almost always carried out. This is often achieved by heating the RTIL in vacuo for several hours and then conducting the remainder of the experiment under an inert atmosphere.[61-63,75-78] Other reported methods include performing the entire experiment under vacuum conditions[39,45,53] or

employing molecular sieves.[79] In many applications, the presence of water may not pose a significant problem and such measures may not be called for. However, the amount of water present should ideally always be measured (Karl Fischer titration is a commonly employed technique) and reported so as to facilitate the accurate comparison of various literature data.

2.2.7 Voltammetry in Ionic Liquids

Once an ionic liquid solution as been sufficiently prepared, there are no additional difficulties in applying any standard electrochemical technique, just as it would be used with more traditional molecular solvents. For example, their comparable conductivities mean that no extra countermeasures against uncompensated solution resistance should be necessary for RTILs than are applied to common organic solvent/electrolyte mixtures. However, the much slower rate of mass transport in ionic liquids has important consequences for the interpretation of experimental data and can significantly alter the experimental conditions under which a true limiting current is obtained from those that the unwary electrochemist may initially expect. In a recent publication that illustrates this point, Boxall and coworkers describe apparently anomalous results in which they obtained current maxima in rotating disk voltammograms for the oxidation of ferrocene in $[C_4mim][[PF_6]$.[61] On closer inspection however, they determined that this was exactly as predicted by theory when the much larger viscosity of the solvent was taken into account, and over 100 revolutions of the disk were necessary to approach the true Levich limiting current following application of the potential step.

Another area in which care must be taken is the use of ultramicroelectrodes (UMEs). In traditional organic solvents, a disk electrode with a diameter of 50 μm or less

would be considered a UME and expected to produce steady-state voltammetry at scan rates of a few hundred mV per second when employed to study simple solution phase electrochemical reactions. As explained in the previous chapter, however, the true definition of a UME requires its critical dimension to be smaller than the length of the diffusion layer developed adjacent to it over the experimental timescale. The size of the diffusion layer for any species is proportional to the square root of its diffusion coefficient and hence in RTIL solutions this region is much more contracted than in traditional aqueous or organic media. As a result, a given electrode may behave as a UME in these latter solvents and yet give rise to peak-shaped cyclic voltammetry in ionic liquids. Recalling equation (1.31), the condition for true steady-state voltammetry at a disk in a potential sweep experiment is that $v \ll RTD/nFr_d^2$. Taking 1 x 10^{-11} m^2 s^{-1} as a typical diffusion coefficient, this corresponds to a scan rate of ca. 10 mV s^{-1} for a 5 μm radius disk at 298 K. Clearly therefore, in terms of practically accessible scan rates, electrodes of this dimension lie in an intermediate range between true peak-shaped and steady-state behaviour, and any attempt to

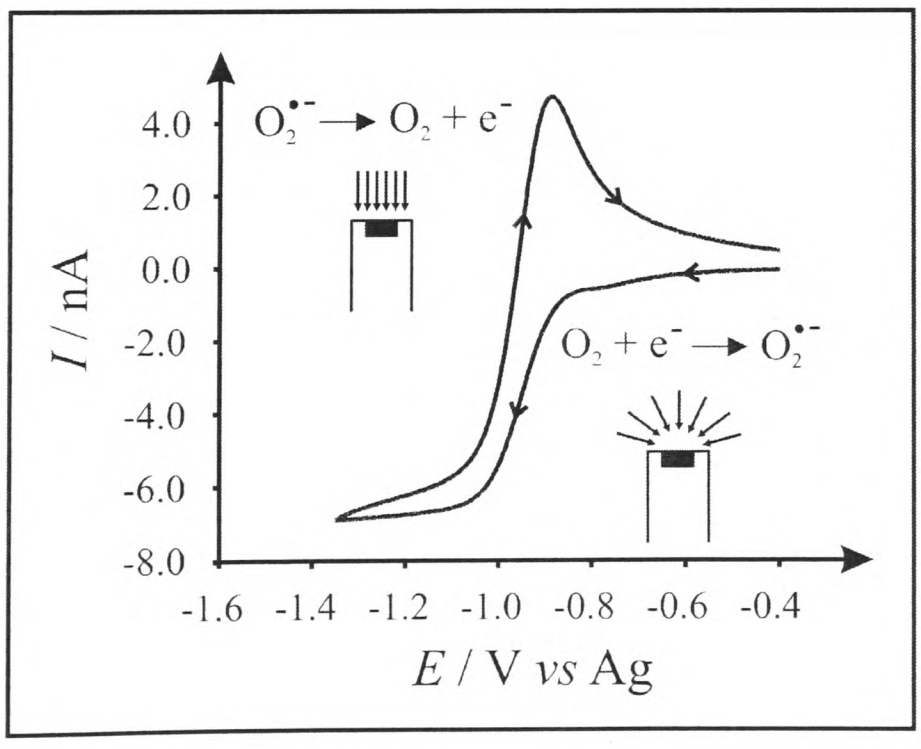


Figure 2.3
A cyclic voltammogram showing the reduction of oxygen in the room temperature ionic liquid $[N_{6222}][NTf_2]$ at a gold disk electrode, r_d = 5 μm, v = 0.5 V s^{-1}, T = 308 K. Inset is a schematic indicating the dominant mode of diffusion to the electrode surface responsible for dictating the shape of the forward and reverse waves respectively (see text).

extract 'limiting' current values from such voltammetry may result in an overestimate. A beautiful illustration of the effect of different diffusion domains on the voltammetry at a UME is provided in Figure 2.3 which depicts the reduction of dioxygen in the RTIL $[N_{6222}][NTf_2]$ at a 5 μm radius gold disk and its subsequent re-oxidation on the reverse scan (at a scan rate of 500 mV s^{-1}). In this medium, the diffusion coefficient of oxygen has been determined to be more than an order of magnitude larger than product of its reduction, superoxide.[60] Consequently, while the shape of the forward wave (reduction of oxygen to superoxide) is chiefly dictated by convergent diffusion to the electrode surface and shows steady-state behaviour, the re-oxidation wave of superoxide has a significant contribution from planar diffusion and thus is strongly peak shaped. Overall therefore, a single cyclic voltammogram is produced demonstrating both steady-state and transient behaviour.

2.3 Electrochemical Applications of Ionic Liquids

Having established a general picture of ionic liquids as electrochemical solvents, this section moves on to consider specific examples of their use from the scientific literature. While many studies have applied RTILs as novel media for organometallic catalysis and organic synthesis,[11,80-85] the number of electrochemical investigations is slim in comparison. Moreover, as Figure 2.1 illustrates, despite a clearly positive trend in the use of second-generation RTILs over the last decade, a large percentage of the reported electrochemical studies still involve haloaluminate derivatives. Nevertheless, the enhanced water-stability of non-haloaluminate RTILs has simplified the apparatus required for their study, bringing them closer to the open-bench and expanding the field of ionic liquid researchers. The fruits of this labour are reviewed below by considering in turn the various areas of fundamental voltammetric

Table 2.3
Reported diffusion coefficients (D / 10^{-12} m^2 s^{-1}) for a selection of molecular and ionic species dissolved in non-haloaluminate room temperature ionic liquids.

Diffusing Species	RTIL Solvent	Diffusion Coefficient / 10^{-12} m^2 s^{-1}		Reference
Ferrocene	$[C_2mim][BF_4]$	51	(295 K)	[77]
	$[C_2mim][BF_4]$	39	(298 K)	[86]
	$[C_4mim][PF_6]$	3.0	(293 K)	[87]
	$[C_2mim][NTf_2]$	6.3	(293 K)	[88]
TMPD [a]	$[C_4mim][PF_6]$	2.6	(295 K)	[39]
Tetrathiafulvalene	$[C_2mim][BF_4]$	42	(295 K)	[77]
Anthracene	$[C_2mim][NTf_2]$	53	(293 K)	[88]
Durene	$[C_2mim][NTf_2]$	27	(293 K)	[88]
MV^{2+} [b]	$[C_4mim][BF_4]$	1.5	(295 K)	[39]
$Ru(bpy)_3^{2+}$ [c]	$[N_{4441}][NTf_2]$	0.12		[63]
Li^+	$[C_4mim][PF_6]$	1.9		[62]
Na^+	$[C_4mim][PF_6]$	1.4		[62]
K^+	$[C_4mim][PF_6]$	4.5		[62]
Ag^+	$[C_2mim][BF_4]$	60	(298 K)	[78]
Br^-	$[C_4mim][NTf_2]$	14	(293 K)	[89]
I^-	$[C_2mim][NTf_2]$	27	(298 K)	[90]

[a] TMPD = *N*,*N*,*N*',*N*'-tetramethylphenylenediamine
[b] MV = methylviologen; 1,1'-dimethyl-4,4'-bipyridinium
[c] bpy = 2,2'-bipyridinyl

investigation, electroanalysis, electrodeposition, electrosynthesis, and finally the application of RTILs in electrochemical devices.

2.3.1 Fundamental Voltammetric Studies

Thus far, a significant amount of work has focused on reproducing the voltammetry of simple, well-behaved redox systems and comparing the results to those previously reported in more conventional solvents, such as acetonitrile and N,N-dimethylformamide. The techniques most widely employed have been chronoamperometry and cyclic voltammetry, each providing reproducible data in a range of ionic liquids. The extent of most studies has been to measure a diffusion coefficient and this has consistently yielded values ~100 times smaller that those obtained in traditional organic media.[39,62,63,77,78,86-90] Table 2.3 lists a range of such values drawn from the literature, as determined for a variety of molecular and ionic species. Fewer investigations have included an assessment of the rate of

heterogeneous electron transfer, but, where reported, values of k_0 were found to be around one order of magnitude lower than for the equivalent process in a conventional nonaqueous solvents.[78,88] This has been rationalised by analogy with Marcus theory in terms of a greater amount of solvent reorganisation.[88]

Most seldom studied electrochemically in ionic liquids so far are homogeneous chemical processes occurring in the wake of an initial electron transfer. Active in this area has been Hapiot,[88,91,92] who initially investigated the oxidation of several aromatic compounds (anthracene, naphthalene, durene, 1,4-dithiafulvene and veratrole) in four different RTILs, generating their radical cations which were then prone to chemical reaction via first- and second-order kinetic processes.[88] In these examples, the presence of an ionic liquid solvent proved to have little effect on the reaction mechanisms or homogeneous kinetics, save for a systematic decrease in the bimolecular rate constants as compared with acetonitrile. In a subsequent study, however, concerning the kinetics of carbon-halogen bond dissociation within electrogenerated radical anions of 4-chlorobenzophenone and 9-chloroanthracene, ionic liquid solvents $[C_4mim][NTf_2]$, $[N_{4111}][NTf_2]$ and $[N_{4222}][NTf_2]$ were found to significantly alter the relative rate.[91] This proved to be dependant on the extent of charge delocalisation in the radical anion and correlated with the degree of specific solvation by the imidazolium and tetraalkylammonium RTIL cations. Bond and co-worker have also reported a first-order homogeneous rate constant that varied significantly amongst the ionic liquid solvents $[C_4mim][PF_6]$, $[C_2mim][NTf_2]$, $[Py_{14}][NTf_2]$ and $[P_{14.666}][FAP]$ (here for the isomerisation of an organometallic complex, following its initial oxidation), but could offer no explanation to rationalise this behaviour.[93]

In cases where species are poorly soluble in ionic liquids, or, although favoured thermodynamically, the kinetics of the dissolution process are thought to be sluggish, solid-phase voltammetry has become a popular alternative technique with some workers. For example, Bond has regularly employed electrodes on which the electroactive species of interest is mechanically ground into the working electrode surface, which is then immersed into the ionic liquid solvent.[64,87,93] In such a study concerning ferrocene in the RTIL $[C_4mim][PF_6]$ it was demonstrated that voltammetry obtained in this manner is equivalent to that observed for the fully dissolved compound, provided that dissolution of the electrogenerated species is rapid, and that there is sufficient mass of adhered solid.[87] The approach has also been used successfully to analyse the reduction of hemin, a biomimetic, heme-containing protein in the ionic liquids $[C_4mim][PF_6]$ and $[C_8mim][PF_6]$.[94]

2.3.2 Electroanalysis

The low volatility and thermal stability of RTILs render them potentially advantageous media for the development of sensors that are both robust and simple in design. Electrochemical efforts in this area have largely involved the detection of gaseous analytes,[60,75,76,95-104] but also the quantification of trace halide impurities in the ionic liquids themselves.[105,106] In the latter case, Compton and Hardacre have applied various electroanalytical techniques to detect chloride in $[C_4mim][BF_4]$, $[C_4mim][PF_6]$ and $[C_4mim][NTf_2]$ at a silver electrode.[105] Most successful amongst these was cathodic stripping voltammetry, able to determine chloride concentrations down to the parts per billion level, this being of particular benefit in the NTf_2^- RTIL where quantification via other means has proved problematic. Regarding the electrochemical detection of gases in ionic liquid media, both ammonia and sulfur

dioxide have been recently investigated,[102-104] but the most attention by far has been focussed on the one-electron reduction of oxygen to superoxide.

The first such study in a non-haloaluminate RTIL was performed by AlNashef et al., who conducted voltammetry a glassy carbon macroelecrode in $[C_4mim][PF_6]$ and 1-butyl-2,3-dimethylimidazolium hexafluorophosphate, $[C_4dim][PF_6]$. The electrogenerated superoxide ion was found to be stable in $[C_4mim][PF_6]$, whilst in the second ionic liquid it reacted with trace protonic impurities, the downfall of an earlier study in a chloroaluminate RTIL.[107] Subsequent reports have found the reduction to be chemically reversible a range of sufficiently pure ionic liquids, and the determined diffusion coefficients and solubility of oxygen are compared below in Table 2.4. The most popular choice of RTIL cationic component has been the imidazolium species, although Katayama has suggested that these ions are susceptible to nucleophilic attack by the superoxide radical anion.[100] When conducted at disks of micrometer dimension, the process can give rise to distinctive voltammetry as seen earlier in

Table 2.4
Diffusion coefficient (D / 10^{-10} m^2 s^{-1}) and solubility ($[O_2]$ / mM) data for oxygen in several non-haloaluminate room temperature ionic liquids.

RTIL Solvent	Diffusion Coefficient / 10^{-10} m^2 s^{-1}	Solubility / mmol dm^{-3}	Temperature / K	Method of Analysis	Reference
$[C_2mim][NTf_2]$	7.3	3.9	293	CA[b]	[60]
	2.5	10.8	293	CA	[96]
$[C_4dim][NTf_2]$[a]	2.1	7.2	293	CA	[96]
$[C_8mim][NTf_2]$	2.8	8.3	293	CA	[96]
$[C_{10}mim][NTf_2]$	2.5	13.0	293	CA	[96]
$[C_5mim][FAP]$	3.5	9.7	293	CA	[96]
$[C_4mim][PF_6]$	2.2	3.6	298	CV	[75]
$[C_2mim][BF_4]$	17	1.1	298	HCC[c]	[97]
$[C_3mim][BF_4]$	13	0.97	298	HCC	[97]
$[C_4mim][BF_4]$	12	1.1	298	HCC	[97]
$[N_{6222}][NTf_2]$	1.5	11.6	293	CA	[60]
$[Py_{14}][NTf_2]$	1.8	13.6	298	CA	[101]

[a] $[C_4dim]$ = 1-butyl-2,3-dimethylimidazolium
[b] CA = chronoamperometry
[c] HCC = hydrodynamic chronocoulometry

Figure 2.3, and arising from the vastly different diffusion coefficients of oxygen and superoxide (in this example $D(O_2)/D(O_2^{-\bullet}) = 33$).[60]

A key challenge in constructing an electrochemical oxygen sensor is to account for the susceptibility of superoxide to reaction with carbon dioxide, since both gases are commonly present in most practical applications. The complication stems from the fact that the ensuing reaction involves a second electron transfer and so, overall, the reduction of a single oxygen molecule requires between one and two electrons, depending on the rate of the homogeneous steps.

$$\begin{aligned} &O_2 + e^- \rightleftharpoons O_2^{-\bullet} \\ &2CO_2 + O_2 + 2e^- \rightarrow C_2O_6^{2-} \end{aligned} \qquad (2.01)$$

AlNashef and colleagues confirmed an increase in the reductive current and a loss of the back peak (corresponding to re-oxidation of superoxide) following the addition of carbon dioxide to a system of O_2 / $[C_4mim][PF_6]$.[76] This was further quantified by Buzzeo et al., who determined the following mechanism as being most likely:[95]

$$\begin{aligned} &O_2 + e^- \rightleftharpoons O_2^{-\bullet} \\ &O_2^{-\bullet} + CO_2 \rightarrow CO_4^{-\bullet} \\ &CO_4^{-\bullet} + CO_2 \rightarrow C_2O_6^{-\bullet} \\ &C_2O_6^{-\bullet} + e^- \rightleftharpoons C_2O_6^{2-} \text{ or } C_2O_6^{-\bullet} + O_2^{-\bullet} \rightarrow C_2O_6^{2-} + O_2 \end{aligned} \qquad (2.02)$$

In the final step, the peroxydicarbonate radical anion is reduced either directly at the electrode surface or homogeneously in solution by superoxide. In the latter case, this regenerates oxygen, the subsequent heterogeneous reduction of which gives rise to the second electron transfer observed voltammetrically. Overall second-order rate constants of $(1.4 \pm 0.4) \times 10^3$ M^{-1} s^{-1} and $(1.7 \pm 0.5) \times 10^3$ M^{-1} s^{-1} were reported in ionic liquids $[C_2mim][NTf_2]$ and $[N_{6222}][NTf_2]$ respectively.

The most developed RTIL-based amperometric oxygen sensor that has appeared in the literature thus far is probably that of Ohsaka, who has reported the construction of glassy carbon electrodes coated in porous polyethylene membranes and saturated with RTILs $[C_2mim][BF_4]$ or $[C_4mim][PF_6]$.[98,99] These sensors were found to function well in a dry oxygen atmosphere, displaying a wide detection range and a response time of 20 s to reach 90% of the maximum current change following a perturbation in $[O_2]$. Introducing water vapour, however, brought about a current increase attributed to disproportionation of the superoxide into oxygen and hydrogen peroxide in the presence of protons (and presumably also a decrease in the viscosity of the solvent matrix). This clearly limits practical application of the sensor, even in environments where carbon dioxide is absent.

2.3.3 Electrodeposition

Room temperature ionic liquids hold two main advantages over the aqueous solvents traditionally employed for electrodeposition. For one thing, their wide potential windows permit the deposition of metals that are simply inaccessible in the latter. In addition, however, higher quality deposits with more variable morphologies may be created due to the absence of the hydrogen evolution process that is often concomitant with the process in an aqueous medium. As such, this was the subject of numerous early studies in the haloaluminate ionic liquids.[13] Their water-instability and the required high-temperature conditions, however, complicate the process and compromise efficiency. In addition, haloaluminates can prevent the deposition of semiconductors due to the early deposition of aluminium. For these reasons, non-haloaluminate RTILs have recently been explored as a more practical choice for the electrodeposition of a variety of species.[73,108-118]

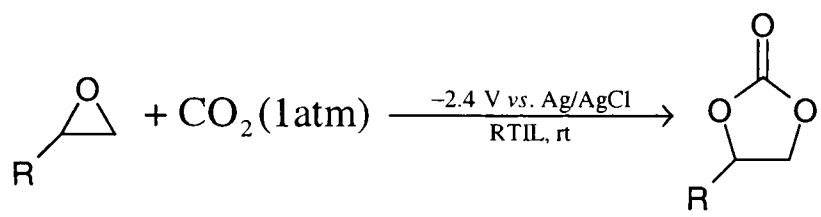
Chen has studied the electrodeposition of copper from a Cu(I) solution in $[C_2mim][BF_4]$ at glassy carbon, tungsten and platinum electrodes.[73] Addition of $[C_2mim][Cl]$ was necessary to facillitate dissolution of the Cu(I), through complexation with the free chloride ions. Dense copper deposits were obtained on tungsten wires, as evidenced by scanning electron microscopy (SEM) and recovered undamaged by washing with organic solvents. Subseqent work by this author has involved the deposition of cesium in $[N_{4441}][NTf_2]$.[108] At a tungsten electrode, the reduction of Cs(I) occurred too close to the cathodic potential limit to allow the recovery of Cs, however, substituting for a hanging mercury drop electrode reduced the reduction potential significantly through the formation of a Cs(Hg) amalgam. This may have application in the treatment of aqueous radioactive waste. In a further example of metal deposition, Freyland and co-workers have reported the reduction of $TiCl_4$ in the RTIL $[C_4mim][NTf_2]$.[109,110] Their preliminary study on highly oriented pyrolytic graphite (HOPG) revealed the growth of Ti nanowires at the HOPG step edges.[109] They later carried out the same deposition on Au(111) with in situ monitoring of the growth pattern by scanning tunnelling microscopy (STM).[110]

The group that has been most productive in the area of electrodeposition in non-haloaluminate RTILs, however, is that of Endres, who initially spent considerable effort investigating the deposit of germanium films on Au(111) from Ge(IV) halide salts in $[C_4mim][PF_6]$.[111-115] Several facets of the growth mechanism are reported along with STM, SEM and X-ray diffraction analyses of the morphology under various conditions. Other reports detail the deposition of nanoscale silicon at HOPG in $[Py_{14}][NTf_2]$,[116] and, most recently, the reduction of tantalum pentafluoride to elemental Ta at various metallic electrodes in the same RTIL.[117,118]

2.3.4 Electrosynthesis

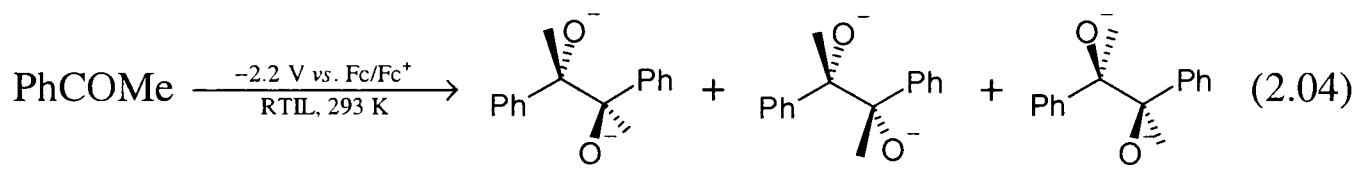
The ability of non-haloaluminate RTILs to dissolve a wide range of compounds while remaining air and water stable, with the added potential for recycling the solvent has encouraged their use in a great number of general synthetic investigations.[11,80-85] Furthermore, in electrosynthesis specifically, the intrinsic conductivity of these ionic liquids eliminates the need to add a supporting electrolyte, serving to both simplify the experimental set up and facilitate product separation. Unsurprisingly therefore, there have been several recent reports exploring their use for such a purpose.[42,43,79,92,119-124] Beginning by considering electrocatalysis, Gaillon and Bedioui have investigated the activation of molecular oxygen by the biomimetic Jacobsen's epoxidation catalyst in $[C_4mim][PF_6]$.[119] They were able to characterise voltammetrically the various stages of the catalytic cycle, including the key formation of a highly reactive Mn(V) intermediate, and anticipate extending the technique to the preparatory scale for the epoxidation of selected olefins. A preparative electrolysis of PhBr and $PhCh_2Br$ to the dimers biphenyl and 1,2-diphenylethane has already been reported by Jouikov in the RTIL $[C_4mim][NTf_2]$ using a Ni(II) complex as the electrocatalyst.[120] In the latter case the product was obtained in 75 % yield, with no evidence of side-reactions. Usefully, the catalyst remained in the ionic liquid as the product was extracted with cyclohexane and, after washing, was available for reuse with fresh substrate material. A Ni(I) catalyst was similarly employed by Sweeny and Peters to dehalogenate C_2H_5I and $C(Cl_2)FC(F_2)Cl$ (Freon® 113) in $[C_4mim][BF_4]$.[79] While these examples offer little comparison on performance compared with more traditional solvents, they do at least demonstrate the potential of RTILs as media for transition metal-based electrocatalysis.

In terms of syntheses involving direct carbon-carbon bond formation from electrogenerated intermediates, Yang and coworkers have reported the cycloaddition of carbon dioxide to epoxides in several imidazolium ionic liquids under mild conditions.[43]



(2.03)

Potentiostatting at –2.4 V *vs.* Ag/AgCl electrogenerates the CO_2 radical anion which then reacts with the epoxide. The best yields were obtained in $[C_4mim][BF_4]$ in as yet unoptimised conditions. Direct formation of new C-C bonds was also achieved by Barhdadi et al. who performed an electroreductive homocoupling of alkyl- and benzylhalides in $[C_8mim][BF_4]$.[121] Product separation and solvent recycling was again facilitated by the hydrophobicity of this ionic liquid, whereby the reaction products were easily separated by conventional extraction techniques and the RTIL washed with aqueous $NaBF_4$, dried and reused. Most recently, Hapiot has studied the electrochemical pinacol coupling of acetophenone in three ionic liquid solvents:[92]



(2.04)

Besides the reported operational simplicity and ease of product separation, use of RTILs was found to strongly affect both the kinetics and stereoselectivity of the reaction, depending upon the strength of the interactions between the RTIL cation and the electrogenerated acetophenone radical anions.

Several electropolymerisations have also been conducted in ionic liquid solvents, with promising overall results.[42,122,123] Synthesis of the electroactive polymer, poly(3-(4-fluorophenyl)thiophene (PFPT), for example, was achieved via the oxidation of 2-(4-fluorophenyl)thiophene at a Pt electrode in two imidazolium-based

RTILs.[122] Its voltammetric behaviour resembled that previously reported in nonaqueous solvents, albeit with slower ion insertion kinetics and a more rapid loss of electroactivity upon continual cycling. Similarly, pyrrole has been polymerised in the RTILs $[C_2mim][BF_4]$, $[C_2mim][PF_6]$ and $[C_2mim][CF_3SO_3]$.[123] The choice of anion proved important, with the rate of polymerisation significantly increased in the ionic liquid containing $CF_3SO_3^-$. As the most viscous RTIL in use, this was rationalised along the lines of electrogenerated radicals accumulating in the vicinity of the electrode surface under the slow diffusion conditions. This optimal solvent was later employed in a related study involving thiophene and aniline monomers.[124] Finally, mechanically strong and highly conductive electrolyte films with potential windows in excess of 3 V have been polymerised from various vinyl species in $[C_2mim][BF_4]$ and $[C_4pyr][BF_4]$.[42] These conducting polymer electrolytes provide one, thus far popular, route for the incorporation of RTILs into a variety of electrochemical devices, and it is to these that attention now turns.

2.3.5 Applications in Electrochemical Devices

Many electrochemical appliances are based on an aqueous, gel or polymer electrolytes, the properties of which (e.g. their conductivity and stability) can dictate the level of performance and overall lifetime. The application of RTILs as electroactive components in a number of devices such as fuel cells, capacitors and solar cells has recently been explored.[32,52,125-129] A prominent example by Lu et al. describes the use of $[C_4mim][BF_4]$ and $[C_4mim][PF_6]$ as electrolyte systems for π-conjugated polymers in electrochemical mechanical actuators, electrochromic devices and numeric displays.[125] Long periods of stable device performance were achieved with negligible loss of electroactivity; for example, a polyaniline

electrochromic window showed no appreciable current decrease over one million cycles in [C_4mim][BF_4]. Ito and co-workers have explored the use of RTIL [C_2mimF·2.3HF] in both solar cell and capacitor applications.[52,126] In their dye-sensitised solar cell, despite employing this low viscous ionic liquid, the efficiency was still less than that obtained using LiI / MeCN.[126] In the capacitative arrangement, the performance was strongly dependent on the applied voltage and characterised overall as being intermediate between currently employed aqueous and nonaqueous systems.[52] In any case, it seems unlikely that ionic liquids based on HF will appeal commercially. Most recently, Dupont has considered the use of [C_4mim][BF_4] and [C_4mim][PF_6] as electrolytes in a fuel cell.[127] The [C_4mim][BF_4]-based system gave an excellent response, exhibiting 67% efficiency for an alkaline fuel cell operating at room temperature, whereas the [C_4mim][PF_6] ionic liquid only reached a maximum efficiency of 28%. Both cells, however, were highly sensitive to water contamination, the presence of which decreased efficiency (to 42% and 16% respectively at 10% (v/v) of water).

2.4 Summary

A decade after they were first prepared, this chapter has considered the use of non-haloaluminate ionic liquids as alternative solvents in which to carry out electrochemical processes. The wide electrochemical windows and high intrinsic conductivities displayed by these compounds commend their use for such a purpose and to date they have been successfully applied to study a number of simple redox couples, the voltammetry of which is characterised by extremely slow rates of diffusion, a direct consequence of the high viscosities also typical of ionic liquids. In terms of the interfacial kinetics and any follow up chemistry, the number of

investigations to characterise this is still low, however, a survey of the literature data that is available reveals that overall RTILs display rather similar behaviour to conventional aprotic organic solvent/electrolyte mixtures. A decrease in the rate of electron transfer kinetics has been consistently observed, but mechanistically, any subsequent chemical reactions have followed the same route as previously established, albeit with a decrease in bimolecular reaction rates. A comprehensive model of the electrical double layer and the corresponding potential distribution set up at the electrode/ionic liquid interface is still awaited, however, and in its absence even something as fundamental as the applicability of the simple Butler-Volmer model cannot be immediately assured. Additionally, much more physical data (solubilities, etc.) will be required before ionic liquids can come to be regarded as mainstream electrochemical solvents, although collecting it will clearly be no small undertaking, owing to the sheer number of different cation/anion combinations that exist.

In addition to simple voltammetric investigations, room temperature ionic liquids solvents have been used in various other electrochemical applications. Regarding their analytical utility, under controlled conditions, RTILs have proved to be viable solvents for the electrochemical detection of a number of molecules, particularly gaseous species. The slow equilibration times and sensitivity of the current response to moisture contamination are clear drawbacks however, the latter especially so in the case of any sensor intended for operation under atmospheric conditions. The corollary to this of course, is that an ionic liquid may make an ideal component for an alternative type of humidity sensor. In other electrochemical fields, water should not pose a significant problem so long as sufficient drying protocols are implemented,

just as would be carried out with more traditional organic solvents. RTILs, after all, are by no means unique in their tendency to absorb moisture. Rather, it is the large effect on their properties caused by even a small level of aqueous impurity that should always be taken into account.

In terms of use as solvents for electrosynthesis, the recyclability and facile product separation possible with ionic liquids certainly appeal, and the handful of studies so far performed have demonstrated promising results producing good to excellent product yields, comparable to those of conventional solvents. Whether or not the low diffusion rates will hamper scale-up of these procedures remains in question however, and additional activation techniques such as sonication or application of microwaves may be necessary for RTIL based electrosyntheses to approach commercialisation.[130,131] It is in the area of electrodeposition where non-haloaluminate ionic liquids seem to offer the greatest benefits and fewest drawbacks, however, combining an ability to dissolve a wide selection of metal compounds with a broad accessible potential range. Considering the improved quality of deposits, the ease of product refinement and the capability to deposit elements that are otherwise inaccessible, it is surely only a matter of time until these second generation RTILs overtake their haloaluminate predecessors in popularity for this purpose.

As Figure 2.1 confirms, in the ten years since their inception, the popularity of non-haloaluminate ionic liquids has risen steadily. With even more stable cation/anion combinations under constant development and existing RTILs becoming progressively more available and inexpensive, an increasing amount of research involving these compounds is anticipated over the next few years, whereupon the potential of ionic liquids in electrochemistry may be fully realised.

2.5 The Aims of the Work Reported in this Thesis

Most simply put, this work aims to contribute to the understanding of how RTILs may act as solvents in which to conduct electrochemistry. To achieve this, it is proposed to adopt a strategy of transposing to an ionic liquid environment several redox systems previously characterised in more traditional nonaqueous media. Then, by scrutinizing the various stages of these electrochemical processes, the extent to which established behaviours are reproduced may be determined as well as identifying any aspects where new considerations are necessary or where previously reliable assumptions must be reassessed. Application of the standard electrochemical techniques of cyclic voltammetry and chronoamperometry is intended, with the expectation of first validating the suitability of established analytical methods and, where necessary, extending the theory. Judicious choice of chemical system will then allow the three general stages of an electrochemical mechanism, namely mass transport, heterogeneous electron transfer and homogeneous chemical reaction to each be investigated. The proposed work is largely fundamental in nature, however, it is anticipated that research of this kind will be crucial in adapting a reaction to run at optimum efficiency in an ionic liquid solvent, as and when RTILs are identified as superior candidates for a given electrochemical process.

Before turning to consider the data, however, chapter three provides details on all commonly utilised experimental materials, equipment and methodologies involved in carrying out the work that is subsequently reported.

2.6 References

[1] M.C. Buzzeo, R.G. Evans, R.G. Compton, *ChemPhysChem* **2004**, *5*, 1106.

[2] P. Walden, *Bull. Acad. Imper. Sci. (St. Petersburg)* **1914**, 405.

[3] R.J. Gale, B. Gilbert, R.A. Osteryoung, *Inorg. Chem.* **1978**, *17*, 2728.

[4] J.C. Nardi, C.L. Hussey, L.A. King, US-Pat 4122245, **1978**.

[5] C.L. Hussey in *Advances in Molten Salt Chemistry* (Eds.: G. Mamantov, C. B. Mamantov), Elsevier, Amsterdam, **1983**, 185.

[6] C.L. Hussey, *Pure Appl. Chem.* **1988**, *60*, 1763.

[7] C.L. Hussey in *Chemistry of Nonaqueous Solutions - Current Progress* (Eds.: G. Mamantov, A. I. Popov), VCH, New York, **1994**, 227.

[8] J. Dupont, C.S. Consorti, J. Spencer, *J. Braz. Chem. Soc.* **2000**, *11*, 337.

[9] H. Olivier, *J. Mol. Catal. A - Chem.* **1999**, *146*, 285.

[10] K.R. Seddon, *Kinet. Catal.* **1996**, *37*, 693.

[11] T. Welton, *Chem. Rev.* **1999**, *99*, 2071.

[12] R.T. Carlin, J.S. Wilkes in *Chemistry of Nonaqueous Solutions - Current Progress* (Eds.: G. Mamantov, A. I. Popov), VCH, New York, **1994**, 277.

[13] F. Endres, *ChemPhysChem* **2002**, *3*, 144.

[14] M.J. Earle, K.R. Seddon, *Pure Appl. Chem.* **2000**, *72*, 1391.

[15] P. Wasserscheid, T. Welton, *Ionic Liquids in Synthesis*, Wiley-VCH, Weinheim, **2003**.

[16] R.D. Rogers, K.R. Seddon, *Ionic Liquids: Industrial Applications for Green Chemistry*, ACS Symp. Ser. #818, **2002**.

[17] Y. Ito, T. Nohira, *Electrochim. Acta* **2000**, *45*, 2611.

[18] S. Geetha, D.C. Trivedi, *Bull. Electrochem.* **2003**, *19*, 37.

[19] J.S. Wilkes, M.J. Zaworotko, *J. Chem. Soc., Chem. Commun.* **1992**, 965.

[20] J. Fuller, R.T. Carlin, H.C. De Long, D. Haworth, *J. Chem. Soc., Chem. Commun.* **1994**, 299.

[21] A.E. Visser, R.P. Swatloski, W.M. Reichert, S.T. Griffin, R.D. Rogers, *Ind. Eng. Chem. Res.* **2000**, *39*, 3596.

[22] V.R. Koch, C. Nanjundiah, G.B. Appetecchi, B. Scrosati, *J. Electrochem. Soc.* **1995**, *142*, L116.

[23] P. Bonhôte, A.-P. Dias, M. Armand, N. Papageorgiou, K. Kalyanasundaram, M. Grätzel, *Inorg. Chem.* **1996**, *35*, 1168.

[24] J. Sun, M. Forsyth, D.R. MacFarlane, *J. Phys. Chem. B* **1998**, *102*, 8858.

[25] D.R. MacFarlane, P. Meakin, J. Sun, N. Amini, M. Forsyth, *J. Phys. Chem. B* **1999**, *103*, 4164.

[26] H. Matsumoto, T. Matsuda, Y. Miyazaki, *Chem. Lett.* **2000**, 1430.

[27] R.P. Swatloski, J.D. Holbrey, R.D. Rogers, *Green Chem.* **2003**, *5*, 361.

[28] A. Noda, M.A.B.H. Susan, K. Kudo, S. Mitsushima, K. Hayamizu, M. Watanabe, *J. Phys. Chem. B* **2003**, *107*, 4024.

[29] M.A.B.H. Susan, A. Noda, S. Mitsushima, M. Watanabe, *Chem. Commun.* **2003**, 938.

[30] A.B. McEwen, E.L. Ngo, K. LeCompte, J.L. Goldman, *J. Electrochem. Soc.* **1999**, *146*, 1687.

[31] S. Forsyth, J. Golding, D.R. MacFarlane, M. Forsyth, *Electrochim. Acta* **2001**, *46*, 1753.

[32] J. Fuller, A.C. Breda, R.T. Carlin, *J. Electrochem. Soc.* **1997**, *144*, L67.

[33] V.R. Koch, L.A. Dominey, C. Nanjundiah, M.J. Ondrechen, *J. Electrochem. Soc.* **1996**, *143*, 798.

[34] P.A.Z. Suarez, S. Einloft, J.E.L. Dullius, R.F. De Souza, J. Dupont, *J. Chim. Physique* **1998**, *95*, 1626.

[35] J. Pernak, A. Czepukowicz, R. Pozniak, *Ind. Eng. Chem. Res.* **2001**, *40*, 2379.

[36] C. Nanjundiah, S.F. McDevitt, V.R. Koch, *J. Electrochem. Soc.* **1997**, *144*, 3392.

[37] S.V. Dzyuba, R.A. Bartsch, *ChemPhysChem* **2002**, *3*, 161.

[38] P.A.Z. Suarez, C.S. Consorti, R.F. De Souza, J. Dupont, R.S. Goncalves, *J. Braz. Chem. Soc.* **2002**, *13*, 106.

[39] U. Schröder, J.D. Wadhawan, R.G. Compton, F. Marken, P.A.Z. Suarez, C.S. Consorti, R.F. de Souza, J. Dupont, *New J. Chem.* **2000**, *24*, 1009.

[40] J.D. Wadhawan, U. Schröder, A. Neudeck, S.J. Wilkins, R.G. Compton, F. Marken, C.S. Consorti, R.F. De Souza, J. Dupont, *J. Electroanal. Chem.* **2000**, *493*, 75.

[41] J. Golding, S. Forsyth, D.R. MacFarlane, M. Forsyth, G.B. Deacon, *Green Chem.* **2002**, *4*, 223.

[42] A. Noda, M. Watanabe, *Electrochim. Acta* **2000**, *45*, 1265.

[43] H. Yang, Y. Gu, Y. Deng, F. Shi, *Chem. Commun.* **2002**, 274.

[44] H. Matsumoto, M. Yanagida, K. Tanimoto, M. Nomura, Y. Kitagawa, Y. Miyazaki, *Chem. Lett.* **2000**, 922.

[45] A.M. Leone, S.C. Weatherly, M.E. Williams, H.H. Thorp, R.W. Murray, *J. Am. Chem. Soc.* **2001**, *123*, 218.

[46] D.R. McFarlane, J. Sun, J. Golding, P. Meakin, M. Forsyth, *Electrochim. Acta* **2000**, *45*, 1271.

[47] J.M. Pringle, J. Golding, C.M. Forsyth, G.B. Deacon, M. Forsyth, D.R. MacFarlane, *J. Mater. Chem.* **2002**, *12*, 3475.

[48] A.I. Bhatt, I. May, V.A. Volkovich, M.E. Hetherington, B. Lewin, R.C. Thied, N. Ertok, *J. Chem. Soc., Dalton Trans.* **2002**, 4532.

[49] D.R. MacFarlane, J. Golding, S. Forsyth, M. Forsyth, G.B. Deacon, *Chem. Commun.* **2001**, 1430.

[50] D.R. MacFarlane, S.A. Forsyth, J. Golding, G.B. Deacon, *Green Chem.* **2002**, *4*, 444.

[51] R. Hagiwara, T. Hirashige, T. Tsuda, Y. Ito, *J. Electrochem. Soc.* **2002**, *149*, D1.

[52] M. Ue, M. Takeda, A. Toriumi, A. Kominato, R. Hagiwara, Y. Ito, *J. Electrochem. Soc.* **2003**, *150*, A499.

[53] T. Hatazawa, R.H. Terrill, R.W. Murray, *Anal. Chem.* **1996**, *68*, 597.

[54] A.P. Abbott, G. Capper, D.L. Davies, H.L. Munro, R.K. Rasheed, V. Tambyrajah, *Chem. Commun.* **2001**, 2010.

[55] R.J.C. Brown, P.J. Dyson, D.J. Ellis, T. Welton, *Chem. Commun.* **2001**, 1862.

[56] D.R. Lide, *Handbook of Chemistry and Physics: 81st Edition*, CRC Press, **2000**.

[57] K.M. Kadish, J.Q. Ding, T. Malinski, *Anal. Chem.* **1984**, *56*, 1741.

[58] A.P. Abbott, *ChemPhysChem* **2004**, *5*, 1242.

[59] V.M. Hultgren, A.W.A. Mariotti, A.M. Bond, A.G. Wedd, *Anal. Chem.* **2002**, *74*, 3151.

[60] M.C. Buzzeo, O.V. Klymenko, J.D. Wadhawan, C. Hardacre, K.R. Seddon, R.G. Compton, *J. Phys. Chem. A* **2003**, *107*, 8872.

[61] D.L. Boxall, J.J. O'Dea, R.A. Osteryoung, *J. Electrochem. Soc.* **2002**, *149*, E468.

[62] D.L. Boxall, R.A. Osteryoung, *J. Electrochem. Soc.* **2002**, *149*, E185.

[63] B.M. Quinn, Z. Ding, R. Moulton, A.J. Bard, *Langmuir* **2002**, *18*, 1734.

[64] J. Zhang, A.M. Bond, W.J. Belcher, K.J. Wallace, J.W. Steed, *J. Phys. Chem. B* **2003**, *107*, 5777.

[65] P.A.Z. Suarez, V.M. Selbach, J.E.L. Dullius, S. Einloft, C.M.S. Piatnicki, D.S. Azambuja, R.F. de Souza, J. Dupont, *Electrochim. Acta* **1997**, *42*, 2533.

[66] A.J. Bard, L.R. Faulkner, *Electrochemical Methods: Fundamentals and Applications: 2nd Edition*, John Wiley & Sons, New York, **2001**.

[67] A.B. McEwen, S.F. McDevitt, V.R. Koch, *J. Electrochem. Soc.* **1997**, *144*, L84.

[68] O. Stern, *Z. Elektrochem.* **1924**, *30*, 508.

[69] A.D. Graves, D. Inman, *J. Electroanal. Chem.* **1970**, *25*, 357.

[70] D.W. Armstrong, L. He, Y.-S. Liu, *Anal. Chem.* **1999**, *71*, 3873.

[71] J.G. Huddleston, R.D. Rogers, *Chem. Commun.* **1998**, 1765.

[72] J.G. Huddleston, A.E. Visser, W.M. Reichert, H.D. Willauer, G.A. Broker, R.D. Rogers, *Green Chem.* **2001**, *3*, 156.

[73] P.-Y. Chen, I.W. Sun, *Electrochim. Acta* **1999**, *45*, 441.

[74] K.R. Seddon, A. Stark, M.-J. Torres, *Pure Appl. Chem.* **2000**, *72*, 2275.

[75] I.M. AlNashef, M.L. Leonard, M.C. Kittle, M.A. Matthews, J.W. Weidner, *Electrochem. Solid-State Lett.* **2001**, *4*, D16.

[76] I.M. AlNashef, M.L. Leonard, M.A. Matthews, J.W. Weidner, *Ind. Eng. Chem. Res.* **2002**, *41*, 4475.

[77] J. Fuller, R.T. Carlin, R.A. Osteryoung, *J. Electrochem. Soc.* **1997**, *144*, 3881.

[78] Y. Katayama, S. Dan, T. Miura, T. Kishi, *J. Electrochem. Soc.* **2001**, *148*, C102.

[79] B.K. Sweeny, D.G. Peters, *Electrochem. Commun.* **2001**, *3*, 712.

[80] J. Dupont, R.F. De Souza, P.A.Z. Suarez, *Chem. Rev.* **2002**, *102*, 3667.

[81] R. Sheldon, *Chem. Commun.* **2001**, 2399.

[82] P. Wasserscheid, W. Keim, *Angew. Chem. Int. Ed.* **2000**, *39*, 3772.

[83] L. Olivier-Bourbigou, L. Magna, *J. Mol. Catal. A.* **2002**, *182-183*, 419.

[84] D. Zhao, W. M., Y. Kou, E. Min, *Catal. Today* **2002**, *74*, 157.

[85] C.M. Gordon, *Appl. Catal. A.* **2001**, *222*, 101.

[86] M. Kosmulski, R.A. Osteryoung, M. Ciszkowska, *J. Electrochem. Soc.* **2000**, *147*, 1454.

[87] J. Zhang, A.M. Bond, *Anal. Chem.* **2003**, *75*, 2694.

[88] C. Lagrost, D. Carrié, M. Vaultier, P. Hapiot, *J. Phys. Chem. A* **2003**, *107*, 745.

[89] G.D. Allen, M.C. Buzzeo, C. Villagran, C. Hardacre, R.G. Compton, *J. Electroanal. Chem.* **2005**, *575*, 311.

[90] R. Kawano, M. Watanabe, *Chem. Commun.* **2003**, 330.

[91] C. Lagrost, S. Gmouh, M. Vaultier, P. Hapiot, *J. Phys. Chem. A* **2004**, *108*, 6175.

[92] C. Lagrost, P. Hapiot, M. Vaultier, *Green Chem.* **2005**, *7*, 468.

[93] J. Zhang, A.M. Bond, *J. Phys. Chem. B* **2004**, *108*, 7363.

[94] D.L. Compton, J.A. Laszlo, *J. Electroanal. Chem.* **2002**, *520*, 71.

[95] M.C. Buzzeo, O.V. Klymenko, J.D. Wadhawan, C. Hardacre, K.R. Seddon, R.G. Compton, *J. Phys. Chem. B* **2004**, *108*, 3947.

[96] M.C. Buzzeo, C. Hardacre, R.G. Compton, *Anal. Chem.* **2004**, *76*, 4583.

[97] D. Zhang, T. Okajima, F. Matsumoto, T. Ohsaka, *J. Electrochem. Soc.* **2004**, *151*, D31.

[98] R. Wang, O.S. Hoyano, T. Okajima, F. Kitamura, T. Ohsaka, *Chemical Sensors* **2004**, *20*, 151.

[99] R. Wang, S. Hoyano, T. Ohsaka, *Chem. Lett.* **2004**, *33*, 6.

[100] Y. Katayama, H. Onodera, M. Yamagata, T. Miura, *J. Electrochem. Soc.* **2004**, *151*, A59.

[101] Y. Katayama, K. Sekiguchi, M. Yamagata, T. Miura, *J. Electrochem. Soc.* **2005**, *152*, E247.

[102] M.C. Buzzeo, D. Giovanelli, N.S. Lawrence, C. Hardacre, K.R. Seddon, R.G. Compton, *Electroanalysis* **2004**, *16*, 888.

[103] D. Giovanelli, M.C. Buzzeo, N.S. Lawrence, C. Hardacre, K.R. Seddon, R.G. Compton, *Talanta* **2004**, *62*, 904.

[104] Q. Cai, Y. Xian, H. Li, Y. Zhang, J. Tang, L. Jin, *Huadong Shifan Daxue Xuebao, Ziran Kexueban* **2001**, *3*, 57.

[105] C. Villagran, C.E. Banks, C. Hardacre, R.G. Compton, *Anal. Chem.* **2004**, *76*, 1998.

[106] L. Xiao, K.E. Johnson, *J. Electrochem. Soc.* **2003**, *150*, E307.

[107] M.T. Carter, C.L. Hussey, S.K.D. Strubinger, R.A. Osteryoung, *Inorg. Chem.* **1991**, *30*, 1149.

[108] P.-Y. Chen, C.L. Hussey, *Electrochim. Acta* **2004**, *49*, 5125.

[109] I. Mukhopadhyay, W. Freyland, *Langmuir* **2003**, *19*, 1951.

[110] I. Mukhopadhyay, C.L. Aravinda, D. Borissov, W. Freyland, *Electrochim. Acta* **2005**, *50*, 1275.

[111] F. Endres, C. Schrodt, *Phys. Chem. Chem. Phys.* **2000**, *2*, 5517.

[112] F. Endres, *Phys. Chem. Chem. Phys.* **2001**, *3*, 3165.

[113] F. Endres, *Electrochem. Solid-State Lett.* **2002**, *5*, C38.

[114] F. Endres, Z. el Abedin Sherif, *Chem. Commun.* **2002**, 892.

[115] F. Endres, S. Zein El Abedin, *Phys. Chem. Chem. Phys.* **2002**, *4*, 1649.

[116] S. Zein El Abedin, N. Borissenko, F. Endres, *Electrochem. Commun.* **2004**, *6*, 510.

[117] S. Zein El Abedin, H.K. Farag, E.M. Moustafa, U. Welz-Biermann, F. Endres, *Phys. Chem. Chem. Phys.* **2005**, *7*, 2333.

[118] S. Zein El Abedin, U. Welz-Biermann, F. Endres, *Electrochem. Commun.* **2005**, *7*, 941.

[119] L. Gaillon, F. Bedioui, *Chem. Commun.* **2001**, 1458.

[120] M. Mellah, S. Gmouh, M. Vaultier, V. Jouikov, *Electrochem. Commun.* **2003**, *5*, 591.

[121] R. Barhdadi, C. Courtinard, J.Y. Nedelec, M. Troupel, *Chem. Commun.* **2003**, 1434.

[122] E. Naudin, H.A. Ho, S. Branchaud, L. Breau, D. Bélanger, *J. Phys. Chem. B* **2002**, *106*, 10585.

[123] K. Sekiguchi, M. Atobe, T. Fuchigami, *Electrochem. Commun.* **2002**, *4*, 881.

[124] K. Sekiguchi, M. Atobe, T. Fuchigami, *J. Electroanal. Chem.* **2003**, *557*, 1.

[125] W. Lu, A.G. Fadeev, B. Qi, E. Smela, B.R. Mattes, J. Ding, G.M. Spinks, J. Mazurkiewicz, D. Zhou, G.G. Wallace, D.R. MacFarlane, S.A. Forsyth, M. Forsyth, *Science* **2002**, *297*, 983.

[126] H. Matsumoto, T. Matsuda, T. Tsuda, R. Hagiwara, Y. Ito, Y. Miyazaki, *Chem. Lett.* **2001**, 26.

[127] R.F. de Souza, J.C. Padilha, R.S. Goncalves, J. Dupont, *Electrochem. Commun.* **2003**, *5*, 728.

[128] H. Randriamahazaka, C. Plesse, D. Teyssie, C. Chevrot, *Electrochem. Commun.* **2003**, *5*, 613.

[129] K. Xu, M.S. Ding, T.R. Jow, *J. Electrochem. Soc.* **2001**, *148*, A267.

[130] C. Villagran, C.E. Banks, W.R. Pitner, C. Hardacre, R.G. Compton, *Ultrasonics Sonochemistry* **2005**, *12*, 423.

[131] U. Kumar Sur, F. Marken, B.A. Coles, R.G. Compton, J. Dupont, *Chem. Commun.* **2004**, 2816.

3 General Experimental Methods

This chapter presents general experimental details for the various investigations reported in this thesis, including all protocols and methodologies that are used as standard throughout the work. Descriptions of any apparatus or experimental procedures that are specific to an individual study are better located, and will be given in the relevant results chapter.

3.1 Chemical Reagents

All chemicals acquired commercially, as listed in Table 3.1, were used as received without any additional purification. As RTILs have only recently entered the mainstream chemical manufacturing industry (with Acros Organics and Merck KGaA both bringing out ranges within the last two years), research in the area has up to now

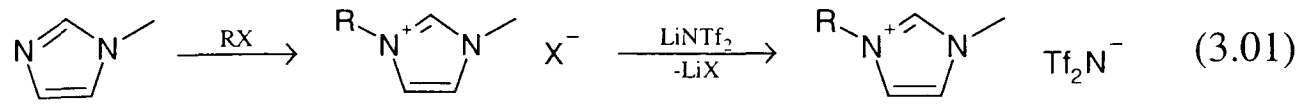
Table 3.1
All purchased chemicals used in performing the experiments reported within this thesis, along with their purity and commercial source.

Name	Formula / Abbreviation	Supplier	Quality
Ferrocene	Cp_2Fe	Aldrich	98%
N,N,N',N'-Tetramethyl-*p*-phenylenediamine	TMPD	Aldrich	98%
Catechol	$C_6H_6O_2$	Aldrich	>99%
p-Chloroaniline	PCA	Aldrich	98%
Potassium hexacyanoferrate(II) trihydrate	$K_4Fe(CN)_6.3H_2O$	Lancaster	99%
2,2,6,6-Tetramethylpiperidine-N-oxyl	TEMPO	Aldrich	98%
N,N-Dimethyl-*p*-toluidine	DMT	Aldrich	99%
Ethyl viologen diperchlorate	$EV(ClO_4)_2$	Aldrich	98%
Tetrabutylammonium perchlorate	TBAP	Fluka	puriss, >99%
Tetrabutylammonium hexafluorophosphate	$TBAPF_6$	Fluka	purum, >98%
Tetrabutylammonium tetraphenylborate	$TBABPh_4$	Aldrich	99%
Potassium chloride	KCl	Riedel-de Haën	analytical grade
Acetonitrile	MeCN	Fisher Scientific	>99.99%
Ethanol	EtOH	Hayman Ltd.	>99.85%
Oxygen	O_2	BOC	
Nitrogen	N_2	BOC	
Argon	Ar	BOC	

Table 3.2
The room temperature ionic liquids used in the investigations reported within and a reference to the literature procedure employed in their synthesis.

Chemical Name	Formula	Reference
1-Ethyl-3-methylimidazolium bis(trifluoromethylsulfonyl)imide	$[C_2mim][NTf_2]$	[2]
1-Butyl-3-methylimidazolium bis(trifluoromethylsulfonyl)imide	$[C_4mim][NTf_2]$	[2]
1-Octyl-3-methylimidazolium bis(trifluoromethylsulfonyl)imide	$[C_8mim][NTf_2]$	[2]
1-Decyl-3-methylimidazolium bis(trifluoromethylsulfonyl)imide	$[C_{10}mim][NTf_2]$	[2]
n-Hexyltriethylammonium bis(trifluoromethylsulfonyl)imide	$[N_{6222}][NTf_2]$	[2]
N-Butylpyridinium bis(trifluoromethylsulfonyl)imide	$[C_4pyr][NTf_2]$	[2]
Tris(*n*-hexyl)tetradecylphosphonium bis(trifluoromethylsulfonyl)imide	$[P_{14.666}][NTf_2]$	[2]
N-methyl-N-butylpyrrolidinium bis(trifluoromethylsulfonyl)imide	$[Py_{14}][NTf_2]$	[3]
Tris(*n*-hexyl)tetradecylphosphonium trifluorotris(pentafluoroethyl)phosphate	$[P_{14.666}][FAP]$	donated by Merck KGaA

required an initial in-house synthesis and purification of the ionic liquids themselves. In this regard, the work reported herein has benefited from a collaborative affiliation with the group of Professor Christopher Hardacre at the Queen's University Ionic Liquid Laboratories (QUILL, University of Belfast).[1] The nine different RTILs employed in the experiments reported in the chapters that follow are listed for convenience in Table 3.2. Of these, eight were prepared in Belfast according to published procedures and the ninth, $[P_{14.666}][FAP]$, kindly donated by Merck KGaA. From the table it is evident that the most popular synthetic route is that first reported by Bonhote et al.[2] In this two-step process, the cation is initially formed as an organic halide salt via alkylation of an amine, phosphine, pyridine etc. using a haloalkane. This is followed by a metathesis in aqueous $LiNTf_2$, as illustrated below for the case of an imidazolium RTIL:



(3.01)

The metathesis can lead to halide impurities remaining in the ionic liquid, which for these water insoluble bistriflimide RTILs can be minimised by repeated aqueous extraction. The level of chloride content was monitored using ion chromatography down to a reported detection limit of ~7 ppm (depending on the exact cation/anion combination).[4] After purification, the viscosity of each batch of ionic liquid was measured by means of a Brookfield cone and plate viscometer (LVDV-II), following a literature protocol.[5]

Ionic liquid solutions of volume 1 mL or greater were prepared using the standard gravimetric laboratory technique. Microlitre volume solutions were made more conveniently via a procedure involving a volatile co-solvent. This required the initial preparation of a stock solution of acetonitrile containing the intended analyte, an appropriate aliquot of which was then mixed with ~20 μL of RTIL, the specific quantities calculated each time to provide, in the absence of the acetonitrile, an ionic liquid solution of the desired concentration. The majority of acetonitrile was removed by allowing it to evaporate over time under ambient conditions, however, purging with dry argon or exposure to a vacuum prior to the collection of electrochemical data served to drive off any residual amount, in addition to trace atmospheric gases.

3.2 Electrodes and Potentiostat

Routine electrochemical experimentation in RTIL or conventional organic solvents was performed using micrometer dimension disk working electrodes composed of either gold ($2r_d$ = 5, 10, 12.5 μm), platinum ($2r_d$ = 10, 100 μm) or glassy carbon (GC, $2r_d$ = 11 μm). These were either purchased (10 μm Au, Pt and 11 μm GC, Cypress Systems, Kansas, U.S.A.) or constructed in-house by sealing a gold or platinum wire (Advent Research Materials Ltd., Oxfordshire) into soft capillary glass, the end of

which was polished to expose a disk-shaped cross-section of wire.[6] Immediately prior to use, the surface of each electrode was renewed by polishing, first using a 1.0 μm alumina-water slurry (Buehler, Illinois, U.S.A.) on a polishing pad (Kemet, Kent) followed by a 0.3 μm alumina-water slurry (Buehler) on a polishing cloth (Microcloth, Buehler). Periodic inspection of the electrodes using optical microscopy was performed to ensure that the disk had not recessed into the glass surface. The diameter was calibrated electrochemically via curve-fitting to chronoamperometric measurements made on a 2 mM ferrocene solution in acetonitrile containing 0.1 M TBAP, using a diffusion coefficient taken from the literature.[7,8] This method was considered to be more accurate than a single calculation based on a measured steady-state current.

A 0.5 mm diameter silver wire (Advent, 99.99%) was employed as a quasireference electrode and, where necessary, a 0.05 mm diameter nickel wire (Advent, 99.7%) coiled into a spiral functioned as the counter. The electrodes were housed within a Faraday cage to minimise interference from extraneous electromagnetic fields. A computer-controlled μ-Autolab (Eco-Chemie, Utrecht, Netherlands) was used to manipulate the potential at the working electrode and measure the current response.

3.3 Additional Apparatus

Experiments involving >1 mL of solution were performed using a standard cell arrangement; a five-armed, 50 mL vessel contained the electrolyte in which both disk, reference and counter were immersed. Measurements on μL-quantities of RTIL solution were instead conducted using a custom-built glass cell, illustrated in Figure 3.1, that was designed to maintain the sample within a controlled atmosphere. The working electrodes were modified with a section of disposable micropipette tip to

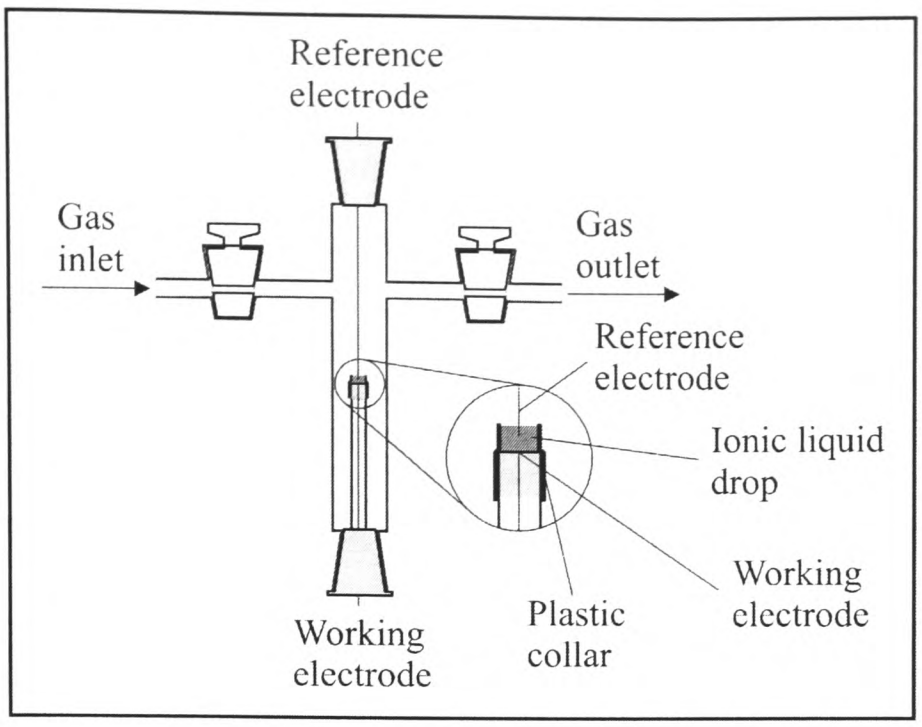


Figure 3.1
A cross-section of the glass cell used to conduct electrochemical experiments on μL samples of ionic liquids under conditions of controlled atmosphere.

create a small recess above each disk (and its insulation) into which a sample (~ 20 μL) of ionic liquid solution could be placed. This assembly was then slotted into the bottom of the cell, and a wire reference inserted from the opposite end completed a two-electrode electrochemical circuit. The two horizontal arms were equipped with taps, such that the cell could be both evacuated and/or filled with gas from an external source. Vacuum conditions were created using a Metrovac rotary pump GDR1 (0.05 Torr, Associated Electrical Industries Ltd, Manchester) connected directly to the cell.

Temperature regulation was achieved by placing each electrochemical cell within a thermostatted box (see Figure 3.2), which in these instances also served as the Faraday cage. The walls of the box consisted of aluminium sheets separated by insulating Supawool 607™ (RS Components Ltd., Northants.). Heat was supplied from a process heater mat (RS Components) located at the base of the cage and dispersed throughout it by a fan on the rear wall. The internal temperature was monitored by a platinum resistance thermometer (nominal resistance 100 Ω at room temperature) linked to a commercially available temperature controller (CAL 3200,

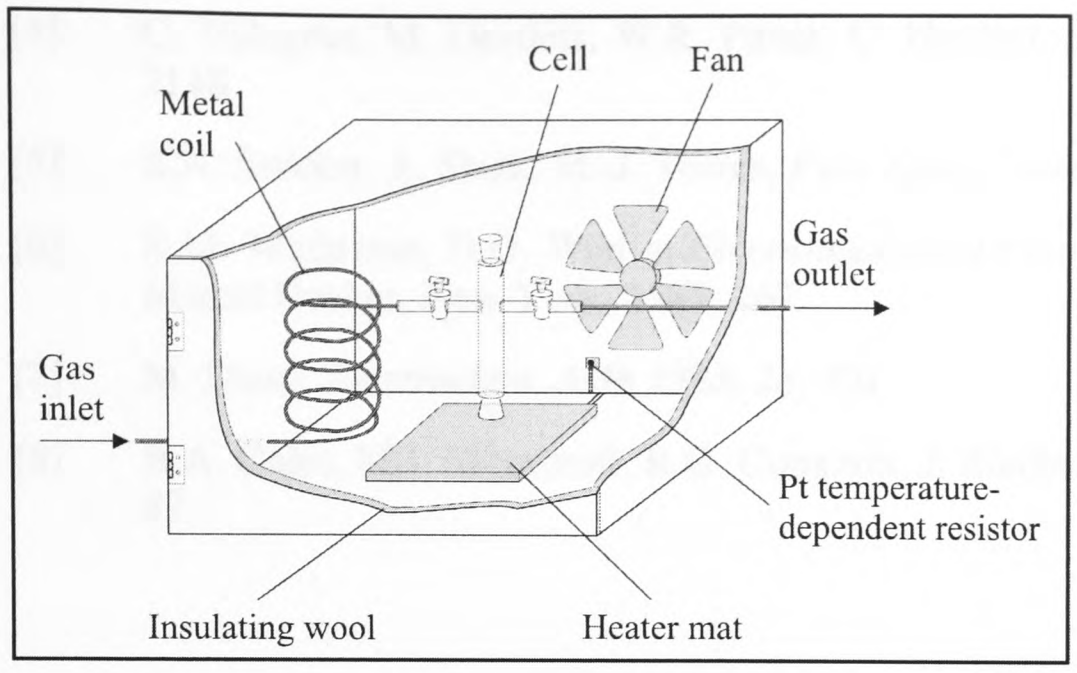


Figure 3.2
A schematic diagram of the temperature-regulated box.

CAL Controls Ltd., Herts.) situated outside the cage. When the volume of solution was sufficient (> 1 mL), the probe from a second digital thermometer was placed directly into the cell. This assembly provided a working temperature range for experiments from room temperature up to 348 K. Gas mixtures were introduced through a coiled metal pipe inside the box to allow the gas time to reach the appropriate temperature, prior to it entering the electrochemical cell. The gas then exited the box via an exhaust.

The next chapter begins the presentation of research original to this thesis by exploring in a range of nonhaloaluminate room temperature ionic liquids the voltammetric behaviour of two phenylenediamine species, a simple and well-characterised redox system in conventional organic media.

3.4 References

[1] http://quill.qub.ac.uk/

[2] P. Bonhôte, A.-P. Dias, M. Armand, N. Papageorgiou, K. Kalyanasundaram, M. Grätzel, *Inorg. Chem.* **1996**, *35*, 1168.

[3] D.R. MacFarlane, P. Meakin, J. Sun, N. Amini, M. Forsyth, *J. Phys. Chem. B* **1999**, *103*, 4164.

[4] C. Villagran, M. Deetlefs, W.R. Pitner, C. Hardacre, *Anal. Chem.* **2004**, *76*, 2118.

[5] K.R. Seddon, A. Stark, M.-J. Torres, *Pure Appl. Chem.* **2000**, *72*, 2275.

[6] R.M. Wightman, D.O. Wipf in *Electroanalytical Chemistry* (Ed.: A. J. Bard), Marcel Dekker, New York, **1989**, 267.

[7] M. Sharp, *Electrochim. Acta* **1983**, *28*, 301.

[8] B.A. Coles, M.J. Moorcroft, R.G. Compton, *J. Electroanal. Chem.* **2001**, *513*, 87.

4

Oxidation of N,N,N',N'-Tetraalkyl-*para*-phenylenediamines in a Series of Room Temperature Ionic Liquids Incorporating the Bis(trifluoromethylsulfonyl)imide Anion

The five room temperature ionic liquids: 1-alkyl-3-methylimidazolium bis(trifluoromethylsulfonyl)imide ($[C_n mim][NTf_2]$, n = 2,4,8,10) and n-hexyltriethylammonium bis(trifluoromethylsulfonyl)imide ($[N_{6222}][NTf_2]$) were investigated as solvents in which to study the electrochemical oxidation of N,N,N',N'-tetramethyl-*para*-phenylenediamine (TMPD) and N,N,N',N'-tetrabutyl-*para*-phenylenediamine (TBPD), using 20 μL samples under vacuum conditions. The effect of dissolved atmospheric gases on the accessible electrochemical window was probed and determined to be less significant than seen previously for ionic liquids containing alternative anions. Chronoamperometric transients recorded at a disk electrode were analysed via a process of nonlinear curve fitting to yield values for the diffusion coefficients of the electroactive species without requiring a knowledge of their initial concentration. Comparison of experimental and simulated cyclic voltammetry was then employed to corroborate these results and estimate diffusion coefficients for the electrogenerated species. The most significant consequence of changing the cationic component of the ionic liquid proved to be its effect on the solvent viscosity, η; the diffusion coefficient of each species was found to be approximately inversely proportional to η across the series of ionic liquids, in accordance with Walden's rule. This work has been published in the *Journal of Electroanalytical Chemistry*.[1]

4.1 Introduction

Since they were first prepared and characterised in the late nineties,[2,3] ionic liquids incorporating the bis(trifluoromethylsulfonyl)imide anion ($N(SO_2CF_3)_2^-$ ≡ NTf_2^-) have been employed as solvents in numerous chemical studies, in areas such as organic synthesis,[4,5] polymerisation,[6,7] enzyme catalysis,[8-10] and in devices such as sensors and supercapacitors.[11,12] Like all room temperature ionic liquids, these salts possess a number of desirable properties including high thermal stability, negligible vapour pressure, an ability to solubilise a wide range of organic and inorganic compounds and, of particular value to the electrochemist, a large intrinsic conductivity and wide electrochemical window. In any investigation involving ionic liquids, the potential ability of water to disrupt these properties is always a pertinent factor to consider, and this is one area where the NTf_2^- anion can offer an improvement over some alternative counter-ions. Properties such as miscibility with other liquids are considered to be almost exclusively determined by the anionic component of an ionic liquid,[13] and so RTILs based on the hydrophobic NTf_2^- anion are found to be water immiscible.[3] This has been rationalised in terms of the poor hydrogen-bonding ability of the NTf_2^- anion due to extensive delocalisation of the negative charge amongst the F_3CO_2S- groups.[3] Even then, some water-insoluble ionic liquids have been shown to absorb considerable quantities of water which can cause significant changes in their physical and chemical properties.[14] In the case of [NTf_2]-based RTILs, however, the saturated water content is typically found to be less than 2% and so its presence causes a smaller effect, a fact once again attributable to the hydrophobicity of the anion.[3] The exact nature or chain length of alkyl substituents on the organic cation in these ionic liquids generally plays a less

significant role in dictating the properties,[13,15] and structural variation provides the potential for 'fine-tuning' in order to more closely meet the specific solvent properties required. In this investigation five separate ionic liquids are employed, all containing the bis(trifluoromethylsulfonyl)imide anion. In four of these liquids the cationic component consists of a 1-alkyl-3-methylimidazolium ion, with the alkyl chain at the 1-position varying between 2 and 10 carbon atoms in length ([$C_n$mim], n = 2,4,8,10), whereas in the fifth compound a n-hexyltriethylammonium cation, [N_{6222}], is employed as the counter-ion (see Figure 4.1 for structures).

The potential use of RTILs incorporating the bis(trifluoromethylsulfonyl)imide anion as electrochemical solvents has already been the subject of several investigations. For example, the diffusion coefficient of $Ru(bpy)_3^{2+}$ was recently determined in a RTIL of the type [NR_3R'][NTf_2] using a chronoamperometric technique.[16] More recently, Lagrost et al. studied the reactivity of electrogenerated organic radical cations in several ionic liquids, including [C_2mim][NTf_2] and [C_4mim][NTf_2].[17] These reports demonstrate that the standard electrochemical methodologies employed with more traditional aqueous and organic solvents can be successfully adapted for use with RTILs so long as important differences, such as the much greater viscosities of these

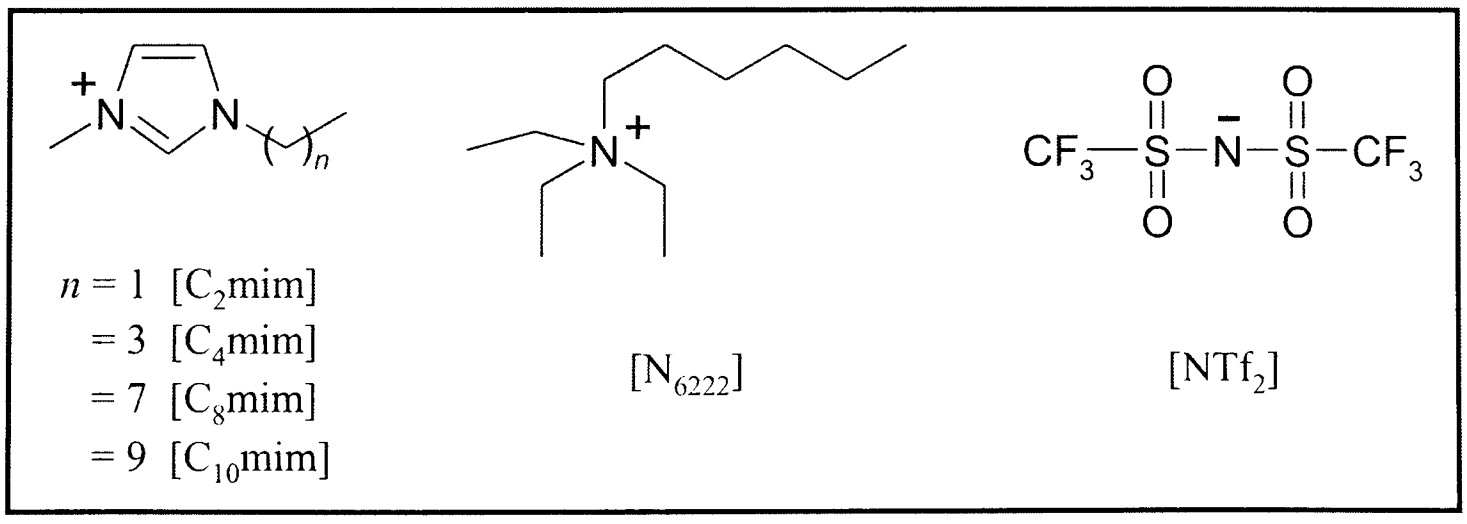


Figure 4.1
Structures of the ions comprising the room temperature ionic liquids under investigation.

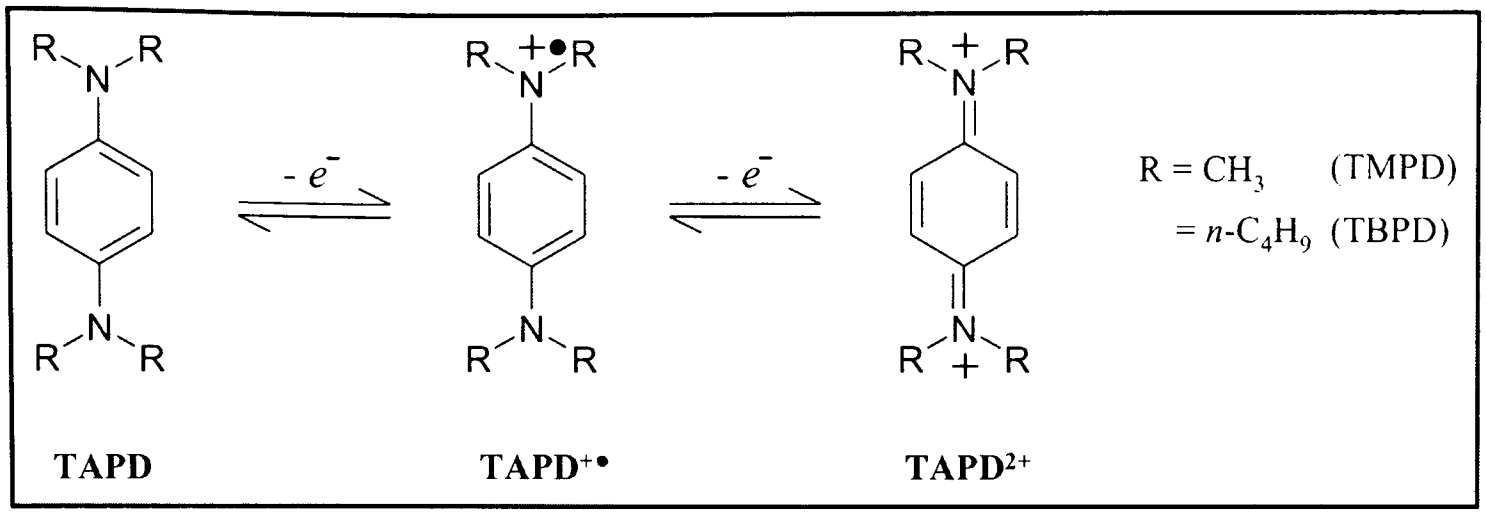


Figure 4.2
The two successive one-electron oxidations of N,N,N',N'-tetraalkyl-*para*-phenylenediamine.

compounds are taken into account. In the present study the electrochemical properties of two N,N,N',N'-tetraalkyl-*para*-phenylenediamines (TAPDs, A = methyl, *n*-butyl), compounds known to undergo two reversible, one-electron oxidations (see Figure 4.2),[14,18] are investigated in a range of ionic liquids using both cyclic voltammetry and chronoamperometry at a disk electrode. The work was carried out using an electrochemical cell specifically designed to allow interrogation of μL-quantities of solution under conditions of high vacuum (see section 3.3).[14] This cell permits voltammetry to be carried out over a period of several hours following evacuation until a steady and reproducible voltammetric response is attained, at which point the solution is assumed essentially anhydrous. Diffusion coefficients are then determined through the analysis of the chronoamperometric data. A major advantage of this technique is that a knowledge of the bulk concentration of the electroactive species is not required; the diffusion coefficient may be calculated based solely on the measurement of a single chronoamperometric transient and a value for the disk radius.[19-21] This is significant, since when preparing solutions of solids compounds in μL-quantities of ionic liquid, an accurate value for the concentration can be difficult to ascertain; standard micropipettes are not designed for use with such

viscous liquids and gravimetric techniques require a value for the density, which is not always available. The mass would also change once all absorbed water vapour had been driven off in vacuo. Furthermore, as in the next chapter where the electroactive species under investigation is a gas, a concentration-independent method of analysis is becomes all the more beneficial since solubility data for gases in ionic liquids is even more sparse. Some successful attempts to evaluate diffusion coefficients in RTIL solvents through analysis of chronoamperometric data collected at microelectrodes have been recently reported.[16,22,23]

The aims of the work were thus two-fold. On the one hand, the relatively straightforward redox properties of TMPD and TBPD could be used to test the proposed methodology for determination of diffusion coefficients in microsamples of ionic liquid solution, which, if successful, could then be applied to more complex electrochemical investigations. At the same time, however, the results from different ionic liquids could then be compared to investigate the potential for fine-tuning, i.e. the extent of variation in their solvent properties on changing the nature of the cation.

4.2 Experimental Section

In addition to matters already covered in chapter three, the sample of N,N,N',N'-tetrabutyl-*para*-phenylenediamine (TBPD) was provided by the group of Professor David J. Walton (University of Coventry), having been synthesised according to a literature procedure.[24] Its characteristics are reported elsewhere.[18]

This study utilised a gold disk working electrode, nominal diameter 12.5 μm. As the work predated construction of the temperature-regulated box, all experiments were carried out under ambient conditions of 293 ± 2 K.

4.3 Theory Section

4.3.1 Simulation of Cyclic Voltammetry

The time dependent equations describing the mass transport of species TAPD (A) and $TAPD^{+\bullet}$ (B) to a disk electrode of radius r_d written in cylindrical coordinates r, z are:

$$\frac{\partial[\mathrm{A}]}{\partial t} = D_{\mathrm{A}}\left(\frac{\partial^2[\mathrm{A}]}{\partial r^2} + \frac{1}{r}\frac{\partial[\mathrm{A}]}{\partial r} + \frac{\partial^2[\mathrm{A}]}{\partial z^2}\right)$$
$$\frac{\partial[\mathrm{B}]}{\partial t} = D_{\mathrm{B}}\left(\frac{\partial^2[\mathrm{B}]}{\partial r^2} + \frac{1}{r}\frac{\partial[\mathrm{B}]}{\partial r} + \frac{\partial^2[\mathrm{B}]}{\partial z^2}\right) \qquad (4.01)$$

where D_A and D_B are the diffusion coefficients of species TAPD and $TAPD^{+\bullet}$. The solution is assumed to contain only TAPD at the beginning of the electrolysis. It follows that the initial conditions for the equations (4.01) are

$$[\mathrm{A}] = [\mathrm{A}]_{bulk}\ ;\ [\mathrm{B}] = 0 \qquad (4.02)$$

The boundary conditions corresponding to the partial differential equations (4.01) for the disk are as follows:

$z = 0,\ 0 \le r \le r_d$ $\qquad D_{\mathrm{A}}\left.\frac{\partial[\mathrm{A}]}{\partial z}\right|_{z=0} = \left(k_f[\mathrm{A}] - k_b[\mathrm{B}]\right)_{z=0}$;

$$D_{\mathrm{B}}\left.\frac{\partial[\mathrm{B}]}{\partial z}\right|_{z=0} = -D_{\mathrm{A}}\left.\frac{\partial[\mathrm{A}]}{\partial z}\right|_{z=0}$$

$z = 0,\ r > r_d$ $\qquad \left.\frac{\partial[\mathrm{A}]}{\partial z}\right|_{z=0} = \left.\frac{\partial[\mathrm{B}]}{\partial z}\right|_{z=0} = 0 \qquad (4.03)$

all $z,\ r = 0$ $\qquad \left.\frac{\partial[\mathrm{A}]}{\partial r}\right|_{r=0} = \left.\frac{\partial[\mathrm{B}]}{\partial r}\right|_{r=0} = 0$

$z, r \to \infty$ $\qquad [\mathrm{A}] \to [\mathrm{A}]_{bulk}\ ;\ [\mathrm{B}] \to 0$

where k_f and k_b (cm s^{-1}) denote the forward and reverse rates for the oxidation of

TAPD, which have a potential dependence described by the Butler-Volmer theory as:

$$k_f = k_0 \exp\left(\frac{(1-\alpha)F}{RT}\left(E - E_f^0\right)\right) = k_0 e^{(1-\alpha)\theta}$$
$$k_b = k_0 \exp\left(-\frac{\alpha F}{RT}\left(E - E_f^0\right)\right) = k_0 e^{-\alpha\theta} \qquad (4.04)$$

where α is the transfer coefficient, E_f^0 is the formal electrode potential, $\theta = (F/RT)\left(E - E_f^0\right)$ is a dimensionless potential, k_0 is the standard electrochemical rate constant, R is the universal gas constant, and T is the absolute temperature.

The conformal mapping of the initial half-infinite simulation area in the cylindrical coordinates onto a closed box in the transformed coordinates developed by Amatore and Fosset[25] was used to create a spatial grid for the numerical simulation of the initial and boundary value problem (4.01–4.04). The application of this transformation allows one to handle the edge singularity that arises from the non-uniform accessibility of the disk electrode, as reflected in the discontinuous boundary conditions (4.03). The Alternating Direction Implicit (ADI) method [26-28] was used to solve the mathematical model (4.01–4.04) numerically in two dimensions. The ADI method applied to the problem under consideration produces banded pentadiagonal systems of linear equations which were solved using the generalised Thomas algorithm.[28] The current flowing at the electrode surface was calculated using the following expression:

$$I = 2\pi F D_{\mathrm{A}} \int_0^{r_d} \left(\frac{\partial[\mathrm{A}]}{\partial z}\right)_{z=0} r\,\mathrm{d}r \qquad (4.05)$$

The computer program implementing the ADI method for the mathematical model (4.01–4.05) was written in Borland Delphi™ 6 Professional Edition by Dr. Oleksiy

V. Klymenko (then University of Oxford) and executed on a PC with Intel Pentium 4 2GHz and 1Gb of RAM. A more detailed description of this simulation procedure has been previously published.[29,30] A typical computation time for simulation of one cyclic voltammogram was approximately 10 seconds.

4.3.2 Determination of Diffusion Coefficients

The diffusion coefficients of compounds dissolved in acetonitrile (containing 0.1 M TBAP) were calculated from the steady state limiting current (I_{ss}) obtained from cyclic voltammetry at a scan rate of 10 mV s^{-1}, using the equation below,

$$D = \frac{I_{ss}}{4nFr_d c} \qquad (4.06)$$

where D is the diffusion coefficient, F is the Faraday constant, n represents the number of electrons transferred, r_d the microelectrode radius and c is the concentration of the redox active compound.

In order to evaluate diffusion coefficients of species dissolved in ionic liquids a chronoamperometric method was employed. Recalling section 1.5.1, the time-dependant current response, I, due to diffusive mass transport following a potential step at a disk electrode has been formulated by Aoki and Osteryoung as:[31,32]

$$I = 4nFr_d Dcf(\tau) \qquad (4.07)$$

the appropriate form of $f(\tau)$ being dependant on the magnitude of $\tau = 4Dt/r_d^2$. Taking 1.0 x 10^{-11} $m^2 s^{-1}$ as a typical value of a diffusion coefficient within an ionic liquid solvent, τ enters the long-time regime ($\tau > 0.82$) after about 1 s for the case of a 12.5 μm diameter disk, whereupon equation (1.27) applies. Accordingly, transient data recorded over a period of 1-10 s following the potential step was analysed via equations (4.07) and (1.27) to yield values for the diffusion coefficient and

concentration of the electroactive species within each RTIL. Using an approach similar to Carlin et al.,[22] a method of nonlinear curve fitting was employed using Origin 6.0 (Microcal Software, Inc.). After inputting the known value of the radius, this software optimised the fit between the theoretical and experimental transients by varying the parameters D and c via a process of Levenberg-Marquardt iteration.

Once the optimal values of D and c had been obtained, they were used to simulate a cyclic voltammogram for comparison with those obtained experimentally. This served both to check the accuracy of the nonlinear fitting technique and also provided a means to estimate a value for the diffusion coefficient of the electrogenerated species by matching the reverse peak of the simulated voltammogram to the experimental data. After inputting the disk radius and the values of D and c determined from the chronoamperometric data, the fit between the simulated and experimental CVs was optimised manually by varying the diffusion coefficient of the electrogenerated species and the rate constant for heterogeneous electron transfer.

4.4 Results and Discussion

4.4.1 Influence of Water Vapour on the RTIL Electrochemical Window

While the saturated water content of bis(trifluoromethylsulfonyl)imide-based ionic liquids has been found to be very low,[3] the presence of even small amounts of water vapour are known to cause a dramatic variation in the solvating properties of RTILs.[14] Accordingly, the voltammetric behaviour of the pure ionic liquids in the presence and absence of atmospheric gases was initially investigated. The electrochemical window of each ionic liquid was probed using cyclic voltammetry, first while the cell was open to the air and subsequently over increasing time under vacuum. Removal of atmospheric gases under vacuum occurred rapidly, with the

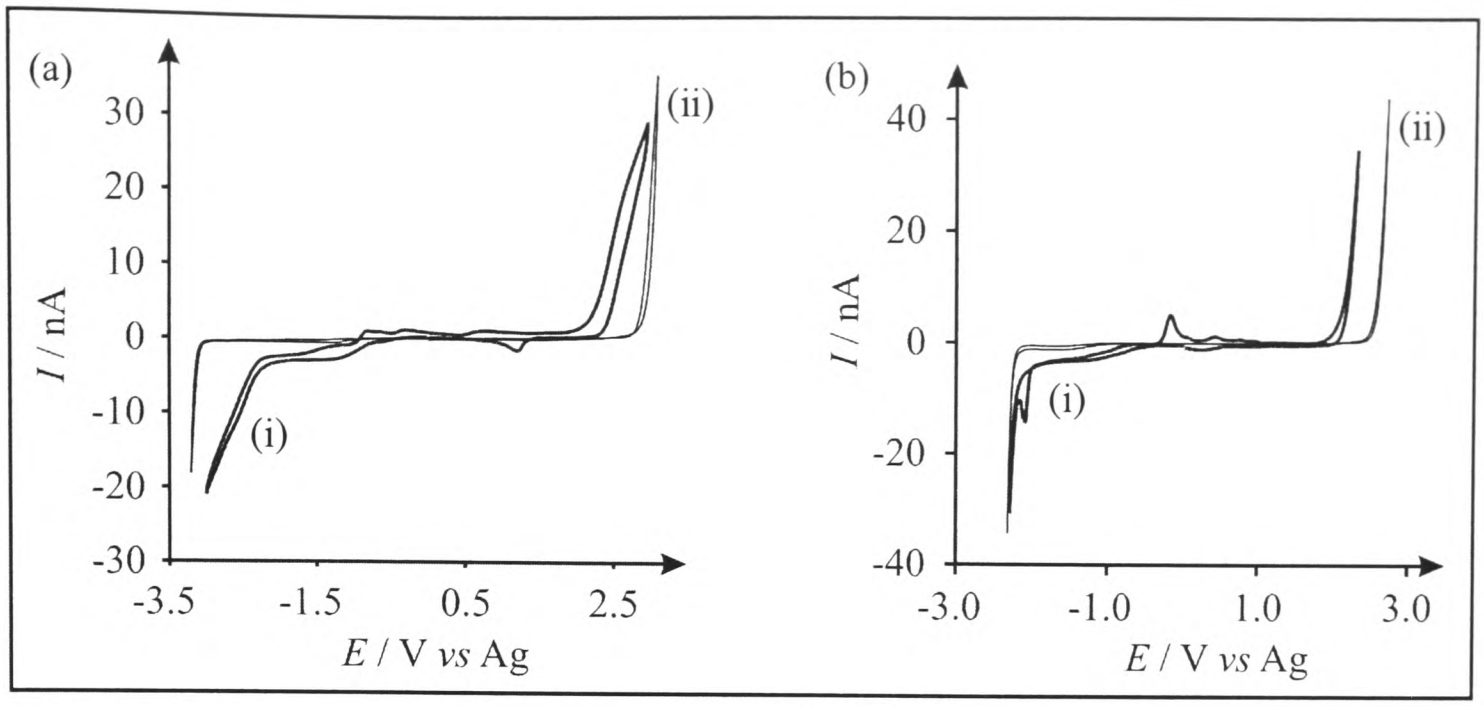


Figure 4.3
Cyclic voltammograms demonstrating the electrochemical windows of (a) $[N_{6222}][NTf_2]$ and (b) $[C_2mim][NTf_2]$ available at a 12.5 μm diameter Au microdisk electrode under (i) atmospheric conditions and (ii) after 60 minutes exposure to a 0.05 Torr vacuum.

voltammetry remaining largely invariant after the first 30 minutes of a 3 hour period of measurement. Figure 4.3 shows CVs recorded for $[N_{6222}][NTf_2]$ and $[C_2mim][NTf_2]$ under atmospheric conditions (Figures 4.3a(i) & 4.3b(i)) and after exposure to the vacuum for 60 minutes (Figures 4.3a(ii) & 4.3b(ii)). In the former case there is a distinct increase of ~0.8 V in both the anodic and cathodic potential limits upon evacuation of the cell, consistent with the interpretation that electrolysis of water can substantially narrow the accessible potential window.[14] In the case of $[C_2mim][NTf_2]$, while the anodic potential limit is substantially shifted, the effect on the cathodic window is considerably smaller and although the preceding baseline is flatter (partially due to removal of the oxygen reduction wave), the ultimate potential of solvent breakdown is almost the same. This behaviour was echoed in the remaining three ionic liquids containing the imidazolium cation; a summary of the electrochemical window data is presented in Table 4.1. The data for $[C_2mim][NTf_2]$ are in excellent agreement with results reported elsewhere at Platinum electrodes,[3] while the window range for $[N_{6222}][NTf_2]$ compares well with that obtained at glassy

Table 4.1
Electrochemical windows, ΔE, of the ionic liquids after 150 minutes exposure to a 0.05 Torr vacuum, determined voltammetrically at a 12.5 μm diameter Au disk, scan rate 200 mV s^{-1}. The point at which the current reaches a magnitude of 5 nA has been used as the definition of the potential limit at each extreme.

	Anodic Limit / V	Cathodic Limit / V	ΔE / V
$[C_2mim][NTf_2]$	-2.24	2.54	4.78
$[C_4mim][NTf_2]$	-2.04	2.72	4.76
$[C_8mim][NTf_2]$	-2.27	2.56	4.83
$[C_{10}mim][NTf_2]$	-2.24	2.65	4.89
$[N_{6222}][NTf_2]$	-3.13	2.86	5.99

carbon electrodes by Sun et al..[33] It is clear from the data that the anodic and cathodic limits of the four $[C_nmim][NTf_2]$ ionic liquids are virtually constant across the series. The anodic limit is governed by oxidation of the bis(trifluoromethyl-sulfonyl)imide anion and is thus expected to remain constant for this series of compounds. The cathodic limit is determined by reduction of the 1,3-dialkyl-imidazolium cation, the relatively low reduction potential of which has been attributed to the H(2) acidity. Other than having a weak inductive effect, varying the length of the alkyl chain would not be expected to significantly alter the acidity of a hydrogen atom in this position. $[N_{6222}][NTf_2]$ has an electrochemical window 1 Volt larger than the other four ionic liquids and this is almost certainly attributable to the greater electrochemical stability of the tetraalkylammonium cation over the imidazolium ion.[33]

4.4.2 Potential Sweep Analysis of TAPD

Having established the time under vacuum required to purge the ionic liquids of undesirable atmospheric gases, the electrochemical behaviour of the phenylenediamines TMPD and TBPD in each of the five ionic liquids was then investigated. Typical cyclic voltammograms obtained for the oxidation of these compounds are exemplified in Figure 4.4 by the systems TMPD in $[C_2mim][NTf_2]$

(Figures 4.4a&c), and TBPD in $[N_{6222}][NTf_2]$ (Figure 4.4b). In all cases two well-defined, reversible oxidation waves were detected which can be readily identified as the first and second one-electron oxidations of the TAPDs:

$$TAPD \rightleftharpoons TAPD^{+\bullet} + e^- \qquad (4.08)$$

$$TAPD^{+\bullet} \rightleftharpoons TAPD^{2+} + e^- \qquad (4.09)$$

Despite these experiments being performed with a 12.5 μm diameter electrode, the current-time behaviour was found to be decidedly peak-shaped at 200 mV s^{-1} (Figures 4.4a&b) and only began to approach a steady-state response at a scan rate of 5 mV s^{-1} (Figure 4.4c). While this may at first seem uncharacteristic of the voltammetry expected from a 'microdisk' electrode, it is a direct consequence of the very low diffusion coefficients of the electroactive species in these ionic liquid solvents. At diffusion coefficients of this magnitude, planar diffusion to the electrode surface is still the dominant form of mass transport and edge effects (which result in steady-state behaviour) only become significant at sufficiently small scan rates.

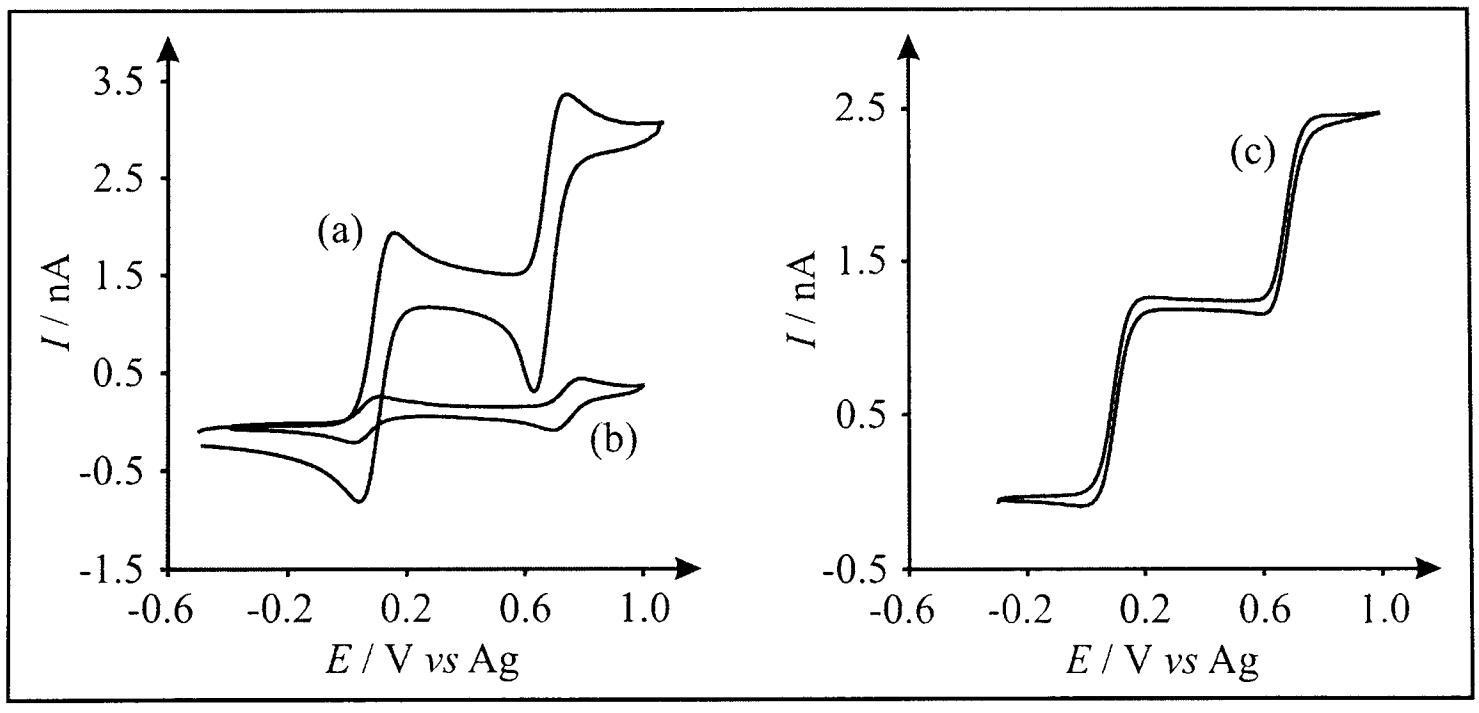


Figure 4.4
Cyclic voltammograms for the oxidation of (a) TMPD in $[C_2mim][NTf_2]$ (scan rate 200 mV s^{-1}), (b) TBPD in $[N_{6222}][NTf_2]$ (scan rate 200 mV s^{-1}) and (c) TMPD in $[C_2mim][NTf_2]$ (scan rate 5 mV s^{-1}) at a 12.5 μm diameter Au disk electrode after at least 60 minutes exposure to a 0.05 Torr vacuum.

Considering again the inequality (1.31) and taking a typical value of D as 1.0×10^{-11} $m^2 s^{-1}$, a true steady-state response at the 12.5 μm diameter disk is only predicted for scan rates below 6.5 mV s^{-1}. Clearly the experimentally practical scan rates accessible for this system fall within an intermediate range between the limiting peak-shaped and steady-state regions, and hence analysis of this voltammetric data to yield values for the diffusion coefficients would not be straightforward.

4.4.3 Chronoamperometric Analysis of TAPD

To make progress it is necessary to consider the chronoamperometric measurements recorded in parallel with the cyclic voltammetry. From this point on, the investigation was limited to the first one-electron oxidation process (formation of the monocation, $TAPD^{+\bullet}$, from the neutral TAPD molecule). In each case the potential was first held for a period of 300 s at a value at least 0.3 V below that at which faradaic currents were first observed to ensure that the two-electrode system had come to equilibrium. The potential was then stepped to an appropriate value beyond the peak potential of the first oxidation process but not sufficiently positive to run into the second oxidative step. Figure 4.5a shows a typical transient recorded for the oxidation of TMPD in $[C_2mim][NTf_2]$ and, for comparison, a transient measured under identical conditions in the pure ionic liquid alone. It can be seen that currents due to the charging of the electrical double layer are negligible compared to those generated by the oxidation reaction of interest, certainly at times greater than 1 s (the beginning point of the analysis). Nevertheless, background transients were recorded for each of the ionic liquids studied and subtracted from those recorded in the presence of the TAPDs before any data analysis was undertaken. As outlined above (see section 4.3), the appropriate Aoki and Osteryoung expression (1.27) was fitted to the experimental

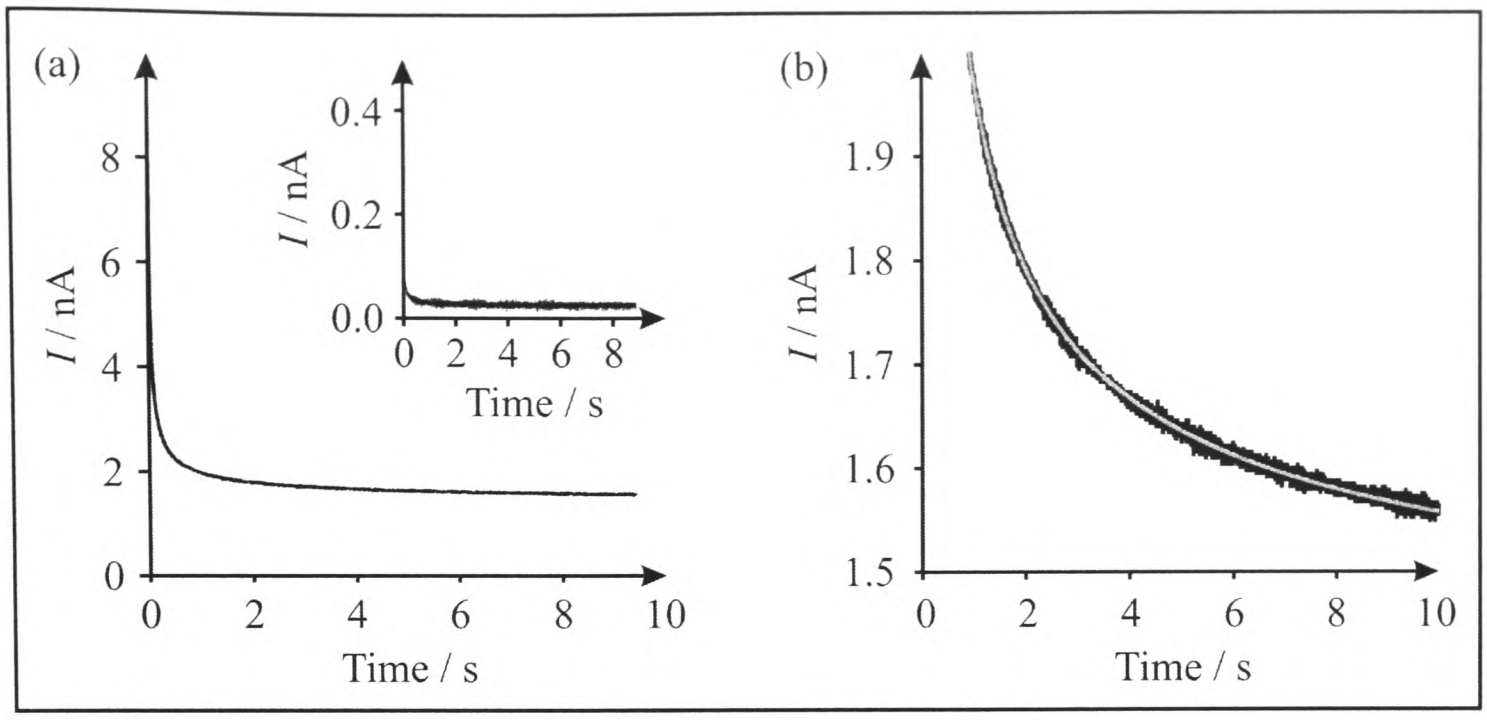


Figure 4.5
(a) A typical potential step chronoamperometric transient recorded at a 12.5 μm diameter Au disk electrode for the oxidation of TMPD in $[C_2mim][NTf_2]$. Inset shows the transient measured in the presence of the solvent alone. (b) A comparison of the experimentally obtained transient with the simulated response, optimised via a process of nonlinear curve fitting (see text).

transient data for times greater than 1 s, using a value for the electrode radius determined from a calibration measurement carried out immediately prior to each experiment. An example of such a fit for the TMPD/$[C_2mim][NTf_2]$ system is shown in Figure 4.5b. The agreement between experiment and theory is excellent in each case, implying that at timescales of above 1 s the oxidation of TAPD is essentially a diffusion-controlled process. The fitting procedure yielded values for both the diffusion coefficient and concentration of the analyte. An immediate validation of the accuracy of this method came from the sensible values obtained for the concentrations of TAPD in the ionic liquid solutions, which were all in close agreement with the values calculated when they were prepared.

4.4.4 Simulating the TAPD Voltammetry

Further verification was sought through simulation of cyclic voltammograms using the derived D and c values, which could then be compared to those recorded experimentally, at a range of scan rates. Cyclic voltammograms simulated for the

oxidation of TMPD in $[C_2mim][NTf_2]$ and TBPD in $[N_{6222}][NTf_2]$ at scan rates of 5 and 200 mV s^{-1} are shown in Figure 4.6, along with the experimental data. In all systems, very close agreement was obtained after optimising the values for the diffusion coefficient of the electrogenerated species and the heterogeneous rate constant for the electron transfer process. The latter fell in the range (0.1–2.5) x 10^{-2} cm s^{-1} for all ten cases, significantly lower than the equivalent values

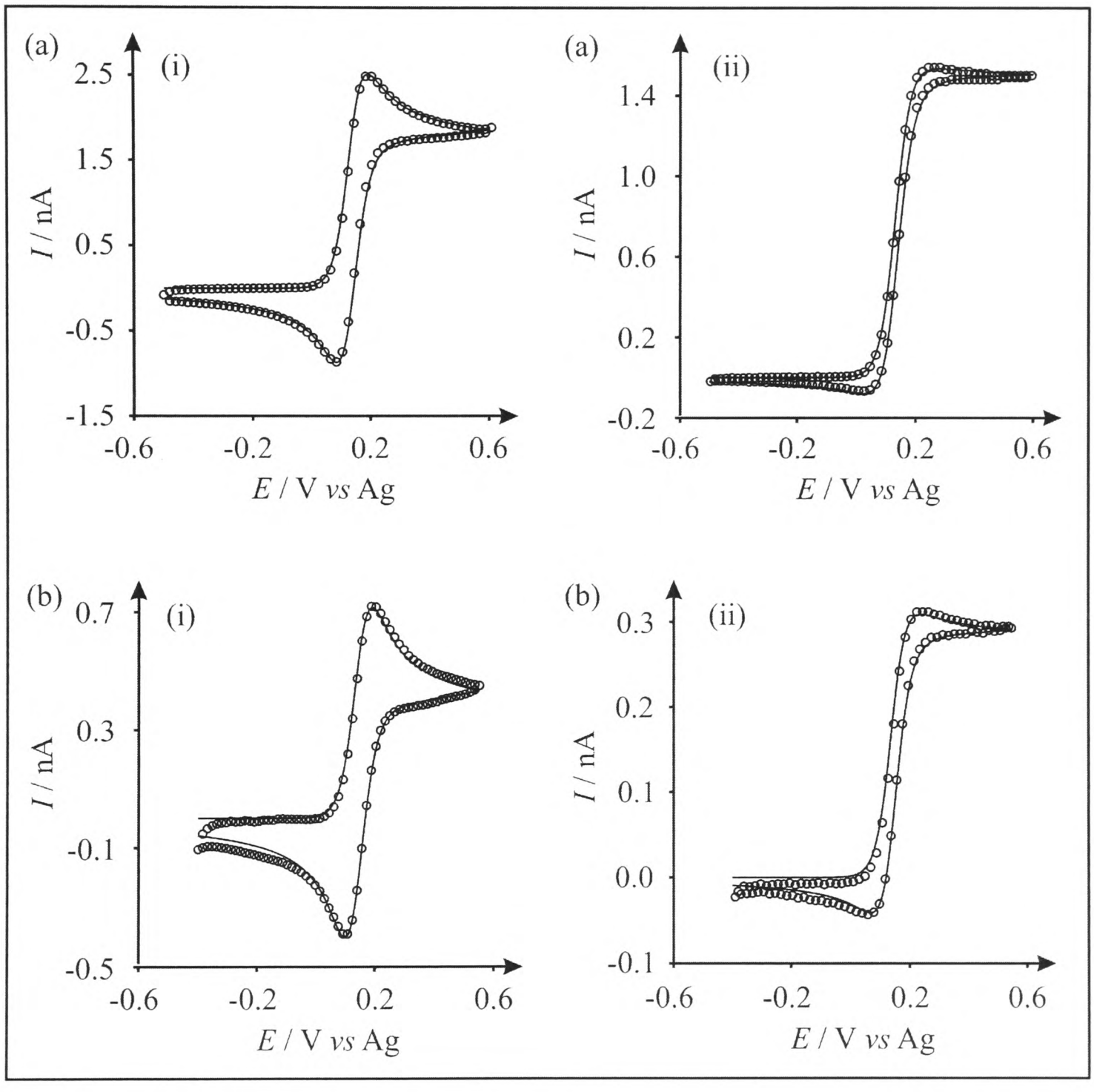


Figure 4.6
Comparison of experimental (○) and simulated (—) voltammograms for the oxidation of TMPD in (a) $[C_2mim][NTf_2]$ and (b) $[N_{6222}][NTf_2]$ at scan rates of (i) 200 mV s^{-1} and (ii) 5 mV s^{-1} using values for D_{TMPD} and c derived from chronoamperometric measurements.

Table 4.2
Diffusion coefficients for TMPD and TBPD in the five RTILs at 20 ± 2 °C determined by nonlinear curve fitting of chronoamperometric transients measured at a 12.5 μm diameter Au disk electrode after at least 60 minutes exposure to a 0.05 Torr vacuum. The viscosity measured for each ionic liquid at 20 °C is also tabulated.

	D_{TMPD} / 10^{-11} m^2 s^{-1} (± 5%)	D_{TBPD} / 10^{-11} m^2 s^{-1} (± 5%)	η / mPa s
$[C_2mim][NTf_2]$	2.62	1.23	32.1
$[C_4mim][NTf_2]$	1.87	0.80	57.6
$[C_8mim][NTf_2]$	1.12	0.40	119.3
$[C_{10}mim][NTf_2]$	1.13	0.52	152.8
$[N_{6222}][NTf_2]$	0.70	0.24	220.0

reported for TMPD and TPBD in acetonitrile of (5.5 ± 0.8) x 10^{-1} cm s^{-1} and (3.0 ± 0.5) x 10^{-1} cm s^{-1} respectively.[34] A summary of the diffusion coefficients is presented in Table 4.2. The margin of error has been calculated based on the averaged results of several different measurements and the effect of the uncertainty in electrode radius on the accuracy of the fitting process. For the systems with the lowest diffusion coefficients, the beginning of the range where the Aoki and Osteryoung equation for $\tau > 0.82$ applies increased above 1 s. In these cases the analysis was repeated from the appropriate starting time until a self-consistent result was obtained.

4.4.5 Discussion

The derived diffusion coefficients compare well with previous literature reports both for similar organic molecules dissolved in these same ionic liquids,[17] and for TMPD measured in different imidazolium-based RTILs.[14] For comparison, the diffusion coefficients of TMPD and TBPD were also measured in acetonitrile (containing 0.1 M TBAP) at 293 K, yielding values of 2.2 x 10^{-9} m^2 s^{-1} and 1.3 x 10^{-9} m^2 s^{-1} respectively (both in excellent agreement with data published elsewhere[34-36]). Clearly there are at least two orders of magnitude difference between the values determined in the ionic liquids and this more conventional solvent-electrolyte system, a fact that has been attributed to the high viscosity of the ionic liquids.[14,17] In order

to explore this relationship, the viscosity, η, of each ionic liquid was measured at 293 K. These data are also given in Table 4.2 and correspond closely with information reported elsewhere in both absolute value,[3,37] and in the linearity observed between viscosity and alkyl chain length, n, for the liquids of type $[C_n\text{mim}][NTf_2]$.[13] While the viscosities of these liquids are much larger than those of aqueous and simple organic media, they are relatively low compared to many other ionic liquids such as those incorporating the hexafluorophosphate or tetrafluoroborate anions. Since H-bonding has been identified as providing a significant contribution to the absolute viscosity,[3] this property is also likely to arise from the weak basicity of the extensively delocalised NTf_2^- anion (*c.f.* the strong H---F interactions in the PF_6^- and BF_4^- compounds[38]).

Since it only relies on a knowledge of the molecular mass and viscosity of the solvent, the model for estimating diffusion coefficients proposed by Wilke and Chang was considered potentially useful in this analysis.[39] Here, D is given by:

$$D = 7.4\times10^{-8}\frac{T\sqrt{xM}}{\eta V^{0.6}} \qquad (4.10)$$

where the various parameters are as defined in section 1.2.2. Diffusion coefficients estimated for the two TAPDs in the various RTILs using (4.10) (with x = 1.0, the value for non-associated solvents) are all too large however, by a factor of 1.5–3.0 and increasing the association coefficient only leads to further discrepancy. On the basis of these results it would seem that the Wilke-Chang theory, developed empirically using data derived from dilute aqueous or simple organic solvents is of limited applicability in the case of ionic liquids and will not be considered further. Figure 4.7 shows plots of diffusion coefficient against reciprocal viscosity for both

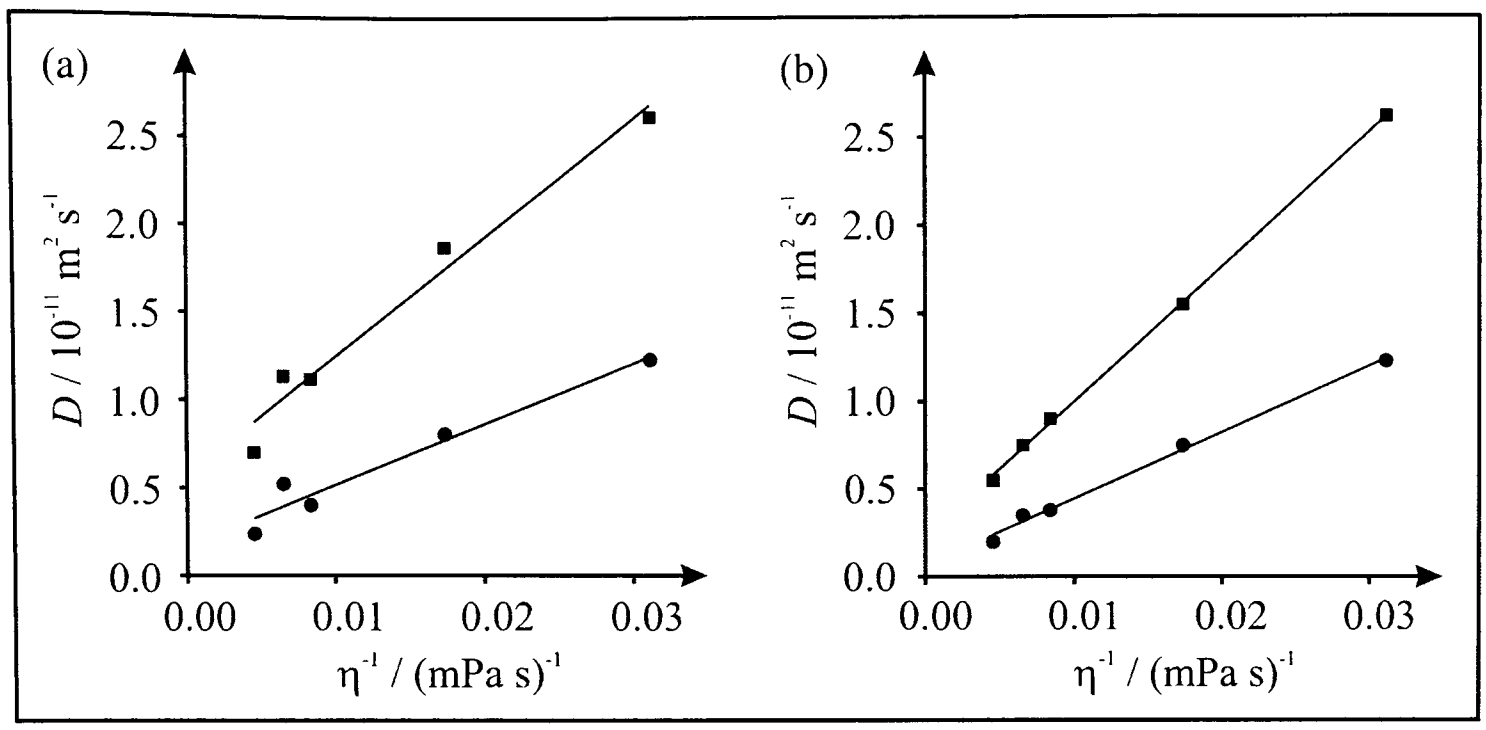


Figure 4.7
Plots of the dependence of diffusion coefficient on the reciprocal viscosity of the ionic liquid solvent for (a) the neutral TAPD species and (b) the radical cations, $TAPD^{+\bullet}$. ■ (TMPD/$TMPD^{+\bullet}$), ● (TBPD/$TBPD^{+\bullet}$).

the neutral TAPDs and the electrogenerated radical cations, $TAPD^{+\bullet}$, the latter data deriving from the optimised voltammetric simulations. For all species there is an excellent linearity between diffusion coefficient and reciprocal viscosity (least squares linear regression gives $R > 0.97$ and intercepts very close to the origin) indicating that the conventional Stokes-Einstein type inverse proportionality between D and η holds in this type of media. In the case of the charged species $TAPD^{+\bullet}$, this trend can also be interpreted as a validation of the empirical observation known as Walden's rule,[40] which states that the product of viscosity and molar conductivity, Λ_m, is approximately constant for the same ions in a variety of solvents. Since $\Lambda_m \propto D$ this may be investigated by looking at the product, $D\eta$. Values for $D\eta$ calculated for the range of five RTILs are all equal to $(1.03 \pm 0.19) \times 10^{-9}$ mPa m^2 and $(4.51 \pm 0.84) \times 10^{-10}$ mPa m^2 for $TMPD^{+\bullet}$ and $TBPD^{+\bullet}$ respectively, suggesting that based on these findings, the range of solvents in which the rule applies can be extended to include ionic liquids.

4.5 Conclusions

For the five studied bis(trifluoromethylsulfonyl)imide-based ionic liquids, exposure to vacuum conditions for short times was found to rapidly purge them of undesirable atmospheric gases, after which they may be readily employed as solvents in which to conduct electrochemical experimentation. Under these conditions, a combination of chronoamperometric measurements and cyclic voltammetry at a disk electrode was successfully applied to probe the mass transport of two species dissolved in μL-samples of the RTILs. Diffusion coefficients were found to be around two orders of magnitude lower than in simple organic solvents, in accordance with previously published findings. Changing the nature of the cationic component of the ionic liquid manifested itself in terms of an effect on the solvent viscosity, which proved sufficient to explain the variation in diffusion coefficient for a given species across the series of RTILs.

In light of this relatively straightforward initial study, it was anticipated that the same methodology could now be employed to investigate a more challenging electrochemical problem. Given the interesting voltammetry reported for the reduction of oxygen in a quaternary alkylammonium ionic liquid (see section 2.2.7), it was to this system that attention next turned.

4.6 References

[1] R.G. Evans, O.V. Klymenko, C. Hardacre, K.R. Seddon, R.G. Compton, *J. Electroanal. Chem.* **2003**, *556*, 179.

[2] V.R. Koch, C. Nanjundiah, G.B. Appetecchi, B. Scrosati, *J. Electrochem. Soc.* **1995**, *142*, L116.

[3] P. Bonhôte, A.-P. Dias, M. Armand, N. Papageorgiou, K. Kalyanasundaram, M. Grätzel, *Inorg. Chem.* **1996**, *35*, 1168.

[4] J.M. Fraile, J.I. García, C.I. Herrerías, J.A. Mayoral, D. Carrié, M. Vaultier, *Tetrahedron: Asymmetry* **2001**, *12*, 1891.

[5] D.W. Kim, C.E. Song, D.Y. Chi, *J. Am. Chem. Soc.* **2002**, *124*, 10278.

[6] C. Hardacre, J.D. Holbrey, S.P. Katdare, K.R. Seddon, *Green Chem.* **2002**, *4*, 143.

[7] E. Naudin, H.A. Ho, S. Branchaud, L. Breau, D. Bélanger, *J. Phys. Chem. B* **2002**, *106*, 10585.

[8] J.A. Laszlo, D.L. Compton, *J. Mol. Catal. B: Enzym.* **2002**, *18*, 109.

[9] M. Eckstein, P. Wasserscheid, U. Kragl, *Bioltechnol. Lett.* **2002**, *24*, 763.

[10] S.H. Schöfer, N. Kaftzik, U. Kragl, P. Wasserscheid, *Chem. Commun.* **2001**, 425.

[11] C. Liang, C.-Y. Yuan, R.J. Warmack, C.E. Barnes, S. Dai, *Anal. Chem.* **2002**, *74*, 2172.

[12] J.D. Stenger-Smith, C.K. Webber, N. Anderson, A.P. Chafin, K. Zong, J.R. Reynolds, *J. Electrochem. Soc.* **2002**, *149*, A973.

[13] S.V. Dzyuba, R.A. Bartsch, *ChemPhysChem* **2002**, *3*, 161.

[14] U. Schröder, J.D. Wadhawan, R.G. Compton, F. Marken, P.A.Z. Suarez, C.S. Consorti, R.F. de Souza, J. Dupont, *New J. Chem.* **2000**, *24*, 1009.

[15] J.G. Huddleston, A.E. Visser, W.M. Reichert, H.D. Willauer, G.A. Broker, R.D. Rogers, *Green Chem.* **2001**, *3*, 156.

[16] B.M. Quinn, Z. Ding, R. Moulton, A.J. Bard, *Langmuir* **2002**, *18*, 1734.

[17] C. Lagrost, D. Carrié, M. Vaultier, P. Hapiot, *J. Phys. Chem. A* **2003**, *107*, 745.

[18] U. Schröder, J. Wadhawan, R.G. Evans, R.G. Compton, B. Wood, D.J. Walton, R.R. France, F. Marken, P.C. Bullman Page, C.M. Hayman, *J. Phys. Chem. B* **2002**, *106*, 8697.

[19] T. Hepel, J. Osteryoung, *J. Phys. Chem.* **1982**, *86*, 1406.

[20] C.P. Winlove, K.H. Parker, R.K.C. Oxenham, *J. Electroanal. Chem.* **1984**, *170*, 293.

[21] G. Denuault, M.V. Mirkin, A.J. Bard, *J. Electroanal. Chem.* **1991**, *308*, 27.

[22] R.T. Carlin, H.C. De Long, J. Fuller, P.C. Trulove, *J. Electrochem. Soc.* **1998**, *145*, 1598.

[23] J.D. Wadhawan, U. Schröder, A. Neudeck, S.J. Wilkins, R.G. Compton, F. Marken, C.S. Consorti, R.F. De Souza, J. Dupont, *J. Electroanal. Chem.* **2000**, *493*, 75.

[24] J.H. Fuhrhop, H. Bartsch, *Liebigs Ann. Chem.* **1983**, 802.

[25] C.A. Amatore, B. Fosset, *J. Electroanal. Chem.* **1992**, *328*, 21.

[26] J. Heinze, *J. Electroanal. Chem.* **1981**, *124*, 73.

[27] J. Heinze, M. Stoerzbach, *Ber. Bunsen. Phys. Chem.* **1986**, *90*, 1043.

[28] I.B. Svir, O.V. Klimenko, R.G. Compton, *Radiotekhnika* **2001**, *118*, 92.

[29] N.V. Rees, O.V. Klymenko, R.G. Compton, M. Oyama, *J. Electroanal. Chem.* **2002**, *531*, 33.

[30] N.V. Rees, O.V. Klymenko, B.A. Coles, R.G. Compton, *J. Electroanal. Chem.* **2002**, *534*, 151.

[31] K. Aoki, J. Osteryoung, *J. Electroanal. Chem.* **1981**, *122*, 19.

[32] K. Aoki, J. Osteryoung, *J. Electroanal. Chem.* **1984**, *160*, 335.

[33] J. Sun, M. Forsyth, D.R. MacFarlane, *J. Phys. Chem. B* **1998**, *102*, 8858.

[34] A.D. Clegg, N.V. Rees, O.V. Klymenko, B.A. Coles, R.G. Compton, *ChemPhysChem* **2004**, *5*, 1234.

[35] S.R. Jacob, Q. Hong, B.A. Coles, R.G. Compton, *J. Phys. Chem. B* **1999**, *103*, 2963.

[36] B.A. Coles, M.J. Moorcroft, R.G. Compton, *J. Electroanal. Chem.* **2001**, *513*, 87.

[37] M.C. Lagunas, W.R. Pitner, J.-A. van den Berg, K.R. Seddon, *ACS Symposium Series* **2003**, *856*, 421.

[38] P.A.Z. Suarez, S. Einloft, J.E.L. Dullius, R.F. De Souza, J. Dupont, *J. Chim. Physique* **1998**, *95*, 1626.

[39] C.R. Wilke, P. Chang, *Am. Inst. Chem. Eng. J.* **1955**, *1*, 264.

[40] P. Walden, *Z. Phys. Chem.* **1906**, *55*, 207.

5

Electroreduction of Oxygen in a Series of Room Temperature Ionic Liquids Composed of Group 15-Centred Ions

The electrochemical reduction of oxygen is reported in four room temperature ionic liquids based on quaternary alkyl -onium cations and heavily fluorinated anions in which the central atom is either nitrogen or phosphorus. Data was collected using cyclic voltammetry and potential step chronoamperometry at gold, platinum and glassy carbon disk electrodes of micrometer dimension under water-free conditions at a controlled temperature. Analysis via fitting to appropriate theoretical equations was then carried out to obtain kinetic and thermodynamic information pertaining to the electrochemical processes observed. In the quaternary ammonium electrolytes, reduction of oxygen was found to occur reversibly to give the stable superoxide species, in an analogous manner to that seen in conventional aprotic solvents such as dimethylsufoxide and acetonitrile. The most significant difference is in the relative rate of diffusion; the diffusion coefficients of oxygen in the RTILs are an order of magnitude lower than in common organic solvents, and for superoxide these values are reduced by a further factor of ten. In the quaternary phosphonium ionic liquids, however, more complex voltammetry is observed, akin to that expected for the reduction of oxygen in acidified organic media. This is shown to be consistent with the occurrence of a proton abstraction reaction between the electrogenerated superoxide and quaternary alkylphosphonium cations following the initial electron transfer. This work has been published in the *Journal of Physical Chemistry B*.[1]

5.1 Introduction

The electrochemistry of dioxygen has been thoroughly investigated in conventional aqueous and organic solvents, and is reviewed in a recent publication by Sawyer,[2] himself a significant contributor in this field. These studies have proven that reduction of the oxygen molecule is a complex process, the outcome of which is highly dependent on the solvent employed and, in particular, its acidity. In aprotic media (acetonitrile, N,N-dimethylformamide, dimethylsulfoxide) a reversible, one-electron reduction occurs to yield the superoxide ion, $O_2^{-\bullet}$.[3-5]

$$O_2 + e^- \rightleftharpoons O_2^{-\bullet} \qquad (5.01)$$

Regardless of solvent, this radical anion is highly reactive and behaves as a strong Brønsted base in the presence of a proton source. Accordingly, addition of a Brønsted acid to the aprotic solvent brings about a change in the observed voltammetry; the reversible one-electron signal is replaced by an irreversible two-electron wave as the electrogenerated superoxide rapidly undergoes a series of protonation and disproportionation steps to ultimately yield hydrogen peroxide as the final product.[3,6,7]

$$O_2 + 2e^- + 2H^+ \rightarrow H_2O_2 \qquad (5.02)$$

Recently, room temperature ionic liquids have become popular alternative solvents in which to conduct electrochemical investigations (for a review see reference [8]) and the reduction of oxygen in these media has already been the subject of several reports.[9-13] The first such study was performed by Carter et al. who reported the voltammetry of dioxygen at a 3 mm diameter glassy carbon (GC) electrode in the basic chloroaluminate binary molten salt 1-ethyl-3-methylimidazolium chloride /

aluminium chloride.[9] A single cathodic peak was observed and interpreted in terms of reaction (5.02) above, i.e. reduction to superoxide followed by fast irreversible reaction with protonic impurities present within the melt. Attempts to stabilise the superoxide by eliminating these protonic impurities proved unsuccessful. In a subsequent investigation, AlNashef and co-workers analysed the reduction of oxygen at a GC macroelectrode in two RTILs consisting of the 1,2-dimethyl-3-butyl-imidazoluim and 1-methyl-3-butylimidazolium cations respectively combined in each case with the hexafluorophosphate anion.[11] In the former ionic liquid, an ill-defined reduction wave with no reverse peak was observed and again attributed to the influence of impurities endemic to the RTIL. In the second ionic liquid however, the electrogenerated superoxide was stable enough to be observed by cyclic voltammetry (reaction (5.01)), and partake in follow up reactions with gaseous carbon dioxide introduced to the RTIL, as explored in a follow-up report.[12] Most recently, Buzzeo et al. have studied the reduction of oxygen in two ionic liquids, 1-ethyl-3-methylimidazolium bis(trifluoromethylsulfonyl)imide, $[C_2mim][NTf_2]$, and *n*-hexyl-triethylammonium bis(trifluoromethylsulfonyl)imide, $[N_{6222}][NTf_2]$, at a 10 μm diameter gold disk electrode.[13] In this investigation, stable superoxide was reported in both liquids and analysis of a combination of chronoamperometric measurements and cyclic voltammetry allowed the diffusion coefficients of both oxygen and superoxide to be determined. The most interesting results were seen for the second ionic liquid, $[N_{6222}][NTf_2]$, in which these diffusion coefficients were found to differ by more than a factor of 30, giving rise to a pronounced asymmetry in the forward and backward voltammetric waves; both transient and steady-state behaviour was observed in a single voltammogram.

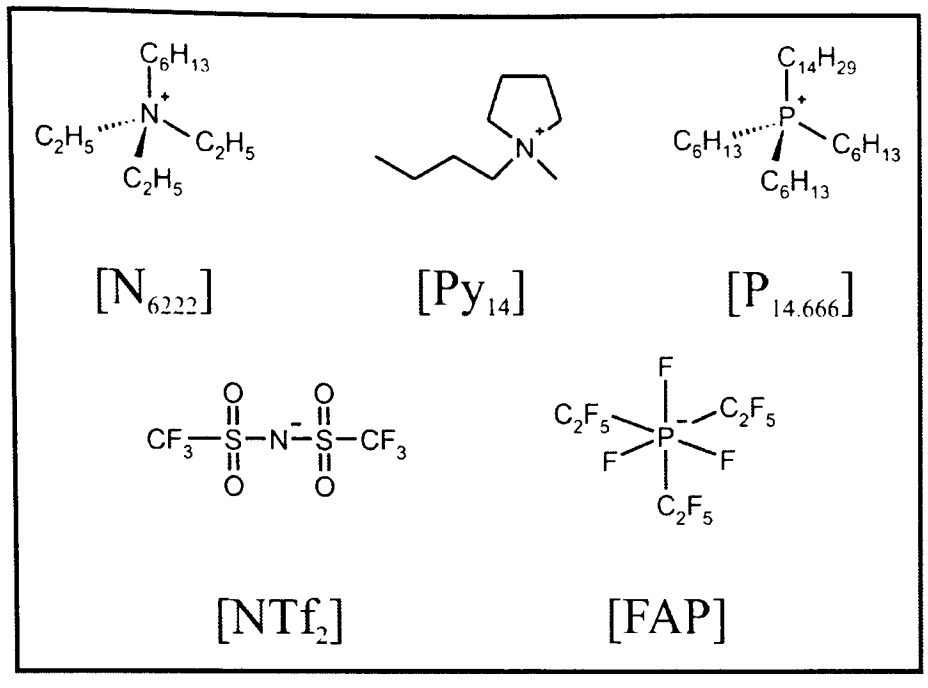


Figure 5.1
Structures of the ions comprising the room temperature ionic liquids under investigation.

In view of these initial results, the aim of the present study was to carry out a comprehensive investigation of the electrogeneration of stable superoxide in various ionic liquid solvents and characterise the heterogeneous kinetics for this process at electrodes composed of different materials (gold, platinum and GC). Four RTILs were employed, all consisting of complex ions based around central nitrogen and phosphorous atoms, namely $[N_{6222}][NTf_2]$; N-methyl-N-butylpyrrolidinium bis(trifluoromethylsulfonyl)imide, $[Py_{14}][NTf_2]$; tris(*n*-hexyl)tetradecylphosphonium bis(trifluoromethylsulfonyl)imide; $[P_{14.666}][NTf_2]$; and tris(*n*-hexyl)tetradecyl-phosphonium trifluorotris(pentafluoroethyl)phosphate, $[P_{14.666}][FAP]$ (for structures see Figure 5.1). The three cations involved are all long chain quaternary alkyl -onium ions, preferred over possible imidazolium-based alternatives due to the more favourable results they yielded in the preliminary study,[13] and, since the reaction of interest is a reduction, the inherently larger cathodic potential windows this type of ionic liquid have been found to possess.[14-16] Early on, it was appreciated that strict control over the experimental temperature would be essential to allow the collection of reliable data. The viscosities of ionic liquids are extremely temperature dependent (a 20% change over 5 K not being uncommon[17]) and the effect of this is felt

electrochemically primarily through the approximately inverse relationship between solution viscosity and rate of diffusion of dissolved species.[18] While this should be a concern in any study, in experiments involving gaseous substrates the effect of temperature variation is exacerbated by its potentially large effect on their solubility. Consequently, a temperature-controlled box was constructed to house the electrochemical cell and thus permit the measurement of reproducible results under well-defined conditions (see section 3.3). With this in place, a series of voltammetric and chronoamperometric experiments were performed, and the resulting data analysed against the appropriate theories to produce a set of thermodynamic and kinetic parameters for the reduction of oxygen. These results are discussed and compared with the equivalent behaviour reported for traditional aprotic solvents.

5.2 Experimental Section

In addition to matters already covered in chapter three, mixtures of oxygen and argon were generated using a Wösthoff triple gas-mixing pump (Bochum, Germany), accurate to ±1%. Nitrogen was connected as the third gas (redundant for the purposes the work reported here) to ensure correct operation of the pump.

This study utilised gold, platinum and GC disk working electrodes, nominal diameters 10 μm (Au, Pt) and 11 μm (GC). The thermostatted box was used to regulate all experiments to a temperature of 308 ± 1 K.

5.3 Theory Section

5.3.1 Analysis of Chronoamperometric Transients

Simultaneous determination of both the diffusion coefficient, D, and initial concentration, $[O_2]$, of oxygen was achieved through analysis of chronoamperometric

measurements conducted at the disk electrodes. Applying the Shoup and Szabo formulation (see section 1.5.1),[19] the time-dependent current response, I, resulting from the diffusion-controlled reduction of oxygen following a potential step at a disk electrode is given by the following expression.

$$I = -4nFD[O_2]r_d\left[0.7854 + 0.8863\tau^{-1/2} + 0.2146e^{-0.7823\tau^{-1/2}}\right] \qquad (5.03)$$

where, as usual, $\tau = 4Dt/r_d^2$. Although an approximation, this single empirical expression is sufficient to describe the current response to within an accuracy of 0.6% over all τ. In the limit of low τ, equation (5.03) simplifies to the Cottrell equation, with an $I \propto [O_2]D^{1/2}$ dependence, whereas at high τ, a steady-state current is attained and $I \propto [O_2]D$. Accordingly, the fitting of experimental data to equation (5.03), recorded over a time incorporating both these regimes allows deconvolution of the parameters D and $[O_2]$ and hence their simultaneous determination. Fitting was achieved using ORIGIN 6.0 (Microcal Software Inc.). After entering a value of r_d, the software was instructed to iterate through various values of D and $[O_2]$ until the fit to the experimental data had been optimised.

5.3.2 Simulation of Cyclic Voltammetry

The mathematical model used to simulate the one-electron reduction of oxygen to superoxide at a disk electrode and its subsequent re-oxidation back to O_2 was identical to the one implemented in an earlier publication which contains a full detailed description of the simulation procedure.[13] Briefly, the pertinent time-dependent mass transport equations and boundary conditions were re-expressed using a coordinate transformation developed by Amatore and Fosset[20] and then solved numerically in two dimensions using the alternating direction implicit (ADI)

method.[21,22] The current-voltage response was then calculated from the resulting concentration profiles. As in the previous study, a spatial grid size of 700 x 700 points (NΘ x NΓ, where Θ and Γ are the transformed grid coordinates) was employed to ensure accurate simulation of both the forward and reverse waves given the expected disparity in the diffusion coefficients of oxygen and superoxide respectively.[13] After inputting the disk radius and the values of D and $[O_2]$ determined from the chronoamperometric analysis, the fit between the simulated and experimental voltammetry was optimised manually by varying the diffusion coefficient of superoxide, the formal electrode potential, E_f^0, the standard electrochemical rate constant, k_0, and the transfer coefficient, α.

In the case of oxygen reduction in the tetraalkylphosphonium-based RTILs, an alternative model was developed, full details of which are provided in an appendix at the end of the chapter. The computer programs implementing the ADI method for each mathematical model were written in Borland Delphi 6 Professional Edition by Dr. Oleksiy V. Klymenko and executed on a PC running a Intel Pentium 4 2GHz processor with 1 GB of RAM.

5.4 Results and Discussion

5.4.1 Reduction of Oxygen in the Quaternary Ammonium RTILs

To remove atmospheric oxygen and water vapour initially present in the ionic liquids, the cell was purged with pure argon prior to the commencement of any controlled addition of oxygen. The level of these impurities was monitored by running background cyclic voltammograms, and one hour of purging was found to be more than sufficient to obtain a constant response. While the amount of water remaining

after this one hour preparatory stage was never explicitly measured, it was felt that owing to the subsequent observation of (chemically) reversible O_2 voltammetry (see below) the cell was thereafter operating under essentially anhydrous conditions. Upon addition of controlled amounts of oxygen to the cell, the time taken for equilibration between the gaseous and dissolved O_2 was determined by recording voltammograms periodically until the reduction wave reached a maximum. The time taken to attain equilibrium was dependent on the volume of ionic liquid placed in the cell; with larger volumes the gas has further to diffuse from the surface to the electrode tip. The amount of RTIL used was optimised at 10 μL whereupon a delay of twenty minutes between altering the oxygen level and making electrochemical measurements ensured that full equilibration had occurred. The circuits regulating the temperature were activated at the beginning of the one-hour purge with pure argon so that the cell had ample time to reach this selected temperature prior to the introduction of oxygen. These procedures were adopted for the collection of all the data reported below.

Figure 5.2 displays cyclic voltammograms recorded for the reduction of oxygen (100 v/v%) in $[N_{6222}][NTf_2]$ at each of the three electrode materials: Au, Pt and GC. In accordance with the previous findings in this ionic liquid (at a Au electrode only),[13] distinctively asymmetric voltammetry is observed corresponding to the electrochemically reversible one-electron reduction of oxygen to give stable superoxide, which is subsequently reoxidised (equation (5.01)). At the metal electrodes, a small pre-wave is apparent just prior to the onset of oxygen reduction. This is attributed to the presence of an unknown trace impurity in the ionic liquid, which could not be removed by any amount of purging with argon or exposure to vacuum conditions. By using 25 v/v% as a lower bound for the various oxygen

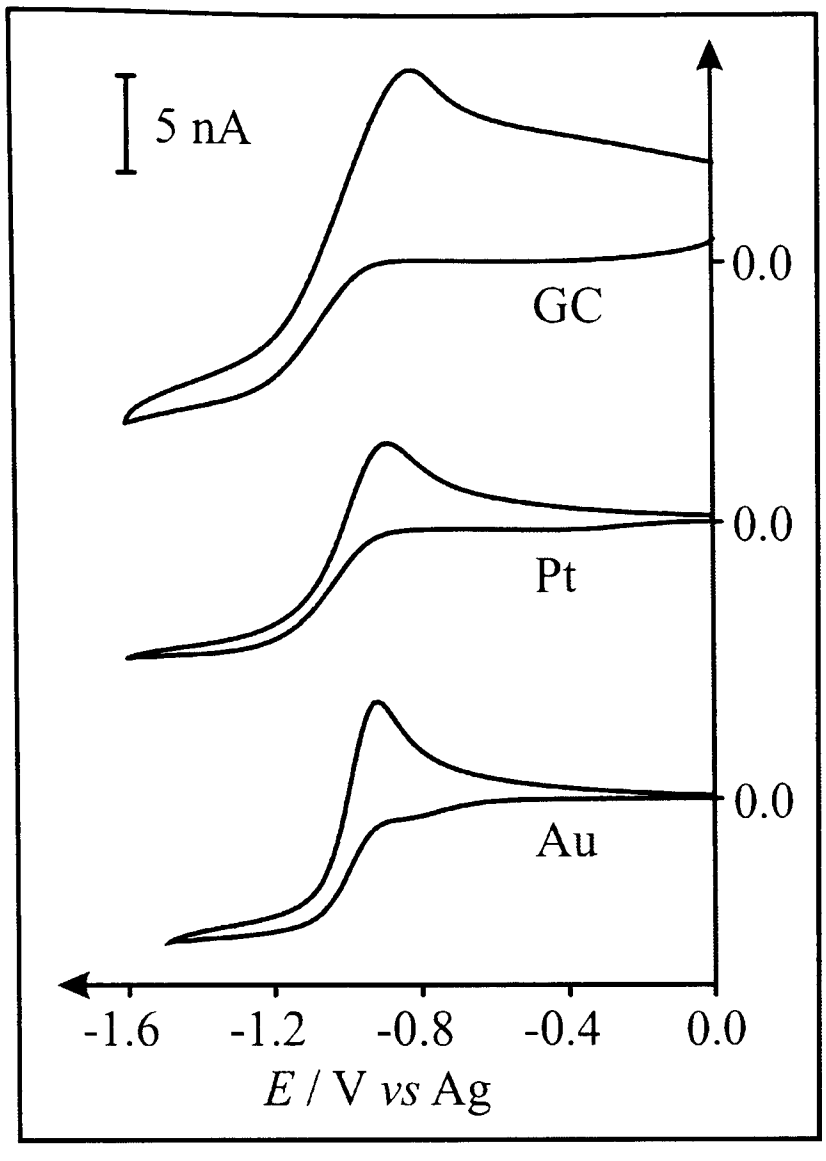


Figure 5.2
Cyclic voltammograms showing the reduction of oxygen in $[N_{6222}][NTf_2]$ at Au, Pt and GC disk electrodes, nominal radii 10 μm (Au, Pt) and 11 μm (GC), at a scan rate of 0.5 V s^{-1} and temperature of 308 K.

concentrations introduced to the cell, however, the influence of this small signal on the overall voltammetry remained minimal. The reduction of oxygen in the second quaternary ammonium RTIL under study, $[Py_{14}][NTf_2]$, followed the same pattern, as shown at a Au electrode in Figure 5.3 which exemplifies the typical voltammetric response of these systems to gradual exposure to increasing oxygen concentrations (25 – 100 v/v % in 15% increments). In all cases, the trend in limiting current for the forward process with concentration of oxygen added showed an excellent linearity.

As outlined in the theoretical section, a chronoamperometric method was applied to deduce the concentration, $[O_2]$, and diffusion coefficient, $D(O_2)$, of the electroactive species in the ionic liquids. To ensure that the two-electrode system was initially at equilibrium, the potential was held at a point corresponding to the passage of no faradaic current for a period of 300 seconds before being instantaneously stepped to a

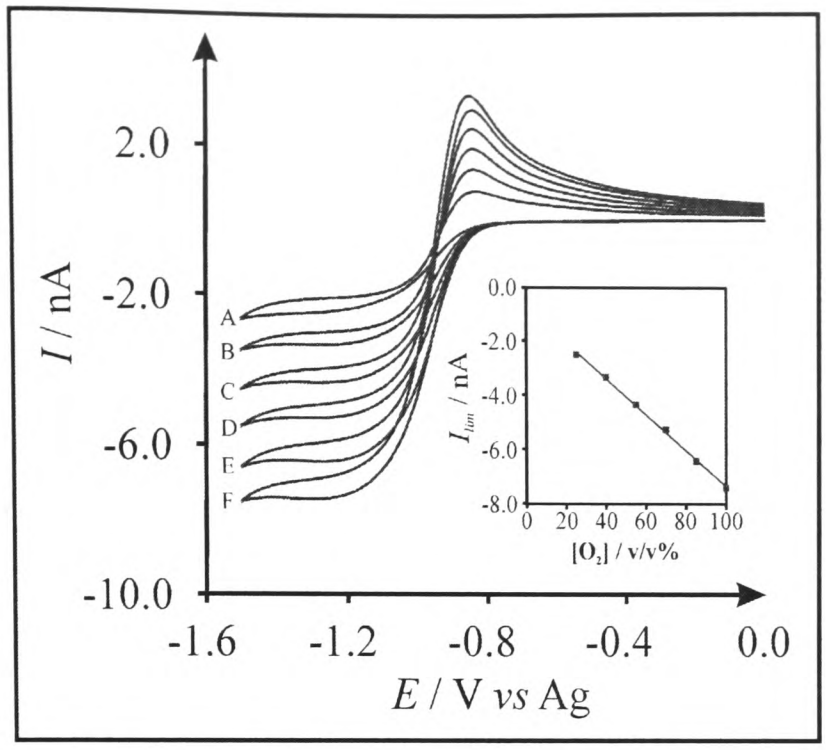


Figure 5.3
Cyclic voltammograms showing the reduction of (A) 25 (B) 40 (C) 55 (D) 70 (E) 85 and (F) 100 v/v% oxygen in $[Py_{14}][NTf_2]$ at a 10 µm Au disk electrode, ν= 0.5 V s^{-1}, T = 308 K. Inset shows the variation of limiting current with the proportion of oxygen in the gas phase (R^2 = 0.9983).

potential in the plateau region of the reductive wave. Transients were recorded at each of the six oxygen concentrations shown in Figure 5.3. To eliminate the influence of background currents (including those attributed to the low level impurity identified above), the transient for the lowest concentration, 25 v/v%, was subtracted from all the others. The corrected data was then analysed according to the Shoup & Szabo expression[19] to yield unique values for the parameters $[O_2]$ and $D(O_2)$ in each ionic liquid. A comparison of the experimental and fitted transients is shown in Figure 5.4 for the oxygen / $[N_{6222}][NTf_2]$ system at a Au electrode. The fits are very close and

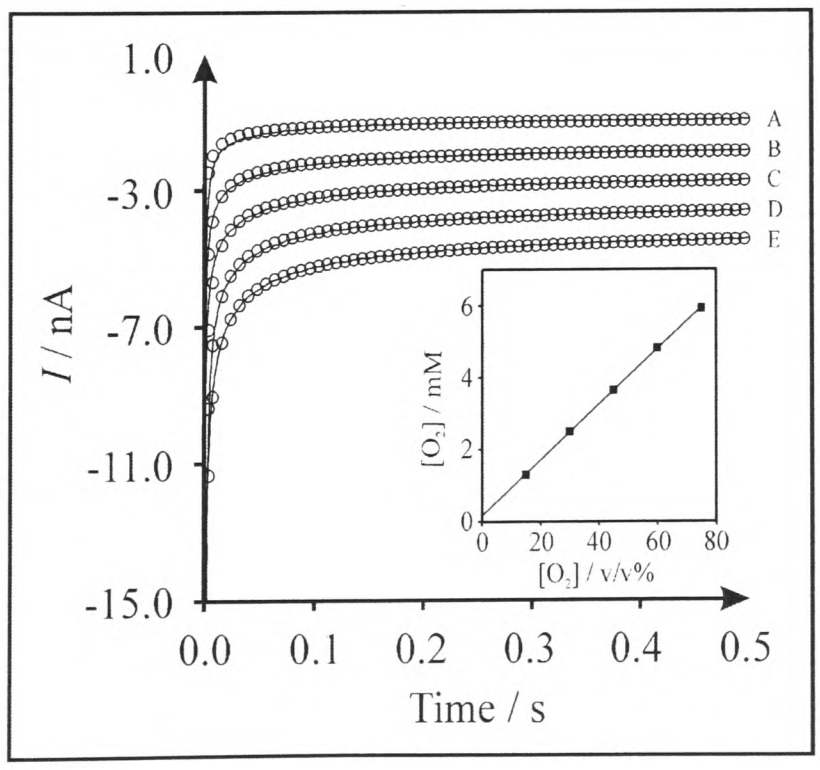


Figure 5.4
Experimental (—) and fitted theoretical (○) chronoamperometric transients for the reduction of (A) 15 (B) 30 (C) 45 (D) 60 and (E) 75 v/v% oxygen in $[N_{6222}][NTf_2]$ at a 10 µm Au disk electrode, T = 308 K. Inset shows the variation of oxygen concentration in solution (deduced from the transients) with the proportion of oxygen in the gas phase (R^2 = 0.9994). Fitting parameters are listed in Table 5.1.

the concentrations deduced directly proportional to the fraction of oxygen introduced to the cell. These data are typical of the results seen at the Au and Pt electrodes in both RTILs. At the GC electrode, however, the transients recorded were of lower quality and analysis by this means was unsuccessful. This is believed to be related to the rather large background current obtained at this electrode, which, as can be seen in Figure 5.2, is much larger than those present at the two metal electrodes and is beginning to swamp the signal of interest even using a pure oxygen atmosphere. Nevertheless, the data from two separate runs at each of the other two electrodes were averaged to give the final results, reported in Table 5.1. Encouragingly, these values are of the same order as equivalent data reported for oxygen in other ionic liquids.[11,13,23-25] Direct comparison is possible with the earlier work on $[N_{6222}][NTf_2]$ in which a concentration of 11.6 mM and diffusion coefficient of 1.5×10^{-10} m^2 s^{-1} were obtained at 293 K.[13] These results match up well with those from the current investigation and the discrepancy can be rationalised by considering the variation in temperature. A temperature increase would be expected to provoke an increase in the diffusion rate (owing to a decrease in the solvent viscosity) and at the same time a reduction in solubility of any gaseous solute, just as the data shows. Of the two quaternary ammonium RTILs studied, oxygen diffusion was more rapid in the

Table 5.1
Saturated concentration values and diffusion coefficients for oxygen in the four room temperature ionic liquid solvents at standard pressure and 308 K. Values are deduced from chronoamperometric measurements assuming in each case a simple one-electron transfer process.

	$[O_2]$ / mM	$D(O_2)$ / 10^{-10} m^2 s^{-1}
$[N_{6222}][NTf_2]$	8.9 ± 0.8	3.2 ± 0.3
$[Py_{14}][NTf_2]$	6.1 ± 0.8	5.2 ± 0.4
$[P_{14.666}][NTf_2]$	6.0 ± 0.5	7.5 ± 0.6
$[P_{14.666}][FAP]$	7.8 ± 1.5	6.1 ± 1.1

pyrrolidinium salt and this is again in accordance with its lower viscosity compared to that of $[N_{6222}][NTf_2]$ (95 mPa s *vs* 220 mPa s at 293 K).

To determine the remaining parameters for the electrochemical couple, experimental voltammograms were compared with computer simulations, starting with the now known values for $[O_2]$ and $D(O_2)$, and varying $D(O_2^{-\bullet})$, E_f^0, k_0 and α in order to reproduce the observed voltammetry as closely as possible. A good fit was achieved for each system, as displayed in Figure 5.5, and the optimal parameters are listed in

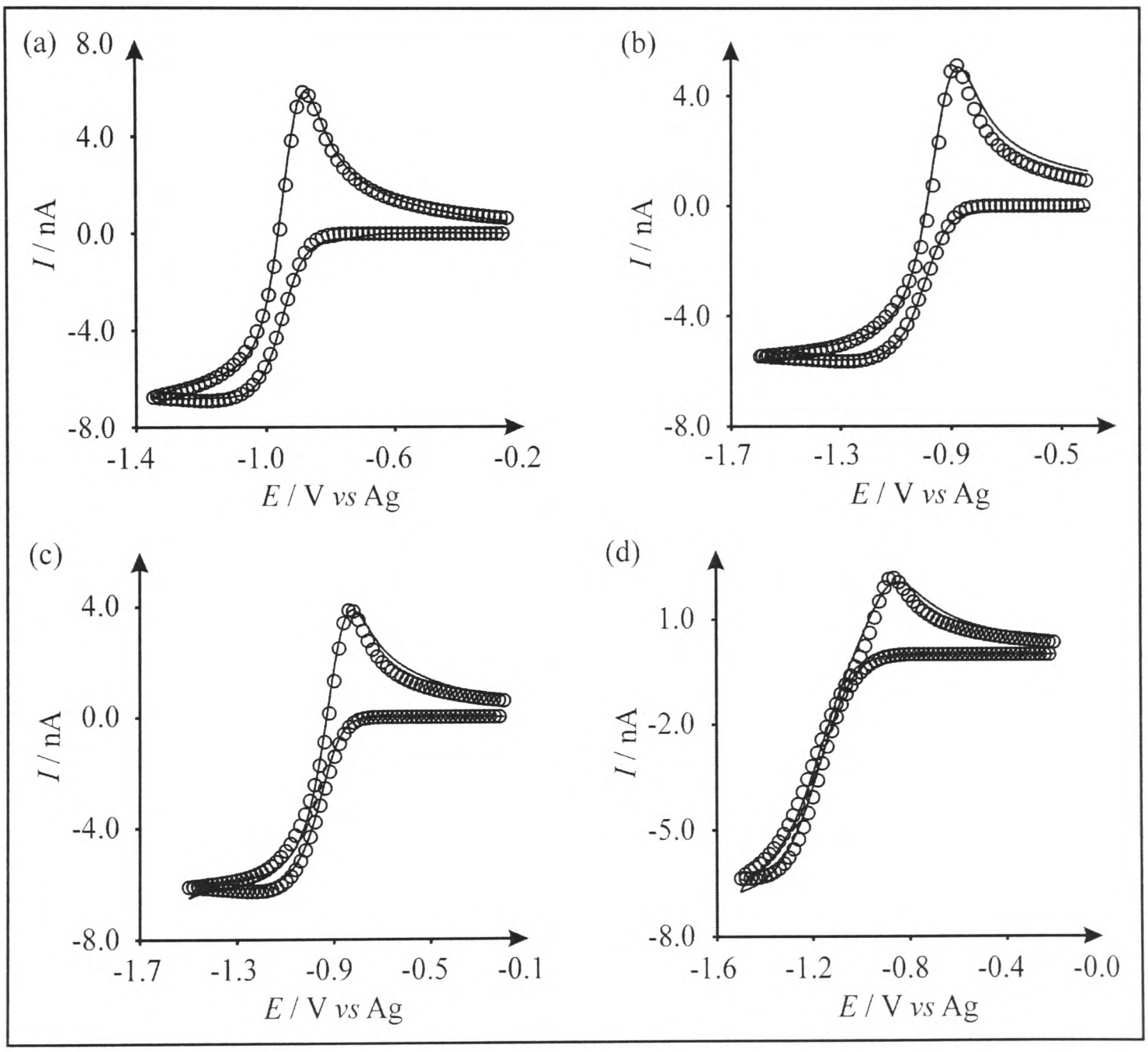


Figure 5.5
Comparison of experimental (—) and simulated (○) cyclic voltammograms for the reduction of oxygen in RTILs containing quaternary ammonium cations at 10 μm Au and Pt disk electrodes, $v = 1.0$ V s^{-1}. (a) Au / $[N_{6222}][NTf_2]$ (b) Au / $[Py_{14}][NTf_2]$ (c) Pt / $[N_{6222}][NTf_2]$ (d) Pt / $[Py_{14}][NTf_2]$. Simulation parameters are listed in Table 5.2.

Table 5.2
Electrochemical parameters for the reversible one-electron reduction of oxygen in two quaternary ammonium room temperature ionic liquids at 308 K.

		$D(O_2^{-\bullet})$ / 10^{-11} m^2 s^{-1}	E_f^0 / V *vs* Ag	k_0 / 10^{-3} cm s^{-1}	α
$[N_{6222}][NTf_2]$					
	Au	1.45	-0.89	5.0	0.35
	Pt	1.55	-0.91	3.0	0.33
$[Py_{14}][NTf_2]$					
	Au	3.35	-0.87	3.5	0.38
	Pt	3.50	-0.86	0.8	0.35

Table 5.2. Several points concerning these results merit some comment. The first thing to notice is that the values of $D(O_2^{-\bullet})$ and E_f^0 obtained for the same ionic liquid at the Au and Pt electrodes respectively are very similar. This bodes well for the accuracy of the simulations, since both these properties of the system should be independent of the electrode material. In both ionic liquids, the heterogeneous rate constant is lower on Pt than Au and the electron transfer coefficients are significantly below 0.5. This behaviour is analogous to that seen for reduction of oxygen in traditional organic solvents where low transfer coefficients at metal electrodes and especially sluggish kinetics at platinum electrodes have previously been reported.[3,5,26] Finally, regarding the superoxide diffusion coefficients, they are confirmed as being over an order of magnitude lower than those of oxygen in the same media. Presumably, this results from the difference in the strength of the coulombic forces between these highly ionic solvents and the neutral oxygen molecule and superoxide radical anion respectively. In any case, the combination of this disparity in the diffusion rates of the reduced and oxidised species with a disk electrode of appropriate radius explains the observed asymmetry in the voltammetry of this system. Over the same experimental timescale, the faster diffusion rate of oxygen causes a convergent diffusion layer to develop at the electrode surface leading

to steady-state behaviour, whereas supply of the more slowly moving superoxide is always dominated by planar diffusion normal to the surface, resulting in a peak-shaped transient reverse wave.

5.4.2 Reduction of Oxygen in the Quaternary Phosphonium RTILs

The second part of this investigation involves the voltammetry of oxygen in the two ionic liquids containing the quaternary phosphonium cation, $[P_{14.666}]$. Figure 5.6 shows cyclic voltammograms for the reduction of 100 v/v% O_2 in the RTIL $[P_{14.666}][FAP]$ at Au and Pt electrodes. While a steady-state forward wave similar to that seen for the quaternary ammonium ionic liquids is again observed, the oxidation peaks are broader and further removed from the initial reductive wave, in the case of the Pt electrode markedly so. The limiting currents derived from the forward wave again varied linearly with the proportion of oxygen gas introduced and a chronoamperometric analysis equivalent to the one described in the previous section (i.e. assuming that the process involved was the one-electron reduction of oxygen) was performed to attempt to deduce the O_2 concentration and diffusion coefficient. A

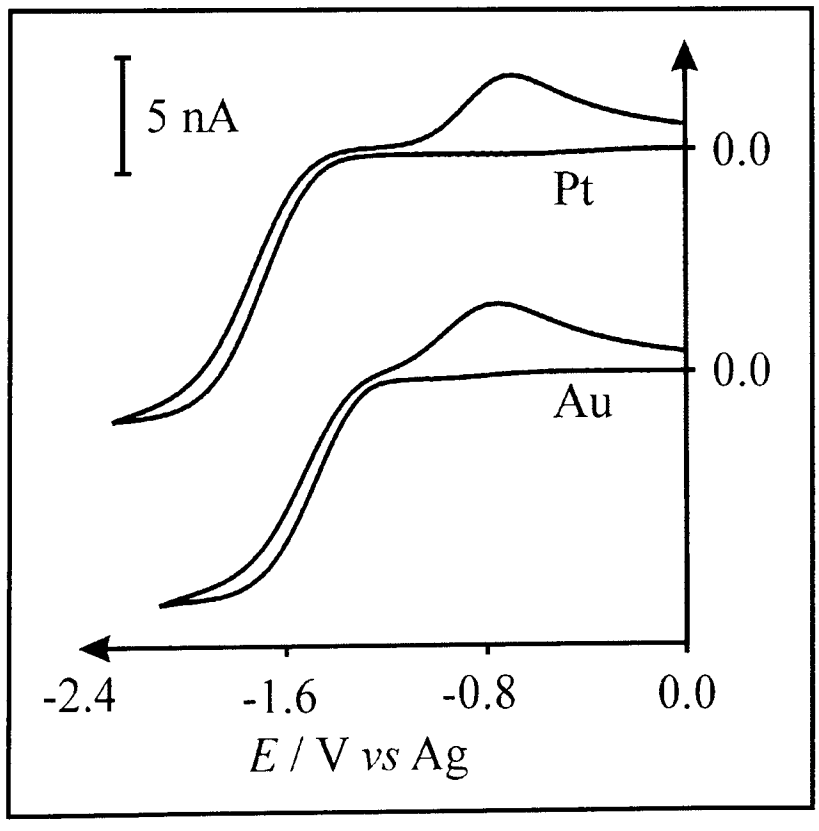


Figure 5.6
Cyclic voltammograms showing the reduction of oxygen in $[P_{14.666}][FAP]$ at 10 μm Au and Pt disk electrodes, $\nu = 0.5$ V s^{-1}, $T = 308$ K.

good correlation was again achieved and the derived values for $[O_2]$, and $D(O_2)$ are given in Table 5.1. It is interesting to note that the oxygen solubility does not vary significantly between the $[NTf_2]$ and [FAP] anions despite the large increase in the fluorine content. Using these values, a simulation of the observed voltammetry was attempted using the above model for a simple reversible single electron transfer. However, whilst the reductive wave could be quite successfully modelled, it was impossible to achieve at the same time a satisfactory fit of the back peak. This simple mechanism was therefore deemed inconsistent with the observed results. The current-voltage profile was in fact much more reminiscent of the voltammetry of oxygen in an aprotic solvent following the addition of a proton source (see above). Since the only species present are oxygen and the solvent itself, the most likely proton source is the quaternary phosphonium cation.

On this basis, an alternative mechanism is proposed involving α-proton abstraction from $[P_{14.666}]$ by superoxide:

$$O_2^{-\bullet} + R_3\overset{+}{P}CH_2R' \rightarrow HO_2^{\bullet} + R_3P{=}CHR' \qquad (5.04)$$

This is by no means unfeasible considering that the reaction of phosphonium ions with strong bases is well established, most notably in the Wittig alkene synthesis, in which the initial step is deprotonation to give a phosphorus ylide.[27] Furthermore, this would explain why a similar process is not observed with the quaternary ammonium salts, whose chemistry bears little in common with their phosphonium analogues; unlike nitrogen, phosphorus is able to adopt a pentacovalent state and is much better at stabilising a negative charge at an α-C.[27] One possible fate for the protonated form of superoxide is to undergo disproportionation to give hydrogen peroxide and regenerate oxygen:

$$2HO_2^{\bullet} \rightarrow H_2O_2 + O_2 \qquad (5.05)$$

In this way, the number of electrons for the forward process may vary between one and two, depending on the rate of reactions (5.04) and (5.05) relative to the experimental timescale. Having recognised this, it must be appreciated that the diffusion coefficients given for oxygen in Table 5.2 for the two phosphonium derived ionic liquids should be considered as upper bounds and their true values may be somewhat lower, depending on the exact number of electrons transferred. The peak observed on the reverse scan may result from oxidation of the phosphorus ylide or, conceivably, either the perhydroxyl radical itself or some oxygen derived species produced in follow up reactions. On repetitive cycling, the voltammetry showed little change and the emergence of no new peaks, implying that the oxidation is irreversible. In experiments with conventional organic solvents, the equivalent peak has been attributed to oxidation of the conjugate base from the Brønsted acid added as a proton source (here, the phosphorus ylide).[3,7] The electrochemical properties of phosphorus ylides have not been widely studied, but a single report on several such compounds in acetonitrile suggests that they are susceptible to being oxidised irreversibly to give highly reactive radical anions.[28]

To corroborate the proposed mechanism, the voltammetry of oxygen in $[N_{6222}][NTf_2]$ was reinvestigated upon addition of a proton source. A 25 mM solution of catechol in $[N_{6222}][NTf_2]$ was prepared, and Figure 5.7 shows the reduction of 100 v/v% oxygen at a Pt electrode in both the pure ionic liquid and the acidified solution. As catechol is a stronger acid than the $[P_{14.666}]$ ion, a shoulder due to the reduction of protons may be observed on the forward wave in the latter voltammogram. Nevertheless, the effect on the back peak is clear; the sharp peak at –0.89 V *vs* Ag is replaced by a broader

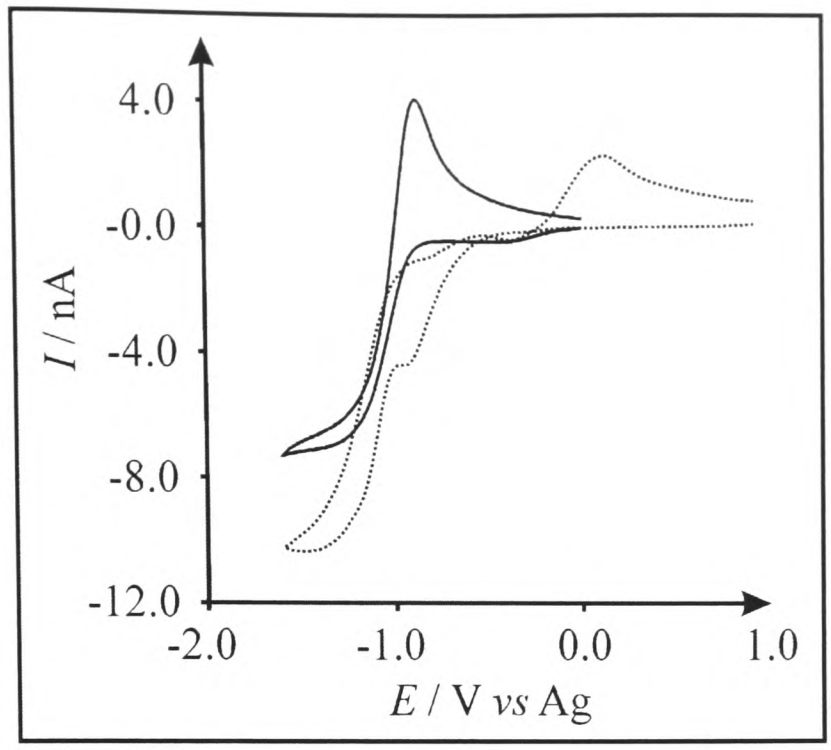


Figure 5.7
Cyclic voltammograms showing the reduction of 100 v/v % oxygen in $[N_{6222}][NTf_2]$ at a 10 μm Pt disk electrode in the presence (····) and absence (—) of 25 mM catechol, $v = 0.5$ V s^{-1}, $T = 308$ K.

signal displaced by *ca.* 0.8 V from the reduction wave, just as was observed in the phosphonium-based ionic liquids. This would suggest that the electroactive product responsible for the back peak is common to both systems, and is therefore an oxygen-derived species.

A full theoretical treatment of the voltammetry of oxygen in quaternary phosphonium RTILs is not straightforward given the number of species involved and the uncertainty in the exact nature of the follow up chemistry after the proton abstraction step. By employing a general $\vec{E}C\vec{E}$ model, however, it is possible to characterise the heterogeneous steps of the mechanism. Applying this model, the reaction is considered to proceed via an initial one-electron heterogeneous electron transfer followed by a diffusion-controlled, first-order, irreversible chemical step to yield another electroactive species, which then undergoes the second one-electron heterogeneous electron transfer (in the opposite direction to the first):

$$\begin{aligned} O_2 + e^- &\rightleftharpoons O_2^{\cdot-} && \vec{E} \\ O_2^{\cdot-} &\rightarrow \rightarrow X(\mathrm{Red}) && C \\ X(\mathrm{Red}) &\rightarrow X(\mathrm{Ox}) + e^- && \overleftarrow{E} \end{aligned} \qquad (5.06)$$

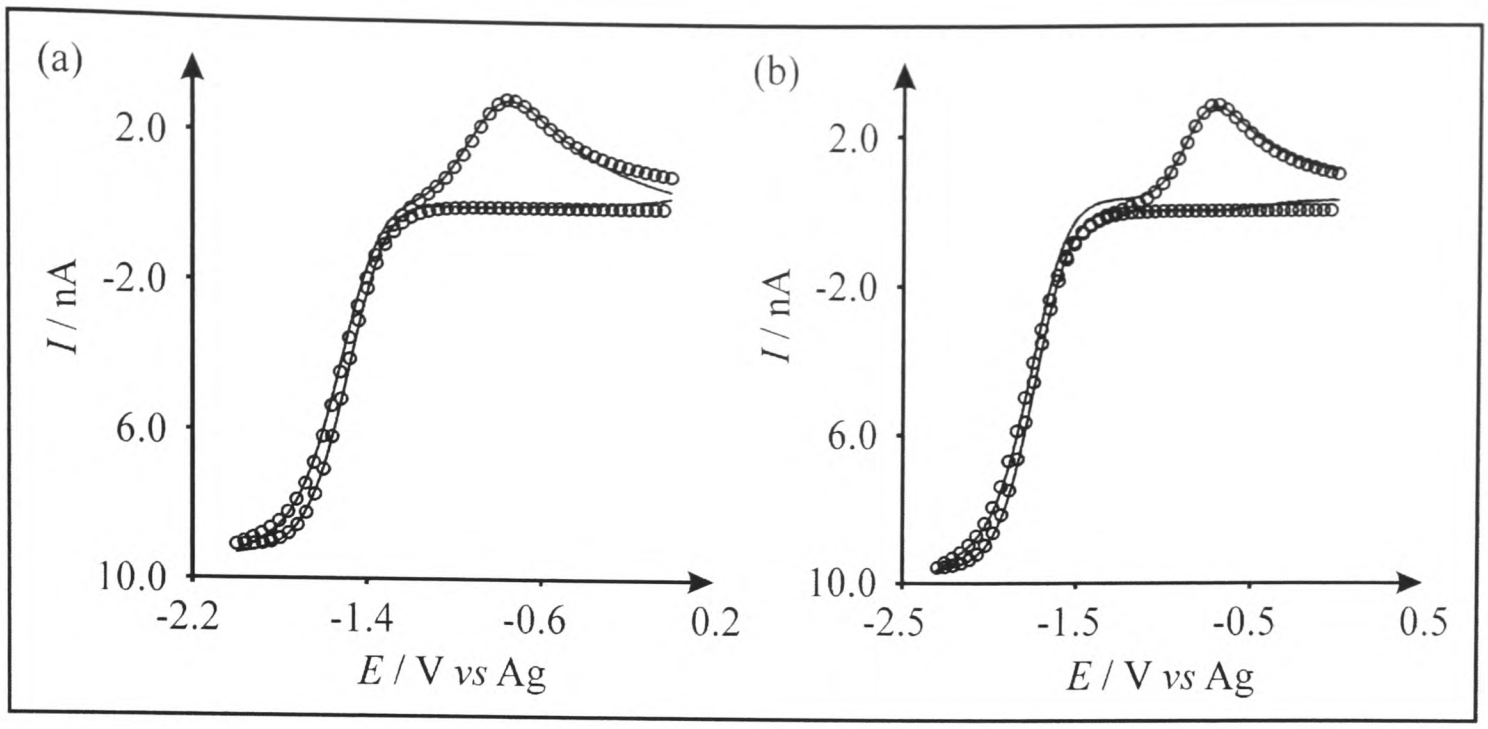


Figure 5.8
Comparison of experimental (—) and simulated (○) cyclic voltammograms for the reduction of oxygen in $[P_{14.666}][FAP]$ at 10 μm (a) Au and (b) Pt disk electrodes, v= 0.5 V s^{-1}. Simulation parameters are listed in Table 5.3.

where X(Red) and X(Ox) represent the reduced and oxidised forms of the electroactive species responsible for the oxidation peak on the reverse scan. The full details of this simulation are provided in an appendix. Fitting to the experimental voltammetry was achieved by applying the values of c and $D(O_2)$ calculated from the chronoamperometric measurements and then varying the remaining parameters systematically. The optimised values are shown in Table 5.3 and examples of the fits are displayed in Figure 5.8.

Table 5.3
Electrochemical parameters for the reduction of oxygen via an $\bar{E}C\bar{E}$ mechanism in two quaternary phosphonium room temperature ionic liquids at 308 K. The superscripts ' and '' refer to the first and second heterogeneous steps respectively, and X represents the species that undergoes the second electron transfer (see text).

		$E_f^{0'}$ / V *vs* Ag	k_0' / 10^{-3} cm s^{-1}	α'	D(X) / 10^{-11} m^2 s^{-1}	α''
$[P_{14.666}][NTf_2]$						
	Au	-0.75	1.77	0.38	0.59	0.63
	Pt	-0.75	0.14	0.31	0.41	0.69
$[P_{14.666}][FAP]$						
	Au	-1.10	0.11	0.32	0.31	0.75
	Pt	-1.10	0.05	0.25	0.37	0.75

5.5 Conclusions

Four room temperature ionic liquids comprised of group 15-centred cations and anions have been employed as electrolytes in which to study the electrochemical reduction of dioxygen. In the quaternary ammonium RTILs $[N_{6222}][NTf_2]$ and $[Py_{14}][NTf_2]$ the reduction was found to proceed reversibly (in the chemical sense) via the loss of one-electron to yield the superoxide radical which was stable in these media. Voltammetric and chronoamperometric data was analysed against the appropriate theoretical models to extract a full set of thermodynamic and kinetic parameters for this electrochemical couple. While the diffusion coefficients of oxygen and superoxide are found to be 10-100 times smaller than in simple organic solvents, in accordance with previous findings (and a consequence of the higher viscosity of RTILs), the results indicate that the process is otherwise not significantly altered; trends in the behaviour of the heterogeneous rate constant and electron transfer coefficient at different electrode materials were preserved. In contrast, the voltammetry of oxygen in the quaternary phosphonium RTILs $[P_{14.666}][NTf_2]$ and $[P_{14.666}][FAP]$ was found to proceed by a different mechanism. The presence of the weakly acidic $[P_{14.666}]$ renders superoxide unstable in these solvents with respect to the formation of a perhydroxyl radical and phosphorus ylide and, through follow up homogeneous reactions, the partial regeneration of O_2. Reduction of oxygen is therefore irreversible, involving the transfer of between one and two electrons. This behaviour represents an intermediate case between the one-election reduction of oxygen in aprotic organic solvents and the two-electron process observed in aqueous solution where the protonation and subsequent reactions of the superoxide are extremely rapid. Although a complete characterisation of this reaction scheme in the

RTILs will require further experimentation, a partial parameterisation of the heterogeneous steps was achieved through the application of a generalised $\vec{E}C\vec{E}$ mechanism.

5.6 Appendix: Simulating the $\vec{E}C\vec{E}$ Mechanism

The reaction mechanism described for the reduction of oxygen in the quaternary phosphonium ionic liquids may be written in symbolic form as:

$$\begin{aligned} &A + e^- \rightleftharpoons B \\ &B \underset{k^-}{\overset{k^+}{\rightleftharpoons}} C \\ &C \rightleftharpoons D + e^- \end{aligned} \qquad (5.07)$$

where A is oxygen, B is superoxide, k^+ is the rate constant of the forward homogeneous reaction and k^- is the rate constant of the reverse reaction. As explained above, the identity of species C is not known with absolute certainty. It is either some oxygen-derived species or the phosphorus ylide, but in the absence of further experimentation, neither possibility can be entirely ruled out. In any case, species D is then the product of its oxidation.

Reaction scheme (5.07) is considered as taking place at a disk electrode under cyclic voltammetric conditions. The mass transport equations describing the concentration distribution of the species in the solution are

$$\begin{aligned} \frac{\partial[A]}{\partial t} &= D_A\left(\frac{\partial^2[A]}{\partial r^2}+\frac{1}{r}\frac{\partial[A]}{\partial r}+\frac{\partial^2[A]}{\partial z^2}\right) \\ \frac{\partial[B]}{\partial t} &= D_B\left(\frac{\partial^2[B]}{\partial r^2}+\frac{1}{r}\frac{\partial[B]}{\partial r}+\frac{\partial^2[B]}{\partial z^2}\right)-k^+[B]+k^-[C] \\ \frac{\partial[C]}{\partial t} &= D_C\left(\frac{\partial^2[C]}{\partial r^2}+\frac{1}{r}\frac{\partial[C]}{\partial r}+\frac{\partial^2[C]}{\partial z^2}\right)+k^+[B]-k^-[C] \end{aligned} \qquad (5.08)$$

where D_A is the diffusion coefficient of species A etc., r and z are cylindrical coordinates and t is time. Initially the solution contains only species A at a bulk concentration, $[A]_{bulk}$, which leads to the following initial conditions:

$$\begin{aligned} &[A](r,z,0) = [A]_{bulk} \\ &[B](r,z,0) = [C](r,z,0) = 0 \end{aligned} \tag{5.09}$$

The system of partial differential equations (5.08) must be completed with the following boundary conditions given by applying the Butler-Volmer theory at the electrode surface, a no flux condition at the insulator and symmetry axes and bulk concentration values far away from the electrode:

$$z = 0,\ 0 \le r \le r_d \qquad D_A \left.\frac{\partial [A]}{\partial z}\right|_{z=0} = \left(k_f'[A] - k_b'[B]\right)_{z=0};$$

$$D_B \left.\frac{\partial [B]}{\partial z}\right|_{z=0} = -D_A \left.\frac{\partial [A]}{\partial z}\right|_{z=0};\ D_C \left.\frac{\partial [C]}{\partial z}\right|_{z=0} = k_f'' [C]_{z=0}$$

$$z = 0,\ r > r_d \qquad \left.\frac{\partial [A]}{\partial z}\right|_{z=0} = \left.\frac{\partial [B]}{\partial z}\right|_{z=0} = \left.\frac{\partial [C]}{\partial z}\right|_{z=0} = 0 \tag{5.10}$$

$$\text{all } z,\ r = 0 \qquad \left.\frac{\partial [A]}{\partial r}\right|_{r=0} = \left.\frac{\partial [B]}{\partial r}\right|_{r=0} = \left.\frac{\partial [C]}{\partial r}\right|_{r=0} = 0$$

$$z, r \to \infty \qquad [A] \to [A]_{bulk};\ [B] \to 0;\ [C] \to 0$$

Here, the forward (marked with a subscript *f*) and backward (marked with a subscript *b*) heterogeneous rate constants are given by

$$k_f' = k_0' \exp\left(\frac{-\alpha' F}{RT}\left(E - E_f^{0\prime}\right)\right);\quad k_b' = k_0' \exp\left(\frac{(1-\alpha') F}{RT}\left(E - E_f^{0\prime}\right)\right)$$

$$k_f'' = k_0'' \exp\left(\frac{(1-\alpha'') F}{RT}\left(E - E_f^{0\prime\prime}\right)\right) \tag{5.11}$$

where k_0' and k_0'' are the standard heterogeneous rate constants, α' and α'' are transfer coefficients and $E_f^{0\prime}$ and $E_f^{0\prime\prime}$ are the formal potentials of the redox couples A/B and C/D in the first and the third steps of (5.07) respectively.

The boundary condition for species C at the electrode surface given in (5.10) is used instead of the full Butler-Volmer expression due to the high irreversibility of the third reaction in mechanism (5.07) (see above); the reduction of species D back to C contributes negligibly to the current and thus the corresponding term $(-k_b''[\mathrm{D}])$ has been dropped from the boundary condition. Consequently, the mass transport equation for species D has not been considered. It follows that in this case it is impossible to determine the values of the standard heterogeneous rate constant k_0'' and the formal potential $E_f^{0\prime\prime}$ independently. Indeed, the boundary condition for species C depends only on k_f'' and not on k_b''. The former may be represented as:

$$k_f'' = k_0'' \exp\left(\frac{(\alpha''-1)FE_f^{0\prime\prime}}{RT}\right)\exp\left(\frac{(1-\alpha'')FE}{RT}\right) = k_0(\alpha'')\exp\left(\frac{(1-\alpha'')FE}{RT}\right) \quad (5.12)$$

Obviously there are an infinite number of pairs k_0'', $E_f^{0\prime\prime}$ corresponding to the same value of $k_0(\alpha'')$. Therefore it is impossible to find a unique solution for these two parameters. The current flowing at the surface of a disk electrode is given by the following integral:

$$I = 2\pi F D_{\mathrm{A}} \int_0^{r_d} \left(\frac{\partial[\mathrm{C}]}{\partial z} - \frac{\partial[\mathrm{A}]}{\partial z}\right)_{z=0} r\,\mathrm{d}r \quad (5.13)$$

The mathematical model (5.08–5.10) was normalised with subsequent application of the coordinate transformation developed by Amatore and Fosset for disk electrode geometry.[20] The resulting equations were then discretised according to the ADI

method.[21,22] The banded systems of linear algebraic equations produced by the implicit ADI method were solved using the generalised Thomas algorithm.[29]

An error analysis similar to that described previously[13,30,31] was applied to determine the simulation grid size necessary to achieve the desired accuracy for the expected ranges of the parameter variation. This resulted in a spatial grid size of 350x350 ($N\theta$ x $N\Gamma$) required to achieve the accuracy of not worse than 1%. Such a high number of mesh nodes in space is necessitated by the fact that the diffusion coefficients of the reacting species may differ by more than two orders of magnitude.[13] A typical computational time for simulation of a cyclic voltammogram within 1% accuracy was approximately 20 minutes. However, significantly smaller grids can be used for the initial fitting of the experimental voltammograms with less computational effort and the final verification performed at a 300x300 grid.

The convergence error appeared to be virtually independent of the discretisation in time. Therefore the number of points in time was kept constant at 2000 to ensure the smoothness of the simulated voltammograms.

This study had demonstrated the occurrence of widely differing diffusion coefficients between parent and electrogenerated species in a room temperature ionic liquid and it was decided to next investigate the generality of this phenomenon. Given the success with using chronoamperometric techniques, a double potential step experiment was envisaged to accomplish this. As such, it was first prudent to develop the theory necessary to interpret the current response.

5.7 References

[1] R.G. Evans, O.V. Klymenko, S.A. Saddoughi, C. Hardacre, R.G. Compton, *J. Phys. Chem. B* **2004**, *108*, 7878.

[2] D.T. Sawyer, A. Sobkowiak, J.L. Roberts, *Electrochemistry for Chemists*, Wiley Interscience, New York, **1995**.

[3] D.T. Sawyer, G. Chiericato, Jr., C.T. Angelis, E.J. Nanni, Jr., T. Tsuchiya, *Anal. Chem.* **1982**, *54*, 1720.

[4] J.D. Wadhawan, P.J. Welford, H.B. McPeak, C.E.W. Hahn, R.G. Compton, *Sens. Actuators B* **2003**, *B88*, 40.

[5] D. Vasudevan, H. Wendt, *J. Electroanal. Chem.* **1995**, *392*, 69.

[6] P. Cofre, D.T. Sawyer, *Anal. Chem.* **1986**, *58*, 1057.

[7] C.P. Andrieux, P. Hapiot, J.M. Saveant, *J. Am. Chem. Soc.* **1987**, *109*, 3768.

[8] M.C. Buzzeo, R.G. Evans, R.G. Compton, *ChemPhysChem* **2004**, *5*, 1106.

[9] M.T. Carter, C.L. Hussey, S.K.D. Strubinger, R.A. Osteryoung, *Inorg. Chem.* **1991**, *30*, 1149.

[10] M.C. Buzzeo, O.V. Klymenko, J.D. Wadhawan, C. Hardacre, K.R. Seddon, R.G. Compton, *J. Phys. Chem. B* **2004**, *108*, 3947.

[11] I.M. AlNashef, M.L. Leonard, M.C. Kittle, M.A. Matthews, J.W. Weidner, *Electrochem. Solid-State Lett.* **2001**, *4*, D16.

[12] I.M. AlNashef, M.L. Leonard, M.A. Matthews, J.W. Weidner, *Ind. Eng. Chem. Res.* **2002**, *41*, 4475.

[13] M.C. Buzzeo, O.V. Klymenko, J.D. Wadhawan, C. Hardacre, K.R. Seddon, R.G. Compton, *J. Phys. Chem. A* **2003**, *107*, 8872.

[14] D.R. MacFarlane, P. Meakin, J. Sun, N. Amini, M. Forsyth, *J. Phys. Chem. B* **1999**, *103*, 4164.

[15] K. Xu, M.S. Ding, T.R. Jow, *J. Electrochem. Soc.* **2001**, *148*, A267.

[16] J. Sun, M. Forsyth, D.R. MacFarlane, *J. Phys. Chem. B* **1998**, *102*, 8858.

[17] A.B. McEwen, E.L. Ngo, K. LeCompte, J.L. Goldman, *J. Electrochem. Soc.* **1999**, *146*, 1687.

[18] R.G. Evans, O.V. Klymenko, C. Hardacre, K.R. Seddon, R.G. Compton, *J. Electroanal. Chem.* **2003**, *556*, 179.

[19] D. Shoup, A. Szabo, *J. Electroanal. Chem.* **1982**, *140*, 237.

[20] C.A. Amatore, B. Fosset, *J. Electroanal. Chem.* **1992**, *328*, 21.

[21] J. Heinze, *J. Electroanal. Chem.* **1981**, *124*, 73.

[22] I.B. Svir, O.V. Klimenko, R.G. Compton, *Radiotekhnika* **2001**, *118*, 92.

[23] Y. Katayama, K. Sekiguchi, M. Yamagata, T. Miura, *J. Electrochem. Soc.* **2005**, *152*, E247.

[24] M.C. Buzzeo, C. Hardacre, R.G. Compton, *Anal. Chem.* **2004**, *76*, 4583.

[25] J.L. Anthony, E.J. Maginn, J.F. Brennecke, *J. Phys. Chem. B* **2002**, *106*, 7315.

[26] P.S. Jain, S. Lal, *Electrochim. Acta* **1982**, *27*, 759.

[27] L.D. Quin, *A Guide to Organophosphorus Chemistry*, Wiley, New York, **2000**.

[28] V.I. Monastyrskaya, K.K. Kalnin'sh, B.N. Strunin, A.G. Tsalieva, *Russ. J. Gen. Chem.* **1997**, *67*, 570.

[29] K. Eriksson, D. Estep, P. Hansbo, C. Johnson, *Computational Differential Equations*, Cambridge University Press, Cambridge, **1996**.

[30] O.V. Klymenko, D. Giovanelli, N.S. Lawrence, N.V. Rees, L. Jiang, T.G.J. Jones, R.G. Compton, *Electroanalysis* **2003**, *15*, 949.

[31] N.V. Rees, O.V. Klymenko, R.G. Compton, M. Oyama, *J. Electroanal. Chem.* **2002**, *531*, 33.

6 Double Potential Step Chronoamperometry at Disk Electrodes: Simulating the Case of Unequal Diffusion Coefficients

An efficient approach to the simulation of double potential step chronoamperometry at a disk electrode is presented, based on an exponentially expanding time grid and conformal mapping of the two spatial coordinates. Dimensionless second potential step flux data are calculated as a function of the first potential step duration and the ratio of the diffusion coefficients of the redox species, allowing instant analysis of experimental double potential step chronoamperograms without the need for recourse to simulation. Values of the diffusion coefficients are determined for several test systems and found to be in good agreement with existing literature data. This work involved significant collaboration between the author and Dr. Oleksiy V. Klymenko, the latter's responsibility being to both select the strategy for and program the simulation, while all experimentation and data fitting was carried out by the former. It has been published in the *Journal of Electroanalytical Chemistry*.[1]

6.1 Introduction

In mechanistic electrochemistry, an accurate determination of the diffusion coefficients of all species involved is crucial in order for a rigorous assessment of the heterogeneous and any subsequent homogeneous processes occurring to be made. Yet, while a whole range of electrochemical techniques may be readily analysed to measure the diffusion coefficient of the initial electroactive species, the equivalent parameter for the electrogenerated species is, in general, not so easily gauged. Furthermore, despite being of similar chemical composition and size, these two

species may differ significantly in their rate of diffusion, depending on the solvent system employed and the difference in charge between the two molecules. This point is emphasised in recent reports concerning the reduction of oxygen to superoxide in room temperature ionic liquid solvents;[2,3] the coefficient for the electrogenerated superoxide was consistently determined to be at least one order of magnitude lower than that of the parent oxygen molecule.

Chronoamperometry has been a widely applied technique in electrochemistry for measuring diffusion coefficients[4-6] and even rate constants of homogeneous reactions.[7,8] The main advantage of this method is its simplicity, since it does not require any complicated potential-time dependences. There exist exact solutions or analytical approximations for chronoamperometric currents at electrodes of various shapes and hence with different diffusion patterns such as planar,[9-11] spherical,[9] cylindrical,[12] band[13] and disk electrodes.[14-16] In the case of single potential step chronoamperometry at a disk electrode, the varying influence of both convergent and planar diffusion over the experimental timescale may be exploited to allow deconvolution of both the diffusion coefficient and concentration of the electroactive species from a single transient based only on a knowledge of the disk radius.[17]

The current study focuses on the case of double potential step chronoamperometry at a disk electrode for which both planar and convergent diffusion are significant processes.[4-6,18,19] The current response from such a perturbation is dependent upon the diffusion coefficients of both the initial species and the product of its electrolysis. There have been attempts in the literature to treat this problem analytically. Galus et al. presented an approximate solution to the problem based on the assumptions of equal diffusion coefficients and planar diffusion, which obviously has very limited

applicability.[18] A more accurate solution, also for the case of equal diffusion coefficients was derived by Yu and Zhang.[19] However, the problem at hand has not yet been solved analytically and existing numerical approaches to the simulation of double potential step chronoamperometry at a disk cannot be relied upon since they utilise uniform grids.[5,6] It has been shown that for the case of single potential step chronoamperometry, such an approach introduces a high error into the calculated current for long dimensionless times ($\tau > 0.1$, see below) despite the fact that uniform grid approach is perfectly suited for very short electrolysis times.[20] This is caused by an increasing influence on the current from the boundary singularity, which cannot be properly treated using uniformly spaced grids. Apart from this singularity caused by the electrode geometry, there are also singularities in time arising at the points at which the potential is switched. Since transport-limited conditions are imposed at the electrode surface, the concentration gradients take (theoretically) infinite values at these time points enforcing severe restrictions on the stability of the numerical methods and hence onto the time step length. Therefore, simulations with a time step sufficiently small to eliminate non-physical oscillations in the solution could lead to excessively lengthy CPU times when long transients have to be simulated. The approach described in this chapter is aimed at resolving both time and space singularities while minimising the CPU time required for computation.

6.2 Theory Section

6.2.1 The Mathematical Model

Consider an uncomplicated electron transfer reaction:

$$A \rightleftharpoons B + e^- \qquad (6.01)$$

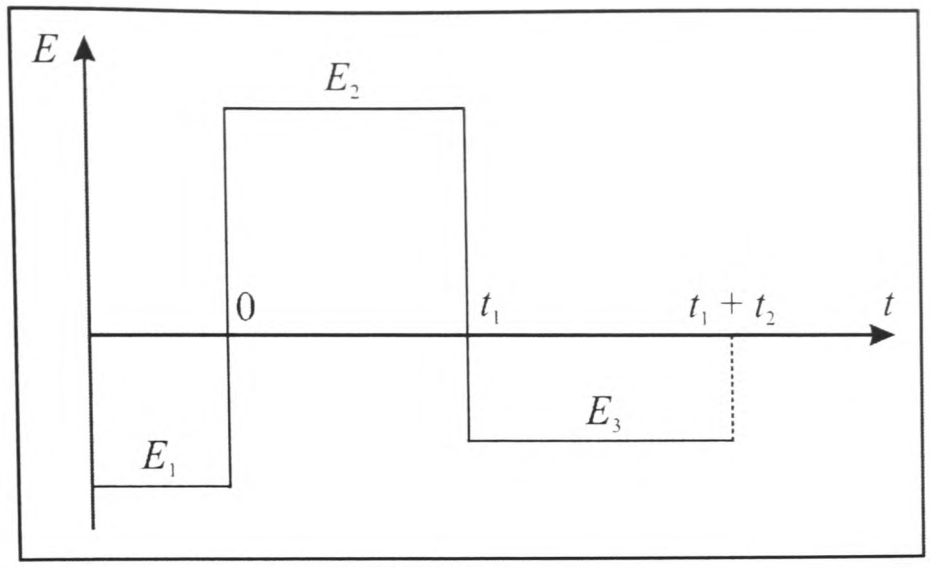


Figure 6.1
The potential waveform applied during a double potential step chronoamperometric experiment.

taking place at the surface of a disk electrode of radius r_d. Suppose that initially, the potential is held at a sufficiently negative value, E_1, with respect to the formal potential of the A/B couple, E_f^0, such that there is negligible current flow. Then, at time $t = 0$ the potential is jumped to a value, E_2, sufficiently positive with respect to E_f^0 to ensure diffusion controlled oxidation in (6.01), and held at this level for t_1 seconds (Figure 6.1). Finally, the potential is again switched such that it is now once more negative with respect to E_f^0, at value E_3, ensuring diffusion-controlled conditions for a reverse (reduction) reaction in (6.01). The duration of the second pulse is denoted by t_2 (Figure 1). The mass transport of species A and B in the bulk solution during the course of the experiment is described by the following system of partial differential equations, written in the cylindrical polar coordinates due to the cylindrical symmetry of the disk electrode:

$$\frac{\partial[\mathrm{A}]}{\partial t} = D_{\mathrm{A}}\left(\frac{\partial^2[\mathrm{A}]}{\partial r^2} + \frac{1}{r}\frac{\partial[\mathrm{A}]}{\partial r} + \frac{\partial^2[\mathrm{A}]}{\partial z^2}\right)$$
$$\frac{\partial[\mathrm{B}]}{\partial t} = D_{\mathrm{B}}\left(\frac{\partial^2[\mathrm{B}]}{\partial r^2} + \frac{1}{r}\frac{\partial[\mathrm{B}]}{\partial r} + \frac{\partial^2[\mathrm{B}]}{\partial z^2}\right) \qquad (6.02)$$

where [ ] denotes concentration, D_{A} and D_{B} the diffusion coefficients of the corresponding species and r, z are the cylindrical coordinates. At the beginning of the

experiment it is assumed that the solution contains exclusively species A at a bulk concentration $[A]_{bulk}$. This forms the initial conditions for equations (6.02):

$$t = 0 \quad [A] = [A]_{bulk}\,; \; [B] = 0 \tag{6.03}$$

Since diffusion-controlled conditions are maintained at the electrode surface at all times (except at the moments when the potential is switched from one value to another; however these changes are assumed to be instantaneous) the boundary conditions at the surface of a disk can be written as:

$$0 < r \le r_d\,, \; z = 0 \qquad [A] = 0\,; \; D_A\, \partial[A]/\partial z = -D_B\, \partial[B]/\partial z \tag{6.04}$$

for the first potential step ($0 < t \le t_1$) and

$$0 < r \le r_d\,, \; z = 0 \qquad [B] = 0\,, \; D_A\, \partial[A]/\partial z = -D_B\, \partial[B]/\partial z \tag{6.05}$$

for the second potential step ($t_1 < t \le t_1+t_2$). Zero flux conditions are imposed at the insulator boundaries and the axis of symmetry:

$$\begin{aligned} r > r_d,\; z = 0 \qquad & \partial[A]/\partial z = \partial[B]/\partial z = 0 \\ r = 0,\; z \ge 0 \qquad & \partial[A]/\partial r = \partial[B]/\partial r = 0 \end{aligned} \tag{6.06}$$

and the bulk concentrations far away from the electrode:

$$r \to \infty\,, \; z \to \infty \qquad [A] \to [A]_{bulk}\,, \; [B] \to 0 \tag{6.07}$$

The mathematical model represented by equations (6.02–6.07) may be cast into a dimensionless form by normalising the spatial coordinates and time as $R = r/r_d$, $Z = z/r_d$, $\tau = D_A\, t/r_d^2$ and the concentrations as $a = [A]/[A]_{bulk}$ and $b = [B]/[B]_{bulk}$. The conformal mapping of the R,Z-plane onto a unit square proposed by Amatore and Fosset is then applied.[21] Although this transformation exhibits best performance at large times (i.e. near steady state) it allows for reasonably accurate results at short times (see ref. [21]) and does not require any further grid adaptation. The following

expressions:

$$R = \sqrt{1-\theta^2}\,/\cos(\pi\Gamma/2)$$
$$Z = \theta\tan(\pi\Gamma/2) \qquad (6.08)$$

relate R and Z to the transformed coordinates θ,Γ. Applying this transformation, the diffusion equations (6.02) are rewritten as:

$$\frac{\partial a}{\partial \tau} = \nabla^2_{\theta,\Gamma} a$$
$$\frac{\partial b}{\partial \tau} = \frac{D_B}{D_A}\nabla^2_{\theta,\Gamma} b \qquad (6.09)$$

where $\nabla^2_{\theta,\Gamma}$ stands for the Laplacian operator in the new coordinates:

$$\nabla^2_{\theta,\Gamma} = \frac{1}{\theta^2 + \tan^2(\pi\Gamma/2)}\left\{\frac{4}{\pi^2}\cos^2\left(\frac{\pi\Gamma}{2}\right)\frac{\partial^2}{\partial\Gamma^2} + \frac{\partial}{\partial\theta}\left[\left(1-\theta^2\right)\frac{\partial}{\partial\theta}\right]\right\} \qquad (6.10)$$

The transformed boundary conditions complementing mass transport equations (6.09) are given in Table 6.1 where τ_1 represents the normalised duration of the first potential step.

The normalised current passing through the electrode surface at any time can be expressed in the new coordinates as

$$g(\tau) = \frac{I}{4FD_A[A]_{bulk} r_d} = \int_0^1 \frac{\partial a}{\partial\Gamma}\mathrm{d}\theta = -\frac{D_B}{D_A}\int_0^1 \frac{\partial b}{\partial\Gamma}\mathrm{d}\theta \qquad (6.11)$$

After normalisation, the mathematical model of the double potential step at a disk

Table 6.1
Boundary conditions for the transformed mass transport equations (6.09).

Boundary	Conditions
$0 \le \theta \le 1, \Gamma = 0$	$a = 0$ $(\tau \le \tau_1)$; $b = 0$ $(\tau > \tau_1)$; $\partial a/\partial\Gamma = -(D_B/D_A)\partial b/\partial\Gamma$ (all τ)
$\theta = 0, 0 < \Gamma < 1$	$\partial a/\partial\theta = \partial b/\partial\theta = 0$
$\theta = 1, 0 < \Gamma < 1$	$\partial a/\partial\theta = \partial b/\partial\theta = 0$
$0 \le \theta \le 1, \Gamma = 1$	$a = 0$; b=0

electrode has only three independent parameters, the dimensionless durations of the potential steps τ_1 and τ_2 and the ratio of the diffusion coefficients of the species A and B, D_A / D_B.

The numerical simulation of the mathematical model given by equations (6.09) and Table 6.1 was performed using the Alternating Direction Implicit (ADI) method at a uniform spatial grid in θ,Γ-coordinates.[2,22,23] The approach to the construction of the time grid is described in the following section.

6.2.2 The Expanding Time Grid

Typically in the numerical simulations of electrochemical problems. discretisation of time derivatives is performed on uniform grids, an approach that allows simplification of the analysis of the numerical scheme and programming. However, the use of uniform grids can lead to an unacceptably large number of time steps and hence to long simulation times. This is caused by requirements on the accuracy and/or stability of the simulation procedure, which introduce restrictions for the length of the time step. The accuracy of the simulation varies at different times since the generally nonlinear function *dc/dt* is sampled at a uniform grid. A better approach for the general case would be an adaptive time grid, although this requires sophisticated analysis and might be computationally rather time consuming. However, in cases where one has a priori knowledge of the concentration behaviour, a nonuniform grid may be predefined, significantly decreasing the amount of computation required.

In the case of the problem under consideration, the time step must be very small after the potential jumps, when rapid changes in the concentration gradients occur near to the electrode surface. However, at larger times the concentration distribution near the electrode becomes near steady-state while the diffusion front continues its

propagation into the bulk of the solution. Because no rapid changes in the concentration distribution take place at those times, the length of the time step here can be much larger than those immediately following a potential step.

Here, an exponentially expanding time grid is adopted following the approach suggested by Amatore and Svir.[20,24] At the beginning of each potential step the simulation is performed at a uniform grid with the step size $\Delta\tau_0$ for a short period of time τ_0. The value of τ_0 must be chosen high enough to ensure that the initial time singularity does not affect the stability of the simulation procedure for $\tau > \tau_0$ ($\tau > \tau_1+\tau_0$ for the second potential step correspondingly). However, it should be small enough to provide the shortest possible simulation time. In the following, the value τ_0 was assumed to be 0.025 and this interval was divided into $N\tau_0 = 500$ initial time steps of length $\Delta\tau_0 = 5 \times 10^{-5}$. This provides efficient smoothening out of the errors in current evaluation caused by the time singularities.

After initial simulation at uniform time grid at the beginning of each potential step the time step is then steadily increased according to the following expression:

$$\Delta\tau_{k+1} = (1+\omega)\Delta\tau_k, \quad \omega > 0, \quad k \geq N\tau_0 \tag{6.12}$$

where k is the time iteration index and ω is the grid expansion coefficient. The time grid is therefore exponentially expanding for the course of simulation (except for the intervals $0 < \tau \leq \tau_0$ and $\tau_1 < \tau \leq \tau_1+\tau_0$) with the expansion speed controlled by the parameter ω.

6.2.3 Fitting and Computation

In order to automatize the fitting process the Nelder-Mead (or downhill simplex) minimisation algorithm was applied.[25,26] The advantage of this algorithm is its easy implementation; the method does not require evaluation of function derivatives and

converges rather quickly provided that a reasonable initial guess is given. The function to be minimised in this case is a weighted sum of squared differences:

$$SSQ\left(D_{\mathrm{A}}, D_{\mathrm{B}}\right) = \sum_{k} w_k \left(i_k - i_k^{th}\right)^2 \qquad (6.13)$$

between the experimentally measured (i_k) and theoretical (i_k^{th}) currents, where w_k is the weight of the *k*th value of the current defined as:

$$w_k = \left(1 + \left| i_k^{th} \right|\right)^{-1} \qquad (6.14)$$

This non-uniform weighting is used here to even out the highly nonuniform current distribution, therefore providing a regular quality of fit.

The program for simulating double potential step chronoamperometry was written in Borland Delphi 7 Professional Edition and executed on a PC with an Intel Pentium 4 3.07 GHz processor and 1Gb of RAM.

6.3 Experimental Section

In addition to matters already covered in chapter three, aqueous solutions were prepared using deionised water from a Vivendi water system with a resistivity not less than 18.2 MΩ cm. Solutions in aqueous and the simple organic solvents were degassed with argon for ten minutes prior to the commencement of electrochemical measurements. A saturated calomel electrode (SCE, Radiometer, Copenhagen) was employed as the reference in the case of aqueous systems. The fast scan voltammetry (> 500 V s^{-1}), which was conducted using a custom built fast scan potentiostat capable of scan rates of up to 2 MV s^{-1} with ohmic drop compensation. This latter potentiostat is analogous to that described and utilised by Amatore et al..[27,28] The potential was applied with a TTi TG1304 programmable function generator (Thurlby

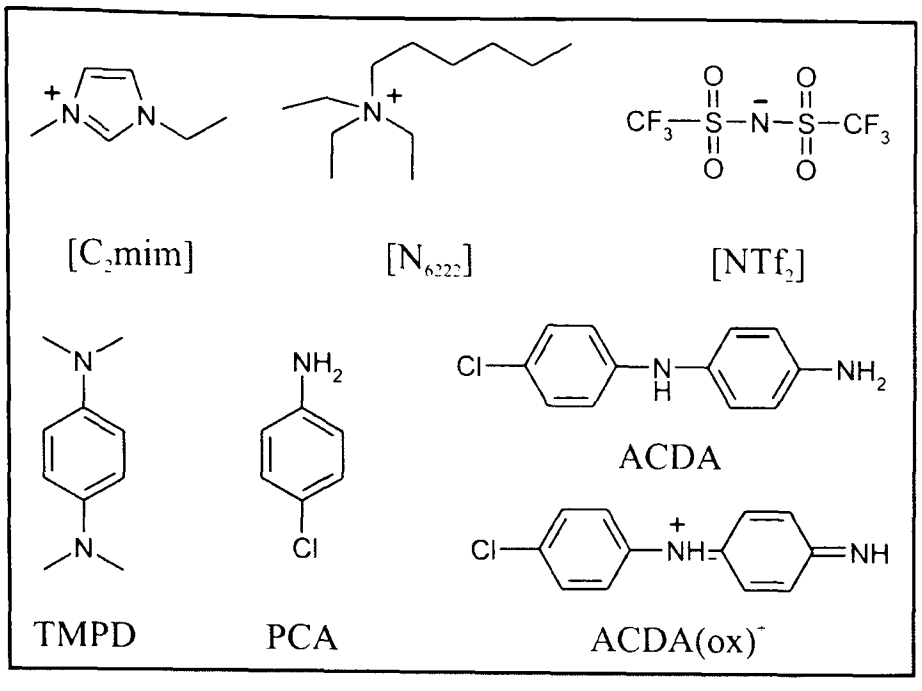


Figure 6.2
Structures of the ions: 1-ethyl-3-methylimidazolium [C_2mim], *n*-hexyltriethylammonium [N_{6222}] and bis(trifluoromethylsulfonyl)imide [NTf_2], the molecules: N,N,N',N'-tetramethyl-*para*-phenylenediamine (TMPD) and *p*-chloroaniline (PCA) and the dimer 4-amino-4'-chloro-diphenylamine in its reduced (ACDA) and oxidised (ACDA(ox)$^+$) forms.

Thandar Instruments Ltd., Huntingdon) and the current recorded with a Tektronix TDS 3032 oscilloscope (300 MHz band-pass, 2.5 GS/s).

This study utilized gold and platinum disk working electrodes, nominal diameters 10 μm (Au) and 100 μm (Pt). The structures of the more complex chemical species are shown in Figure 6.2. Experiments were carried out at a temperature of 298 ± 1 K.

6.4 Results and Discussion

6.4.1 Theoretical Results

Figure 6.3 shows the convergence of the first potential step current to the analytical approximation by Aoki and Osteryoung[14,15] as a function of spatial grid size for a fixed value of the grid expansion parameter $\omega = 10^{-3}$. Note that the errors are plotted against the normalised time introduced in refs. [14,15], $4Dt/r_d^2 = 4\tau$ as τ was defined in section 6.2.1. As the figure shows, a grid of the size $N\theta$ x $N\Gamma$ = 100 x 100 gives a convergence of not worse than 0.5% for all times considered. The highest error in the current is observed at very short times when diffusion towards a disk electrode is mostly planar and the coordinate transformation (6.08) does not perform very well, and around $4\tau = 1$. The latter is attributed to the errors in the approximate solution,

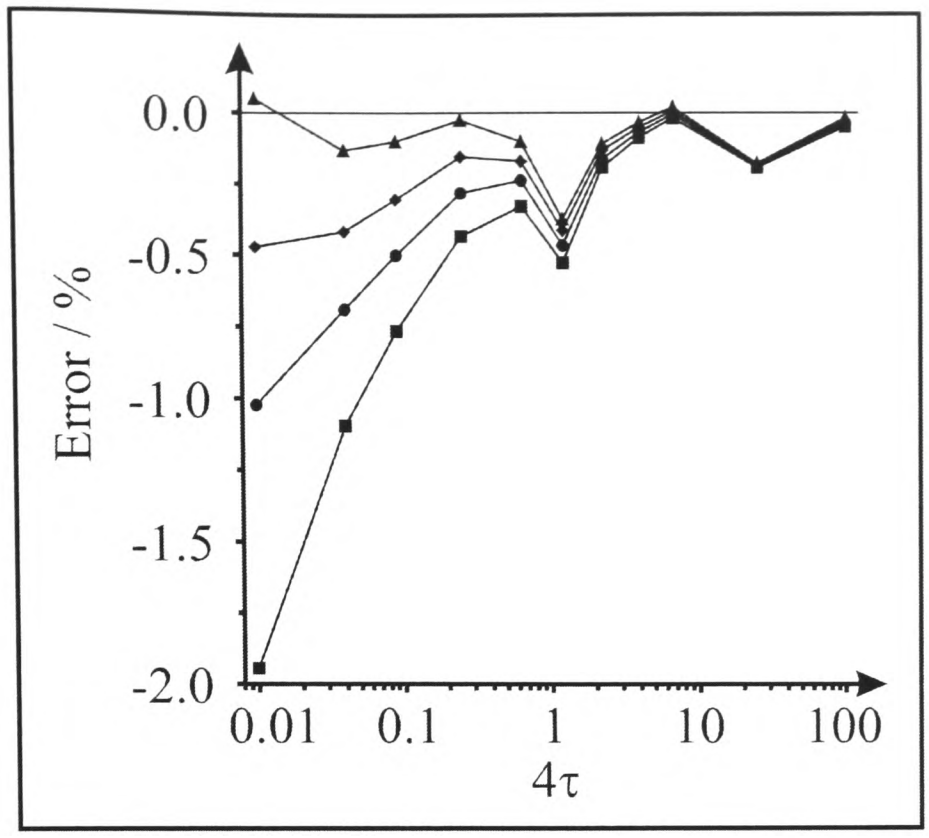


Figure 6.3
Convergence errors in the first step current for different spatial grid sizes, $N\theta$ x $N\Gamma$: (-■-) 50 x 50, (-●-) 70 x 70, (-♦-) 100 x 100, (-▲-) 200 x 200.

since it is constructed of two expressions which are valid for short and long times respectively and connected in the domain $0.82 < 4\tau < 1.44$ within an error of 0.5%.[15] Next, the effect of the grid expansion parameter ω onto the convergence of the first potential step currents was investigated. The results of this analysis are shown in Table 6.2. It is obvious that in the range of ω values considered, the convergence errors are virtually independent of this parameter (higher values of the expansion parameter even lead to slight improvement of the errors for some time points). This is in contrast with the analysis presented in [20] where the Hopscotch method was

Table 6.2
Dependence of the convergence error in the first potential step current on the grid expansion factor.

	Convergence error / %					
4τ	$\omega = 10^{-4}$	$\omega = 10^{-3}$	$\omega = 5 \times 10^{-3}$	$\omega = 10^{-2}$	$\omega = 5 \times 10^{-2}$	$\omega = 0.1$
0.01	-0.45601	-0.45601	-0.45601	-0.45601	-0.45601	-0.45601
0.04	-0.40199	-0.40199	-0.40199	-0.40199	-0.40199	-0.40199
0.09	-0.30527	-0.30527	-0.30527	-0.30527	-0.30527	-0.30527
0.25	-0.15483	-0.15481	-0.15468	-0.15455	-0.15281	-0.13879
0.64	-0.16769	-0.16767	-0.17185	-0.16732	-0.16205	-0.15556
1.21	-0.41528	-0.41526	-0.41498	-0.41454	-0.40863	-0.39796
2.25	-0.13019	-0.13016	-0.12985	-0.12966	-0.12792	-0.11796
4	-0.04096	-0.04094	-0.04062	-0.04012	-0.03871	-0.02335
6.76	0.01364	0.01366	0.01398	0.01430	0.01562	0.01751
25	-0.17139	-0.17137	-0.17102	-0.17054	-0.16807	-0.16649
100	-0.01722	-0.0172	-0.01686	-0.0164	-0.01365	-0.01165

applied. Unlike explicit algorithms such as Hopscotch, implicit methods (i.e. ADI) can cope with propagation of the diffusion layer by more than one spatial step during a single time step. Accordingly, no distortion of the real diffusion propagation speed is expected, permitting the use of ω values up to 0.1. Higher values have not been considered since they do not offer any significant reduction of simulation times. Based on this analysis the value $\omega = 0.05$ was used in the following.

The effect of different diffusion coefficients on the errors in the second potential step current is shown in Figure 6.4. This analysis was performed in the same way as employed previously,[29,30] i.e. by "converging" the current. The data shown were calculated for the dimensionless durations of the two potential steps of $\tau_1 = 10$ and $\tau_2 = 5$. It is obvious that the convergence error increases as the ratio D_A / D_B grows, in agreement with previous findings for the case of cyclic voltammetry.[2] However, even for such an extreme case when the diffusion coefficients are different by a factor of one hundred, a spatial grid of the size $N\theta$ x $N\Gamma$ = 100 x 100 is sufficient to achieve a convergence error of less that one percent. This resulted in simulation times of under 30 s for all calculations.

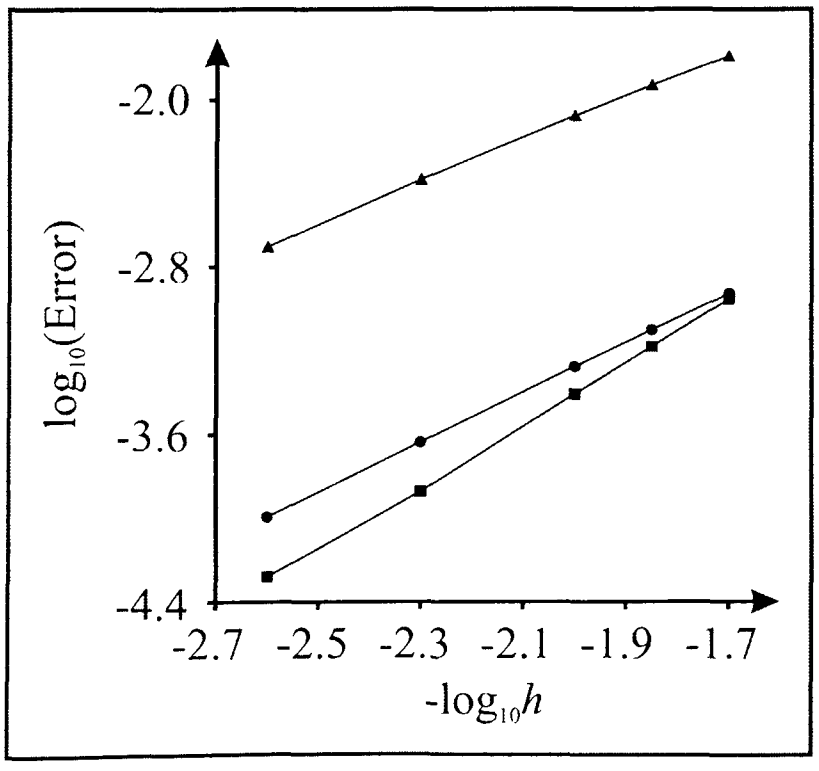


Figure 6.4
Dependence of the convergence error in the second potential step current on the grid step size $h = 1/N\theta = 1/N\Gamma$ for three ratios of D_A / D_B. Step durations were fixed at $\tau_1 = 10$ and $\tau_2 = 5$. (-■-) $D_A / D_B = 1$, (-●-) $D_A / D_B = 10$, (-▲-) $D_A / D_B = 100$.

Finally, Tables 6.3–6.5 present fully dimensionless data for the flux defined by equation (6.11), corresponding to the second potential step. Since the first potential step transient can be fitted using the expressions given in [15,16] there is no need to supply corresponding data pertaining to this period of the *I-t* curve. After the diffusion coefficient D_A has been evaluated from analysis of the first step transient, a double potential step experiment can be run with the duration of the first step corresponding to one of the three dimensionless values assumed in Tables 6.3–6.5, and the data from these tables used to fit the second step current data and obtain the ratio of the diffusion coefficients of A and B.

Table 6.3
Second step fluxes for $\tau_1 = 1$.

D_A / D_B	τ_2 0.01	0.1	0.5	1	2	5	10	25
0.02	-0.6390	-0.1592	-0.0456	-0.0230	-0.0105	-0.0033	-0.0013	-0.0005
0.05	-1.0192	-0.2455	-0.0693	-0.0347	-0.0157	-0.0048	-0.0019	-0.0006
0.1	-1.4415	-0.3387	-0.0940	-0.0468	-0.0210	-0.0064	-0.0025	-0.0007
0.2	-2.0069	-0.4639	-0.1257	-0.0621	-0.0277	-0.0084	-0.0032	-0.0009
0.3	-2.4088	-0.5547	-0.1477	-0.0725	-0.0322	-0.0097	-0.0037	-0.0010
0.4	-2.7248	-0.6275	-0.1649	-0.0805	-0.0357	-0.0107	-0.0041	-0.0011
0.5	-2.9858	-0.6884	-0.1791	-0.0871	-0.0385	-0.0115	-0.0044	-0.0012
0.6	-3.2080	-0.7407	-0.1913	-0.0927	-0.0408	-0.0122	-0.0046	-0.0012
0.7	-3.4011	-0.7866	-0.2021	-0.0976	-0.0428	-0.0128	-0.0048	-0.0013
0.8	-3.5715	-0.8273	-0.2116	-0.1019	-0.0446	-0.0133	-0.0050	-0.0013
1	-3.8607	-0.8968	-0.2281	-0.1093	-0.0477	-0.0141	-0.0053	-0.0014
1.2	-4.0989	-0.9544	-0.2420	-0.1155	-0.0502	-0.0148	-0.0056	-0.0015
1.4	-4.2998	-1.0031	-0.2539	-0.1209	-0.0524	-0.0154	-0.0058	-0.0015
1.6	-4.4724	-1.0451	-0.2644	-0.1256	-0.0543	-0.0160	-0.0060	-0.0016
1.8	-4.6227	-1.0818	-0.2737	-0.1298	-0.0559	-0.0164	-0.0061	-0.0016
2	-4.7552	-1.1142	-0.2820	-0.1336	-0.0575	-0.0168	-0.0063	-0.0017
3	-5.2411	-1.2330	-0.3136	-0.1482	-0.0634	-0.0184	-0.0069	-0.0018
5	-5.7824	-1.3654	-0.3503	-0.1663	-0.0711	-0.0205	-0.0076	-0.0020
10	-6.3817	-1.5114	-0.3914	-0.1875	-0.0809	-0.0233	-0.0086	-0.0022
20	-6.8454	-1.6255	-0.4228	-0.2039	-0.0890	-0.0261	-0.0096	-0.0025
50	-7.2819	-1.7423	-0.4541	-0.2197	-0.0966	-0.0289	-0.0109	-0.0028

Table 6.4
Second step fluxes for $\tau_1 = 5$.

D_A / D_B	τ_2 0.01	0.1	0.5	1	2	5	10	25
0.02	-0.5754	-0.1609	-0.0595	-0.0362	-0.0205	-0.0084	-0.0038	-0.0013
0.05	-0.9288	-0.2524	-0.0926	-0.0561	-0.0316	-0.0129	-0.0058	-0.0018
0.1	-1.3330	-0.3549	-0.1289	-0.0778	-0.0438	-0.0177	-0.0079	-0.0025
0.2	-1.8980	-0.4994	-0.1786	-0.1074	-0.0601	-0.0242	-0.0108	-0.0033
0.3	-2.3202	-0.6099	-0.2156	-0.1291	-0.0721	-0.0289	-0.0129	-0.0039
0.4	-2.6669	-0.7022	-0.2460	-0.1469	-0.0818	-0.0327	-0.0145	-0.0044
0.5	-2.9649	-0.7826	-0.2723	-0.1621	-0.0900	-0.0359	-0.0159	-0.0048
0.6	-3.2280	-0.8543	-0.2957	-0.1756	-0.0973	-0.0387	-0.0172	-0.0052
0.7	-3.4648	-0.9193	-0.3169	-0.1877	-0.1038	-0.0412	-0.0183	-0.0055
0.8	-3.6805	-0.9789	-0.3364	-0.1988	-0.1097	-0.0435	-0.0192	-0.0058
1	-4.0634	-1.0852	-0.3713	-0.2185	-0.1202	-0.0474	-0.0209	-0.0063
1.2	-4.3969	-1.1784	-0.4020	-0.2359	-0.1293	-0.0509	-0.0224	-0.0067
1.4	-4.6930	-1.2615	-0.4296	-0.2514	-0.1374	-0.0539	-0.0237	-0.0071
1.6	-4.9598	-1.3366	-0.4547	-0.2654	-0.1447	-0.0566	-0.0249	-0.0074
1.8	-5.2026	-1.4051	-0.4778	-0.2783	-0.1514	-0.0591	-0.0259	-0.0077
2	-5.4254	-1.4680	-0.4991	-0.2903	-0.1576	-0.0613	-0.0269	-0.0080
3	-6.3262	-1.7233	-0.5867	-0.3394	-0.1828	-0.0704	-0.0307	-0.0091
5	-7.5246	-2.0641	-0.7060	-0.4074	-0.2177	-0.0827	-0.0357	-0.0105
10	-9.1317	-2.5223	-0.8692	-0.5028	-0.2681	-0.1006	-0.0429	-0.0125
20	-10.5314	-2.9248	-1.0136	-0.5891	-0.3159	-0.1188	-0.0504	-0.0145
50	-11.8995	-3.3372	-1.1605	-0.6769	-0.3655	-0.1397	-0.0600	-0.0173

Table 6.5
Second step fluxes for $\tau_1 = 10$.

D_A / D_B	τ_2 0.01	0.1	0.5	1	2	5	10	25
0.02	-0.5607	-0.1611	-0.0631	-0.0402	-0.0244	-0.0113	-0.0057	-0.0021
0.05	-0.9079	-0.2537	-0.0987	-0.0628	-0.0379	-0.0174	-0.0087	-0.0030
0.1	-1.3076	-0.3582	-0.1382	-0.0876	-0.0529	-0.0242	-0.0120	-0.0041
0.2	-1.8719	-0.5071	-0.1929	-0.1220	-0.0733	-0.0334	-0.0165	-0.0056
0.3	-2.2983	-0.6221	-0.2342	-0.1476	-0.0886	-0.0402	-0.0198	-0.0067
0.4	-2.6518	-0.7191	-0.2686	-0.1689	-0.1011	-0.0458	-0.0225	-0.0076
0.5	-2.9581	-0.8043	-0.2986	-0.1873	-0.1119	-0.0506	-0.0249	-0.0083
0.6	-3.2307	-0.8809	-0.3255	-0.2037	-0.1215	-0.0549	-0.0269	-0.0090
0.7	-3.4778	-0.9508	-0.3501	-0.2186	-0.1302	-0.0587	-0.0288	-0.0096
0.8	-3.7045	-1.0153	-0.3728	-0.2324	-0.1382	-0.0622	-0.0304	-0.0102
1	-4.1107	-1.1316	-0.4139	-0.2571	-0.1525	-0.0684	-0.0334	-0.0112
1.2	-4.4689	-1.2349	-0.4506	-0.2792	-0.1651	-0.0738	-0.0360	-0.0120
1.4	-4.7906	-1.3280	-0.4839	-0.2991	-0.1764	-0.0787	-0.0383	-0.0128
1.6	-5.0835	-1.4130	-0.5145	-0.3173	-0.1868	-0.0831	-0.0404	-0.0134
1.8	-5.3529	-1.4914	-0.5429	-0.3343	-0.1964	-0.0872	-0.0423	-0.0141
2	-5.6025	-1.5643	-0.5694	-0.3501	-0.2053	-0.0909	-0.0441	-0.0146
3	-6.6386	-1.8676	-0.6812	-0.4168	-0.2426	-0.1065	-0.0514	-0.0169
5	-8.0975	-2.2969	-0.8421	-0.5139	-0.2968	-0.1285	-0.0615	-0.0201
10	-10.2512	-2.9334	-1.0843	-0.6626	-0.3810	-0.1624	-0.0766	-0.0247
20	-12.3737	-3.5661	-1.3267	-0.8137	-0.4692	-0.1993	-0.0931	-0.0296
50	-14.6613	-4.2738	-1.5978	-0.9838	-0.5707	-0.2450	-0.1150	-0.0363

6.4.2 Chemically Reversible, One-Electron Couples

The double potential step simulation was first applied to the aqueous one-electron oxidation of $Fe(CN)_6^{4-}$ to $Fe(CN)_6^{3-}$, since the diffusion coefficients of both these species are well established in the literature.[31] Double step chronoamperomograms were recorded at a (nominally) 100 μm diameter Pt disk electrode immersed in a 10 mM $Fe(CN)_6^{4-}$ / 0.1 M KCl aqueous solution using the following parameters: E_1 = -0.10 V *vs* SCE, E_2 = +0.60 V *vs* SCE, E_3 = -0.10 V *vs* SCE, t_1 = 10 s, t_2 = 10s. These potentials were chosen such that E_1/E_3 is prior to the onset of any oxidative faradaic process and E_2 lies comfortably in the transport-limited region of the $Fe(CN)_6^{4-}$ oxidative wave. To analyse these transients, the data from the first potential step was initially fitted to the analytical Shoup and Szabo expression (equation (1.28) in secion 1.5.1) to determine the diffusion coefficient for $Fe(CN)_6^{4-}$ after inputting values for the concentration and disk radius (determined by earlier calibration). Having deduced the best-fit value for $D(Fe(CN)_6^{4-})$, the data for both potential steps were analysed using the simulation described above to obtain the final parameter, $D(Fe(CN)_6^{3-})$. A close fit between the experimental and simulated double step transients was obtained, as shown for a typical experimental transient in Figure 6.5(a). The diffusion coefficients determined from multiple scans were averaged to give the final values for $D(Fe(CN)_6^{4-})$ and $D(Fe(CN)_6^{3-})$ which are given in Table 6.6, along with literature values reported for the same experimental conditions. In both cases, agreement with the published data is excellent.

To test the procedure on data collected in organic solvents, the simulation was next used to determine the diffusion coefficients of TMPD and the radical cation, $TMPD^{+\bullet}$, generated via its oxidation in the solvent electrolyte systems (i) ethanol /

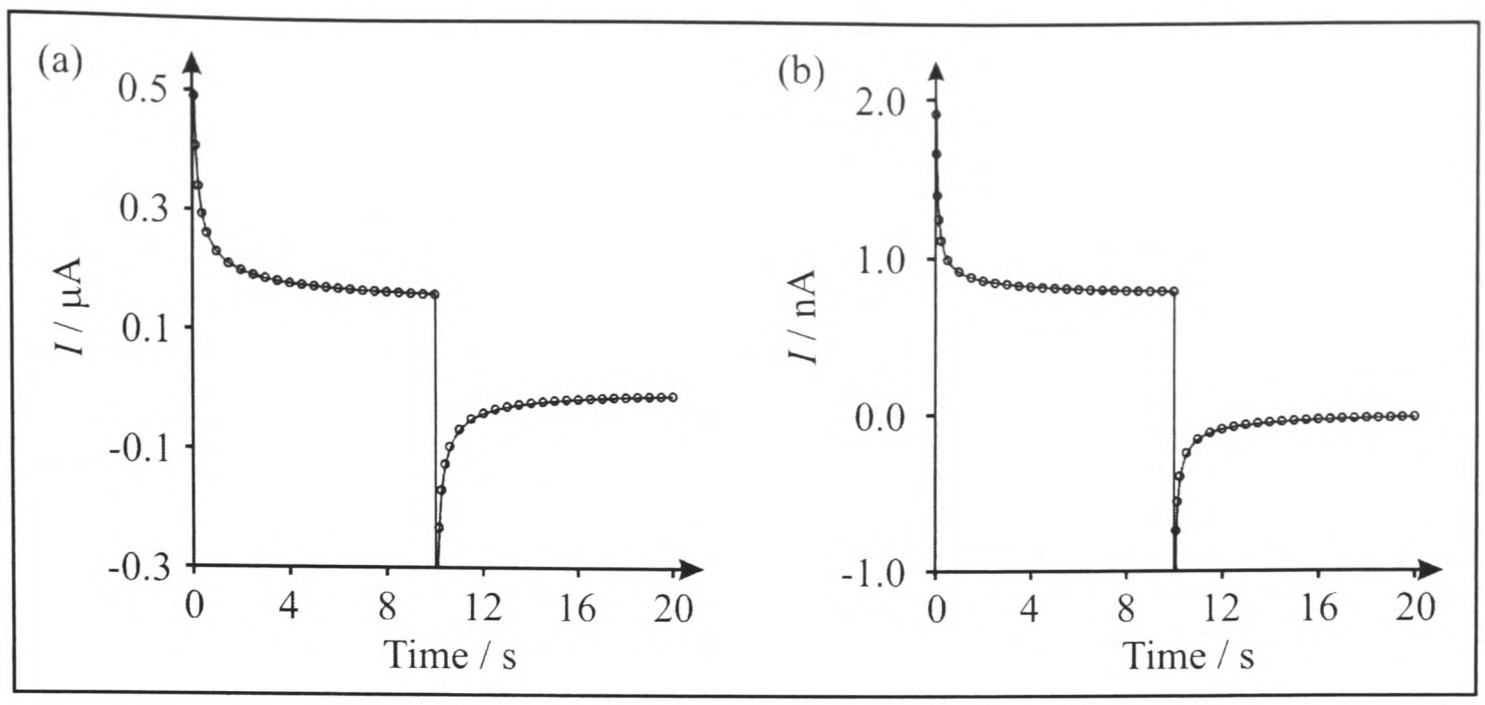


Figure 6.5
Comparison of the fit between experimental and simulated double potential step transients for the systems (a) $Fe(CN)_6^{4-}$ in aqueous 0.1 M KCl at a 100 µm diameter Pt disk and (b) *p*-chloroaniline in $[C_2mim][NTf_2]$ at a 10 µm diameter Au disk.

TBAP and (ii) the room temperature ionic liquid *n*-hexyltriethylammonium bis(trifluoromethylsulfonyl)imide, $[N_{6222}][NTf_2]$. It should be noted that ionic liquids have an inherent conductivity comparable to that of traditional organic solvent/electrolyte mixtures, thus obviating the need for addition of a supporting electrolyte. Ethanol was chosen above other more commonly employed nonaqueous solvents since it has been reported that the difference in rate of diffusion between neutral parent and electrogenerated radical cation is accentuated in more associated solvents.[32] The applied potentials were (i) E_1 = -0.20 V *vs* Ag, E_2 = +0.50 V *vs* Ag, E_3 = -0.20 V *vs* Ag and (ii) E_1 = -0.10 V *vs* Ag, E_2 = +0.60 V *vs* Ag, E_3 = -0.10 V *vs* Ag with all steps being of 10 s duration. Double step chronoamperomograms were recorded at a 10 µm diameter Au disk in systems (i) and (ii) and additionally at a 100 µm diameter Pt disk in system (i), then analysed in the same manner as above to yield diffusion coefficients for each species. These are presented in Table 6.6 along with literature values. The results are again in good agreement with the published data, in

Table 6.6
Diffusion coefficients for a selection of solvent / electrolyte systems determined using double potential step chronoamperometry. The given margins of error are in each case based on the averaging of several (≥ 5) data sets.

Species	Solvent	D / 10^{-11} m^2 s^{-1} (298 ± 1 K)	Reference value / 10^{-11} m^2 s^{-1}		
$Fe(CN)_6^{4-}$	H_2O / 0.1 M KCl	65.8 ± 3.7	65.0	298 K	[31]
$Fe(CN)_6^{3-}$	H_2O / 0.1 M KCl	75.1 ± 9.9	76.3	298 K	[31]
TMPD	EtOH / 0.1 M TBAP	90.6 ± 4.1	96.8	298 K	[32]
	$[N_{6222}][NTf_2]$	0.64 ± 0.03	0.70	293 ± 2 K	[17]
$TMPD^{+\cdot}$	EtOH / 0.1 M TBAP	70.9 ± 9.0	82.3	298 K	[32]
	$[N_{6222}][NTf_2]$	0.50 ± 0.07	0.55	293 ± 2 K	[17]
p-chloroaniline	$[C_2mim][NTf_2]$	4.33 ± 0.90	-		
$ACDA(ox)^+$	$[C_2mim][NTf_2]$	2.51 ± 0.90	-		

the case of system (i), determined using an alternative chronoabsorptometric technique.[32] The diffusion coefficient of TMPD is seen to be two orders of magnitude smaller in the ionic liquid relative to the conventional organic solvent, a direct consequence of the much larger viscosity of the former (167 mPa s *vs* 1.074 mPa s at 298 K[33,34]).

6.4.3 Anodic Dimerisation of p-Chloroaniline

The electrochemically initiated dimerisation of *p*-chloroaniline (PCA) was first characterised by Bacon and Adams in aqueous media,[35] and then more recently, along with several related haloanilines, by Farsang et al. in N,N-dimethylformamide and acetonitrile.[36-39] A detailed investigation in the former organic solvent yielded a mechanism in which PCA undergoes a one-electron oxidation to give a radical cation, which may be rapidly and reversibly deprotonated by the solvent, S.[36] In the rate-determining step, the resulting radical then couples with its parent radical cation (forming a nitrogen-carbon bond) to give, following loss of HCl, the oxidised form of the dimer 4-amino-4'-chlorodiphenylamine (ACDA, for structure see Figure 6.2). Finally, since this species is itself electrochemically active, it may be reversibly reduced and re-oxidised at a lower potential than that required for the initial oxidation

of *p*-chloroaniline.

$$PCA \rightarrow PCA^{+\bullet} + e^- \qquad (6.15)$$

$$PCA^{+\bullet} + S \rightleftharpoons PCA^{\bullet} + SH^+ \qquad (6.16)$$

$$PCA^{+\bullet} + PCA^{\bullet} \rightarrow ACDA(ox)^+ + HCl \qquad (6.17)$$

$$ACDA(ox)^+ + 2e^- + H^+ \rightleftharpoons ACDA \qquad (6.18)$$

In the current investigation, the dimerisation of PCA was studied for the first time in the room temperature ionic liquid solvent 1-ethyl-3-methylimidazolium bis(trifluoromethylsulfonyl)imide, $[C_2mim][NTf_2]$. A voltammogram for the oxidation of 5 mM PCA in $[EMIM][N(Tf)_2]$ at a 10 μm Au disk electrode is shown in Figure 6.6. Qualitatively, the shape of the voltammogram closely resembles the observed behaviour in conventional organic solvents; a sharp irreversible oxidative peak at +1.0 V *vs* Ag followed by a smaller reductive wave peaking at +0.4 V *vs* Ag on the reverse scan. On further cycling, the corresponding oxidation peak to this latter wave appears at +0.5 V *vs* Ag, a region in which there was initially no faradaic

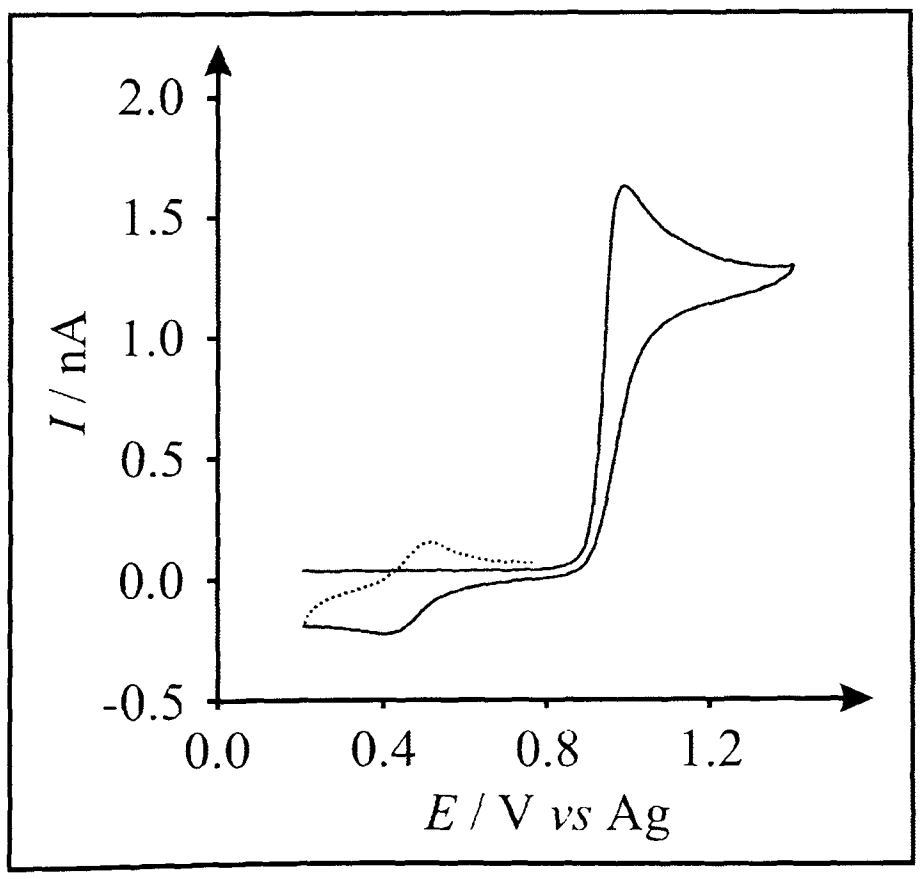


Figure 6.6
Cyclic voltammogram for the oxidation of 5 mM PCA in $[C_2mim][NTf_2]$ at a 10 μm diameter Au disk, 0.2 V s^{-1}. (——) first cycle, (·····) second cycle.

process occuring. A Tafel analysis of the early part of the original oxidative peak yields a gradient less than 60 mV, hinting at the presence of a follow up homogeneous process that could be second order in the electroactive species (after an initial electrochemically reversible heterogeneous step). By analogy with the previous reports,[35,36] the principal peak may be identified as arising from the oxidation of PCA (equation 6.15), and the smaller peaks due to the reduction and re-oxidation of its dimer ADCA (equation 6.18).

In an attempt to quantify the rate constants for this process, the system was subjected to a variable scan rate study in an attempt to out-run the homogeneous kinetics. Cyclic voltammograms were recorded for a 50 mM solution of PCA at a 10 μm Au disk electrode over a range of 2.8–168.0 kV s^{-1}. As the scan rate was increased, a back peak for the initial oxidation process at +1.0 V *vs* Ag did begin to emerge, however, even at the highest scan rates employed, the dimerisation process could not be entirely out-run. Consequently it proved impossible to characterise the electron transfer process by this means. While no kinetic information could be deduced, double potential step chronoamperometry could be applied however, to determine the diffusion coefficients of PCA and the dimer in its oxidised form. Since the homogeneous reactions (6.16–6.17) occur so rapidly, for the purposes of modelling this system, the mechanism can be effectively reduced to

$$2A \rightleftharpoons B + 2e^- \qquad (6.20)$$

$$B + 2e^- \rightleftharpoons C \qquad (6.21)$$

where A represents PCA and B and C are the oxidised and reduced forms of the dimer ACDA respectively. Furthermore, the fact that one molecule of B is formed for every two molecules of A is cancelled by the fact that B subsequently undergoes a

two electron reduction, such that the simulation developed earlier for the simple reversible one-electron couple is entirely appropriate for this problem also. Accordingly, double step chronoamperomograms were recorded (E_1 = +0.60 V *vs* Ag, E_2 = +1.20 V *vs* Ag, E_3 = 0.00 V *vs* Ag, t_1 = 10 s, t_2 = 10s, see Figure 6.5(b)) and analysed as above to yield the two diffusion coefficients that are given in Table 6.6. Encouragingly, the diffusion coefficient of the dimer is found to be almost half that of monomeric *p*-chloroaniline.

6.5 Conclusions

A new approach to the simulation of the double potential step chronoamperometry at a disk electrode has been developed based on the conformal mapping of the spatial coordinates and a time grid with a constant time step at the beginning of each potential pulse which then increases geometrically for the remaining duration. The accuracy of the calculations has been tested, both theoretically and against experimental measurements, demonstrating a high efficiency for the proposed technique. Dimensionless data for the second potential step transient has been generated which can be readily applied to the analysis of further experimental data, eliminating a need for any additional computation.

Having constructed the required experimental apparatus and developed and validated the necessary analytical tools, the path was now clear to commence a systematic study of diffusion in room temperature ionic liquid solvents, as a function of both the temperature and the charge located on the diffusing species.

6.6 References

[1] O.V. Klymenko, R.G. Evans, C. Hardacre, I.B. Svir, R.G. Compton, *J. Electroanal. Chem.* **2004**, *571*, 211.

[2] M.C. Buzzeo, O.V. Klymenko, J.D. Wadhawan, C. Hardacre, K.R. Seddon, R.G. Compton, *J. Phys. Chem. A* **2003**, *107*, 8872.

[3] R.G. Evans, O.V. Klymenko, S.A. Saddoughi, C. Hardacre, R.G. Compton, *J. Phys. Chem. B* **2004**, *108*, 7878.

[4] W. Hyk, A. Nowicka, Z. Stojek, *Anal. Chem.* **2002**, *74*, 149.

[5] J.V. Macpherson, P.R. Unwin, *Anal. Chem.* **1997**, *69*, 2063.

[6] H. Ikeuchi, M. Kanakubo, *J. Electroanal. Chem.* **2000**, *493*, 93.

[7] M.L. Olmstead, R.S. Nicholson, *Anal. Chem.* **1969**, *41*, 851.

[8] A. Bewick, D. Serve, T.A. Joslin, *J. Electroanal. Chem.* **1983**, *154*, 81.

[9] A.J. Bard, L.R. Faulkner, *Electrochemical Methods: Fundamentals and Applications: 2nd Edition*, John Wiley & Sons, New York, **2001**.

[10] J.C. Myland, K.B. Oldham, *Electrochem. Commun.* **2004**, *6*, 344.

[11] F.G. Cottrell, *Z. Physik. Chem.* **1902**, *42*, 385.

[12] A. Szabo, D.K. Cope, D.E. Tallman, P.M. Kovach, R.M. Wightman, *J. Electroanal. Chem.* **1987**, *217*, 417.

[13] K. Aoki, K. Tokuda, H. Matsuda, *J. Electroanal. Chem.* **1987**, *230*, 61.

[14] K. Aoki, J. Osteryoung, *J. Electroanal. Chem.* **1981**, *122*, 19.

[15] K. Aoki, J. Osteryoung, *J. Electroanal. Chem.* **1984**, *160*, 335.

[16] D. Shoup, A. Szabo, *J. Electroanal. Chem.* **1982**, *140*, 237.

[17] R.G. Evans, O.V. Klymenko, C. Hardacre, K.R. Seddon, R.G. Compton, *J. Electroanal. Chem.* **2003**, *556*, 179.

[18] Z. Galus, J.O. Schenk, R.N. Adams, *J. Electroanal. Chem.* **1982**, *135*, 1.

[19] J.-S. Yu, Z.-X. Zhang, *J. Electroanal. Chem.* **1997**, *439*, 73.

[20] C. Amatore, I. Svir, *J. Electroanal. Chem.* **2003**, *557*, 75.

[21] C.A. Amatore, B. Fosset, *J. Electroanal. Chem.* **1992**, *328*, 21.

[22] J. Heinze, *J. Electroanal. Chem.* **1981**, *124*, 73.

[23] I.B. Svir, O.V. Klimenko, R.G. Compton, *Radiotekhnika* **2001**, *118*, 92.

[24] C. Amatore, A. Oleinick, I. Svir, *J. Electroanal. Chem.* **2004**, *564*, 245.

[25] W.H. Press, S.A. Teukolsky, W.T. Vetterling, B.P. Flannery, *Numerical Recipies in C: The Art of Scientific Computing*, Cambridge University Press, Cambridge, **1992**.

[26] D.M. Himmelblau, *Applied Nonlinear Programming*, McGraw-Hill, New York, **1972**.

[27] C. Amatore, E. Maisonhaute, G. Simonneau, *J. Electroanal. Chem.* **2000**, *486*, 141.

[28] C. Amatore, E. Maisonhaute, G. Simonneau, *Electrochem. Commun.* **2000**, *2*, 81.

[29] O.V. Klymenko, D. Giovanelli, N.S. Lawrence, N.V. Rees, L. Jiang, T.G.J. Jones, R.G. Compton, *Electroanalysis* **2003**, *15*, 949.

[30] N.V. Rees, O.V. Klymenko, R.G. Compton, M. Oyama, *J. Electroanal. Chem.* **2002**, *531*, 33.

[31] R.N. Adams, *Electrochemistry at Solid Electrodes*, Marcel Dekker, New York, **1969**.

[32] R.L. Wang, K.Y. Tam, R.G. Compton, *J. Electroanal. Chem.* **1997**, *434*, 105.

[33] J. Sun, M. Forsyth, D.R. MacFarlane, *J. Phys. Chem. B* **1998**, *102*, 8858.

[34] D.R. Lide, *Handbook of Chemistry and Physics: 81st Edition*, CRC Press, **2000**.

[35] J. Bacon, R.N. Adams, *J. Am. Chem. Soc.* **1968**, *90*, 6596.

[36] C. Amatore, G. Farsang, E. Maisonhaute, P. Simon, *J. Electroanal. Chem.* **1999**, *462*, 55.

[37] M. Kadar, Z. Nagy, T. Karancsi, G. Farsang, *Electrochim. Acta* **2001**, *46*, 3405.

[38] M. Kadar, Z. Nagy, T. Karancsi, G. Farsang, *Electrochim. Acta* **2001**, *46*, 1297.

[39] M. Kadar, Z. Tokats, T. Karancsi, G. Farsang, *Electroanalysis* **1999**, *11*, 809.

7

A Comparative Electrochemical Study of Diffusion in Room Temperature Ionic Liquid Solvents *versus* Acetonitrile

Measurements on the diffusion coefficients of the neutral molecule N,N,N',N'-tetramethyl-*para*-phenylenediamine and the radical cation and dication generated by its one- and two-electron oxidation respectively are reported over the range 298-348 K in both acetonitrile and four room temperature ionic liquids. Data were collected using single and double potential step chronoamperometry at a gold disk electrode of micrometer dimension, and analysed via fitting to the appropriate analytical expression or, where necessary, simulation. The variation of diffusion coefficient with temperature was found to occur in an Arrhenius-type manner for all combinations of solute and solvent. For a given ionic liquid, the diffusional activation energies of each species were not only closely equivalent to each other, but also to the RTIL's activation energy of viscous flow. In acetonitrile supported with 0.1 M tetrabutylammonium perchlorate, the ratio of diffusion coefficients of the radical cation and dication to the neutral molecule were calculated as 0.89 ± 0.05 and 0.51 ± 0.03 respectively. In contrast, amongst the ionic liquids the same ratios were determined to be on average 0.53 ± 0.04 and 0.33 ± 0.03. The consequences of this dissimilarity are considered in terms of the modelling of voltammetric data gathered within ionic liquid solvents. This work has been published in *ChemPhysChem*.[1]

7.1 Introduction

In solution phase chemistry, diffusion processes are frequently important in determining the overall rate of multi-step chemical reactions. In such cases, an

accurate knowledge of the diffusion coefficients of reactant, intermediate and product species may be crucial to a successful analysis of the kinetics and reaction mechanism. When electrochemical steps are involved, a diffusion coefficient for the initial electroactive species is generally straightforward to determine via a range of methods, however, in the case of the electrogenerated species, this quantity is rarely as easily ascertained. This often leads to use of the approximation that these two quantities are equal, an approximation that has proved to be sound in the case of many redox systems in conventional organic solvents.[2-4] Wang et al., for example, measured the diffusion coefficients of a number of radical ions electrogenerated from various aromatic organic molecules in acetonitrile.[4] The ratio of the diffusion coefficients of radical ion to neutral parent was found to be 0.96 or higher in each case. It was argued that for these highly charge-delocalised radical species in this non-associated solvent, the solvent-radical ion interactions were essentially equal to those for the solvent-neutral parent.

With a high thermal stability, negligible vapour pressure, a high intrinsic conductivity and a wide electrochemical window typically featured amongst their properties, room temperature ionic liquids are currently attracting a wealth of attention both from within the electrochemical community and beyond.[5,6] In order to facilitate their use (in the former category at least), a sound understanding of the nature of the mass transport processes occurring in these solvents and their similarity to those already established for more common aqueous and organic solvents would be highly beneficial. A brief comparison of the diffusion coefficients for a given species in both traditional molecular solvents and RTILs reveals the most striking difference: the latter are routinely 10-100 times smaller at room temperature, a fact which may be

ascribed to the considerably larger viscosities of which ionic liquids are possessed. This difference alone results in important consequences for the interpretation of electrochemical data, and several cautionary remarks have already appeared in the literature.[5,7,8] Other previous investigations have examined the effect on diffusion of varying the water content of the ionic liquid and, most recently, varying the concentration of the diffusing species itself.[9,10] Regarding the ratio of diffusion coefficients between reactant and electrogenerated species under these conditions, a recent report concerning the one-electron reduction of dioxygen to superoxide in several RTILs produced values of ~0.1 for this parameter.[11] Whilst the oxygen system can be considered a rather extreme case, it does emphasise a need to re-evaluate any assumption of equal diffusion coefficients in this new reaction medium.

Herein, the rate of diffusion is explored as a function of both temperature and the magnitude of the charge residing on the species in motion. Four RTILs were utilised, each incorporating the bis(trifluoromethylsulfonyl)imide anion, [NTf_2], paired in turn with cations: 1-ethyl-3-methylimidazolium, [C_2mim]; 1-decyl-3-methylimidazolium, [C_{10}mim]; N-butylpyridinium [C_4pyr]; and tris(*n*-hexyl)tetradecylphosphonium,

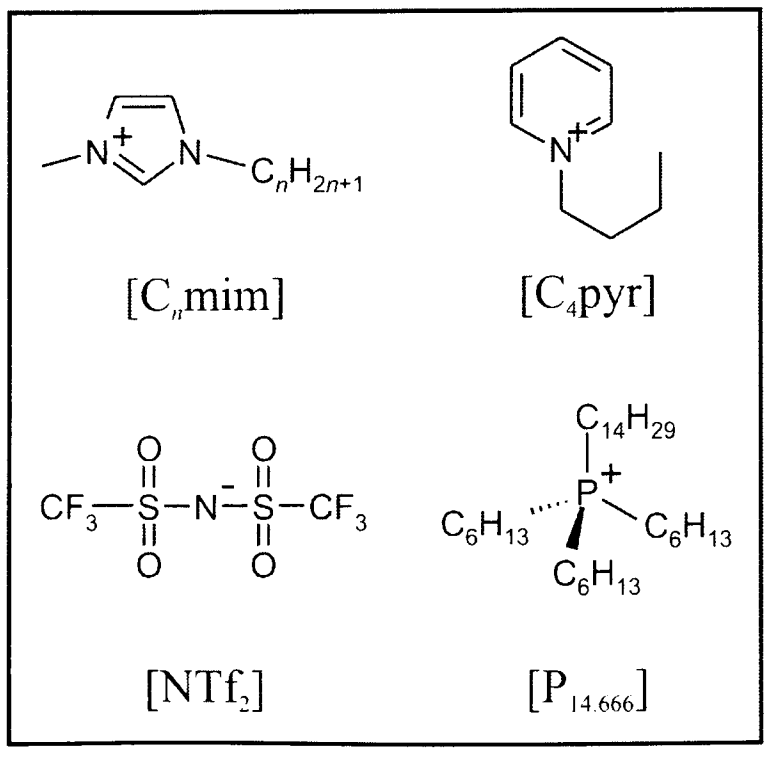


Figure 7.1
Structures of the ions comprising the room temperature ionic liquids under investigation.

$[P_{14.666}]$, respectively (for structures see Figure 7.1). These were selected to enable the study to span a range of viscosities, neat $[P_{14.666}][NTf_2]$ being more than twelve times as viscous as $[C_2mim][NTf_2]$ at 298 K (400 mPa s *vs* 31 mPa s) and the remaining two RTILs occupying intermediate values. The molecule N,N,N',N'-tetramethyl-*para*-phenylenediamine, TMPD, was chosen as the diffusional probe. Previous reports have demonstrated that TMPD undergoes two well-defined, reversible one-electron oxidations in ionic liquid media,[8,10] just as it does in simple organic solvents:

$$TMPD \rightleftharpoons TMPD^{+\bullet} + e^- \qquad (7.01)$$

$$TMPD^{+\bullet} \rightleftharpoons TMPD^{2+} + e^- \qquad (7.02)$$

The application of different electrode potentials thus provides access to species with formal charges of 0, +1 and +2 respectively. A generic complication of using a system with two successive electron transfers, however, is the possible (thermodynamically favoured) conproportionation reaction between TMPD and $TMPD^{2+}$ that could occur in the diffusion layer adjacent to the electrode surface and affect any voltammetry were it not accounted for.[12,13] To circumvent this problem, use of solutions of neutral TMPD was restricted to the study of TMPD and $TMPD^{+\bullet}$ only, while a solution of bulk $TMPD^{+\bullet}$ was employed separately to interrogate the ions $TMPD^{+\bullet}$ and $TMPD^{2+}$. As such, the two species susceptible to conproportionation were never found in bulk solution together and hence this potential side-reaction avoided.

The method of choice for the determination of diffusion coefficients was double potential step chronoamperometry at a disk electrode of micrometer dimension. The electroactive species (TMPD or $TMPD^{+\bullet}$) was subjected to a potential step to a point

at which its one-electron oxidation occurs at a diffusion-controlled rate. Subsequently, a second potential step applied in the reverse direction causes the electrogenerated $TMPD^{+\bullet}$ or $TMPD^{2+}$ to be re-reduced, again, under diffusional control. Under such conditions, analysis of the *I-t* data from the initial step is possible using a simple analytical expression.[14] The equivalent data for the second step is a more complex function of both diffusion coefficients and must be deconvoluted via comparison with a model. This was achieved using the previously described approach to the simulation of double potential step chronoamperometry at disks, which allows for simultaneous determination of the diffusion coefficient of both reactant and electrogenerated species, and has already been successfully applied to analyse data gathered in ionic liquid solutions.[15] Overall therefore, these measurements provide sufficient information to characterise the diffusion of all three species: TMPD, $TMPD^{+\bullet}$ and $TMPD^{2+}$ over a range of temperatures.

7.2 Experimental Section

In addition to matters already covered in chapter three, N,N,N',N'-tetramethyl-*para*-phenylenediamine tetrafluoroborate, $TMPD^{+}BF_4^{-}$, was provided by Professor Stephen G. Davies (University of Oxford) having been prepared following the procedure reported by Yamauchi et al..[16] TMPD (500 mg, 3.04 mmol) was dissolved in a solution of MeOH (12 mL) and H_2O (9 mL) containing $NaBF_4$ (4.49 g, 40.9 mmol). The solution was cooled to 263 K and a 0.252 M solution of Br_2 (15.7 mL, 3.95 mmol) added dropwise. The resultant crystals were filtered off and washed with cold MeOH followed by Et_2O. The crude product was recrystalised from MeOH to furnish $TMPD^{+}BF_4^{-}$ (248 mg, 0.987 mmol, 32%) as a purple solid; m.p. 118-119 °C

(MeOH) [Lit. m.p. 126-127 °C (decomposed) (MeOH)],[16] ESR hyperfine coupling constants (MeCN) a^{H}_{CH} = 0.690 mT [Lit. 0.677 mT], $a^{H}_{CH_3}$ = 0.197 mT [Lit. 0.199 mT], a^{N} = 0.695 mT [Lit. 0.705 mT].[17]

Bulk electrolysis of TMPD to $TMPD^{+\bullet}$ in acetonitrile was carried out using a 100 mL cell consisting of two compartments, separated by a ceramic frit, and employing a conventional three-electrode arrangement. In one compartment were placed the TMPD solution, a reticulated vitreous carbon working electrode (5x1x1 cm^3, 10 PPI, The Electrosynthesis Company Inc., Lancaster, NY, USA) and $Ag/AgNO_3$ reference (constructed in-house), with a graphite rod counter electrode in supported acetonitrile occupying the second. Constant bubbling with Argon (BOC, Surrey, UK), presaturated with MeCN, provided vigorous stirring throughout the electrolysis.

This study utilized a gold disk working electrode, nominal diameter 10 μm.

7.3 Results and Discussion

7.3.1 Analysis of Chronoamperometric Data

The diffusion coefficients of TMPD, its radical cation and dication were probed over a range of temperatures using double potential step chronoamperometry. To determine the appropriate points at which to initiate and then step the potential, a cyclic voltammogram was first recorded, such as the one shown in Figure 7.2(a) for $TMPD^{+\bullet}$ in $[C_2mim][NTf_2]$. Based on this, the potential region corresponding to the passage of no faradaic current was identified (in Figure 7.2(a) this is around +0.15 V *vs* Ag) and the potential held in this region for 50 s to ensure that the two-electrode system had stabilised. It was then stepped to a more positive value in the mass transport-limited region of the adjacent oxidation process (around +0.75 *vs* Ag in

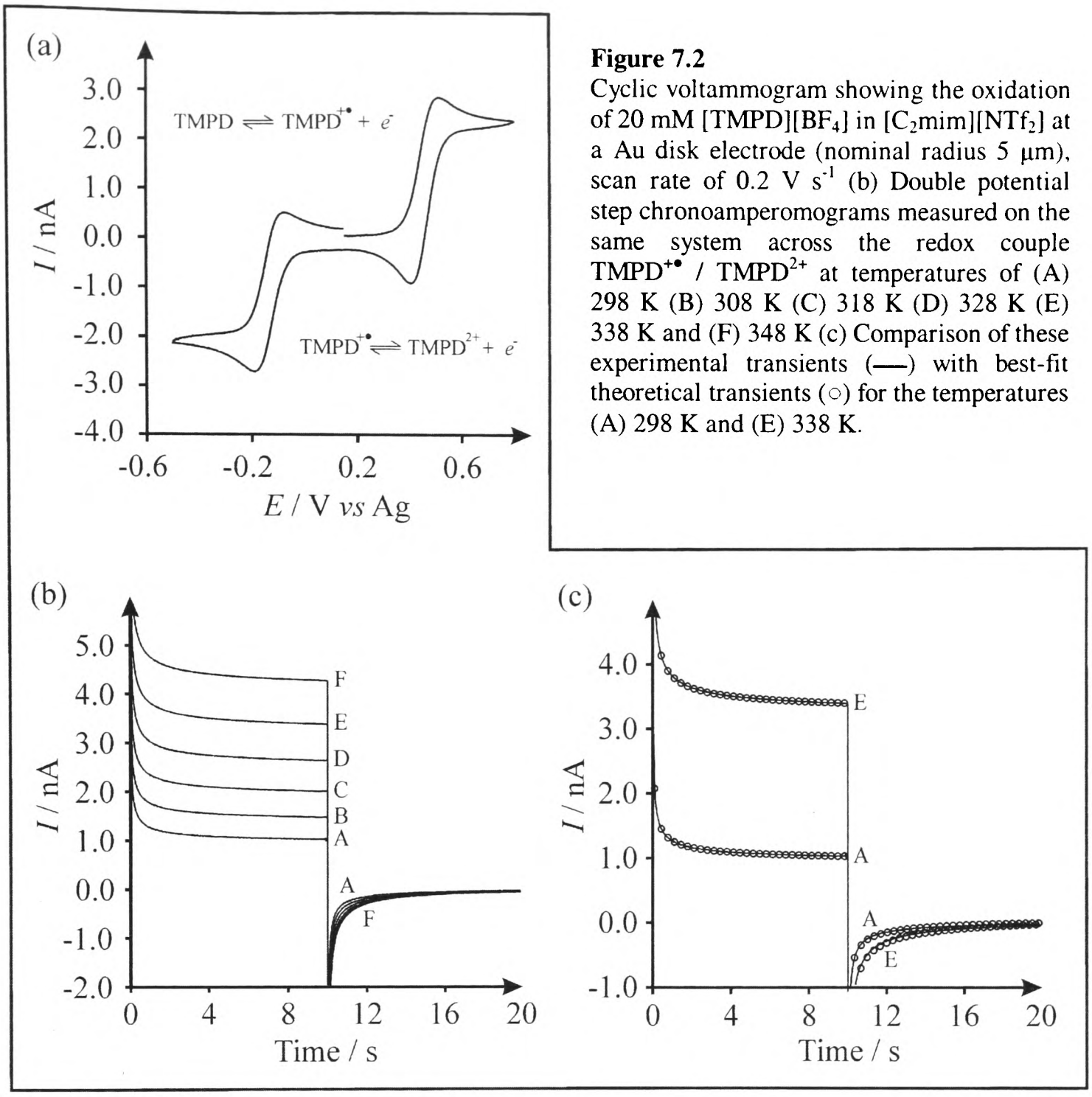


Figure 7.2
Cyclic voltammogram showing the oxidation of 20 mM [TMPD][BF_4] in [C_2mim][NTf_2] at a Au disk electrode (nominal radius 5 μm), scan rate of 0.2 V s^{-1} (b) Double potential step chronoamperomograms measured on the same system across the redox couple $TMPD^{+\bullet}$ / $TMPD^{2+}$ at temperatures of (A) 298 K (B) 308 K (C) 318 K (D) 328 K (E) 338 K and (F) 348 K (c) Comparison of these experimental transients (—) with best-fit theoretical transients (○) for the temperatures (A) 298 K and (E) 338 K.

Figure 7.2(a)) and held for 10 s. Finally, the potential was stepped back to its original value, and the current response monitored for a further 10 s. Such double potential steps were recorded from room temperature up to 348 K at 10 K intervals, and Figure 7.2(b) shows the resulting set of scans for the $TMPD^{+\bullet}$ / [C_2mim][NTf_2] system. As in the previous studies on TMPD,[8] background chronoamperograms recorded under the same conditions in the pure ionic liquid alone revealed currents negligible in comparision to those generated by the faradaic processes of interest. Consequently, baseline correction of the data prior to its analysis was not deemed necessary.

In order to extract diffusion coefficients from these transients, the data from the first potential step (which depends on diffusion of the electroactive species only) were first fitted to the Shoup and Szabo analytical expression (equation (1.28) in section 1.5.1). The fit was optimized by using the nonlinear curve fitting function within ORIGIN 6.0 (Microcal Software Inc.) by varying *D*, the only unknown parameter. Examples of the resulting fits are shown in Figure 7.2(c) for two of the chronoamperograms for the $TMPD^{+\bullet}$ / $[C_2mim][NTf_2]$ system. As no equivalent analytical expression exists to describe the current-time behaviour of the second potential step, it became necessary to employ a computer simulation to model this section of the data, full details of which were described in the previous chapter.[15] This latter section of the current-time profile is a function of the diffusion coefficients of both the reduced and oxidized species involved in the electrochemical couple as well as the length of the first potential step. However, with the former quantity now known from analysis of the first step data, the simulation program was instructed to vary the latter, until the closest match was achieved. Two of the fits so obtained are shown in the latter half (10-20 s) of Figure 7.2(c) for $TMPD^{+\bullet}$ in $[C_2mim][NTf_2]$.

7.3.2 Results in Acetonitrile

In order to provide the means to compare data from the RTILs with that derived from acetonitrile, diffusion of the three phenylenediamine species was first studied in solutions of the latter, although the volatility of this solvent necessitated the use of a more restricted temperature range ($\leq$ 323 K). Since relatively few studies on diffusion in ionic liquids have been reported, this also afforded the chance to compare diffusional parameters obtained using our proposed strategy with corresponding data from the literature. Measurements on the neutral compound were made using several

~10 mL solutions of varying TMPD concentration (0.5–5.0 mM), supported with 0.1 M TBAP. The diffusion coefficient of TMPD was confirmed to be independent of concentration within this range. A solution of the radical cation was then prepared by bulk electrolysis of 2 mM TMPD at a potential just beyond the peak of its first oxidation. The process took approximately 2 hours and was considered complete when the current had decreased to ~0.3 % of its initial value. Double step chronoamperometry performed on ~20 mL of this solution then furnished the necessary information on the radical and dication species. Additional measurements on the neutral molecule and radical cation were performed using the alternative supporting electrolytes: $TBAPF_6$ and $TBABPh_4$ (both 0.1 M). Having extracted diffusion coefficients at each temperature, all the data were then analysed via plots of ln D versus $1/T$ as a test of conformity to an Arrhenius-type relationship:

$$D = D_0 e^{-E_a/RT} \qquad (7.03)$$

where E_a is a diffusional activation energy for the species of interest in the solvent at hand and D_0 is a constant corresponding to the hypothetical diffusion coefficient at $1/T \rightarrow 0$. For each species, the plot was linear ($R^2 \geq 0.995$) and the resulting parameters are listed in Table 7.1. The diffusional activation energy of TMPD in acetonitrile, determined to be 10.7 ± 0.5 kJ mol^{-1}, is in excellent agreement with the literature.[18-20] In the MeCN / TBAP system, the ratio of the diffusion coefficients of the radical cation and neutral TMPD, R_1 (=D(TMPD$^{+\bullet}$)/D(TMPD)), was found to be 0.89 ± 0.05 (taken at the midpoint temperature, 308 K, with an error margin based on the uncertainty in the two coefficients at this point). This compares to values from previous reports under the same conditions of 0.99 ± 0.10 and 0.79 ± 0.02.[4,13] A larger discrepancy was seen in the case of the dication, where the ratio of diffusion

Table 7.1
Arrhenius parameters for the variation with temperature (293–323 K) in diffusion coefficient ($D = D_0\exp(-E_{a,D}/RT)$ of species TMPD, its radical cation, $TMPD^{+\bullet}$, and dication, $TMPD^{2+}$, in acetonitrile and various supporting electrolytes. Diffusion parameters in regular font were derived from single step potential chronoamperograms, whilst those in italics were determined via the analysis of double potential step data.

MeCN / 0.1 M X X:	TMPD D_0 / m^2 s^{-1}	$E_{a,D}$ / kJ mol^{-1}	$TMPD^{+\bullet}$ D_0 / m^2 s^{-1}	$E_{a,D}$ / kJ mol^{-1}
TBAP	1.65×10^{-7}	10.7	1.39×10^{-7}	10.5
$TBAPF_6$	1.34×10^{-7}	10.1	9.31×10^{-8}	9.6
$TBABPh_4$	1.91×10^{-7}	11.0	1.84×10^{-7}	11.4
	$TMPD^{2+}$ D_0 / m^2 s^{-1}	$E_{a,D}$ / kJ mol^{-1}	R_1 $D_{308}^{TMPD^{+\bullet}} / D_{308}^{TMPD}$	R_2 $D_{308}^{TMPD^{2+}} / D_{308}^{TMPD}$
TBAP	*9.81×10^{-8}*	*11.1*	0.88 ± 0.05	0.51 ± 0.03
$TBAPF_6$	-	-	0.85 ± 0.05	-
$TBABPh_4$	-	-	0.84 ± 0.05	-

coefficients, R_2 ($=D(TMPD^{2+})/D(TMPD)$), was down to 0.51 ± 0.03. This trend is consistent with a similar study in acetonitrile on tetracyanoquinodimethane, its radical anion and dianion in which the ratio of diffusion coefficients of the latter two to the former were reported to be 0.94 ± 0.04 and 0.63 ± 0.03 respectively.[12] It is also evident from Table 7.1 that varying the identity of the anion in the supporting electrolyte has, within experimental error, virtually no effect on the magnitude or ratio of the diffusion coefficients of the neutral and radical TMPD species, implying that the radical cation is not ion paired in this medium.

7.3.3 Results in Room Temperature Ionic Liquids

Turning next to the ionic liquids, as all the diffusion data reported herein for RTIL solvents was derived from the same experimental procedure, initially some preliminary work was necessary to determine and validate an efficient and accurate operating protocol. Once the gold disk electrode had been immersed in a small amount of RTIL containing the electroactive species of interest and positioned within

the apparatus, as described in the previous section, the cell was placed under vacuum at room temperature to minimize the presence of volatile impurities (oxygen, water vapour, residual acetonitrile). The level of these impurities was monitored by periodically recording background voltammograms, and 30 minutes under these conditions was found to be ample time to obtain a constant signal. Consequently, an initial 30 minute purge was routinely performed prior to the collection of any data, and the vacuum maintained throughout the entire experiment to preserve these conditions. It was then general practice to perform all desired scans at the lowest temperature, increase the temperature slightly and re-run these scans, and then repeat this cycle up to the highest temperature of interest. As anticipated, the magnitude of both the oxidative and reductive currents increased with increasing temperature as a result of an increase in the rate of diffusion of the electroactive species to the electrode surface. During a preliminary run, on each occasion that the internal temperature was increased, the diffusion-limited current for oxidation of the electroactive species was monitored to gauge the length of time necessary for it to settle at a new maximum. Here it was found that waiting 10 minutes after the internal thermometer had first registered the new target temperature before taking a measurement was prudent in order to be confident that the RTIL solution had experienced the full temperature increase. The concentration of the electroactive species was chosen to be 20 mM for all RTIL experiments. As a result of the lower currents generated in these viscous media, this seemingly high concentration is necessary to boost the strength of the faradaic response against the background.[21] Doherty has recently reported a concentration dependence on the diffusion of ferrocene in the RTIL 1-butyl-3-methylimidazolium bis(trifluoromethylsulfonyl)-

imide;[9] their electrochemically determined diffusion coefficient showed a small, but linear increase with low ferrocene concentrations which progressed to an stronger increase at higher concentrations (> 35 mM). The occurrence of this apparent enhancement in the diffusion rate was not rationalised. With this in mind, a brief investigation was undertaken to compare the chronoamperometrically determined diffusion coefficients of TMPD in $[C_4pyr][NTf_2]$ at several analyte concentrations over a 5–40 mM range. The results did not reveal a trend and all the determined values were statistically equivalent, within the accuracy of the technique. It would seem therefore, that the possibility of concentration-augmented diffusion should not be a major concern, for the phenylendiamine system at least. Nevertheless, in the current study, solutions 20 mM in the electroactive species were always employed to ensure that any concentration-dependent phenomenon could not obfuscate the effects of changing the variables under investigation here. Finally, generation of the $TMPD^{+\bullet}$ via bulk electrolysis was not practical here given the size of the working electrode and the two-electrode setup. Instead, a quantity of the tetrafluoroborate salt of the radical cation was synthesized (see section 7.2), and thus solutions of it could be directly prepared.

Having developed a reliable method of data acquisition, the determination of diffusion coefficients for the neutral, monocationic and dicationic phenylenediamine species in each of the four ionic liquids was attempted at several intervals over a 50 K temperature range. Wherever possible, this was achieved via the collection of first potential step data since its analysis involves a single unknown parameter (and requires minimal computation time relative to that required when employing the computer simulation for the second step). In principle, this was possible for both the

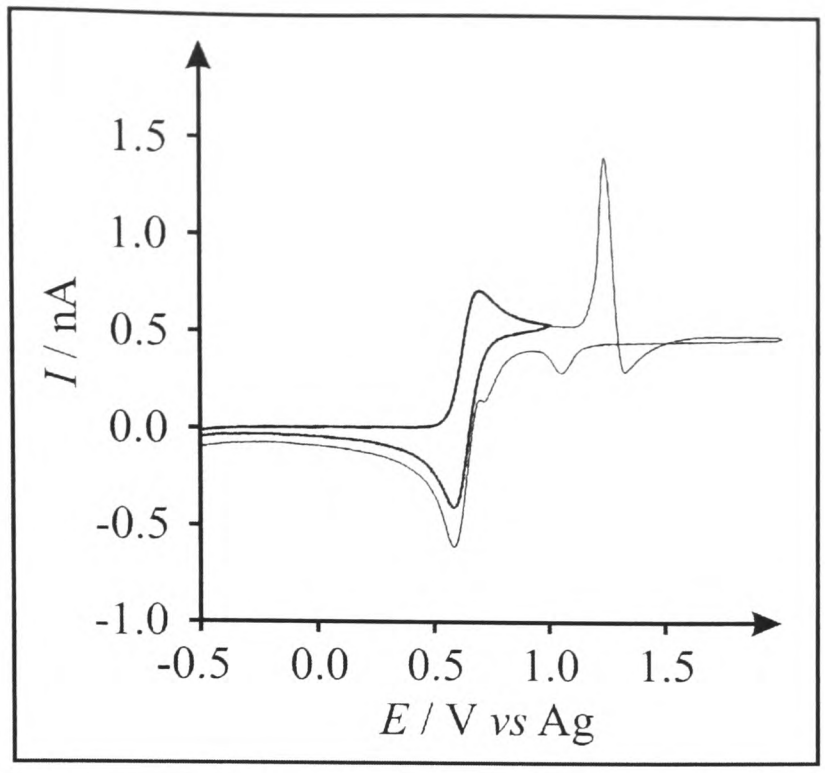


Figure 7.3
Cyclic voltammograms showing the oxidation of 20 mM TMPD in $[P_{14.666}][NTf_2]$ at a Au disk electrode (nominal radius 5 μm), scan rate of 0.2 V s^{-1}, sweep reversed at (—) +1.0 V *vs* Ag and (—) +2.0 V *vs* Ag.

neutral compound and the radical cation in each RTIL, since solutions of these species could be readily prepared. This leaves the dication, for which probing via second potential step data derived from oxidation of the radical cation solution was the sole option. In practice, the only deviation from this strategy arose for the case when the RTIL $[P_{14.666}][NTf_2]$ was used as the solvent. Here, whilst relatively normal voltammetry was observed for the oxidation and immediate re-reduction of TMPD / $TMPD^{+\bullet}$ (Figure 7.3, thick line), sweeping the potential further positive to promote the formation of the dication resulted in an anomalous wave-shape (Figure 7.3, thin line). As the only incidence of this phenomenon in the present study, its occurence is indicative of chemical reaction taking place between the phenylenediamine cations and the tris(*n*-hexyl)tetradecylphosphonium ion, $[P_{14.666}]$. Evidence of similar behaviour with electrogenerated species has been noted previously in a study of the reduction of dioxygen in both $[P_{14.666}][NTf_2]$ and a second RTIL comprised of this cation.[11] In these cases, deprotonation by superoxide of an alkyl carbon alpha to the phosphorus atom was postulated to be taking place, leading to the formation of additional electroactive species and the regeneration of O_2. These results, combined

with the present findings, would seem to suggest that in the use of $[P_{14,666}]$-based ionic liquids, the solvent ions should not be dismissed as mere spectators, but are in fact quite capable of modifying the chemical process of interest. The consequences for the current investigation were that the diffusion rate of the radical cation was instead gauged from second step data for the neutral compound, whereas this property of the dication was rendered inaccessible.

Even in the absence of solvent effects however, the determination of a diffusion coefficient for $TMPD^{2+}$ in this, the most viscous of the RTILs under investigation may have been hindered by another complicating factor, encountered for all systems while recording the second potential step. It was found experimentally that the latter half of the current-time profile for any double potential step chronoamperogram measured across the $TMPD^{+\bullet}$ / $TMPD^{2+}$ couple varied depending on exactly where in the diffusion controlled region the potential was stepped. At more positive potentials, the curves were distorted from the theoretically-predicted shape; in particular, they had a tendency to climb into positive current values after the initial few seconds, a fact that is clearly irreconcilable with a simple re-reduction of the dication taking place on this backward step. Such behaviour can instead be rationalised in terms of a

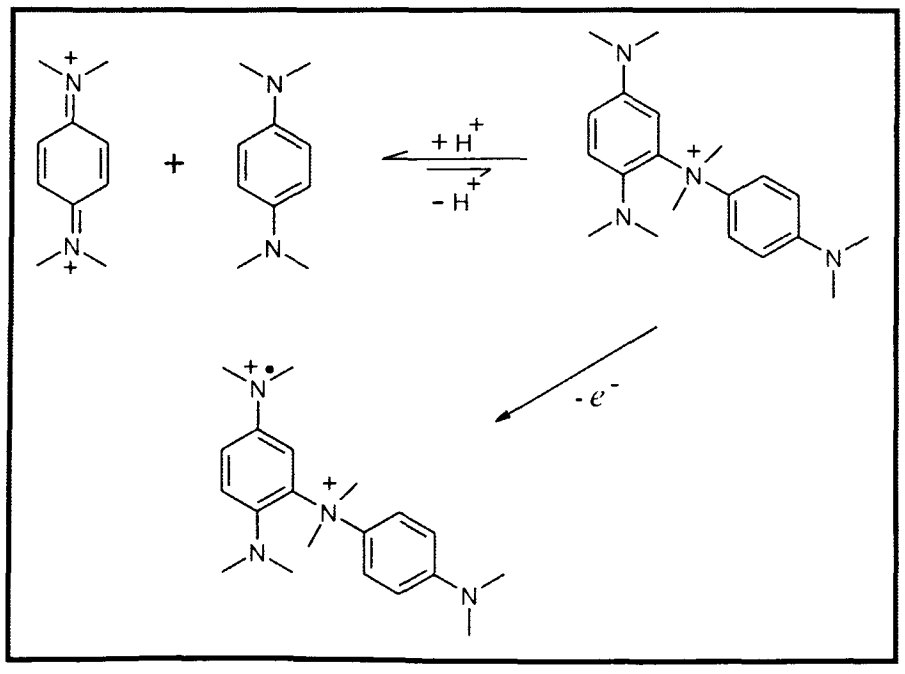


Figure 7.4
Dimerisation reaction between the neutral cation and TMPD.

dimerisation reaction between the dication and neutral TMPD (see Figure 7.4) as the latter begins to form at potentials approaching the reduction of $TMPD^{+\bullet}$. This dimer is itself electroactive, but being positively charged would be expected to oxidise at a potential more positive than for the first oxidation of the monomer. Thus if the second step is made to a potential greater than this value, oxidation of the dimer can occur, driving the coupling reaction and giving rise to an overall positive current:

$$TMPD + TMPD^{2+} \rightleftharpoons Dimer^{+} + H^{+} \xrightarrow{-e^-} Dimer^{2+} \qquad (7.04)$$

By ensuring that the second step potential is sufficiently negative however, this side reaction may never become favoured and the measured current is truly that due to the re-reduction of $TMPD^{2+}$ only. This in effect places a more restrictive upper bound on the potential range available in which to locate the second step, the lower bound of which is obviously the onset of reduction of the radical cation. In practice, the size of this window varied with solvent and although the double step experiment could be accommodated when using acetonitrile and the RTILs $[C_2mim][NTf_2]$ and $[C_4pyr][NTf_2]$, it had shrunk sufficiently in $[C_{10}mim][NTf_2]$ to prevent a determination of the diffusion coefficient of $TMPD^{2+}$ in this ionic liquid by chronoamperometric means.

Exceptional cases aside, there remained ten combinations of phenylenediamine species and ionic liquid from which variable temperature diffusion coefficient data was successfully gleaned. For each of these, analogous chronoamperograms to those shown in Figure 7.2(b) were obtained from at least three separate experimental runs, to ensure the collection of reliable data. As with acetonitrile, the derived diffusion coefficients were then analysed in terms of an Arrhenius-type behaviour, and Figure 7.5 shows several of the resulting plots for (a) TMPD in each of the four RTILs and

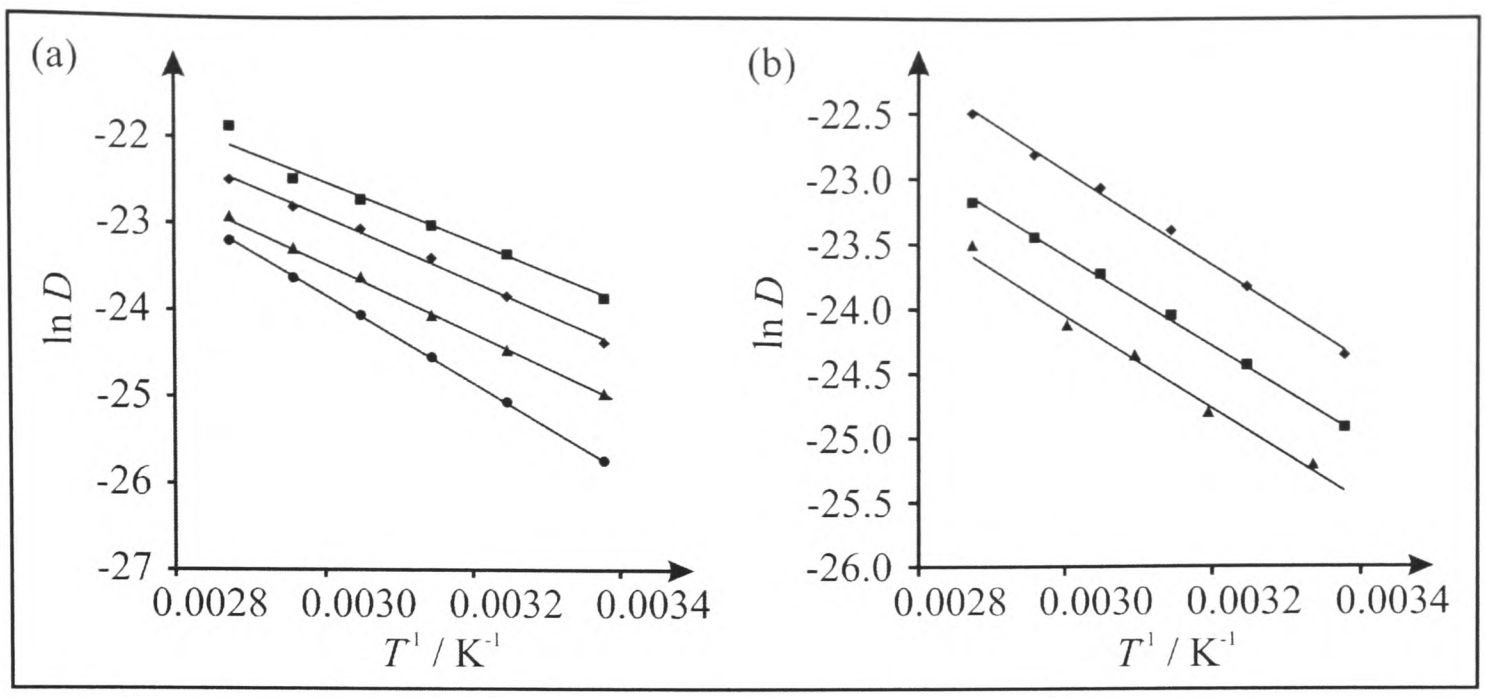


Figure 7.5
Arrhenius Plots of ln D *vs* T^{-1} over the range 298–348 K for the diffusion coefficients of (a) TMPD in the RTILs (■) $[C_2mim][NTf_2]$ (♦) $[C_4pyr][NTf_2]$ (▲) $[C_{10}mim][NTf_2]$ (●) $[P_{14.666}][NTf_2]$ and (b) (♦) TMPD (□) $TMPD^{+\bullet}$ (Δ) $TMPD^{2+}$ in the RTIL $[C_4pyr][NTf_2]$

(b) the three phenylenediamine species in $[C_4pyr][NTf_2]$. In all cases, a high degree of linearity is observed ($R^2 \geq 0.98$). Table 7.2 then summarises this temperature-dependent diffusion coefficient data for each system in terms of the two parameters D_0 and E_a. Based on the analysis of multiple runs, an error margin of 6% (single step) and 16% (double step) on any diffusion coefficient calculated using these parameters in the range 293-348 K is appropriate. Viscosity data for the four neat ionic liquids was also collected over the same temperature range and displays a similar linearity when itself subjected to an Arrhenius-type analysis (here dynamic viscosity, $\eta = \eta_0 e^{Ea/RT}$). The resulting parameters are also included in Table 7.2.

7.3.4 Discussion

Examining this table, a major conclusion to be drawn is that the activation energy for the diffusion of the neutral, cationic and dicationic forms of TMPD are, within experimental error, essentially the same. There is considerable data to suggest that the diffusional activation energy in solvents such as acetonitrile or N,N-

Table 7.2
Arrhenius parameters for the variation with temperature (298–348 K) in neat solvent viscosity ($\eta = \eta_0 \exp(E_{a,\eta}/RT)$ and diffusion coefficient ($D = D_0 \exp(-E_{a,D}/RT)$ of species TMPD, its radical cation, $TMPD^{+\bullet}$, and dication, $TMPD^{2+}$, in four room temperature ionic liquids. Diffusion parameters in regular font were derived from single step potential chronoamperograms, whilst those in italics were determined via the analysis of double potential step data.

	Viscosity η_0 / mPa s	$E_{a,\eta}$ / kJ mol^{-1}	Diffusion TMPD D_0 / m^2 s^{-1}	$E_{a,D}$ / kJ mol^{-1}
$[C_2mim][NTf_2]$	3.36 x 10^{-4}	28.5	4.54 x 10^{-6}	28.3
$[C_4pyr[NTf_2]$	4.61 x 10^{-4}	29.6	6.70 x 10^{-6}	30.5
$[C_{10}mim][NTf_2]$	1.89 x 10^{-4}	33.1	8.61 x 10^{-6}	32.7
$[P_{14.666}][NTf_2]$	4.52 x 10^{-5}	39.5	1.62 x 10^{-4}	41.8
	Diffusion $TMPD^{+\bullet}$ D_0 / m^2 s^{-1}	$E_{a,D}$ / kJ mol^{-1}	Diffusion $TMPD^{2+}$ D_0 / m^2 s^{-1}	$E_{a,D}$ / kJ mol^{-1}
$[C_2mim][NTf_2]$	1.51 x 10^{-6}	27.0	*8.71 x 10^{-7}*	*26.9*
$[C_4pyr[NTf_2]$	2.19 x 10^{-6}	29.2	*1.86 x 10^{-6}*	*30.0*
$[C_{10}mim][NTf_2]$	5.86 x 10^{-6}	33.2	-[a]	-[a]
$[P_{14.666}][NTf_2]$	*1.24 x 10^{-6}*	*43.2*	-[a]	-[a]
	R_1 $D_{323}^{TMPD^{+\bullet}} / D_{323}^{TMPD}$		R_2 $D_{323}^{TMPD^{2+}} / D_{323}^{TMPD}$	
$[C_2mim][NTf_2]$	0.54 ± 0.03		0.33 ± 0.05	
$[C_4pyr[NTf_2]$	0.53 ± 0.03		0.33 ± 0.05	
$[C_{10}mim][NTf_2]$	0.57 ± 0.03		-[a]	
$[P_{14.666}][NTf_2]$	0.46 ± 0.07		-[a]	

[a] Determination prevented due to interfering homogeneous processes (see text)

dimethylformamide is approximately independent of molecular size or identity[20,22] and this may point to a similarity in mechanism of transport between RTILs and simple organic solvents. Furthermore, the diffusional activation energy and the activation energy of viscous flow for the ionic liquid medium in which the diffusion takes place are also essentially equivalent, indicating an inverse linear relationship between diffusion and viscosity, as commonly seen in conventional molecular solvents and often embodied using the classical Stokes-Einstein relation:

$$D = \frac{kT}{6\eta\pi a} \qquad (7.05)$$

where k is the Boltzmann constant and a the hydrodynamic radius of the diffusing species. Use of this equation to estimate the radius of the TMPD molecule in the RTIL solvents (by approximating it as spherical) typically gives values one-half to one-third of that calculated using molecular volumes (3.4 Å).[23] Disagreement is not unexpected however, considering the wealth of experimental evidence to suggest that this simple hydrodynamic theory is quantitatively inadequate when any of the following conditions are fulfilled: (i) the diffusing molecule is small in comparison with the molecules of the solvent (ii) the solvent has a high viscosity and (iii) solute-solvent interaction can occur.[24]

The last two columns of Table 7.2 show the ratios, R_1 and R_2, of diffusion coefficients of the radical cation and dication to that of the neutral parent (calculated at 323 K, but virtually independent of temperature over the studied range since $E_{a,D}$ is approximately the same for each species). In distinct contrast to acetonitrile, the diffusion coefficient of $TMPD^{+\bullet}$ is consistently around half that of TMPD throughout the ionic liquids studied. It would seem that the effect of any charge present on the diffusing species is much more considerable in these highly associated solvents. Removal of a second electron achieves another significant drop in the diffusion coefficient, again more prominent than in comparison with acetonitrile (R_2 = 0.33 *vs* 0.51), where the presence of charge only now becomes important in influencing the magnitude of D. Finally, it is noteworthy that the ratios R_1 and R_2 showed little variation among the different ionic liquids themselves. This is likely due to solvation of the positively charged TMPD species being dominated in each case by the common anion [NTf_2], since the RTILs employed only varied structurally in terms of their cationic component.

7.4 Conclusions

Diffusion of the TMPD molecule, its radical cation and dication was investigated over a 50 K temperature range in four room temperature ionic liquids and the conventional solvent acetonitrile (supported with 0.1 M TBAP). Diffusion coefficients were successfully determined for each of these species using a combination of single and double potential step chronoamperometry, except for the dication in the two most viscous RTILs, $[C_{10}mim][NTf_2]$ and $[P_{14.666}][NTf_2]$, where involvement of this species in secondary reactions precluded such an evaluation. An Arrhenius relationship between diffusion coefficient and temperature was uniformly followed, and the diffusional activation energy was approximately constant for all three species in a given solvent. Furthermore, this diffusional activation energy was found to be virtually equivalent to the activation energy of viscous flow in each ionic liquid, demonstrating a qualitative conformity to the simple Stokes-Einstein relation. Whereas in acetonitrile the diffusion coefficient of the TMPD radical cation was only slightly diminished from that of neutral TMPD (R_1 = 0.89), throughout the ionic liquids studied this ratio was around 0.5. In the case of the dication, the diffusion coefficient was significantly lower in all cases, but again more exaggerated in the RTILs (R_2 = 0.32 *vs* 0.51). In chapter four,[8] the unsuitability of the empirical Wilke-Chang expression[25] for estimating diffusion coefficients in ionic liquid media was demonstrated. Now, use of a second recourse of the electroanalyst, namely the assumption of equal diffusion coefficients for an electrochemical reaction system has also been shown to be potentially unwise when the solvent in question is a RTIL.

Having applied electrochemistry to investigate the translational movement of species within ionic liquid solutions, the next chapter continues the diffusional analysis by supplementing this technique with electron spin resonance measurements to additionally probe rotational motion.

7.5 References

[1] R.G. Evans, O.V. Klymenko, P.D. Price, S.G. Davies, C. Hardacre, R.G. Compton, *ChemPhysChem* **2005**, *6*, 526.

[2] R.L. Wang, K.Y. Tam, F. Marken, R.G. Compton, *Electroanalysis* **1997**, *9*, 284.

[3] R.G. Compton, B.A. Coles, R.A. Spackman, *J. Phys. Chem.* **1991**, *95*, 4741.

[4] R.L. Wang, K.Y. Tam, R.G. Compton, *J. Electroanal. Chem.* **1997**, *434*, 105.

[5] M.C. Buzzeo, R.G. Evans, R.G. Compton, *ChemPhysChem* **2004**, *5*, 1106.

[6] T. Welton, *Chem. Rev.* **1999**, *99*, 2071.

[7] D.L. Boxall, J.J. O'Dea, R.A. Osteryoung, *J. Electrochem. Soc.* **2002**, *149*, E468.

[8] R.G. Evans, O.V. Klymenko, C. Hardacre, K.R. Seddon, R.G. Compton, *J. Electroanal. Chem.* **2003**, *556*, 179.

[9] C.A. Brooks, A.P. Doherty, *Electrochem. Commun.* **2004**, *6*, 867.

[10] U. Schröder, J.D. Wadhawan, R.G. Compton, F. Marken, P.A.Z. Suarez, C.S. Consorti, R.F. de Souza, J. Dupont, *New J. Chem.* **2000**, *24*, 1009.

[11] R.G. Evans, O.V. Klymenko, S.A. Saddoughi, C. Hardacre, R.G. Compton, *J. Phys. Chem. B* **2004**, *108*, 7878.

[12] Z. Rongfeng, D.H. Evans, *J. Electroanal. Chem.* **1995**, *385*, 201.

[13] N. Leventis, X. Gao, *J. Electroanal. Chem.* **2001**, *500*, 78.

[14] D. Shoup, A. Szabo, *J. Electroanal. Chem.* **1982**, *140*, 237.

[15] O.V. Klymenko, R.G. Evans, C. Hardacre, I.B. Svir, R.G. Compton, *J. Electroanal. Chem.* **2004**, *571*, 211.

[16] J. Yamauchi, H. Fujita, Y. Deguchi, *Bull. Chem. Soc. Jpn.* **1979**, *52*, 2819.

[17] J.A. Weil, J.R. Bolton, J.E. Wertz, *Electron Paramagnetic Resonance: Elementary Theory and Practical Applications*, John Wiley, New York, **1994**.

[18] H. Fernandez, M.A. Zon, *J. Electroanal. Chem.* **1990**, *283*, 251.

[19] M.A. Zon, H. Fernandez, L. Sereno, J.J. Silber, *Electrochim. Acta* **1987**, *32*, 1733.

[20] S.R. Jacob, Q. Hong, B.A. Coles, R.G. Compton, *J. Phys. Chem. B* **1999**, *103*, 2963.

[21] C. Lagrost, D. Carrié, M. Vaultier, P. Hapiot, *J. Phys. Chem. A* **2003**, *107*, 745.

[22] B.A. Coles, M.J. Moorcroft, R.G. Compton, *J. Electroanal. Chem.* **2001**, *513*, 87.

[23] A. Kapturkiewicz, W. Jaenicke, *J. Chem. Soc., Faraday Trans.* **1987**, *83*, 2727.

[24] H.J.V. Tyrrell, K.R. Harris, *Diffusion in Liquids: A Theoretical and Experimental Study*, Butterworths & Co. Ltd., **1984**.

[25] C.R. Wilke, P. Chang, *Am. Inst. Chem. Eng. J.* **1955**, *1*, 264.

8

An Electrochemical and ESR Study on the Molecular Dynamics of TEMPO in Room Temperature Ionic Liquid Solvents

Measurements on the temperature variation of the translational and rotational diffusion coefficients of neutral radical species 2,2,6,6-tetramethylpiperidine-N-oxyl (TEMPO) are reported in five room temperature ionic liquids. Data pertaining to translation was obtained from chronoamperometric measurements at gold and platinum disk electrodes, involving the reversible oxidation of the molecule. Rotational information was accessed through the use of electron spin resonance (ESR) spectroscopy; slow rotational diffusion of the probe results in asymmetry in its ESR spectrum, the severity of which depends on the temperature. In some cases the observed *D-T* behaviour may be rationalized using simple hydrodynamic theories, while in others it points to an increased level of ordering within the liquid structure. This work has been published in *ChemPhysChem*.[1]

8.1 Introduction

The field of room temperature ionic liquid research is currently very active, with the potential of fashioning 'greener' alternatives to traditional molecular solvents driving intensive studies into their application across many chemical disciplines, including the synthetic and electrochemical industries.[2,3] Characterisation of the transport properties and solvating ability of this new class of reaction media will presumably form an important part in realising this endeavour to its full potential, although to date, reports on more fundamental investigations of this nature have been less common. To aid in this effort, the previous chapter explored the temperature

dependence of the translational diffusion of probe molecules N,N,N',N'-tetramethyl-*para*-phenylenediamine, its radical cation and dication in several RTIL solvents, by means of a chronoamperometric technique.[4] Amongst these species, the variation in translational diffusion coefficient, D_T, with temperature in each ionic liquid was found to obey an Arrhenius relation of general form:

$$f = f_0 e^{E_a/RT} \tag{8.01}$$

where E_a represents the activation energy associated with the temperature dependent process, f_0 is a constant of proportionality and in the current context, $f = 1/D_T$. Furthermore, the diffusional activation energies calculated by plotting $\ln f$ versus $1/T$ and measuring the slope were, for a given RTIL, largely independent of solute charge or size. Subjecting the measured viscosity, η, of the ionic liquids at each temperature to the same analysis (with $f = \eta$ in equation (8.01)) systematically yielded an activation energy of viscous flow that also closely resembled this diffusional E_a. This implies an inverse linear relationship between translational diffusion coefficient and solvent viscosity, akin to that commonly observed in conventional molecular solvents and generally formulated in terms of the Stokes-Einstein equation:

$$D_T = \frac{kT}{6\eta\pi a} \tag{8.02}$$

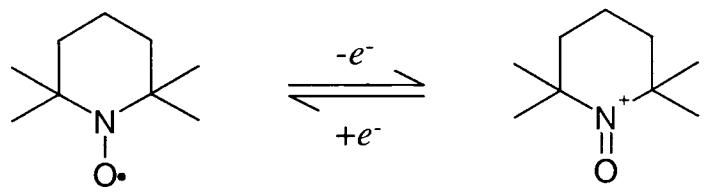
where a is the hydrodynamic radius of the (spherical) diffusing molecule.

The study at hand aims to build on this work by now expanding the investigation to include rotational diffusion. The equivalent hydrodynamic description of molecular rotation in a liquid is given by the Debye-Stokes-Einstein equation:

$$\tau_R = \frac{1}{6D_R} = \frac{4\pi\eta a^3}{3kT} \tag{8.03}$$

where D_R and τ_R are termed the rotational diffusion coefficient and rotational correlation coefficient, respectively. Note that an inverse linear relationship between rotational diffusion coefficient and solvent viscosity is again predicted. For sufficiently viscous solvents, electron spin resonance can be utilised to measure the rotational correlation coefficient of paramagnetic species via analysis of the spectral line-shapes, a technique which exploits the fact that restricted molecular tumbling of the rotational probe leads to an incomplete averaging of the ESR signal on the experimental timescale, ultimately manifesting as asymmetry in the resulting spectrum. While ESR has seldom been employed to study ionic liquids, the reports that have appeared describe the successful application of this methodology for accessing rotational solvent-solute parameters.[5,6]

The stable free radical 2,2,6,6-tetramethylpiperidine-N-oxyl (TEMPO) was selected as the diffusional probe for this study. In addition to possessing a simple and well-characterised ESR spectrum,[7] it is also capable of being oxidised electrochemically and reversibly through the loss of one electron to yield the corresponding oxammonium cation:[8]



(8.04)

Consequently, information on both translational and rotational diffusion of this molecule may be obtained by separately interrogating it via electrochemical and spectroscopic techniques. Five different ionic liquid solvents were investigated, between them spanning a viscosity range of over one order of magnitude (30.8–440.5 mPa s at 298 K). These were, in order of increasing viscosity, 1-ethyl-3-methylimidazolium bis(trifluoromethylsulfonyl)imide, $[C_2mim][NTf_2]$; N-methyl-N-

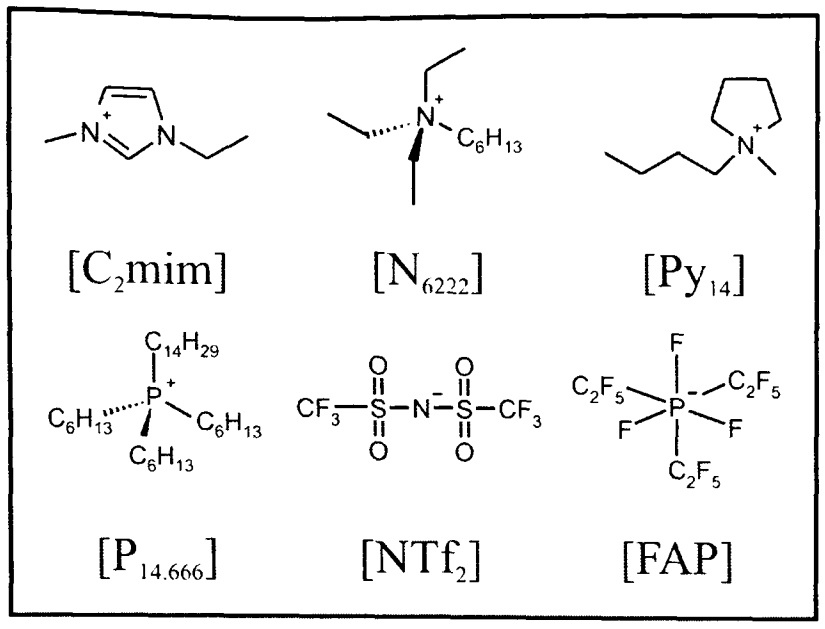


Figure 8.1
Structures of the ions comprising the room temperature ionic liquids under investigation.

butylpyrrolidinium bis(trifluoromethylsulfonyl)imide, $[Py_{14}][NTf_2]$; n-hexyltriethyl-ammonium bis(trifluoromethylsulfonyl)imide, $[N_{6222}][NTf_2]$; tris(n-hexyl)tetra-decylphosphonium bis(trifluoromethylsulfonyl)imide, $[P_{14.666}][NTf_2]$; and tris(n-hexyl)tetradecylphosphonium trifluorotris(pentafluoroethyl)phosphate, $[P_{14.666}][FAP]$ (for structures see Figure 8.1).

8.2 Experimental Section

In addition to matters already covered in chapter three, ESR spectroscopy was conducted with the assistance of Mr. Andrew J. Wain (University of Oxford). Spectra were recorded using a JEOL JES-FA100 X-band spectrometer equipped with a cylindrical (TE_{011}) cavity resonator and a ES-DVT3 variable temperature controller. In order to minimise spectral broadening due to dissolved oxygen and to prevent the absorption of water, ionic liquid solutions were thoroughly degassed with nitrogen and carefully syringed into a silica tube cell of internal diameter 2 mm, which was positioned centrally in the ESR cavity. An atmosphere of nitrogen was maintained above the ionic liquid within the cell throughout the procedure. All ESR experiments employed a microwave power of 1 mW and a modulation width of 0.01 mT.

This study utilized Au and Pt disk electrodes, both with 10 μm nominal diameters.

8.3 Results and Discussion

8.3.1 Viscosity

Initially, the viscosities of the pure ionic liquids were measured as a function of temperature between 288-368 K using a rotational viscometer with cone and plate geometry. These data were analysed in terms of equation (8.01) and the resulting plots of ln η against $1/T$ are shown in Figure 8.2. While the plots are not perfectly linear, as previously reported for these and other ionic liquids,[3,9] a simple Arrhenius relationship is sufficient to describe the variation of viscosity with temperature over the measured range, yielding a linear least squares correlation coefficient not worse than 0.98 for all RTILs. The activation energies of viscous flow extracted from the slope of each plot are listed in Table 8.1. The more viscous ionic liquids have correspondingly larger activation energies.

8.3.2 Translational Diffusion

Next, electrochemical experiments were conducted to collect translational diffusion coefficient data from the RTILs. Figure 8.3(a) shows cyclic voltammograms at three temperatures for the oxidation of a 20 mM TEMPO solution in $[N_{6222}][NTf_2]$ at a

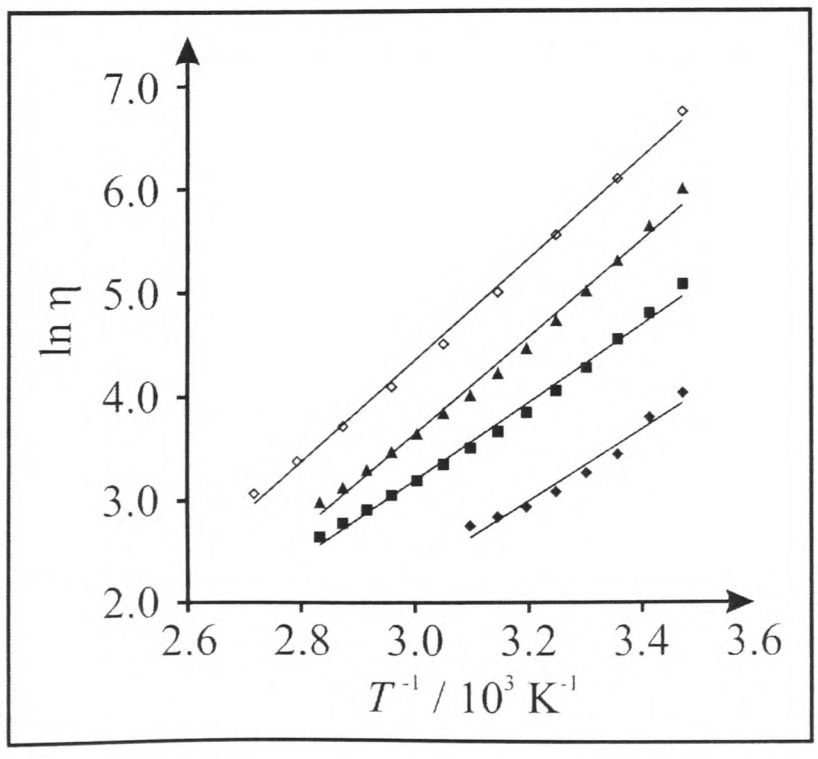


Figure 8.2
Arrhenius Plots of ln η vs $1/T$ over the range 288–368 K for the neat viscosities of room temperature ionic liquids: $[C_2mim][NTf_2]$ (◆), $[Py_{14}][NTf_2]$ (■), $[N_{6222}][NTf_2]$ (▲) and $[P_{14.666}][FAP]$ (◇).

Table 8.1
Activation energies derived from the Arrhenius equation (8.01) for the variation with temperature of neat solvent viscosity and also translational diffusion coefficient and rotational correlation coefficient of TEMPO in five room temperature ionic liquids.

	Viscosity ($f = \eta$) E_a / kJ mol^{-1}	Translational Diffusion ($f = 1/D_T$) E_a / kJ mol^{-1}	Rotational Diffusion ($f = \tau_R$) E_a / kJ mol^{-1}
$[C_2mim][NTf_2]$	28.5	27.9 ± 0.8	27.8 ± 0.3
$[Py_{14}][NTf_2]$	30.9	33.5 ± 0.6	32.1 ± 0.6
$[N_{6222}][NTf_2]$	38.6	40.7 ± 0.2	37.0 ± 1.6
$[P_{14.666}][NTf_2]$	39.5	42.6 ± 0.2	34.0 ± 2.0
$[P_{14.666}][FAP]$	40.5	41.8 ± 1.2	30.7 ± 2.7

(nominally) 10 μm diameter Pt disk electrode. Allowing for the more transient nature of the observed voltammetry due to the generally slower diffusion rates associated with use of RTILs,[3,10] it is otherwise consistent with that reported in traditional non-aqueous solvents.[8] Having located the oxidation potential of TEMPO in the ionic liquid, potential step chronoamperometry was then performed by applying an initial potential corresponding to the passage of no faradaic current then instantaneously stepping it to a value on the plateau of the voltammetric wave and recording the current response for 10 seconds. This procedure was repeated at 10 K intervals over the temperature range 293–348 K. The experimental transients were fitted to the Shoup and Szabo analytical expression for chronoamperometry at a disk electrode in a manner analogous to that explained in the previous chapter,[11,12] and a comparison of experimental and fitted transients are shown for TEMPO / $[N_{6222}][NTf_2]$ in Figure 8.3(b). In this way, translational diffusion coefficients were determined for TEMPO in all five ionic liquids. Data from three separate experimental runs using both Au and Pt electrodes were averaged to give the final D_T values, the negative natural logarithms of which are plotted against $1/T$ for three of the RTILs in Figure 8.3(c). The Arrhenius relation is again rigorously obeyed and the associated activation

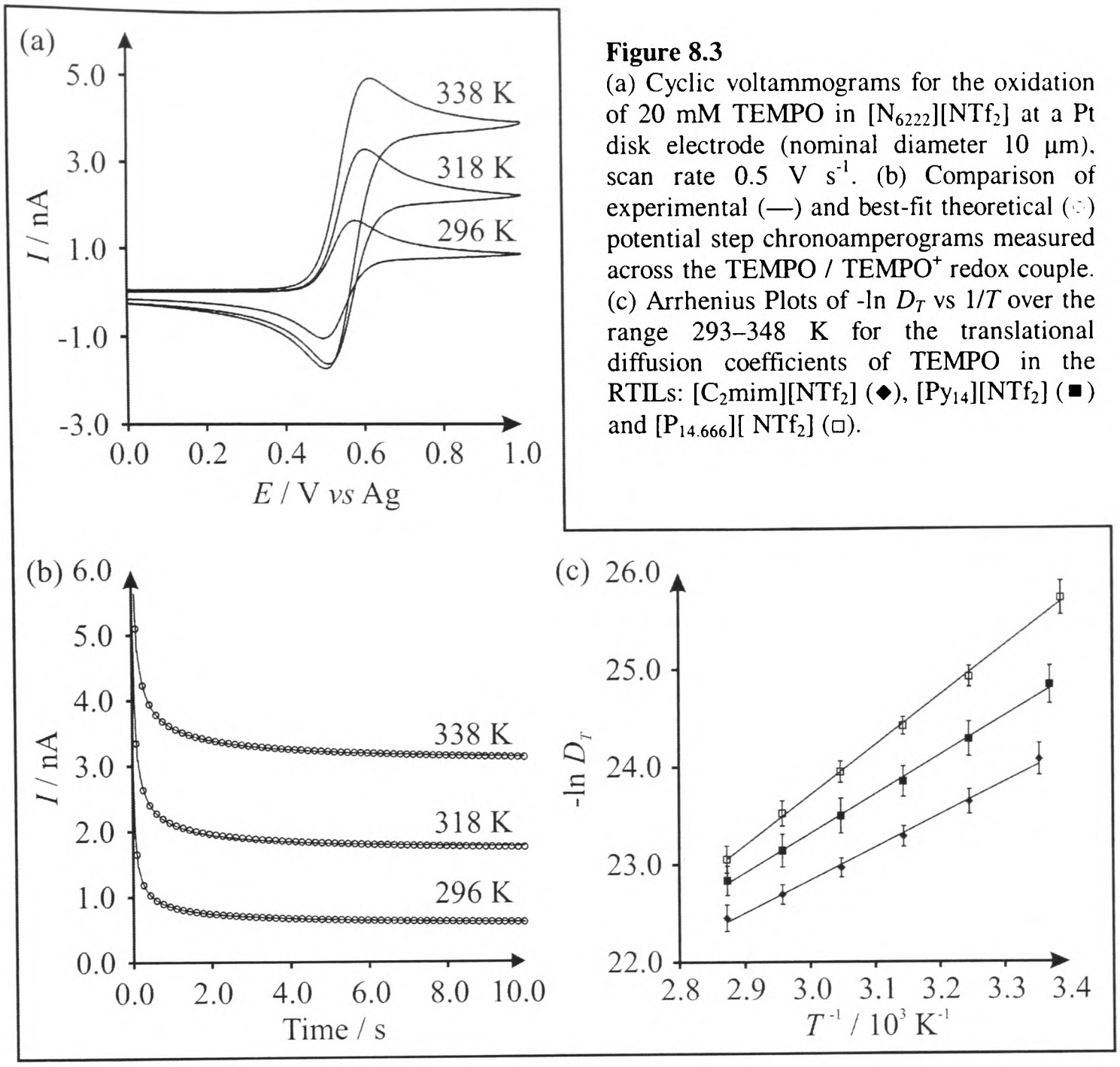


Figure 8.3
(a) Cyclic voltammograms for the oxidation of 20 mM TEMPO in $[N_{6222}][NTf_2]$ at a Pt disk electrode (nominal diameter 10 μm), scan rate 0.5 V s^{-1}. (b) Comparison of experimental (—) and best-fit theoretical (○) potential step chronoamperograms measured across the TEMPO / $TEMPO^+$ redox couple. (c) Arrhenius Plots of -ln D_T vs $1/T$ over the range 293–348 K for the translational diffusion coefficients of TEMPO in the RTILs: $[C_2mim][NTf_2]$ (◆), $[Py_{14}][NTf_2]$ (■) and $[P_{14.666}][NTf_2]$ (□).

energies are summarised in Table 8.1. Just as was observed in the case of the phenylenediamine species,[4] the correlation between the activation energies for diffusion and viscous flow is extremely close, demonstrating once again the conformity of these ionic liquid solutions to the predictions of simple hydrodynamic theory.

8.3.3 Rotational Diffusion

Having characterised the behaviour of both the RTIL neat viscosities and the translational diffusion of TEMPO within them, it only remained to probe the variation with temperature in the rotational motion of this species. Accordingly, ESR spectra of

1 mM TEMPO solutions in the ionic liquids were recorded over the temperature range 243-363 K, two of which are shown in Figure 8.4(a) for $[Py_{14}][NTf_2]$ at 273 and 363 K. As the viscosity of the solution increases with decreasing temperature, rotation of the TEMPO molecule becomes increasingly restricted and the anisotropies in the hyperfine coupling constant and *g*-value are less effectively averaged out. As evident from the figure, the result is an increasing asymmetry in the overall spectra. Over the range $10^{-11} \leq \tau_R \leq 3 \times 10^{-9}$ s (the so-called 'fast-motion' region), rotational correlation coefficients may be obtained via analysis of the ESR line-widths and relative intensities. As detailed in reference [13], within this regime the relation between τ_R and the spectral parameters is given to a good approximation by the following two expressions:

$$\tau_R = -6.1 \times 10^{-10} \Delta H(0) \left[\sqrt{\frac{I_0}{I_{+1}}} - \sqrt{\frac{I_0}{I_{-1}}} \right]$$
$$= +6.0 \times 10^{-10} \Delta H(0) \left[\sqrt{\frac{I_0}{I_{+1}}} + \sqrt{\frac{I_0}{I_{-1}}} - 2 \right] \qquad (8.05)$$

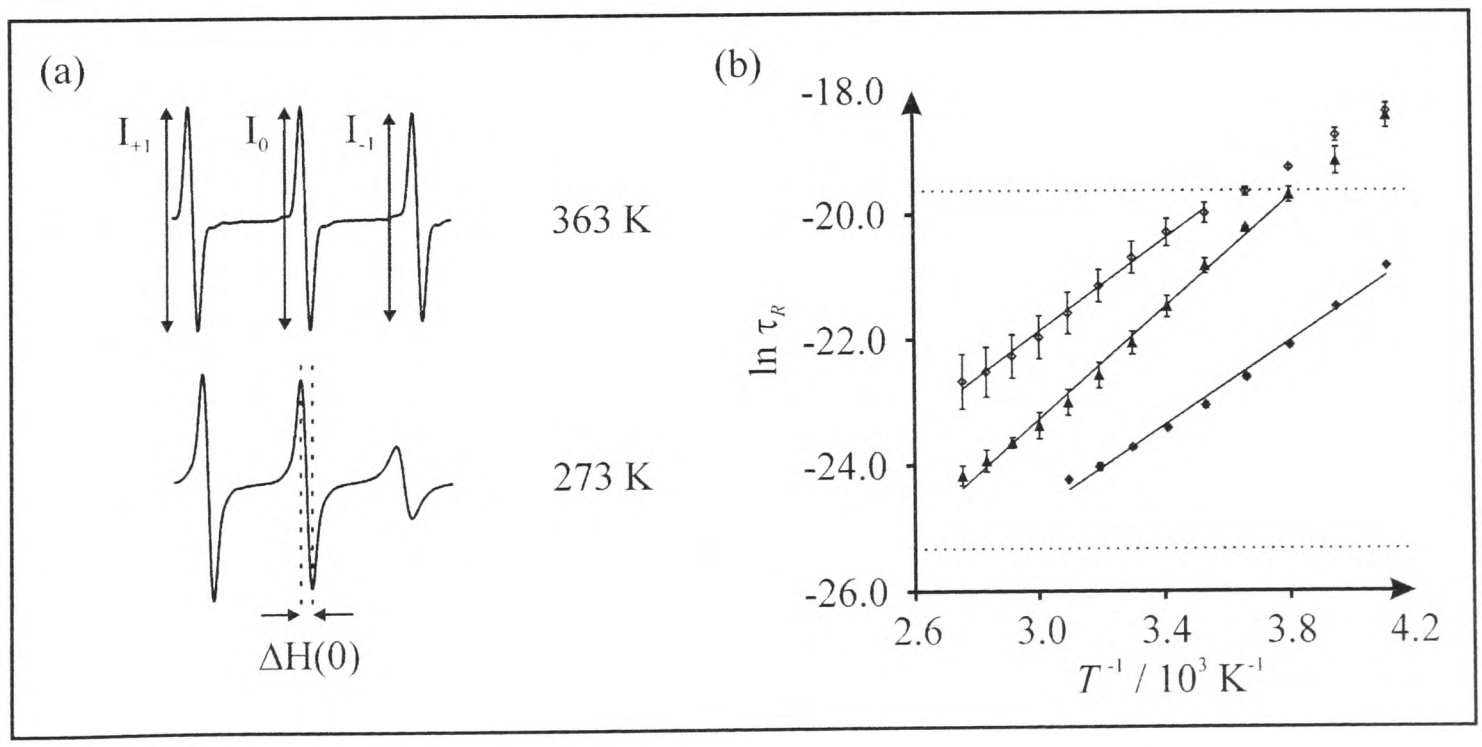


Figure 8.4
(a) ESR spectra for 1 mM TEMPO in $[Py_{14}][NTf_2]$. (b) Arrhenius Plots of ln τ_R vs $1/T$ over the range 243–363 K for the rotational correlation coefficients of TEMPO in the RTILs: $[C_2mim][NTf_2]$ (◆), $[N_{6222}][NTf_2]$ (▲) and $[P_{14.666}][FAP]$ (◇). The dotted horizontal lines demarcate the range of τ_R values in which analysis via the ESR line-shape method is appropriate.

where I_n is the intensity of the ESR line corresponding to $m_I = n$ and $\Delta H(0)$ is the width of the central ($m_I = 0$) line (as defined in Figure 8.4(a)). These two expressions are equivalent in the absence of any inhomogeneous broadening (caused, for example, by unresolved proton hyperfine interactions). No attempt was made to correct for such effects, however, whilst this inevitably places some uncertainty in the absolute τ_R values so calculated, trends in the temperature dependence of this parameter should be largely preserved. The coefficients in equations (8.05) have been determined using typical values for the hyperfine coupling constant and g-value of TEMPO rather than quantities specific to the individual RTIL solvents.[13] Once again however, while minorly affecting the value of τ_R itself, this is irrelevant as far as the calculation of a rotational activation energy is concerned. The variation of ln τ_R with $1/T$ is plotted for three ionic liquids in Figure 8.4(b), where the error bars reflect the resulting uncertainly in the rotational correlation coefficient from applying the two different expressions. Generally, the two values were in close agreement, but displayed a greater level of divergence in the case of the two phosphonium-based RTILs. Also marked are the limits of τ_R between which it is reasonable to employ the line-shape analysis method. At the lowest temperatures the formulae sometimes returned values that fell outside this range; these points were not included when calculating the gradients. All five plots were linear ($R^2 \geq 0.99$) and the rotational activation energies deduced from the slope of each line according to equation (8.01) (with $f = \tau_R$) are reported in the final column of Table 8.1.

The rotational correlation coefficients for TEMPO in the five ionic liquids at 293 K range from 0.07–1.54 ns. Cautionary remarks regarding over-interpretation of these absolute τ_R values not withstanding, it is nevertheless useful to compare the numbers

reported here with those obtained in other ionic liquids using the same approach. Noel et al. measured τ_R = 0.08 ns for TEMPO in the binary ionic liquid [C_2mim][Cl]/ $AlCl_3$ (303 K),[6] and coefficients of 0.46–1.70 ns in a range of imidazolium and tetraalkylammonium RTILs have been reported for the related compound 4-amino-2,2,6,6-tetramethylpiperidine-N-oxyl (293 K),[5] thus the present findings are consistent with the literature. Turning to the activation energies, the situation is not as straightforward as in the case of translational diffusion. In the RTILs [C_2mim][NTf_2], [Py_{14}][NTf_2] and [N_{6222}][NTf_2] the rotational E_a values are again approximately equal to those for viscous flow, in accordance with the Debye-Stokes-Einstein relation (8.03). Similar behaviour, determined via a solvatochromatic method has been reported for several probe molecules in 1-butyl-3-methylimidazolium hexafluorophosphate.[14] In these ionic liquids this is further evidence to suggest a similarity in transport mechanisms to those occurring in simple molecular solvents.

In both the tetraalkylphosphonium-containing RTILs however, the rotational activation energy was 5–10 kJ mol^{-1} lower than activation energy of viscosity flow. Maintaining the analogy with hydrodynamic theory, this would suggest that these ionic liquid solutions contain zones of lower microviscosity than the bulk value which the TEMPO molecules are more likely to inhabit. Hardacre has investigated the crystal structures of long chain alkylimidazolium-based ionic liquids ([$C_n$mim], n > 12) and identified regions consisting of interdigitated linear alkyl chains alternating with regions containing the cationic head-group and anion.[15,16] Moreover, Weiss et al. have reported similar solid structures for various long alkyl-chain phosphonium RTILs, many of which melt into a liquid-crystalline phase in which much of this order is maintained.[17-19] Where studied, this liquid-crystalline structure was largely

unaffected by the addition of up to 20 wt % of a small organic molecule (acetonitrile).[18] If the solute was disrupting the ion-ion interactions the structure would probably be destroyed, suggesting that the added acetonitrile primarily occupies the alkyl region. With their fourteen-carbon alkyl chains, it seems probable that the $[P_{14.666}][NTf_2]$ and [FAP] ionic liquids studied here also adopt this liquid-crystalline conformation. One can then envisage a solution-structure similar to that depicted schematically in Figure 8.5 with the neutral TEMPO species concentrated within these non-polar alkyl layers, and the lower rotational activation energy reflects the contribution from more facile rotation of the probe in these locations. The literature offers some support for this hypothesis, since rotational activation energies measured for TEMPO in a phospholipid (egg lecithin) and 4-oxo-2,2,6,6,-tetramethylpiperidine-N-oxyl in a micellar environment have been reported as 32.2 and 30.5 kJ mol^{-1} respectively.[20,21] As they translate through solution however, the TEMPO molecules must necessarily pass through the more ionic regions and thus the equivalence between translational and viscosity activation energies is still maintained (after all, viscosity reflects the ease of movement of solvent molecules within solution, and so these energies characterise essentially the same process).

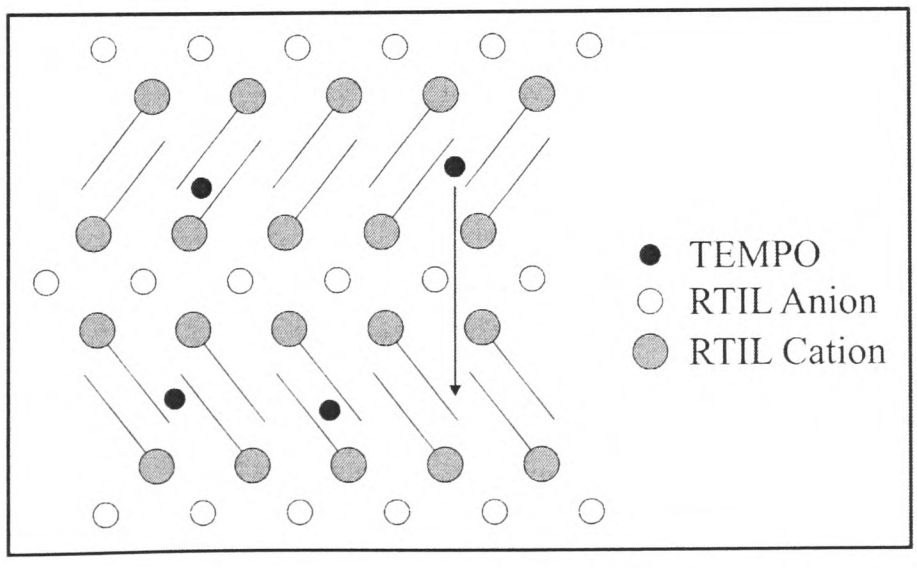


Figure 8.5
Schematic representation of the proposed bilayer structure of two RTILs featuring $[P_{14.666}]$ as their cationic component. Neutral TEMPO resides (and rotates) preferentially in the nonpolar alkyl regions, but its translational diffusion coefficient reflects the necessity to traverse more highly charged zones between the various layers.

8.4 Conclusions

A combined electrochemical and ESR spectroscopic approach has been applied to investigate the translational and rotational diffusive behaviour of probe molecule TEMPO in five room temperature ionic liquids. Over the studied range, the parameters characterising these two types of motion were universally found to follow an Arrhenius dependence on the temperature. In the isotropic RTILs $[C_2mim][NTf_2]$, $[Py_{14}][NTf_2]$ and $[N_{6222}][NTf_2]$ the activation energies derived via this Arrhenius analysis for the translational diffusion coefficient, rotational correlation coefficient and solvent viscosity were essentially equivalent in a given ionic liquid, in compliance with the predictions of simple hydrodynamic theory and suggesting that similar transport mechanisms to those found in simple organic solvents are also in operation here. In the two ionic liquids containing the tris(*n*-hexyl)tetradecyl-phosphonium cation ($[P_{14.666}][NTf_2]$ and $[P_{14.666}][FAP]$), however, the rotational activation energies were determined to be 5–10 kJ mol^{-1} lower than those for viscous flow and translational diffusion. It has been speculated that this is due to the adoption of a more ordered bilayer structure in these systems consisting of alternating ionic and lipophilic regions. The discrepancy in the activation energies then reflects the more significant proportion of time the neutral probe molecule spends rotating in these latter, non-polar locales.

The work reported thus far has both examined heterogeneous kinetics and considered in some detail the issue of diffusive mass transport within room temperature ionic liquid solvents. In the final chapter, it remains to explore the rate of any homogeneous chemistry associated with an electrochemical process.

8.5 References

[1] R.G. Evans, A.J. Wain, C. Hardacre, R.G. Compton, *ChemPhysChem* **2005**, *6*, 1035.

[2] P. Wasserscheid, T. Welton, *Ionic Liquids in Synthesis*, Wiley-VCH, Weinheim, **2003**.

[3] M.C. Buzzeo, R.G. Evans, R.G. Compton, *ChemPhysChem* **2004**, *5*, 1106.

[4] R.G. Evans, O.V. Klymenko, P.D. Price, S.G. Davies, C. Hardacre, R.G. Compton, *ChemPhysChem* **2005**, *6*, 526.

[5] A. Kawai, T. Hidemori, K. Shibuya, *Chem. Lett.* **2004**, *33*, 1464.

[6] M.A.M. Noel, R.D. Allendoerfer, R.A. Osteryoung, *J. Phys. Chem.* **1992**, *96*, 2391.

[7] J.A. Weil, J.R. Bolton, J.E. Wertz, *Electron Paramagnetic Resonance: Elementary Theory and Practical Applications*, John Wiley, New York, **1994**.

[8] W. Suemmermann, U. Deffner, *Tetrahedron* **1975**, *31*, 593.

[9] P. Bonhôte, A.-P. Dias, M. Armand, N. Papageorgiou, K. Kalyanasundaram, M. Grätzel, *Inorg. Chem.* **1996**, *35*, 1168.

[10] R.G. Evans, O.V. Klymenko, C. Hardacre, K.R. Seddon, R.G. Compton, *J. Electroanal. Chem.* **2003**, *556*, 179.

[11] D. Shoup, A. Szabo, *J. Electroanal. Chem.* **1982**, *140*, 237.

[12] R.G. Evans, O.V. Klymenko, P.D. Price, S.G. Davies, C. Hardacre, R.G. Compton, *ChemPhysChem* **2005**, *6*, 526.

[13] B.H. Robinson, H. Thomann, A.H. Beth, P. Fajer, L.R. Dalton in *EPR and Advanced EPR Studies of Biological Systems* (Ed.: L. R. Dalton), C.R.C. Press, Boca Raton, FL, **1985**, 68.

[14] N. Ito, S. Arzhantsev, M. Maroncelli, *Chem. Phys. Lett.* **2004**, *396*, 83.

[15] A. Downard, M.J. Earle, C. Hardacre, S.E.J. McMath, M. Nieuwenhuyzen, S.J. Teat, *Chem. Mater.* **2004**, *16*, 43.

[16] C. Hardacre, J.D. Holbrey, S.E.J. McMath, M. Nieuwenhuyzen, *ACS Symposium Series* **2002**, *818*, 400.

[17] H. Chen, D.C. Kwait, Z.S. Goenen, B.T. Weslowski, D.J. Abdallah, R.G. Weiss, *Chem. Mater.* **2002**, *14*, 4063.

[18] G.A.N. Gowda, H. Chen, C.L. Khetrapal, R.G. Weiss, *Chem. Mater.* **2004**, *16*, 2101.

[19] D.J. Abdallah, A. Robertson, H.-F. Hsu, R.G. Weiss, *J. Am. Chem. Soc.* **2000**, *122*, 3053.

[20] C.F. Polnaszek, S. Schreier, K.W. Butler, I.C.P. Smith, *J. Am. Chem. Soc.* **1978**, *100*, 8223.

[21] H. Yoshioka, *J. Am. Chem. Soc.* **1979**, *101*, 28.

9

A Kinetic Study of the Reaction between N,N-Dimethyl-*para*-toluidine and its Electrogenerated Radical Cation in a Room Temperature Ionic Liquid

The reaction between N,N-dimethyl-*para*-toluidine (DMT) and the radical cation generated through its one-electron oxidation has been studied electrochemically in the room temperature ionic liquid N-methyl-N-butylpyrrolidinium bis(trifluoromethyl-sulfonyl)imide, $[Py_{14}][NTf_2]$. Kinetic information obtained as linear sweep and cyclic voltammetry collected at 5 μm, 10 μm and 0.3 mm diameter platinum disk electrodes over a range of initial substrate concentrations and scan rates spanning five orders of magnitude was complemented by chronoamperometric measurements designed to probe the rate of diffusion. At the fastest scan rates the homogeneous reactions following the initial electron transfer were effectively out-run, facilitating an assessment of the electrode kinetics using DIGISIM® and a validated Nicholson's method. Through digital simulation the voltammetry was then shown to be consistent with a mechanism established for the same reaction in acetonitrile, involving dimerisation of the DMT radicals following an initial and rate-determining proton transfer step. After careful consideration of all parameters, a bimolecular rate constant of $(3.4 \pm 1.1) \times 10^2$ dm^3 mol^{-1} s^{-1} was deduced by fitting the data. This was compared to the equivalent value for acetonitrile and, in light of this, the implications on the viability of ionic liquids for use as alternative mainstream solvents briefly assessed. This work is in press at *ChemPhysChem*.[1]

9.1 Introduction

Room temperature ionic liquids are becoming increasingly familiar within the chemical community, having been proposed for some time now, principally on environmental grounds, as potential industrial replacements for volatile organic solvents.[2] For any given process, however, the effect of an ionic liquid on the reaction rate and possibly even path is clearly an important factor in determining whether such a transition will ultimately take place. Some general investigation into the similarity in chemical reactivity between RTIL *vs* conventional nonaqueous solvents would therefore seem productive, and in cases where such reactivity is initiated by a heterogeneous electron transfer, electrochemical techniques can be brought to bear in this regard. Electrochemical research involving RTILs has not been lacking thus far,[3] indeed several reports have now evidenced the successful transposition of established electroanalytical procedures to accomplish kinetic studies in these neoteric media.[4-10] The present work aims to complement this by investigating the chemical reactivity of the radical cation generated via the one-electron oxidation of N,N-dimethyl-*para*-toluidine (DMT) in an ionic liquid solvent.

Within the literature that already provides data on such bimolecular processes in RTIL solutions (electrochemical in origin or otherwise), no simple correlation with traditional nonaqueous behaviour has emerged, with the relative reaction rates often depending, unsurprisingly, on the exact nature of the ions comprising the solvent. For the fastest reactions, one might predict with reasonable confidence a diffusion-controlled rate curtailed in proportion to the greater viscosity ionic liquids are known to possess, although work by Neta et al. cautions against the over-interpretation of classical formulae commonly applied to molecular solvents for estimating such

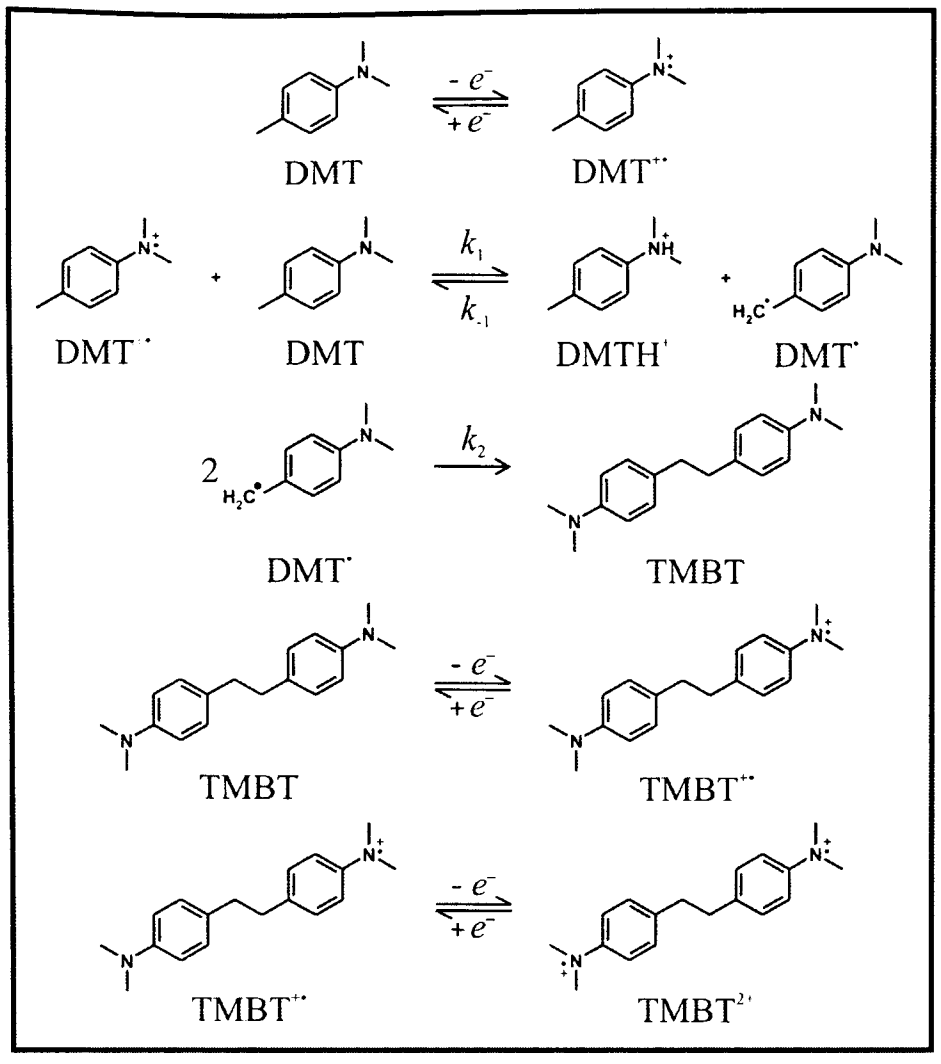


Figure 9.1
Mechanism for the anodic dimerisation of N,N-dimethyl-*para*-toluidine (DMT).

rates.[11] Activated processes, however, could be either driven or impeded depending on specific solvation effects, and while the dimerisation of benzaldehyde radical anions and the reaction of 1,2-dimethylimidazole with benzyl bromide in RTILs display rate constants comparable to those in polar, aprotic solvents,[10,12] Hapiot has reported both a significant decrease and increase in the rates of various electrodimerisation reactions, rationalised in each case using ion-association arguments.[6,8] In all these examples, however, where reported, the rate constants did not differ by more than one order of magnitude from the equivalent value in acetonitrile.

Returning to consider the current investigation, the oxidation of DMT and ensuing reactions have been the subject of a number of studies in acetonitrile,[13-16] the most recent of which has proposed that reaction occurs through the pathway given in Figure 9.1,[16] involving a rate determining acid-base reaction between the $DMT^{+\bullet}$

radical cation and its neutral precursor. Following the deprotonation, the $DMT^{\bullet}$ radicals undergo dimerisation to form N,N,N',N'-tetramethyl-α,α'-bi-*para*-toluidine (TMBT), which is itself susceptible to two successive one-electron oxidations. Such a mechanism containing a mixture of electrochemical and homogeneous steps lends itself to interrogation via electrochemical means, and analysis using a combination of linear sweep and cyclic voltammetry at a disk electrode over a range of electrode radii, concentrations and scan rates yielded a bimolecular rate constant of k_1 = $(5.9 \pm 2.2) \times 10^2$ dm^3 mol^{-1} s^{-1} for the proton transfer reaction. In the following, it was proposed to adopt a similar methodology, having substituted as the solvent the ionic liquid N-methyl-N-butylpyrrolidinium bis(trifluoromethylsulfonyl)imide, $[Py_{14}]$-$[NTf_2]$ (for the structures of the ions see Figure 9.2), selected simply for its favourable conductivity and suitable electrochemical window.[17] Accordingly, transient voltammetric measurements were made at several platinum disk electrodes over a wide scan range with varying initial concentrations of [DMT]. Comparison with the theoretical model developed for this system then permitted elucidation of the various mechanistic parameters in the ionic liquid solvent.

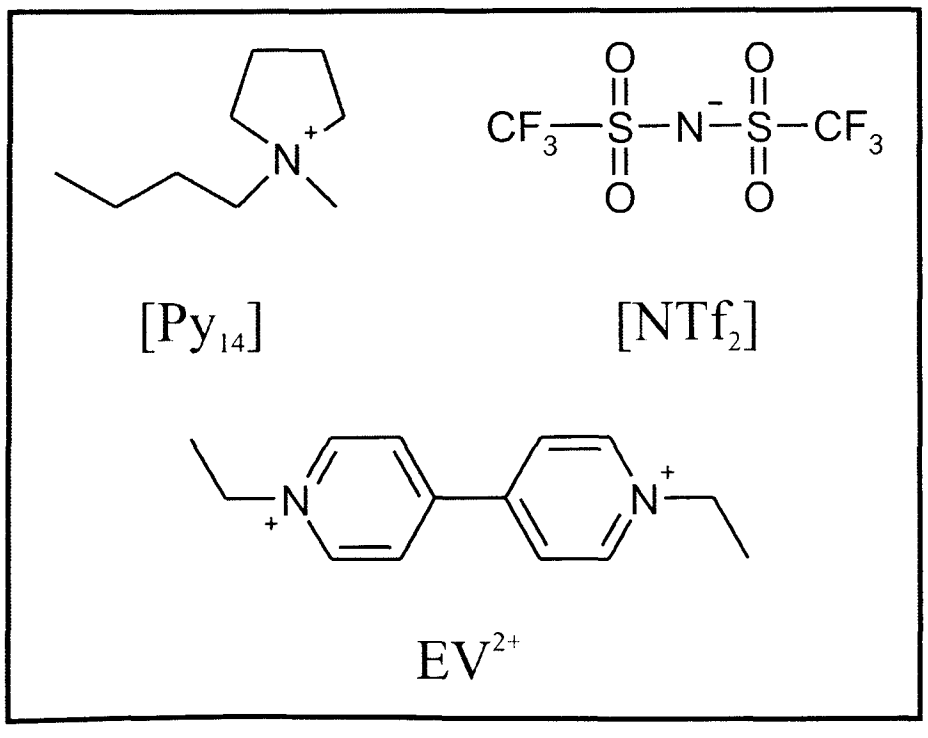


Figure 9.2
Structures of ions involved in this study.

9.2 Experimental Section

In addition to matters already covered in chapter three, the 0.7 mm platinum disk (constructed in-house, mounted in a Teflon support) was polished using 3 μm and then 1 μm diamond spray on a polishing pad (all Kemet). Its precise diameter was determined with the aid of a traveling microscope.

This study utilized three platinum disk working electrodes, nominal diameters 5 μm, 10 μm and 0.7 mm. The experimental temperature was maintained at 298.9 ± 0.8 K.

9.3 Results and Discussion

9.3.1 Voltammetry of DMT in $[Py_{14}][NTf_2]$

The oxidation of DMT in $[Py_{14}][NTf_2]$ was first investigated using linear sweep and cyclic voltammetry at 5 and 10 μm platinum electrodes, and Figure 9.3 (right-hand side) shows a typical CV obtained from a solution containing 20 mM DMT by applying a scan rate of 500 mV s^{-1} at the 10 μm disk. Apart from the slower rate of diffusion in the ionic liquid causing the wave to exhibit a more transient appearance at electrodes of smaller radius,[3,4] the voltammetric profile otherwise closely

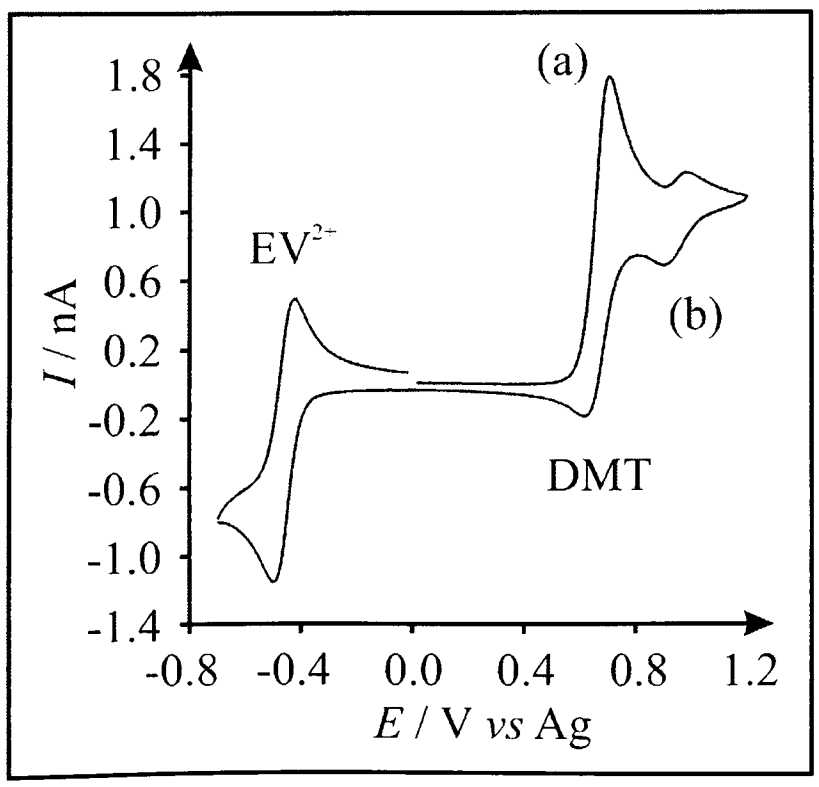


Figure 9.3
Cyclic voltammogram for the electrolysis of a 20 mM solution of EV^{2+} and DMT in $[Py_{14}][NTf_2]$ at a 10 μm diameter platinum disk electrode, scan rate 500 mV s^{-1}.

resembles that observed for the same system in acetonitrile.[16] The size and location of the various peaks can be rationalised by considering the mechanism shown in Figure 9.1, which contains three species capable of undergoing a heterogeneous electron transfer in the potential window of interest, namely the DMT substrate itself and also the dimeric species TMBT and $TMBT^{+\bullet}$. Accordingly, the principal anodic wave (a), primarily attributable to DMT is augmented by oxidation of the neutral dimer, whose standard electrode potential is less than or equal to that of DMT and is thus immediately susceptible to oxidation upon its formation via the two homogeneous steps. At higher potentials, a further one-electron oxidation of the dimer becomes favourable, leading to a distinct second wave (b), which appears reversible. Finally, since (i) most of the $DMT^{+\bullet}$ radical cations have been consumed through chemical reaction and (ii) only one molecule of TMBT is generated for every two DMT molecules initially oxidized, the reverse peak of wave (a) (resulting from the reduction of species $DMT^{+\bullet}$ and $TMBT^{+\bullet}$) is relatively small.

Since the initial data had not revealed anything unexpected or inconsistent with the earlier studies on this system, a raft of further experiments were next undertaken in which the concentration of DMT, [DMT], disk radius, r_d, and scan rate, v, were sequentially varied. To track the first of these parameters, a second species, ethyl viologen (EV^{2+}, for structure see Figure 9.2), was added to the ionic liquid solution to act as an internal standard. This became necessary to overcome the inherent difficulty of accurately preparing μL-quantities of ionic liquid solution of known concentration.[4] As explained in chapter three, the preparation of these ionic liquid solutions proceeded by first dissolving the solutes in acetonitrile. In this initial stock solution, the DMT and EV^{2+} were added in equal concentration on the basis that in

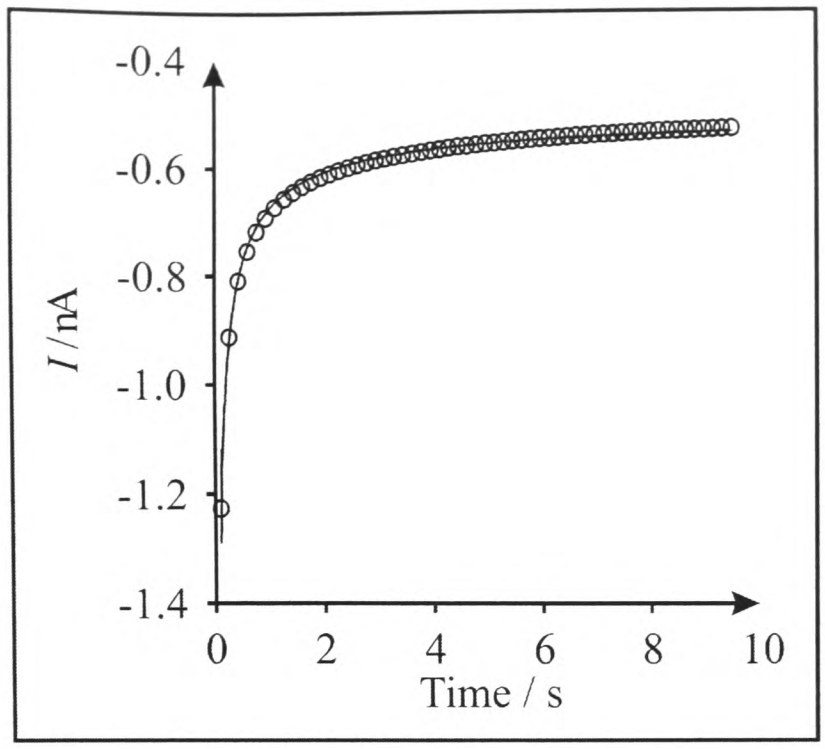


Figure 9.4
Experimental (—) and fitted theoretical (○) chronoamperometric transient for the reduction of 20 mM EV^{2+} in $[Py_{14}][NTf_2]$ at a 10 μm Pt disk electrode.

the final ionic liquid solution, the same would be true. Of the numerous compounds that could have functioned as a simple chemical marker, ethyl viologen diperchlorate was selected for this investigation as both cation and counter-anion are electrochemically inactive in the window encompassing the voltammetry of DMT. At sufficiently cathodic potentials, however, ethyl viologen undergoes a reversible, one-electron reduction (see Figure 9.3, left-hand side) and thus its concentration can be readily determined by electrochemical measurements, specifically chronoamperometry.[4] Then, since they were designed to be equal, the result of this analysis provides the concentration of DMT in the same solution. Application of the chronoamperometric technique is illustrated in Figure 9.4 for the same experiment from which the voltammogram in Figure 9.3 is drawn. The system is perturbed by applying an instantaneous potential step from a region of no faradaic activity to a point at which the one-electron reduction of EV^{2+} occurs at a diffusion controlled rate, and the current response monitored as a function of time (Figure 9.4, solid line). The now familiar Shoup and Szabo analysis then yields simultaneously both unknowns, i.e. the concentration and diffusion coefficient of the electroactive

species.[5,18] This was carried out using the nonlinear curve fitting function available in ORIGIN 6.0 (Microcal Software Inc.) and the optimised fit is shown for the example in Figure 9.4 (open circles). By performing such a measurement on every solution, [DMT] was thus determined each time. For completeness, the diffusion coefficient of EV^{2+} was found to be $(8.05 \pm 0.25) \times 10^{-12}$ m^2 s^{-1}.

Having put in place the necessary prerequisites to allow the parameters to be varied in a controlled manner, an array of voltammograms was then generated across the ranges: r_d = 2.5, 5 μm; (nominal) [DMT] = 2.5, 5, 10, 20, 40 mM; and $5 \leq v \leq 5000$ mV s^{-1}. A selection of the resulting data is displayed in Figure 9.5, which shows the variation with concentration in (a) linear sweep voltammograms at the 5 μm disk, with v = 5 mV s^{-1} and (b) cyclic voltammograms at the 10 μm disk, with v = 500 mV s^{-1}. The actual concentrations (derived from accompanying EV^{2+} chronoamperometric measurements) are listed in the legend, and in each case the plots have been scaled such that the variation in the relative peak heights may be directly gauged. If the

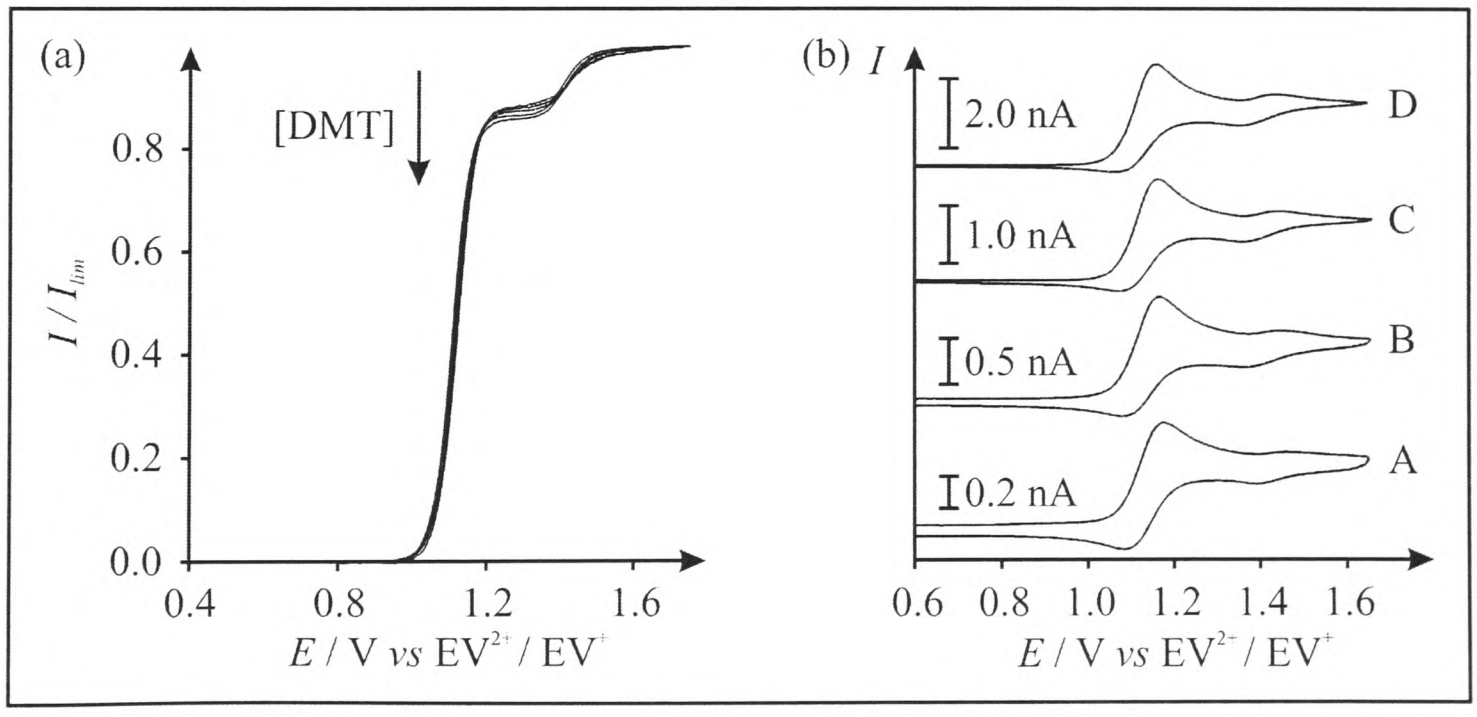


Figure 9.5
(a) Linear sweep voltammograms for the oxidation of 3.7, 6.9, 10.8, 22.0 and 30.8 mM DMT in $[Py_{14}][NTf_2]$ at a 5 μm Pt disk electrode, scan rate 5 mV s^{-1}, normalised by the limiting current on the second plateau. (b) Cyclic voltammograms for the oxidation of (A) 8.7, (B) 11.7, (C) 19.8 and (D) 32.8 mM DMT in $[Py_{14}][NTf_2]$ at a 10 μm Pt disk electrode, scan rate 500 mV s^{-1}.

above mechanism was indeed followed, an increase in concentration should promote the first homogeneous step (which is first-order in [DMT]) and manifest as an increase in the height of the second wave at the expense of the first. Although subtle, the data in Figure 9.5 is consistent with this prediction; in Figure 9.5(a), as [DMT] increases, the height of the first current plateau is seen to decrease slightly relative to the second and in Figure 9.5(b) the second peak becomes less distinguishable and the back peak associated with the first wave more so as the concentration of DMT is reduced.

9.3.2 Diffusion

In a first step towards deconvoluting the various parameters quantifying the electrochemical behaviour of this system, the diffusion coefficient of DMT was determined using the following strategy. If it is assumed that the second homogeneous mechanistic step, involving the dimerisation of two $DMT^{\bullet}$ radicals, is sufficiently rapid that the concentration of $DMT^{\bullet}$ remains effectively zero, the overall process may be reduced to the single equation:

$$DMT \rightarrow \tfrac{1}{2}(1-x)DMTH^{+} + \tfrac{1}{4}(1-x)TMBT^{2+} + xDMT^{+\bullet} + e^{-} \quad (9.01)$$

where the variable x may take the values $0 \leq x \leq 1$ and allows for the uncertainty in the rate constant, k_1, for the reaction between DMT and its radical cation. It can be seen that the rate of this reaction affects only the product distribution and not the number of electrons transferred, which remains constant at one. Formulated in this way, regardless of the rate of the proton transfer reaction, one electron is consumed for each molecule of DMT oxidised. Thus, if the potential is stepped to a point sufficiently beyond the second voltammetric wave that all heterogeneous electron transfers will operate at their diffusion controlled rate, the resulting

chronoamperometric transient can be analysed in the same manner as described above for reduction of the viologen to give, to a good approximation, the diffusion coefficient of DMT. This method is preferable to a simple calculating involving the limiting current, as there is no requirement for the system to reach a steady-state, nor is it required to make any assumption regarding the magnitude of k_1. Transients of this nature were measured and analysed for each studied concentration of DMT at both the 5 and 10 μm disks. The results were averaged to give the diffusion coefficient of DMT in $[Py_{14}][NTf_2]$ as $(1.99 \pm 0.37) \times 10^{-11}$ m^2 s^{-1}.

Ultimately, extraction of further quantitative mechanistic information from the data derived in this section will necessitate simulation of the entire voltammetric wave. Simulating such a five-step mechanism, however, requires the inclusion of numerous parameters, and in order for the results of the final fitting procedure to be as meaningful as possible, it is desirable to fix some of these beforehand through their independent determination. Under the right experimental conditions, the reaction between DMT and its radical cation could be sufficiently out-run that the resulting cyclic voltammetry simply represented the electrochemical oxidation and re-reduction of DMT. The kinetics of this heterogeneous electron transfer could then be parameterised using standard techniques. In terms of our three experimental variables, creating the right conditions involves either minimising r_d or [DMT] or maximising v. Constructing a disk electrode of significantly smaller diameter is impractical and 2.5 mM is already close to the lower limit for generating a measurable current in an ionic liquid solution given their much smaller magnitude in these highly viscous media. Moreover, the extent of variation in the relative wave heights over the range 2.5–40 mM (Figure 9.5) suggests that a considerable decrease in either of these

parameters would be required. Applying faster scan rates was therefore the most likely approach to successfully furthering this investigation.

9.3.3 Heterogeneous Kinetics

Despite what the name may suggest, room temperature ionic liquids are generally more resistive media than more conventional organic solvent / electrolyte systems,[3] thus the application of higher scan rates can not be considered without first addressing the issue of ohmic drop compensation. This proved difficult to implement for the small currents generated at the 5 and 10 μm disks, so a much larger platinum electrode (0.7 mm) was instead employed using a modified set-up (see experimental section and chapter three). In this case, using positive-feedback mode, the potentiostat was able to gauge and correct for an uncompensated resistance of around 2 kΩ. CVs were then recorded for the oxidation of a 10 mM DMT solution over the range $10 \leq v \leq 250$ V s^{-1} and a selection of these are shown in Figure 9.6(a). At these scan rates, the second oxidative peak is absent and the back peak associated with the first wave is much more pronounced, as under these conditions the mechanism has been effectively reduced to the first step only. As the voltammetry display quasireversible behaviour, the variation in the peak-to-peak separation, ΔE_p, with v may be used to determine a rate constant, k_0, for this heterogeneous electron transfer. Adopting the method of Nicholson,[19] assuming that this step involves the concerted transfer of one electron and that the direction of the potential sweep is reversed at least 90 mV beyond the anodic peak, the voltammetric profile may be expressed as a function of the parameter, ψ, defined as:

$$\psi = \frac{(RT)^{1/2}\left(D_O/D_R\right)^{\alpha/2} k_0}{(\pi D_O F v)^{1/2}} \qquad (9.02)$$

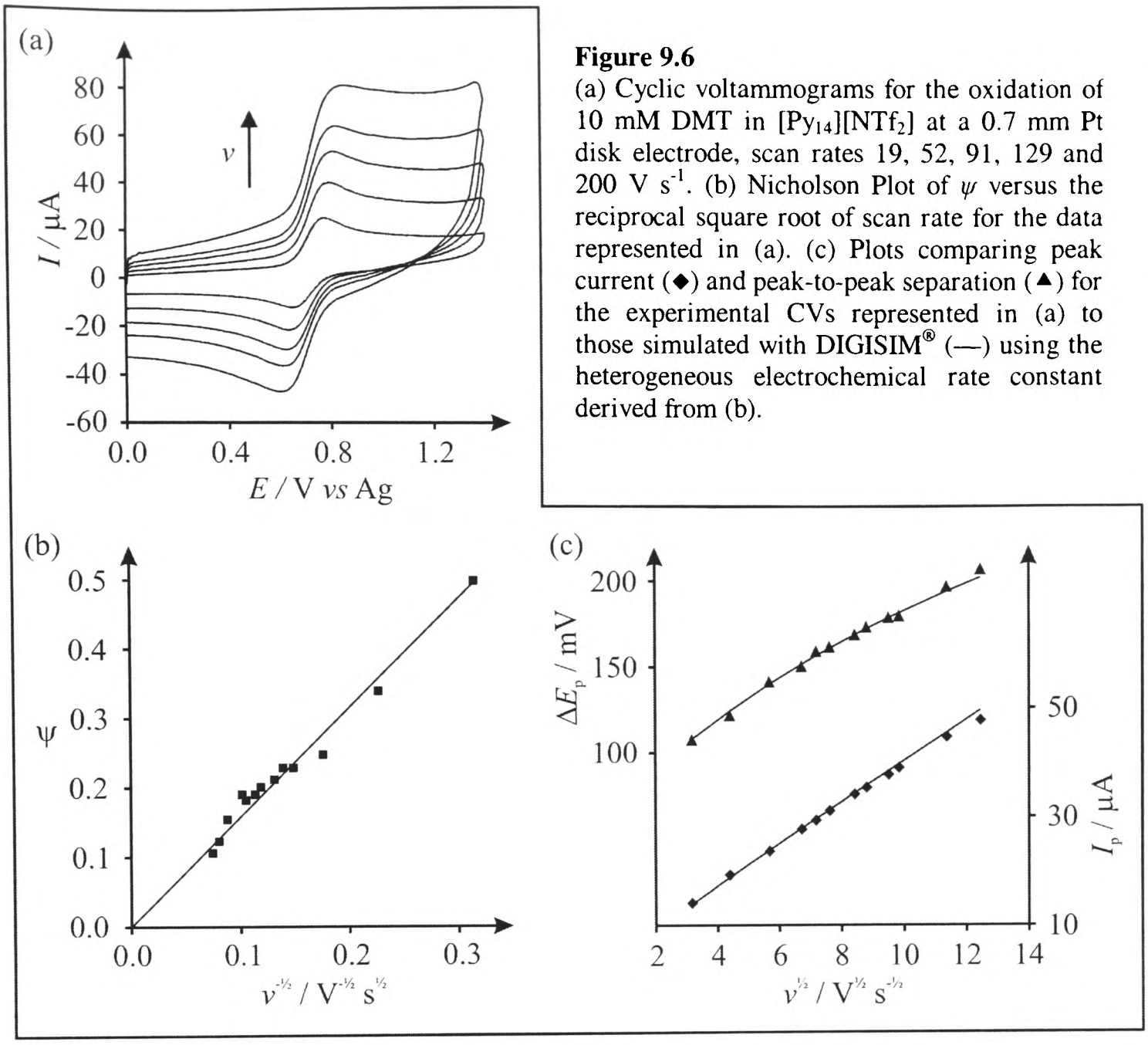


Figure 9.6
(a) Cyclic voltammograms for the oxidation of 10 mM DMT in $[Py_{14}][NTf_2]$ at a 0.7 mm Pt disk electrode, scan rates 19, 52, 91, 129 and 200 V s^{-1}. (b) Nicholson Plot of ψ versus the reciprocal square root of scan rate for the data represented in (a). (c) Plots comparing peak current (◆) and peak-to-peak separation (▲) for the experimental CVs represented in (a) to those simulated with DIGISIM® (—) using the heterogeneous electrochemical rate constant derived from (b).

where the subscripts O and R refer to the species undergoing oxidation and reduction respectively, α is the electron transfer coefficient, and R is the universal gas constant. The heterogeneous rate constant is then determined by relating ψ to ΔE_p at each scan rate. In his original 1965 paper, Nicholson calculated ΔE_p at thirteen values of ψ for the case where $\alpha = 0.5$ and $T = 298$ K.[19] Modern computing methods now render this process facile, and the commercial voltammetric simulation package DIGISIM® (version 3.0, BAS Technicol, USA) was used to re-calculate these peak separations by using equation (9.02) to determine the scan rate associated with each ψ value for a given k_0. The results are compared in Table 9.1, along with some additional simulated values in the region where ΔE_p increases rapidly in Nicholson's table. Comfortingly,

Table 9.1
Variation in the kinetic parameter ψ with the peak-to-peak separation from the cyclic voltammogram of a simple one-electron process with $\alpha = 0.5$ at $T = 298$ K, as determined by Nicholson[4] and using DIGISIM®.

ψ	ΔE_p / mV Nicholson	ΔE_p / mV DIGISIM®	ψ	ΔE_p / mV Nicholson	ΔE_p / mV DIGISIM®
20	61	59	0.35	121	122
7	63	61	0.30	-	130
6	64	62	0.25	141	142
5	65	63	0.23	-	149
4	66	64	0.18	-	164
3	68	66	0.17	-	173
2	72	70	0.15	-	183
1	84	82	0.13	-	193
0.75	92	90	0.12	-	203
0.50	105	105	0.10	212	217

the newly-simulated values correspond within one or two mV to those previously calculated.

Using Table 9.1, a value of ψ was interpolated for each voltammogram and a plot of ψ *vs* $v^{-½}$ constructed, as shown in Figure 9.6(b). According to equation (9.02), this should yield a straight line through the origin, the gradient of which is a function of the heterogeneous rate constant. The plot was indeed linear and based on the diffusion coefficient of DMT derived above, a value for k_0(DMT) of $(7.36 \pm 1.51) \times 10^{-3}$ cm s^{-1} was deduced, its uncertainty reflecting both the scatter in the plot and the weak dependence of ψ on (D_O/D_R) (an α value of 0.5 was assumed). In the latter case, variation of this ratio between one and two was considered, since the work reported in chapter seven has demonstrated that the diffusion coefficient of a related organic radical cation in several RTILs differs by almost 50% from that of its neutral parent.[20] This value of k_0 is one order of magnitude lower than observed for the oxidation of DMT in acetonitrile,[16] a similar finding to that previously observed for the oxidation of several organic molecules in RTIL *vs* conventional nonaqueous environments, and pointing to a more extensive degree of solvent reorganisation

during charge transfer in the former.[6] To validate this assessment of k_0, DIGISIM® was now employed to attempt to recreate the experimental CVs using this value of the heterogeneous rate constant. The good fit between experiment and theory is demonstrated in Figure 9.6(c) where the variation in oxidative peak current and peak-to-peak separation with scan rate for one data set is seen to closely follow the other. This simulation served one other useful purpose, that of defining a rough maximum value for the rate constant of the first homogeneous step (the proton transfer between DMT and its radical cation). The 2^{nd} – 5^{th} steps of the mechanism were added to the program and the voltammogram at the slowest scan rate re-computed with the rate constant k_1 gradually increased from zero. Only at values of $k_1 > 1000$ dm^3 mol^{-1} s^{-1} did the simulated voltammograms begin to deviate from experiment and a second wave start to emerge. This may therefore be considered as an upper-limit on k_1 with which subsequent simulation must be consistent.

9.3.4 Homogeneous Kinetics

Armed now with independent data on the diffusional and electrochemical properties of the system, it remained to determine a homogeneous rate constant for the acid-base reaction between DMT and its radical cation by returning to model the voltammetry from the 5 and 10 μm platinum disks. Since DIGISIM® is only capable of simulating over one spatial dimension, a more sophisticated program was required to accurately account for the contributions of both planar and convergent diffusion under the prevailing conditions.[3,4] The theory developed to compute voltammetic profiles at a disk electrode for the mechanism given in Figure 9.1 and the finite-difference method used in its solution were adopted from the earlier work of Klymenko et al. in which acetonitrile was used as the solvent.[16] As the procedure relies on numerical

approximation to solve key equations, the convergence of the simulation was re-examined in the light of the diffusion coefficient pertinent to the system at hand being significantly smaller than in the previous work (~100 times). As before, the level of convergence was gauged by running the program over a variety of grid sizes ($N\theta$ x $N\Gamma$, where θ and Γ are the transformed grid coordinates) and calculating the relative error in the height of the first peak, ($|I-I_{lim}|/I_{lim}$). Here, I_{lim} represents the limiting value of the peak current, extrapolated to a grid of infinite size. Figure 9.7 shows a logarithmic plot of this relative error against the reciprocal of the grid size parameter, N. The level of convergence proved to be virtually equivalent to that originally found,[16] thus the global reduction in diffusion coefficients was inconsequential in this regard. While fitting the experimental voltammetry, a grid of size 50 x 50 ($N\theta$ x $N\Gamma$) was employed, giving a convergence of 2.9 % and requiring each time approximately two minutes to process on an AMD Athlon™ 2600+ 1.92 GHz PC with 1.00 GB of RAM. Given that the procedure required manual iteration of each parameter, further grid refinement was deemed impractical.

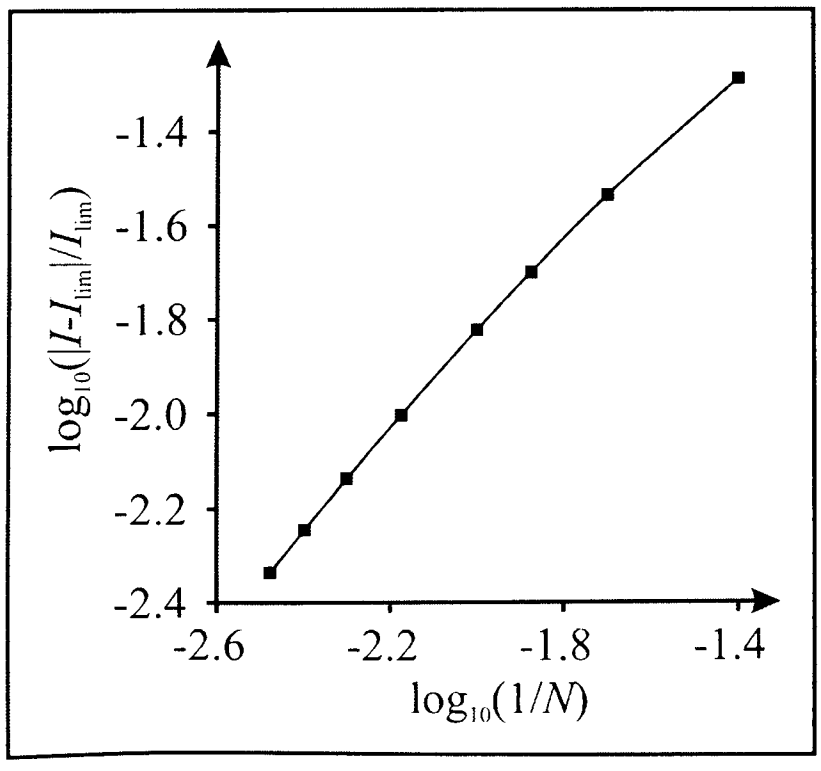


Figure 9.7
Convergence plot for the peak current of the first wave calculated for the case where r_d = 10 μm; [DMT] = 20.8 mM; ν = 500 mV s^{-1} and all other parameters as in Table 9.2.

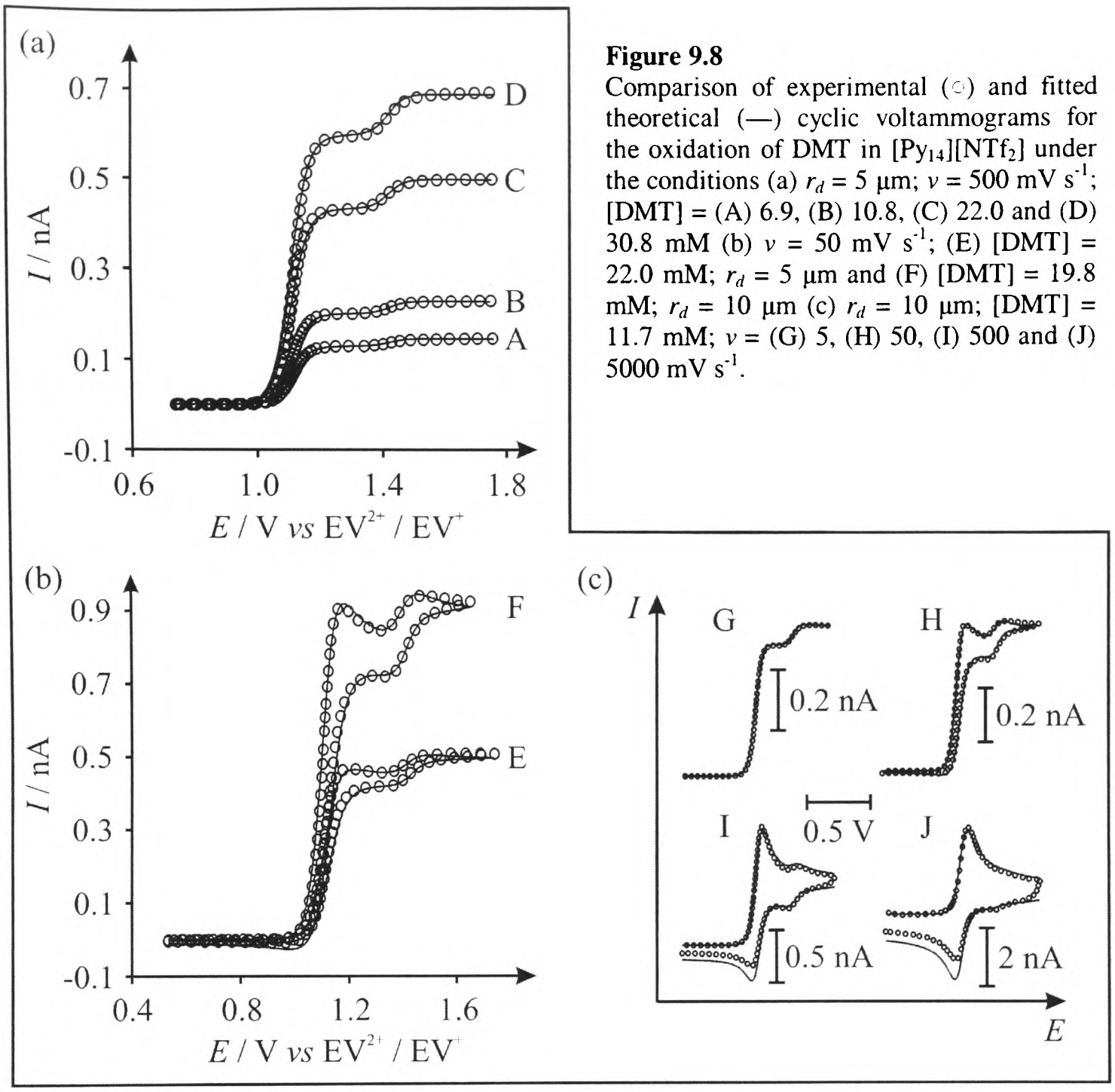


Figure 9.8
Comparison of experimental (○) and fitted theoretical (—) cyclic voltammograms for the oxidation of DMT in $[Py_{14}][NTf_2]$ under the conditions (a) r_d = 5 μm; ν = 500 mV s^{-1}; [DMT] = (A) 6.9, (B) 10.8, (C) 22.0 and (D) 30.8 mM (b) ν = 50 mV s^{-1}; (E) [DMT] = 22.0 mM; r_d = 5 μm and (F) [DMT] = 19.8 mM; r_d = 10 μm (c) r_d = 10 μm; [DMT] = 11.7 mM; ν = (G) 5, (H) 50, (I) 500 and (J) 5000 mV s^{-1}.

With the output of the simulation program confirmed as sound, it was used to reproduce the entire range of voltammetry collected at the 5 and 10 μm working electrodes as closely as possible by varying the remaining unknown parameters. As far as they could be determined, the optimum values of these parameters are summarized in Table 9.2 and the quality of the accompanying fits are exemplified in Figure 9.8 as the (a) concentration, (b) disk radius and (c) scan rate are separately varied. The shape of the voltammetric profile was found to be much more sensitive to the value of certain parameters than it was to others and, as the table shows, this is reflected in the accuracy to which these various quantities may be reported. Crucially

for the purposes of this investigation, the relative height of the two oxidative peaks was strongly dependant on the value of the rate constant for the first homogeneous step, k_1, which could thus be determined reliably to a high precision. Other parameters changed the voltammogram more subtly, or their effects could not be completely deconvoluted from one another. Before drawing any general conclusions therefore, it is appropriate to first assess how the various diffusional, electrochemical and homogeneous kinetic steps were treated in arriving at the optimized fit.

Beginning with the case of diffusion, there are seven distinct species involved in the mechanism, each requiring their own diffusion coefficient to be specified. The coefficient for DMT itself was measured directly, as described above, yet this still left six values for which independent data does not exist. The dimer is not commercially available for separate analysis, nor is the Wilke-Chang method of estimating diffusion coefficients suitable for use with ionic liquids solutions.[4] It was therefore assumed that the ratio of diffusion coefficients between DMT and its dimer was the same as in acetonitrile,[16] and deviation from this value for *D*(TMBT) during the fitting procedure offered no significant improvement. For the various ions, a further assumption was made that the diffusion coefficient of each monomeric species was

Table 9.2
Optimised parameters characterizing the anodic dimerisation of DMT in $[Py_{14}][NTf_2]$ via the mechanism shown in Figure 9.1.

D(DMT)	$(1.99 \pm 0.37) \times 10^{-11}$ m^2 s^{-1}
D(TMBT)	$(1.20 \pm 0.37) \times 10^{-11}$ m^2 s^{-1}
E_f^0 (DMT)	1.12 ± 0.01 V *vs* EV^{2+} / EV^{+}
E_f^0 (TMBT)	1.12 ± 0.01 V *vs* EV^{2+} / EV^{+}
E_f^0 ($TMBT^{+\bullet}$)	1.41 ± 0.01 V *vs* EV^{2+} / EV^{+}
k_0 (DMT)	0.007 ± 0.002 cm s^{-1}
k_0 (TMBT)	0.007 ± 0.002 cm s^{-1}
k_0 ($TMBT^{+\bullet}$)	0.005 ± 0.002 cm s^{-1}
k_1	$(3.4 \pm 1.1) \times 10^2$ dm^3 mol^{-1} s^{-1}
k_2	$\geq 10^5$ dm^3 mol^{-1} s^{-1}
k_{-1}	kinetically insignificant

equal to that of neutral DMT and correspondingly those of the oxidized forms of TMBT were equal to that of their parent. As has already been alluded to above however, although there is considerable evidence for the validity of this assumption when applied to mechanistic electrochemical studies involving conventional solvents,[21-23] contrary behaviour has recently been observed for the case of ionic liquids.[20] It was therefore important to explore the extent of the influence of relative diffusion rates, and to this end subsequent simulations were performed in which, guided by the previous report,[20] the diffusion coefficients of all species with a formal positive charge of one had their diffusion coefficients successively reduced up to a limit of 50% of their initial value. This modification was found to displace the limiting current reached by the first wave to slightly higher values, while the second peak continued to tend to the same absolute maximum, and a corresponding decrease (up to 50%) in the rate constant, k_1, was required to cause the simulated wave to overlay the experimental data once more. Clearly therefore, the diffusion coefficients carry some significance, but without more precise information it is impossible to entirely correct for their effects, thus placing some additional uncertainty on any determination of a rate constant, k_1. At the same time, however, these latter simulations suggest that they do not create order of magnitude level uncertainty, and are unlikely to invalidate the general conclusions.

Turning to the three electrochemical steps of the mechanism, the parameters of relevance here are the heterogeneous rate constant, k_0, the formal electrode potential, E_f^0 and the electron transfer coefficient, α, for each couple. As stated above, a sample of the dimer could not be easily obtained to perform separate studies on its electrochemistry, and so in constructing the simulation these properties were initially

based on those determined independently for DMT from the fast scan data at the 0.7 mm disk. Voltammetrically, the first oxidation process of the dimer is buried under that of DMT itself and so attempting to refine its parameters any further is not viable. The second oxidative wave is distinct, and here a slightly lower value for the heterogeneous rate constant than found for DMT gave an improved fit (see Table 9.2). Its separation from the first oxidation wave of TMBT, assessed by taking the difference: [E_f^0 (TMBT$^{+\bullet}$) - E_f^0 (TMBT)], was found to be virtually identical to the situation in acetonitrile (0.29 V as compared to 0.31 V). Deviation of any transfer coefficient from a value of 0.5 served no purpose.

Finally in this review of the various parameters, it remains to discuss the effect of the homogeneous rate constants for the two bimolecular reactions. The dimerisation step itself, as in the determination of a diffusion coefficient for DMT, was not considered at all rate limiting and treated as totally irreversible with its forward rate constant, k_2, set sufficiently high that any further increase produced an unaltered simulated voltammogram. This threshold occurred at 10^5 dm^3 mol^{-1} s^{-1} and thus k_2 may only be specified in terms of this lower limit, although the Stokes-Einstein-Smoluchowski equation would suggest an upper (diffusion controlled) limit of 10^8 dm^3 mol^{-1} s^{-1} for this ionic liquid. The rate determining reaction between DMT and its radical cation was modelled as reversible with both forward and back rate constants, k_1 and k_{-1} specified. In practice, however, the value of k_{-1} only began to influence the shape of the simulated voltammogram when it considerably exceeded that of k_1, a situation requiring that this equilibrium lie to the right. It was assumed that this was not the case and k_{-1} restricted to values $< k_1$ with the result that this step is rendered effectively irreversible under the experimental conditions. As such, the extent of its

progress was exclusively governed by k_1, whose value could be fine-tuned during the fitting procedure to best match the ratio between the first and second oxidative peaks. Having taken all these factors into consideration, the results are summarized in Table 9.2 and demonstrated in Figure 9.8. The theoretical and experimental voltammetric waves are largely coincident, the only major departure occurring at the highest scan rates (see Figure 6(c)), where the back peak predicted for the first oxidative feature is significantly larger than that actually observed. This is likely due to the fact that an alternative fate for the TMBT dication, specifically deprotonation to yield a stilbene,[14] has been omitted from the modeling, yet in practice occurs to a certain extent. Otherwise, however, there is nothing to suggest that the oxidation of DMT in the ionic liquid $[Py_{14}][NTf_2]$ is inconsistent with the literature mechanism given in Figure 9.1.

9.4 Conclusions

The first-order rate constant for the reaction between the $DMT^{+\bullet}$ radical cation and its neutral precursor in the ionic liquid $[Py_{14}][NTf_2]$ has been determined through rigorous simulation as $k_1 = (3.4 \pm 1.1) \times 10^2$ dm^3 mol^{-1} s^{-1}, which is found to be in accordance with the prediction made during the earlier DIGISIM® modelling. This compares to the value $k_1 = (5.9 \pm 2.2) \times 10^2$ dm^3 mol^{-1} s^{-1}, reported in the case of acetonitrile as the solvent.[16] The outcome of this investigation is therefore in line with previous reports in finding the bimolecular reaction rate in an ionic liquid solution to be indistinct from that observed in a more conventional polar aprotic medium. While a transition from conventional to RTIL solvents will not be centered on this issue, it demonstrates once more that the chemistry itself certainly provides no impediment. Finally, it is worth noting that whereas the dimerisation reactions cited

in the introduction occurred between two charged radicals, in the rate determining step for the DMT system, only one species is charged. The effect of solvation within the ionic liquid may therefore be less of a factor here than in these former instances in which it was identified as a major cause of the variation in rate constant between the two solvent environments.

9.5 Overall Conclusions of the Work Reported in this Thesis

Compared with conventional organic solvents, electrochemistry in ionic liquids may be performed with relatively little additional complexity of experimental set up, and the measurements geared towards and analysed according to traditional strategies, albeit without the benefit of certain simplifications and conveniences established through decades of research in the former. Perhaps the most significant findings have been in the area of mass transport. Beyond the observance of an order of magnitude drop in their absolute value compared to standard nonaqueous media, individually each diffusion coefficient has been shown to follow a reciprocal relationship with the macroscopic viscosity. Moreover, three separate experimental approaches have rigorously demonstrated the greater influence of the charge on a diffusing species, the consequence being a pronounced asymmetry in the rate of diffusion on either side of a redox couple in an ionic liquid. While the effects on homogeneous follow-up chemistry are less meaningfully generalised, this work has concurred with external data in that of the three stages of the electrochemical process, this is the least affected by relocation to an RTIL environment. Heterogeneous electron transfer has been found to be amenable to Butler-Volmer type analysis, providing sensible values of the relevant parameters, and reproducing a factor of ten decrease in the size of the heterogeneous rate constant. Although a more thorough survey of this variable would

have certainly been desirable, it is best studied using a steady-state method, and obtaining a truly limiting current under quiescent conditions has been shown as unfeasible. Much more reliable would be a hydrodynamic approach, rendered impractical over the course of this work, however, due to the sheer volume of ionic liquid solvent necessarily required. A continuation of the work in this direction would nevertheless be most welcome, and with the increasing availability of RTILs in larger quantities, the emergence of such data is soon anticipated.

9.6 References

[1] R.G. Evans, R.G. Compton, *ChemPhysChem* **2005**, in press.

[2] P. Wasserscheid, T. Welton, *Ionic Liquids in Synthesis*, Wiley-VCH, Weinheim, **2003**.

[3] M.C. Buzzeo, R.G. Evans, R.G. Compton, *ChemPhysChem* **2004**, *5*, 1106.

[4] R.G. Evans, O.V. Klymenko, C. Hardacre, K.R. Seddon, R.G. Compton, *J. Electroanal. Chem.* **2003**, *556*, 179.

[5] R.G. Evans, O.V. Klymenko, S.A. Saddoughi, C. Hardacre, R.G. Compton, *J. Phys. Chem. B* **2004**, *108*, 7878.

[6] C. Lagrost, D. Carrié, M. Vaultier, P. Hapiot, *J. Phys. Chem. A* **2003**, *107*, 745.

[7] C. Lagrost, S. Gmouh, M. Vaultier, P. Hapiot, *J. Phys. Chem. A* **2004**, *108*, 6175.

[8] C. Lagrost, P. Hapiot, M. Vaultier, *Green Chem.* **2005**, *7*, 468.

[9] C.A. Brooks, A.P. Doherty, *J. Phys. Chem. B* **2005**, *109*, 6276.

[10] A.P. Doherty, C.A. Brooks, *Electrochim. Acta* **2004**, *49*, 3821.

[11] A. Skrzypczak, P. Neta, *J. Phys. Chem. A* **2003**, *107*, 7800.

[12] A. Skrzypczak, P. Neta, *International Journal of Chemical Kinetics* **2004**, *36*, 253.

[13] R. Hand, M. Melicharek, D.I. Scoggin, R. Stotz, A.K. Carpenter, R.F. Nelson, *Collect. Czech. Chem. Commun.* **1971**, *36*, 842.

[14] M. Melicharek, R.F. Nelson, *J. Electroanal. Chem.* **1970**, *26*, 201.

[15] M. Oyama, M. Goto, H. Park, *Electrochem. Commun.* **2002**, *4*, 110.

[16] N.V. Rees, O.V. Klymenko, R.G. Compton, M. Oyama, *J. Electroanal. Chem.* **2002**, *531*, 33.

[17] D.R. MacFarlane, P. Meakin, J. Sun, N. Amini, M. Forsyth, *J. Phys. Chem. B* **1999**, *103*, 4164.

[18] D. Shoup, A. Szabo, *J. Electroanal. Chem.* **1982**, *140*, 237.

[19] R.S. Nicholson, *Anal. Chem.* **1965**, *37*, 1351.

[20] R.G. Evans, O.V. Klymenko, P.D. Price, S.G. Davies, C. Hardacre, R.G. Compton, *ChemPhysChem* **2005**, *6*, 526.

[21] R.L. Wang, K.Y. Tam, R.G. Compton, *J. Electroanal. Chem.* **1997**, *434*, 105.

[22] R.L. Wang, K.Y. Tam, F. Marken, R.G. Compton, *Electroanalysis* **1997**, *9*, 284.

[23] R.G. Compton, B.A. Coles, R.A. Spackman, *J. Phys. Chem.* **1991**, *95*, 4741.